NASA Technical Memorandum 102817

Suckdown, Fountain Lift, and Pressures Induced on Several Tandem Jet V/STOL Configurations

David C. Bellavia, Douglas A. Wardwell,
Victor R. Corsiglia, and Richard E. Kuhn

March 1991

National Aeronautics and
Space Administration

NASA Technical Memorandum 102817

Suckdown, Fountain Lift, and Pressures Induced on Several Tandem Jet V/STOL Configurations

David C. Bellavia, Douglas A. Wardwell, Victor R. Corsiglia
Ames Research Center, Moffett Field, California

Richard E. Kuhn
STO-VL Technology, San Diego, California

March 1991

National Aeronautics and
Space Administration

Ames Research Center
Moffett Field, California 94035-1000

SYMBOLS

C_m pitching moment coefficient; $C_m = PM/(T * d_e)$

C_p pressure coefficient; $C_p = 2\ \Delta P\ (S_{jet})/T$

d_e equivalent nozzle diameter, in.

$\overline{D}$ equivalent model diameter, in.

h model height, in.

ΔL jet-induced lift, lb

P_{amb} ambient pressure, psia

P_i local static absolute pressure, psia

P_{jet} total absolute pressure at jet exit, psia

PM pitching moment, in·lb

ΔP local pressure difference; $\Delta P = P_i - P_{amb}$, psi

r radial distance from disk center, in.

R disk radius, in.

S_{jet} jet area; one jet = 1.188 in.^{2}, two jets = 2.376 in.^{2}

S_{plan} model planform area, in.^{2}

T thrust, where $T = 7.0\ A_{jet}(\ P_{amb})[(NPR^{0.286}) - 1]$ (lb) for NPR < 1.893

$T = A_{jet}\ (P_{amb})[(1.2679)NPR - 1]$ (lb) for NPR > 1.893

x_{mc} moment center (in. from moment reference); $x_{mc} = (PM/\Delta L) - 17$

SUCKDOWN, FOUNTAIN LIFT, AND PRESSURES INDUCED ON SEVERAL TANDEM JET V/STOL CONFIGURATIONS

David C. Bellavia, Douglas A. Wardwell, Victor R. Corsiglia, and Richard E. Kuhn*

Ames Research Center

SUMMARY

As part of a program to improve the methods for predicting the suckdown and hot gas ingestion for jet V/STOL aircraft in ground effect, a data base is being created that provides a systematic variation of parameters so that a new empirical prediction procedure can be developed. The first series of tests in this program has been completed. This report describes suckdown, fountain lift, and pressures induced on several two-jet V/STOL configurations. It is one of three reports that present the data obtained from tests conducted at Lockheed Aeronautical Systems–Rye Canyon Facility and in the High Bay area of the 40- by 80-Foot Wind Tunnel complex at NASA Ames Research Center.

INTRODUCTION

The propulsion-induced aerodynamics experienced by jet V/STOL aircraft hovering in close proximity to the ground is being studied at NASA Ames Research Center. For a multiple jet configuration in ground effect, a flow field is generated as shown in figure 1. The hot jets impinge on the ground and form a wall jet that entrains surrounding air. This entrainment induces a low-pressure area on the lower surface of the aircraft that causes a suckdown or lift loss. Meanwhile, a fountain upwash is generated in the area between the jets inducing a high-pressure area called fountain lift. The resultant of these two forces is the jet-induced lift, or ΔL. Hot gas ingestion is caused by the hot wall jet being drawn into the engine inlet. This temperature increase can cause inlet distortion, resulting in compressor stall and reduced thrust.

In the 1950's and 1960's, efforts were made to evaluate the effects of propulsion-induced aerodynamics on a diverse set of V/STOL aircraft configurations. Reference 1 describes the first of several efforts to predict the jet-induced lift, but there is no pressure distribution data in that report. Most of the reports available include only force-and-moment data on complete V/STOL configurations.

NASA Ames has been conducting a program to improve the methods for predicting the jet-induced lift and hot gas ingestion on jet V/STOL aircraft in ground effect. As part of this program, a data base is being created that provides a systematic variation of parameters so that a new or

---

*STO-VL Technology, San Diego, California.

modified empirical prediction procedure can be developed. The data will also be useful for the validation of computational fluid dynamics codes.

The first series of tests in this program has been completed. This report is one of three that present the data obtained from tests conducted at Lockheed Aeronautical Systems–Rye Canyon Facility. Reference 2 presents the single-jet data obtained in evaluating the adequacy of this facility. The hot-gas-ingestion data will be presented in a later report.

DESCRIPTION OF RYE CANYON TEST SETUP

Hover Test Rig

The hover test rig (fig. 2) consisted of a movable ground plane, model hardware, and an A-frame structure to support the model hardware. The aluminum ground plane was 8 by 8 ft and was moved vertically by a hydraulically operated scissors lift. The ground plane had a range of motion of 50 in. The A-frame was constructed of square 4-in. steel tubing. Flanges were welded to the attachment points and 1/2-in. bolts were used to clamp them together. The A-frame was 10 ft high and 7 ft wide at the base.

The nozzles were fed from two tandem rectangular plenums (fig. 3) which were supported by the A-frame. High-pressure air was fed to each plenum separately. The plenum pressures were controlled separately but were kept equal to each other. The plenums had a maximum weight flow of 2.5 lb/sec per plenum at a nozzle pressure ratio (NPR) of 6. The flat-plate models were mounted on a six-component strain gage balance (TASK Balance 1.5 MK IIC). The nozzles and plenum were nonmetric; that is, the strain gage balance measured only induced aerodynamic loads on the models.

The entire hover test rig was enclosed in a test cell that was 20 ft wide by 15 ft high by 28.5 ft deep (fig. 4). At one end of the room there was a rollup door that was 16 ft wide and 11 ft high.

Details of Nozzle and Plenum

The ASME nozzles were made of 321 stainless steel and were bolted to the rectangular plenums which were made of 304 stainless steel. As shown in figure 5, the nozzles had three porous plates to improve flow quality. Steel rods 3/8 in. in diameter were welded in place to increase the plenum wall stiffness.

A Kiel probe assembly (figs. 6 and 7), used to sense the total pressure and total temperature, was mounted in each nozzle 3.5 in. from the exit of the ASME nozzle and 2.0 in. (26 hole diameters) downstream of the last porous plate. The Kiel probe had a shield diameter of 0.095 in. At the location of the Kiel probe, the inner diameter of the duct leading to the nozzle was 1.935 in. The nozzle exit diameter was 1.23 in. A gap of 0.050 in. was maintained between the model and the nozzle (fig. 6). A fouling circuit warned of fouling between the nozzle and the model.

Model Hardware

Three model configurations were tested: wing/body, body alone, and delta wing (figs. 8–11). The models were constructed of 1/4-in.-thick aluminum. Each was 34 in. long and had a wing span of 20 in. The jet spacing for all three configurations was the same at 14.7 in. The strain-gage-balance attachment point was at a model station 18 in. from the nose, which was 1 in. aft of the moment reference. The top edges were chamfered as shown in figure 6.

The flat plate wing/body (fig. 9) had a leading-edge sweep angle of 49° and a trailing-edge sweep angle of –8°. It had an aspect ratio of 2.28 and a planform-area-to-jet-area ratio (S_{plan}/S_{jet}) of 105. The equivalent model diameter ($\overline{D}$) was 16.9 in.

The flat plate body (fig. 10) had an S_{plan}/S_{jet} of 50.2 and an equivalent model diameter of 9.95 in.

The flat plate delta wing (fig. 11) had a leading-edge sweep angle of 71° and a trailing-edge sweep angle of –8°. It had an aspect ratio of 1.08, an S_{plan}/S_{jet} of 156, and an equivalent model diameter of 20.1 in. The wing/body and the delta wing are shown installed at the Rye Canyon facility test cell in figures 12 and 13, respectively.

The bottom pressure tap locations for the wing/body and the delta wing are shown in figures 14 and 15, respectively. The wing/body has 67 pressure taps and the delta wing has 78. The pressure taps are distributed in 2-in. increments in the chordwise and spanwise directions except in the area between the jets (fountain area), where they are distributed in 1-in. increments along the longitudinal axis.

For some tests, lift improvement devices (LIDs) were installed on the wing/body configuration (fig. 16). These were constructed of 1 1/2-in.-wide, 1/16-in.-thick steel bent 90° and attached to the bottom of the model so that they protruded down 3/4 in. They were placed at several different stations to evaluate their effectiveness in reducing suckdown.

Instrumentation and Data Acquisition System

The instrumentation system consisted of an HP 9000/200 computer, an HP 6942 multiprogrammer, a hot box, and various sensors. Figure 17 is a schematic of the setup. Figure 18 shows the computer system. A six-component TASK 1.5 MK IIC strain gage balance was used to measure the jet-induced lift on the models. Only three forces were recorded. The axial force component (100 lb maximum) was used to measure the lift loss. The side force components were used to determine the pitching moment. No gage interactions were used in the equations.

The instrumentation also consisted of two nozzle-pressure transducers (100 psig), used to monitor NPR and to calculate thrust, and three 48-port scanivalve modules with 1-psig pressure transducers. Ambient pressure was monitored by a 25-psig transducer.

Three thermocouples were used; one monitored the ambient temperature (Copper-Constantan), and the other two monitored the nozzle air temperature (Chromel-Alumel). All thermocouples were fed into a 150 °F reference junction box.

A group of signal conditioners supplied an excitation voltage to the strain gage balance and all the pressure transducers. Each of these instruments had its own signal conditioner. The output of each instrument was fed back to the signal conditioner and could be monitored in real time on a digital panel meter. The cables that connected the signal conditioners to the strain gage balance and transducers were 50 ft long, as were the wires from the thermocouples to the reference junction.

All instrumentation was then sent to a set of amplifiers (gain = 128). The amplified signals were input to a scanner card in an HP 6942A multiprogrammer. During the data acquisition sequence (fig. 19), the raw voltages were stored in a 64K-word memory buffer in the multiprogrammer. After the acquisition sequence was completed, the voltages were downloaded into the HP 9000/200 computer system, where they were averaged. The raw data were then converted to engineering units, stored on a Bering 20-mB Bernoulli cartridge, and output to an HP 2671G thermal printer.

Nozzle Surveys

The nozzles were surveyed to determine the rate of jet decay along the jet axis and the total pressure profile.

PRESENTATION OF DATA

The data are presented in four sections in the appendix, without analysis. (Data from the nozzle surveys are presented in ref. 2.)

REFERENCES

1. Wyatt, L. A.: Static Test of Ground Effect on Planforms Fitted With a Centrally-Located Round Lifting Jet. Ministry of Aviation, CP-749, June 1962.

2. Bellavia, D. C.; Wardwell, D. A.; Corsiglia, V. R.; and Kuhn, R. E.: Forces and Pressures Induced Circular Plates by a Single Lifting Jet in Ground Effect. NASA TM-102816, 1991.

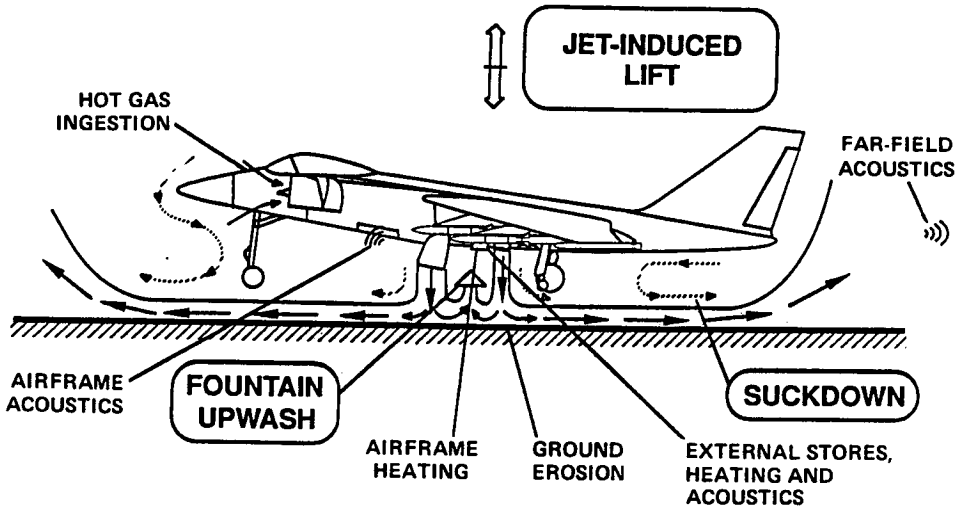

Figure 1. Research topics associated with the flow field of a STOVL aircraft hovering in ground effect.

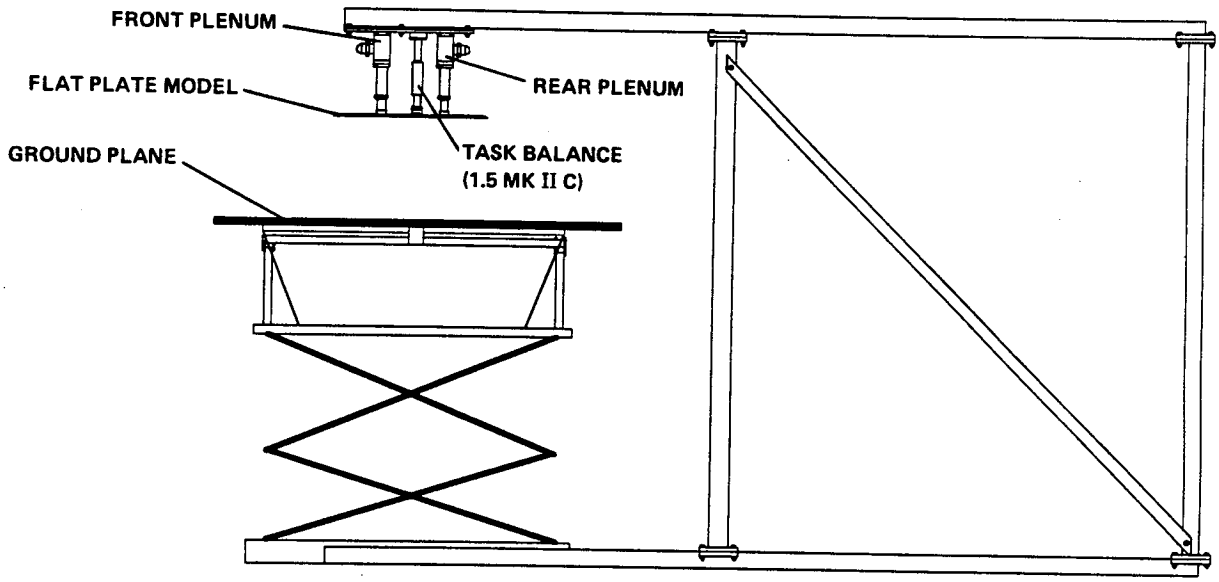

Figure 2. Hover test rig, test cell; located at Lockheed Aeronautical Systems–Rye Canyon Facility.

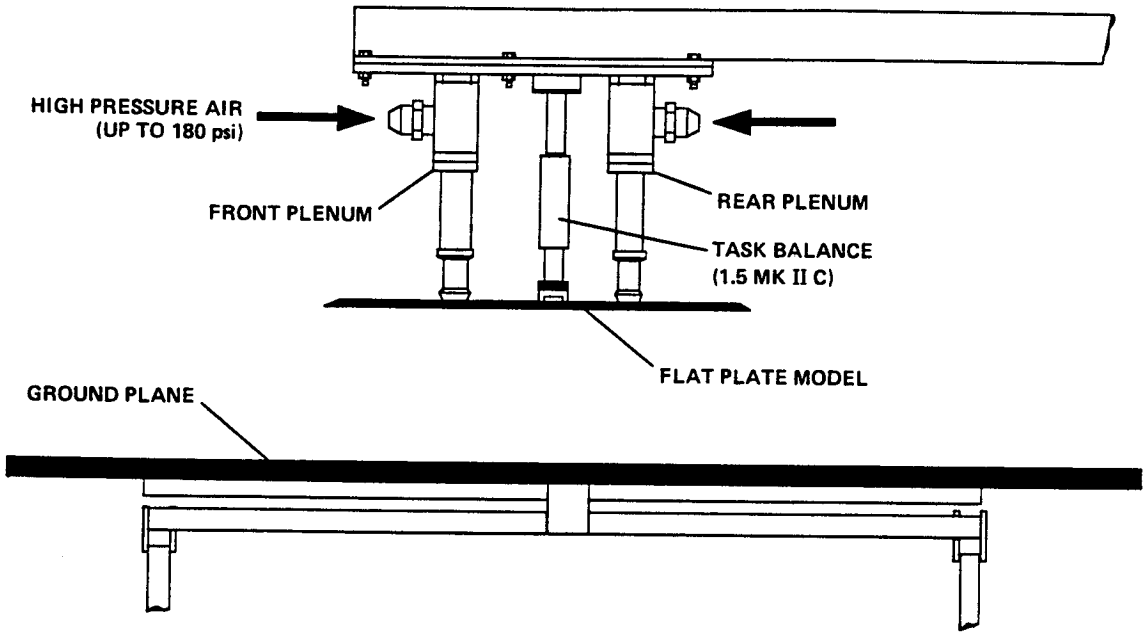

Figure 3. Hover test rig details (test cell).

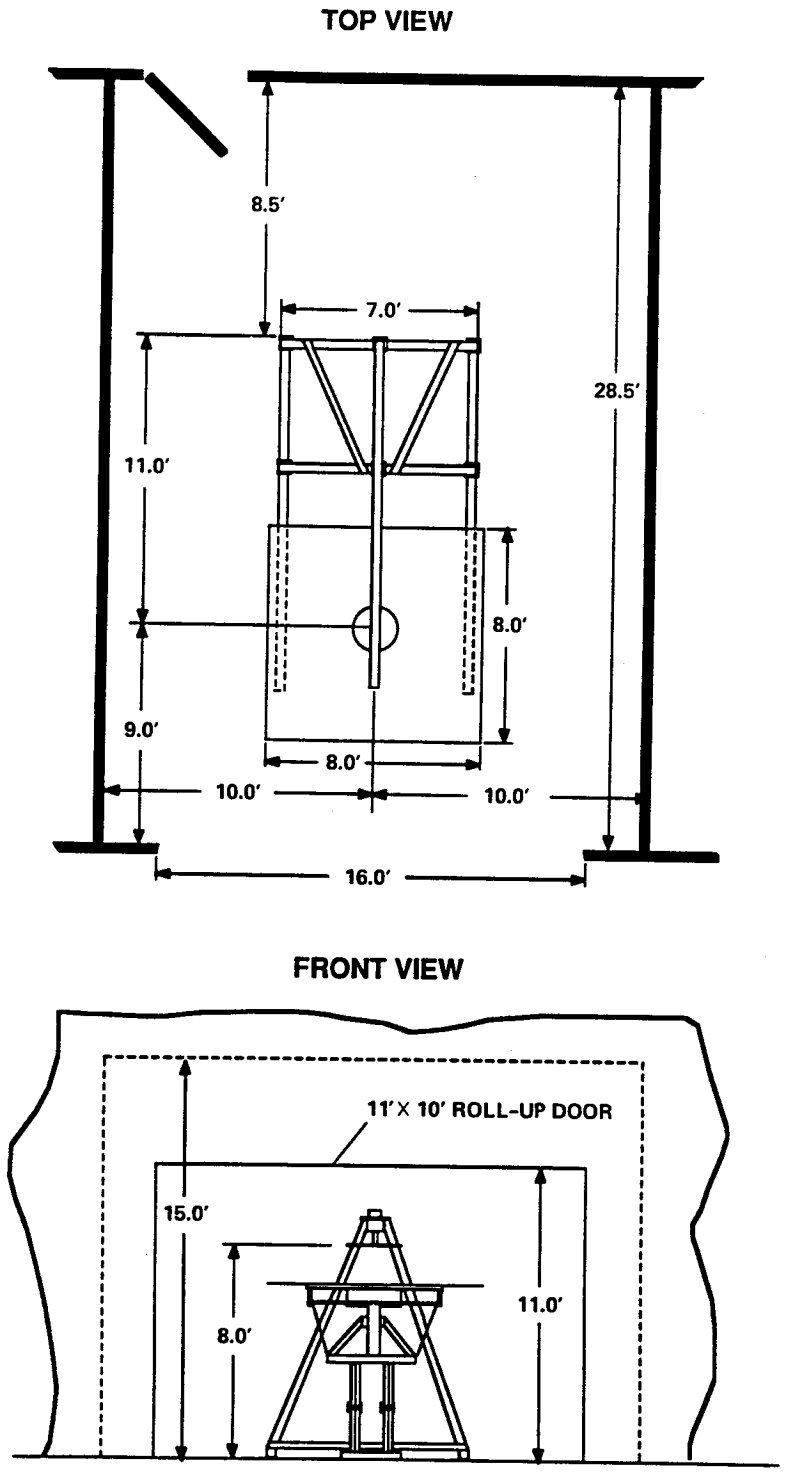

Figure 4. Location of test setup (test cell) relative to walls and ceiling.

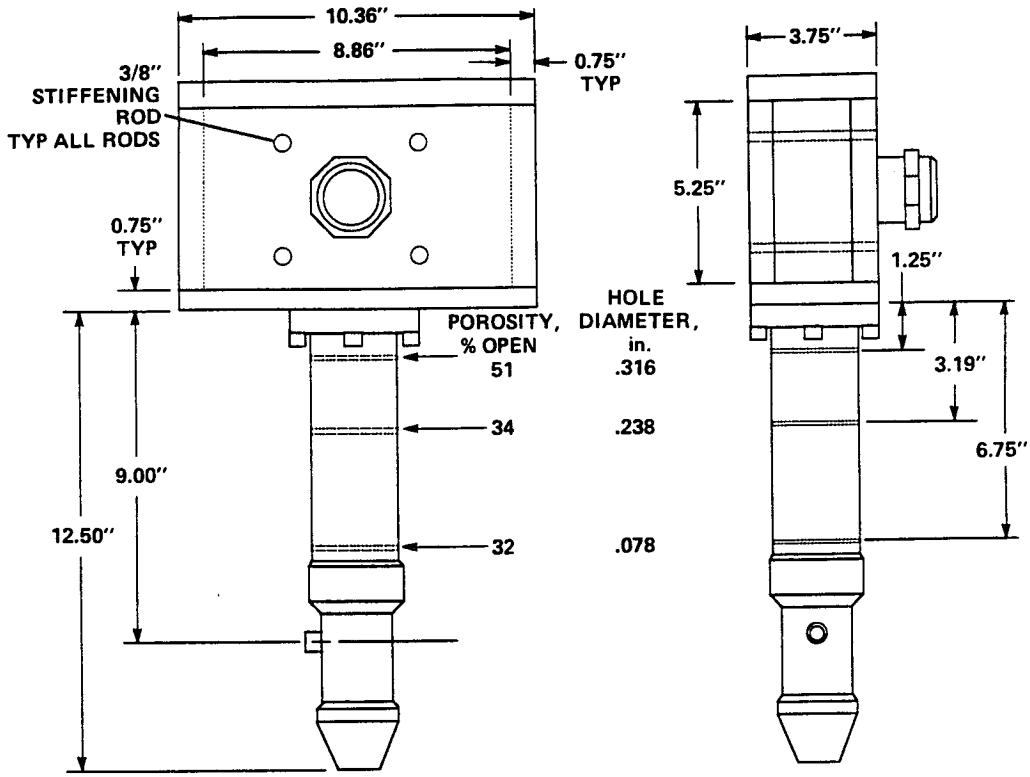

Figure 5. Details of nozzle and plenum assembly.

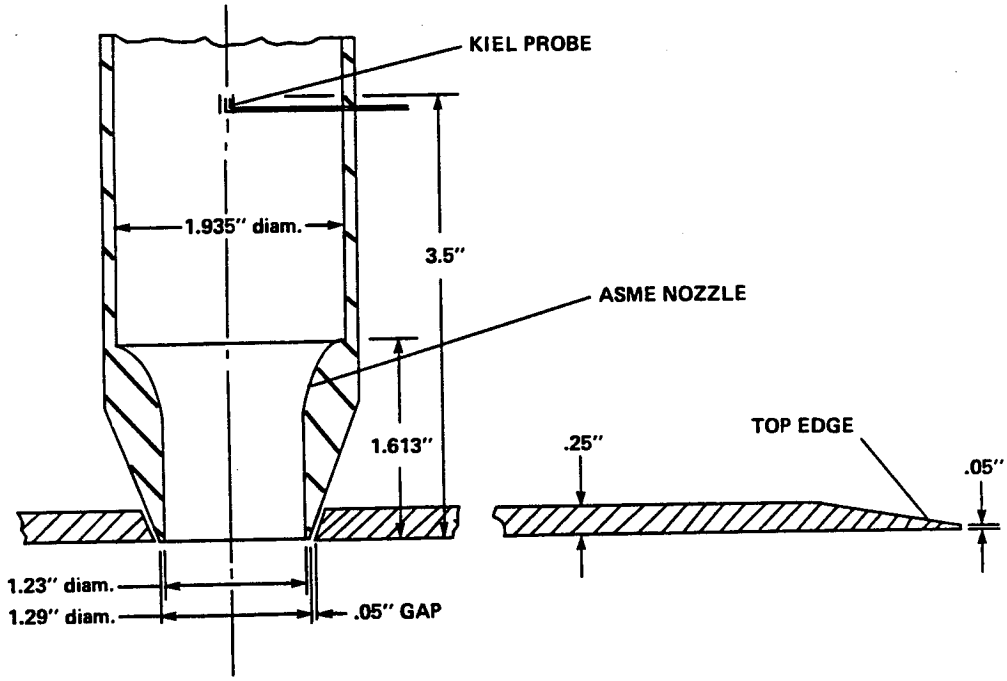

Figure 6. Detail of nozzle exit and flat plate model.

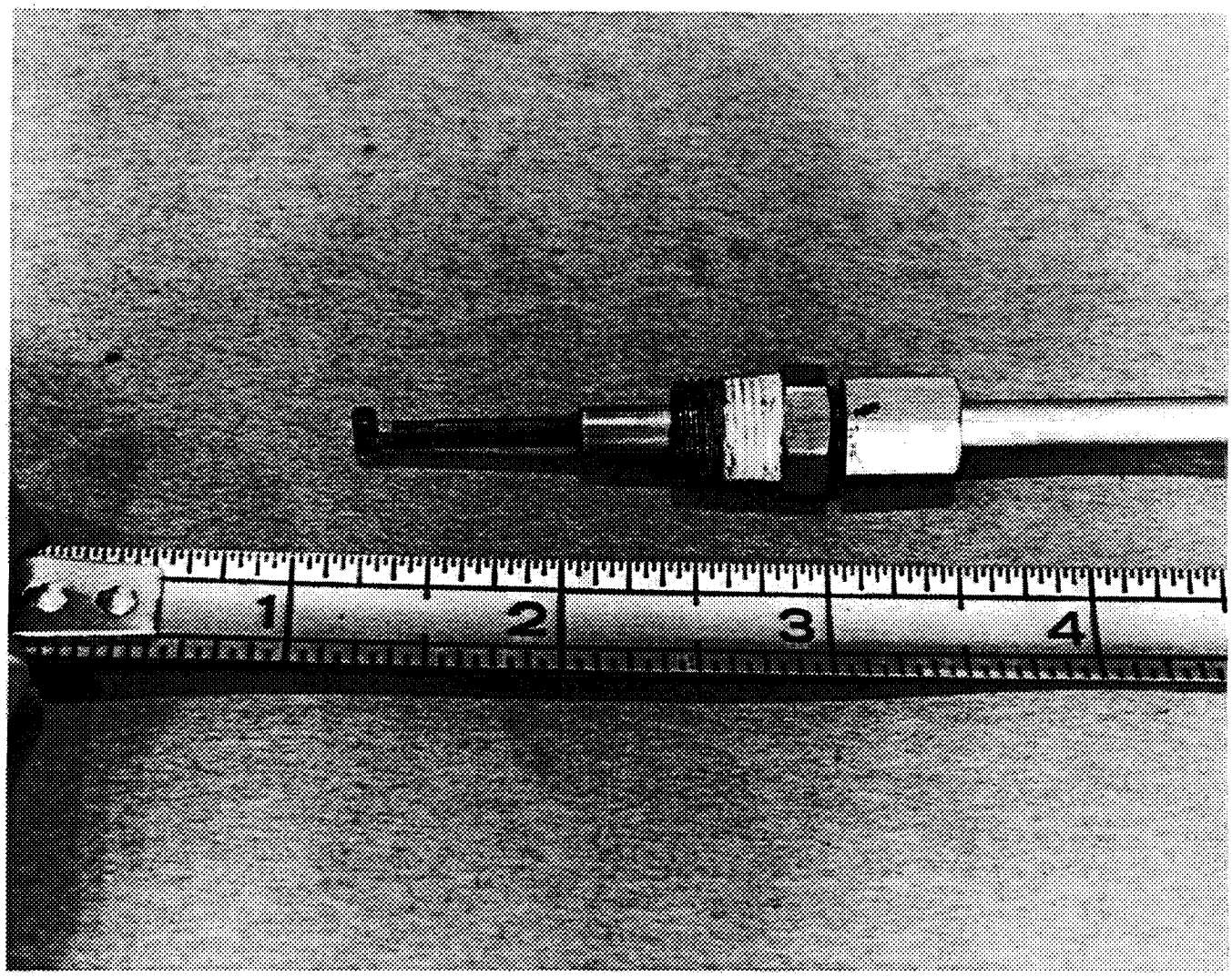

Figure 7. Kiel probe used in nozzle.

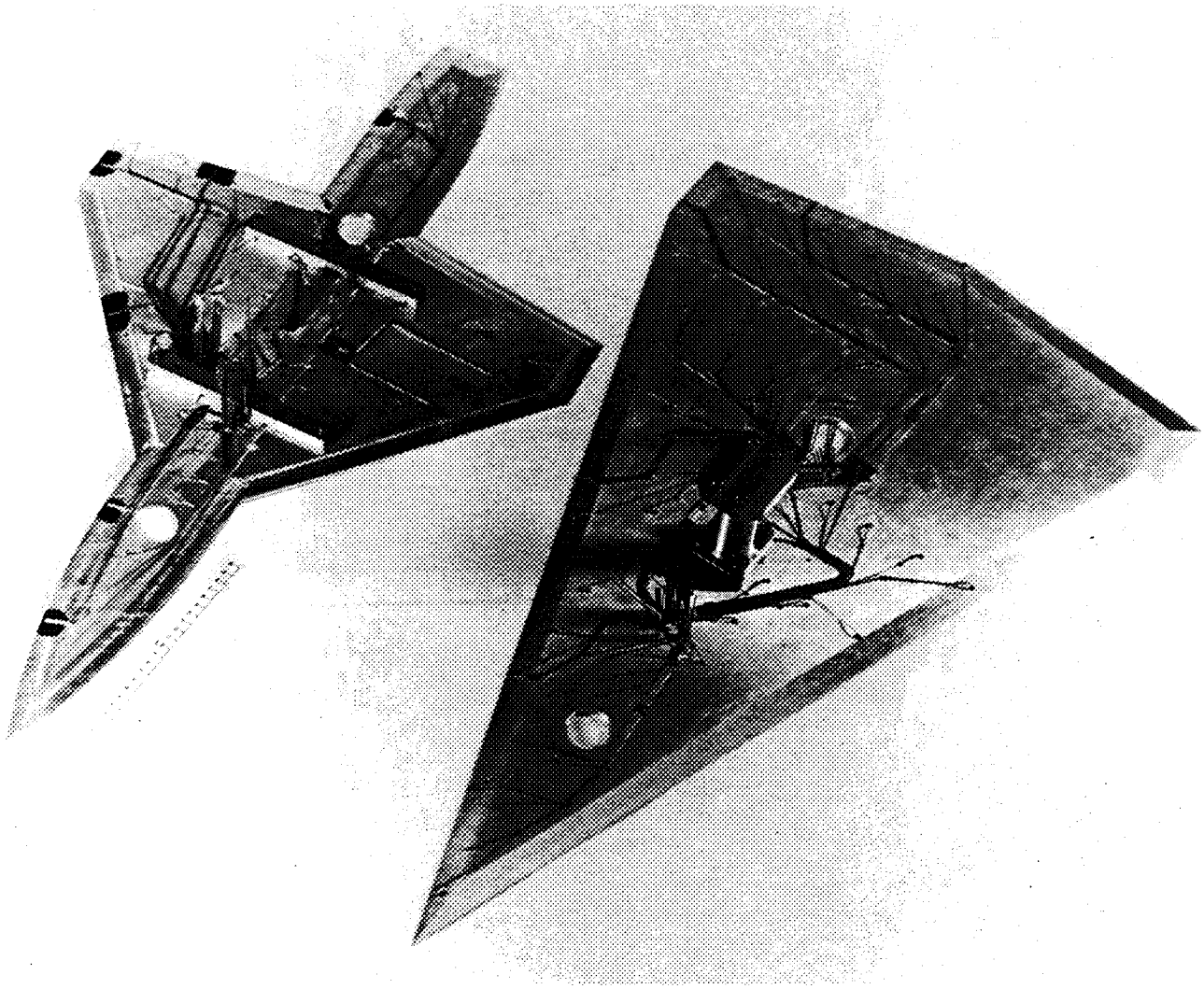

Figure 8. Wing/body model and delta-wing model.

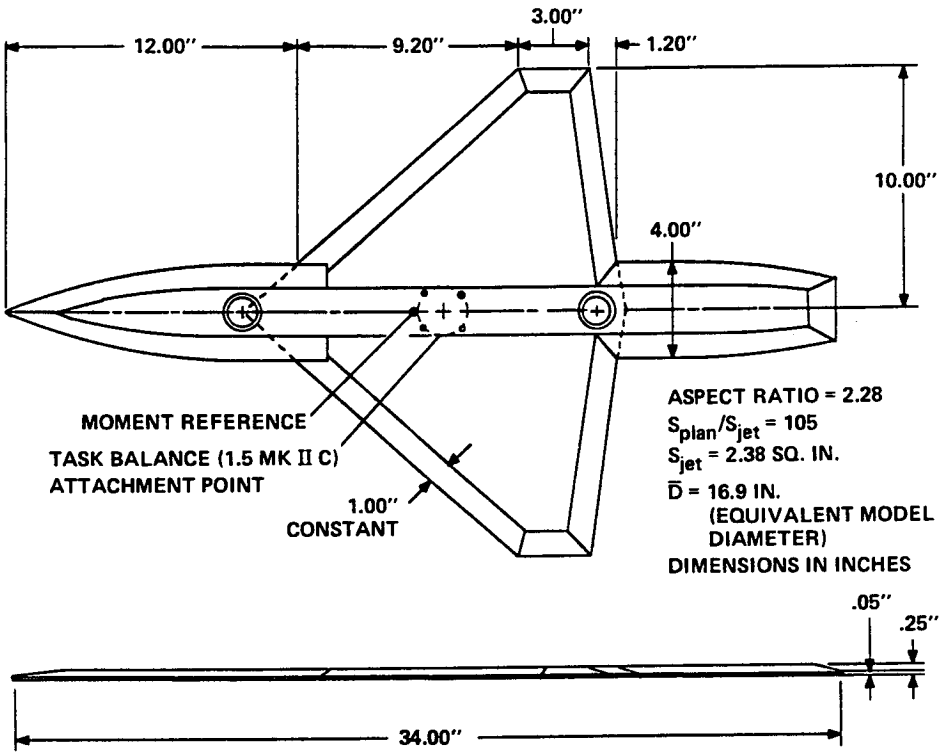

Figure 9. Dimensions of wing/body model.

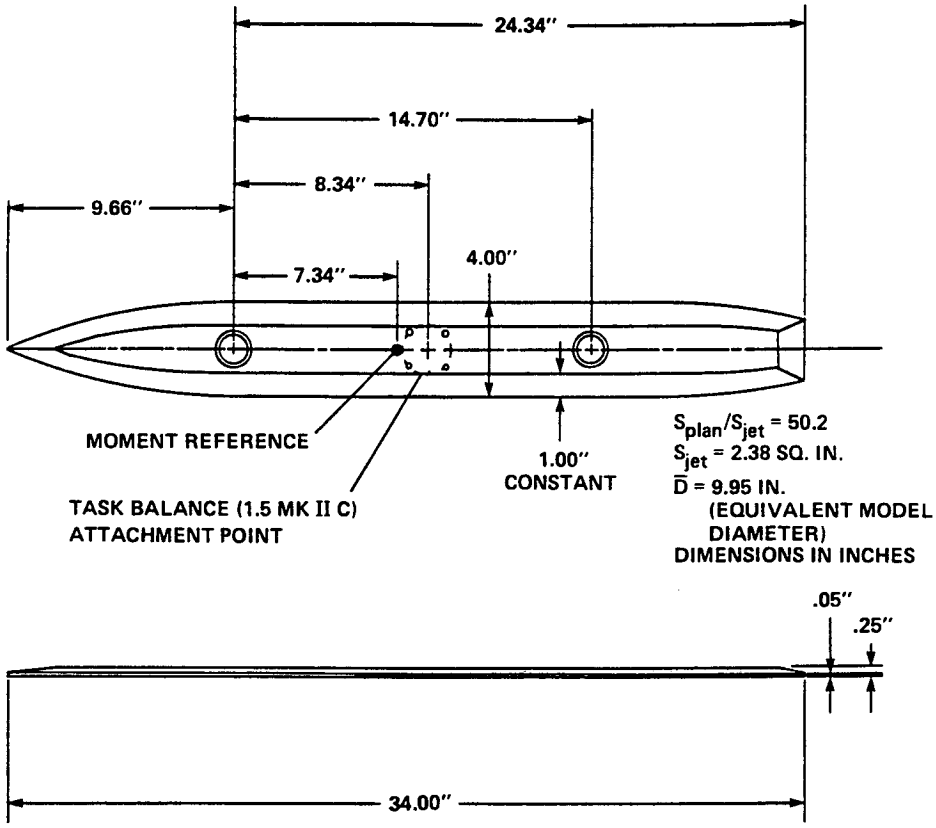

Figure 10. Dimensions of body.

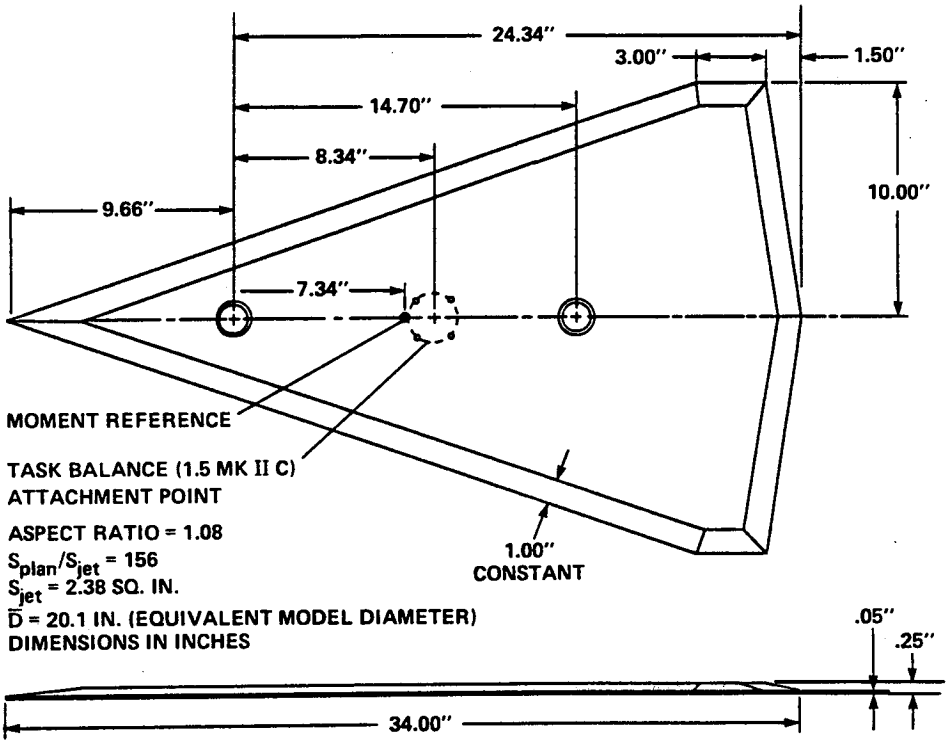

Figure 11. Dimensions of delta-wing model.

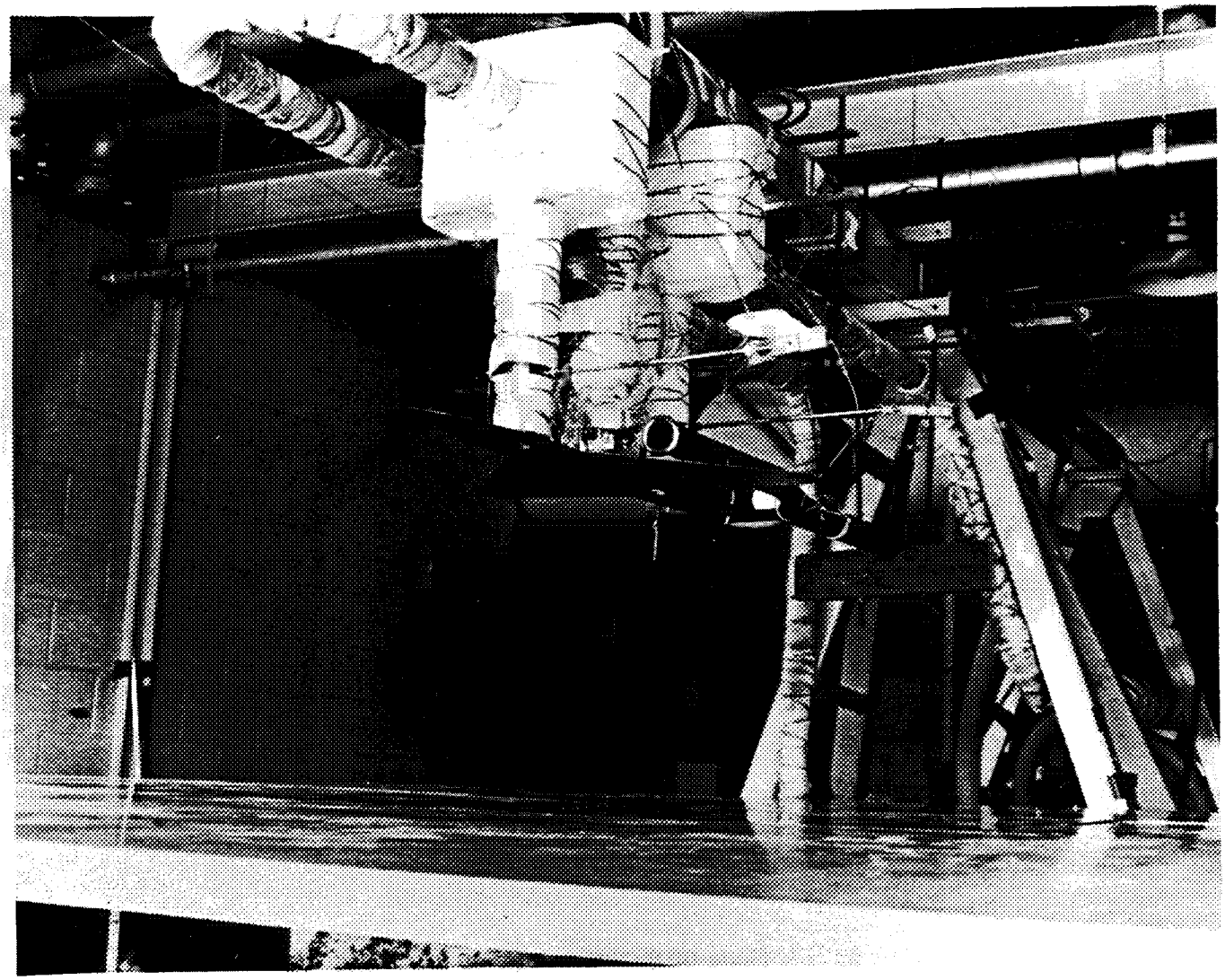

Figure 12. Wing/body model installed in the test cell.

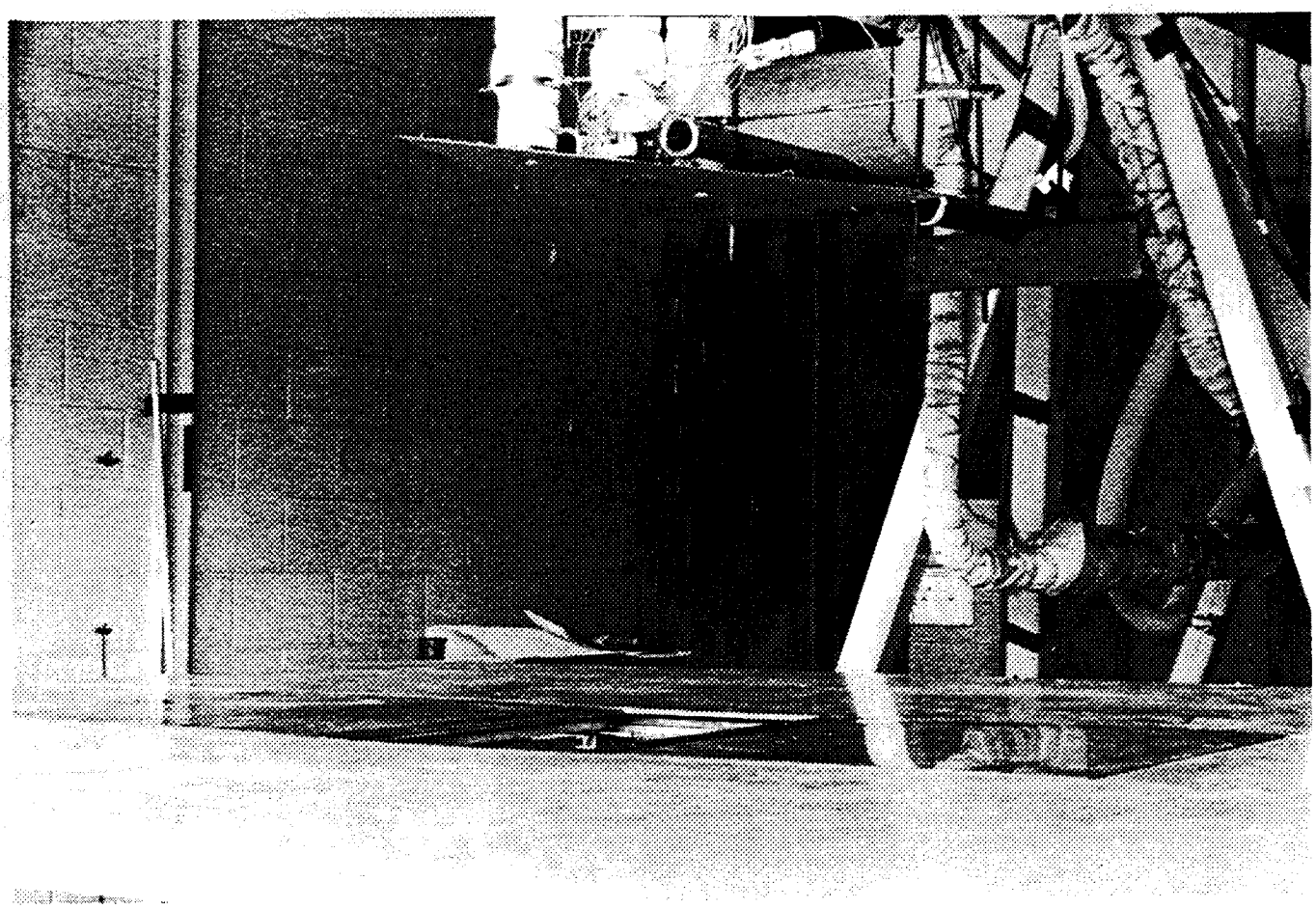

Figure 13. Delta-wing model installed in the test cell.

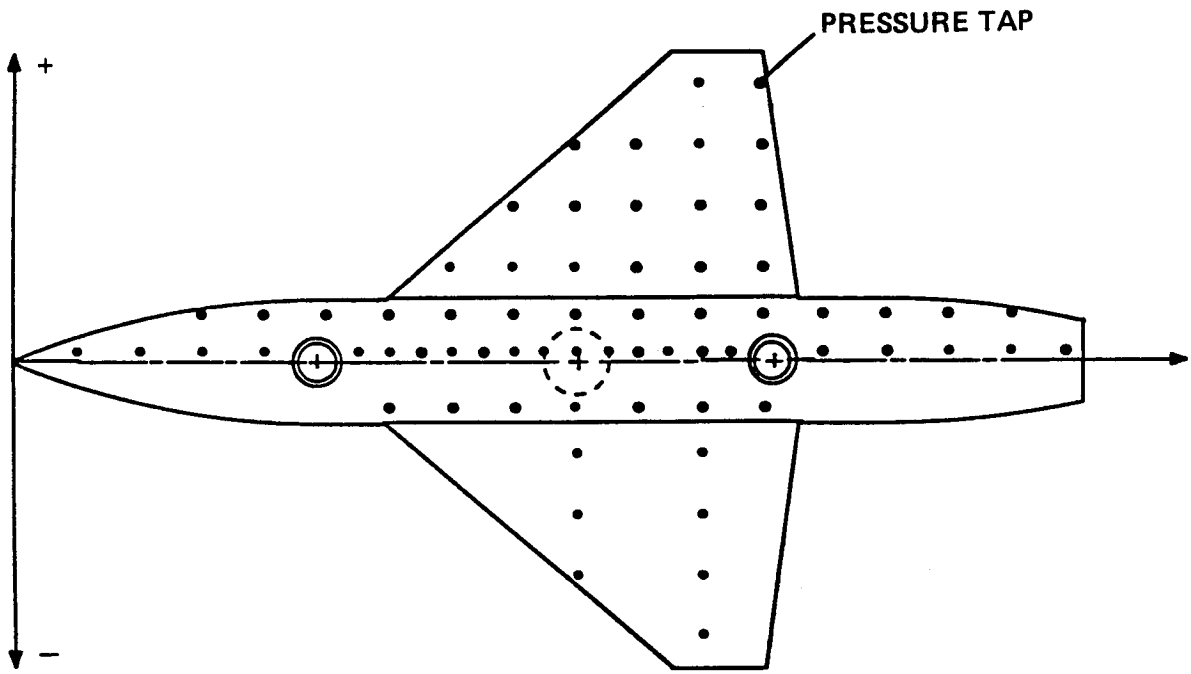

STATION	BUTT LINE (INCHES)										
(INCHES)	0.25	1.5	3	5	7	9	-1.5	-3	-5	-7	-9
2	X										
4	X										
6	X	X									
8	X	X									
10		X									
11	X										
12	X	X					X				
13	X										
14	X	X	X				X				
15	X										
16	X	X	X	X			X				
17	X										
18	X	X	X	X	X		X	X	X	X	
19	X										
20	X	X	X	X	X		X				
21	X										
22	X	X	X	X	X	X	X	X	X	X	X
23	X										
24		X	X	X	X	X	X				
26	X	X									
28	X	X									
30	X	X									
32	X	X									
33.75	X										

Figure 14. Location of pressure taps on the wing/body model.

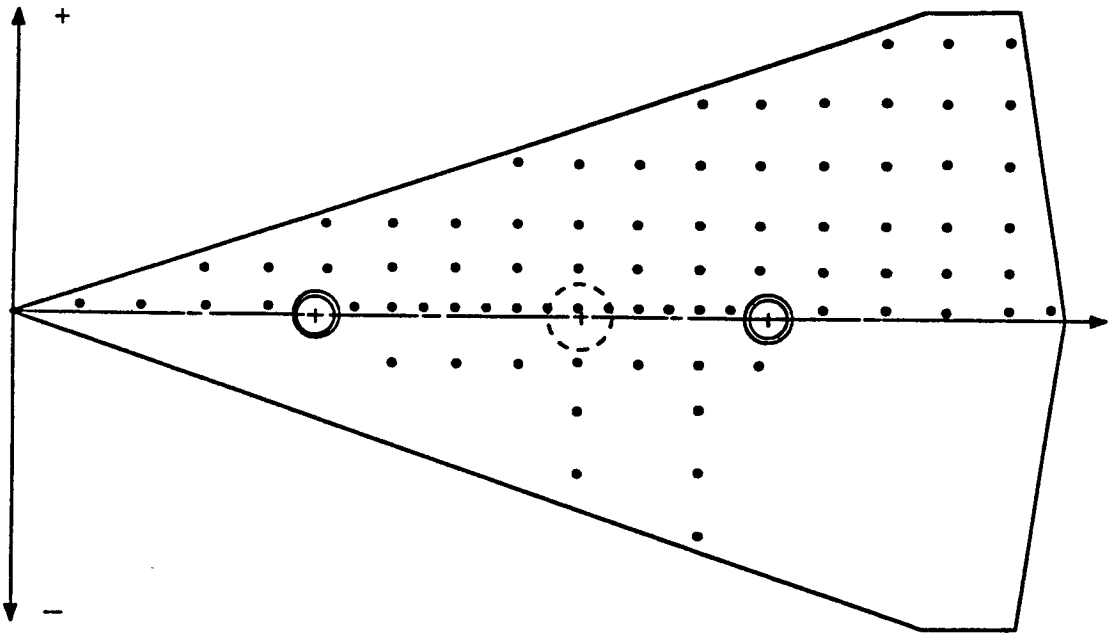

STATION (INCHES)	BUTT LINE (INCHES)									
	0.25	1.5	3	5	7	9	-1.5	-3	-5	-7
2	X									
4	X									
6	X	X								
8	X	X								
10		X	X							
11	X									
12	X	X	X				X			
13	X									
14	X	X	X				X			
15	X									
16	X	X	X	X			X			
17	X									
18	X	X	X	X			X	X	X	
19	X									
20	X	X	X	X			X			
21	X									
22	X	X	X	X	X		X	X	X	X
23	X									
24		X	X	X	X		X			
26	X	X	X	X	X					
28	X	X	X	X	X	X				
30	X	X	X	X	X	X				
32	X	X	X	X	X	X				
33.75	X									

Figure 15. Location of pressure taps on the delta wing model.

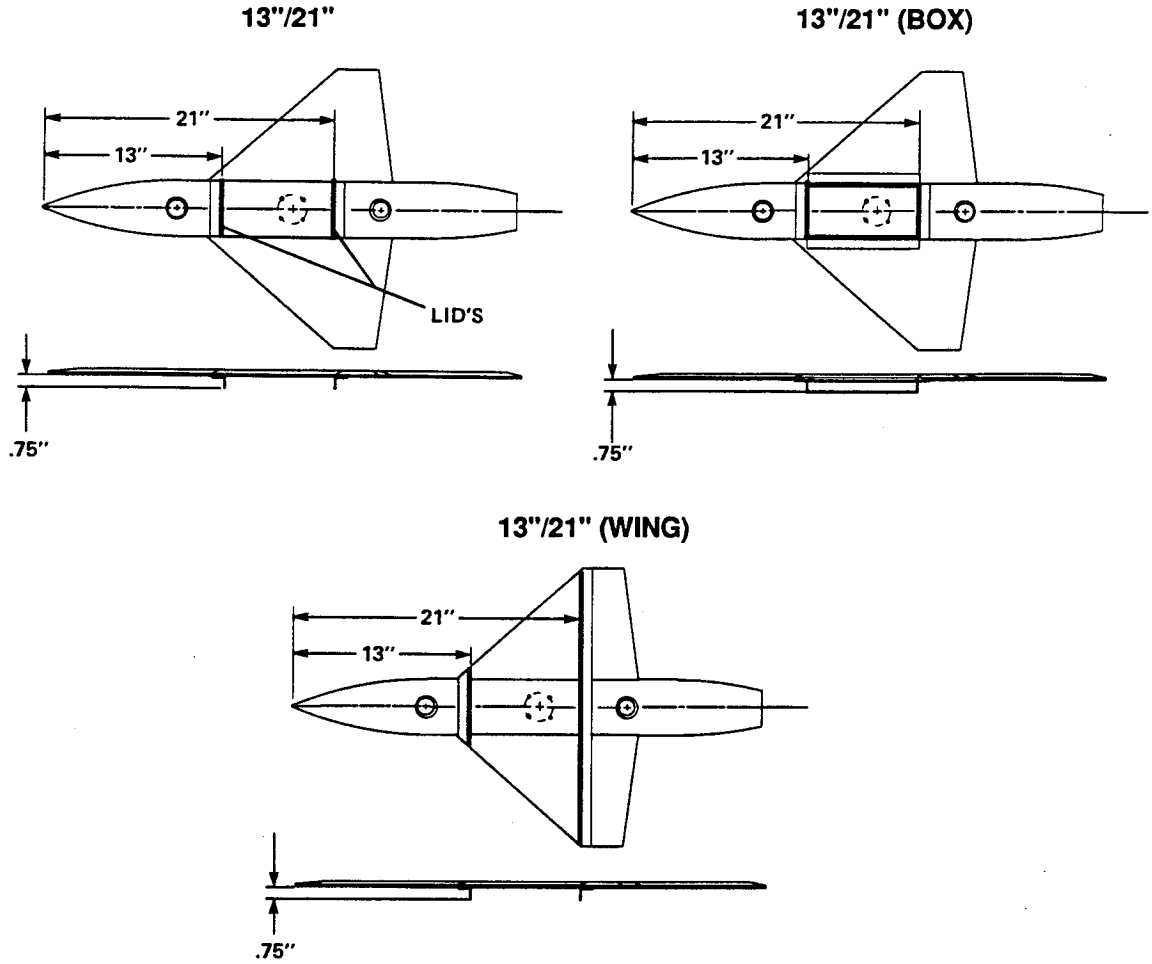

Figure 16. Typical LID configurations.

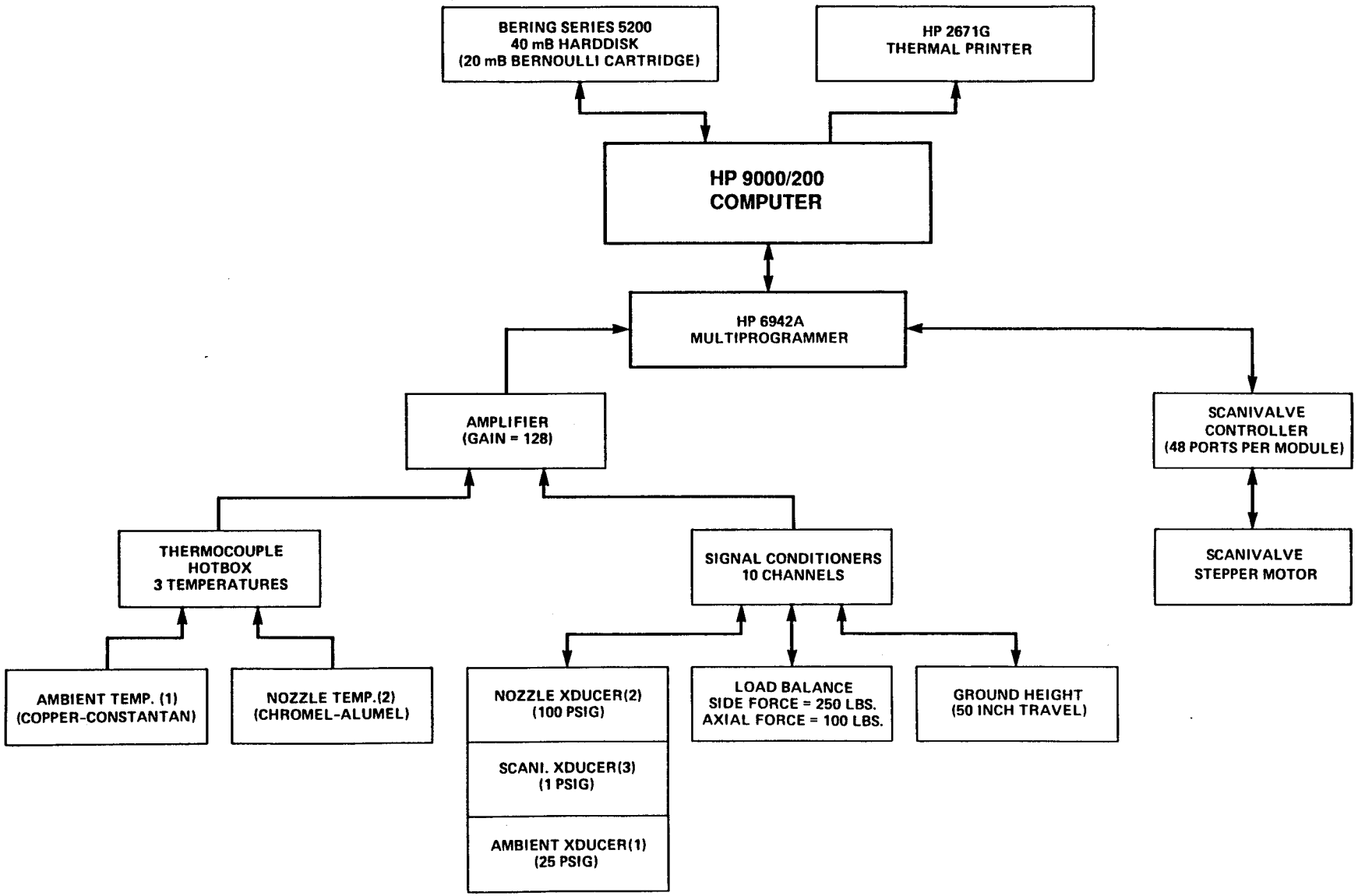

Figure 17. Instrumentation and data acquisition system.

Figure 18. Data acquisition system setup.

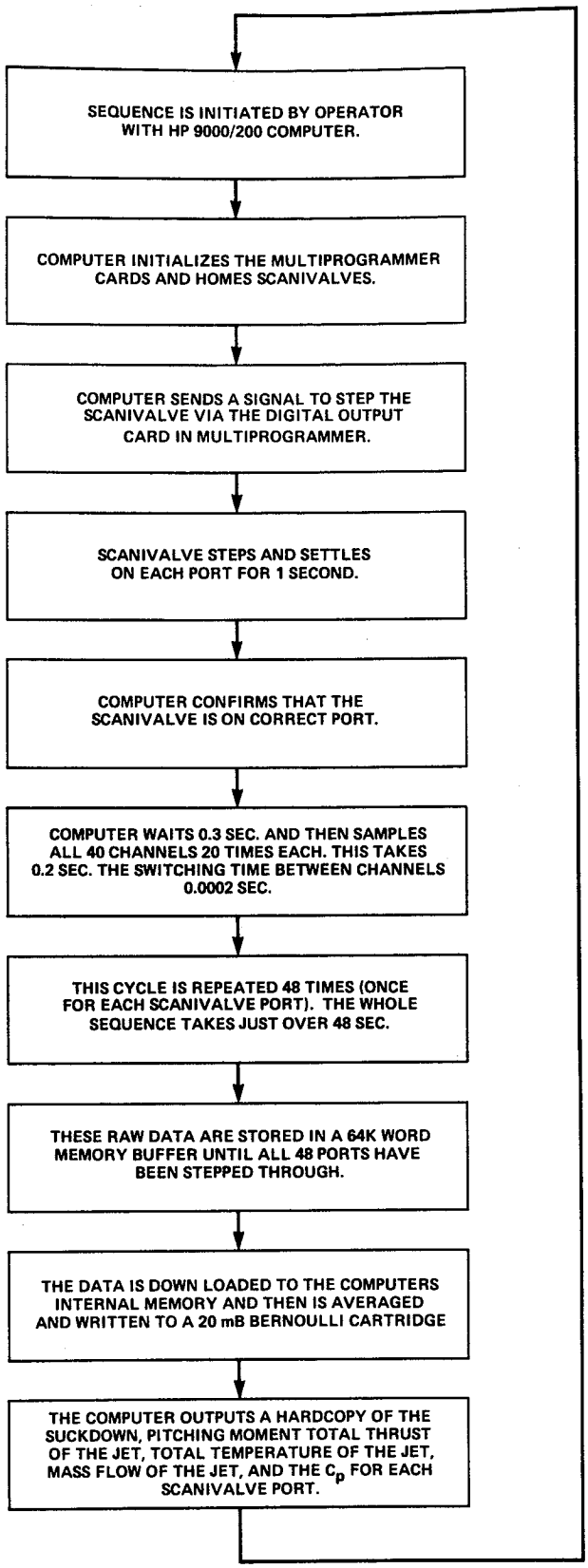

Figure 19. Data acquisition sequence.

APPENDIX

PRESENTATION OF DATA

Most of the data are displayed graphically in section I, as pressure coefficient as a function of station location on the configuration (figs. 20–45). These data are broken into eight groups which represent different planform configurations.

Section II presents lift loss ($\Delta L/T$) as a function of nozzle pressure ratio (P_{jet}/P_{amb}) (figs. 46–53).

Section III presents pitching moment as a function of nozzle pressure ratio (figs. 54–61).

Section IV presents the center of lift as a function of height for various nozzle pressure ratios (figs. 62–69).

Section I

C_p vs. Station

	h/d_e	NPR	Figure number
Group 1 Delta wing, both jets, no LIDs			
	2.3, 3.5, 4.6, 5.8 8.6, 11.5, 14.4, 23.0	2	20a,20b,20c,20d 20e,20f,20g,20h
	2.3, 3.5, 4.6, 5.8, 8.6, 11.5, 14.4, 23.0	3	21a,21b,21c,21d 21e,21f,21g,21h
	2.3, 3.5, 4.6, 5.8, 8.6 11.5, 14.4, 23.0	4	22a,22b,22c,22d,22e 22f,22g,22h
	2.3, 3.5, 4.6, 5.8, 8.6 11.5, 14.4, 23.0	5	23a,23b,23c,23d 23e,23f, 23g,23h
	11.5, 14.4, 17.2 23.0, 23.0, 23.0	6	24a,24b,24c 24d,24e,24f

	h/d_e	NPR	Figure number
Group 2 Delta wing, front jet, no LIDs			
	3.3, 4.9, 6.5, 8.1 12.2, 16.3, 20.3, 32.5	2	25a,25b,25c,25d 25e,25f,25g,25h
	3.3, 4.9, 6.5, 8.1 12.2, 16.3, 32.5	4	26a,26b,26c,26d 26e,26f,26g
	3.3, 4.9, 6.5, 8.1 12.2, 16.3, 20.3, 32.5	6	27a,27b,27c,27d 27e,27f,27g,27h
Group 3 Delta wing, rear jet, no LIDs			
	3.3, 4.9, 6.5, 8.1 12.2, 16.3, 20.3, 32.5	2	28a,28b,28c,28d 28e,28f,28g,28h
	3.3, 4.9, 6.5, 8.1 12.2, 16.3, 20.3, 32.5	4	29a,29b,29c,29d 29e,29f,29g,29h
	4.9, 6.5, 8.1, 12.2 16.3, 20.3, 32.5	6	30a,30b,30c,30d 30e,30f,30g
Group 4 Delta wing, no LIDs			
Both jets	OGE	2,3,4,5,6	31a,31b,31c,31d,31e
Front jet	OGE	2,3,4,5,6	32a,32b,32c,32d,32e
Rear jet	OGE	2,3,4,5,6	33a,33b,33c,33d,33e
Group 5 Body alone, both jets, no LIDs			
	2.3, 3.5, 4.6, 4.6, 5.8 8.6, 11.5, 14.4, 23.0	2	34a,34b,34c,34d,34e 34f,34g,34h,34i
	2.3, 3.5, 4.6, 5.8 8.6, 11.5, 14.4, 23.0	4	35a,35b,35c,35d 35e,35f,35g,35h
	2.3, 3.5, 4.6, 5.8 8.6, 11.5, 14.4, 23.0	6	36a,36b,36c,36d 36e,36f,36g,36h

	h/d_e	NPR	Figure number
Group 6 Body alone, both jets			
LIDs = 15"/19"	2.3, 3.5, 4.6, 5.8 8.6, 11.5, 14.4, 23.0	2	37a,37b,37c,37d 37e,37f,37g,37h
LIDs = 13"/21"	2.3, 3.5, 4.6, 5.8 8.6, 11.5, 14.4, 23.0	2	38a,38b,38c,38d 38e,38f,38g,38h
LIDs = 11"/23"	2.3, 3.5, 4.6, 5.8 8.6, 11.5, 14.4, 23.0	2	39a,39b,39c,39d 39e,39f,39g,39h
LIDs = 13"/21" (BOX)	2.3, 3.5, 4.6, 5.8 8.6, 11.5, 14.4, 23.0	2	40a,40b,40c,40d 40e,40f,40g,40h
Group 7 Wing/body, both jets, no LIDs			
	2.3, 3.5, 4.6, 5.8, 8.6 8.6, 11.5, 14.4, 23.0, 23.0	2	41a,41b,41c,41d,41e 41f,41g,41h,41i,41j
	2.3, 3.5, 4.6, 5.8 8.6, 11.5, 14.4, 23.0	4	42a,42b,42c,42d 42e,42f,42g,42h
	2.3, 3.5, 4.6, 5.8 8.6, 11.5, 14.4, 23.0	6	43a,43b,43c,43d 43e,43f,43g,43h
Group 8 Wing/body, both jets			
LIDs = 12"/21" (wing)	2.3, 3.5, 4.6, 5.8 8.6, 11.5, 14.4, 23.0	2	44a,44b,44c,44d 44e,44f,44g,44h
LIDs = 13"/21" (BOX)	2.3, 3.5, 4.6, 5.8 8.6, 11.5, 14.4, 23.0	2	45a,45b,45c,45d 45e,45f,45g,45h

Section II

ΔL/Thrust

Configuration	NPR	Figure number
Delta wing (both jets)	2, 3, 4, 5, 6	46
Delta wing (front jet)	2, 4, 6	47
Delta wing (rear jet)	2, 4, 6	48
Delta wing (OGE)	2, 3, 4, 5, 6	49
Body (both jets)	2, 4, 6	50
Body (both jets) LIDs	2	51
Wing/body (both jets)	2, 4, 6	52
Wing/body (both jets) LIDs	2	53

Section III

Pitching Moment Coefficient

Configuration	NPR	Figure number
Delta wing (both jets)	2, 3, 4, 5, 6	54
Delta wing (front jet)	2, 4, 6	55
Delta wing (rear jet)	2, 4, 6	56
Delta wing (OGE)	2, 3, 4, 5, 6	57
Body (both jets)	2, 4, 6	58
Body (both jets) LIDs	2	59
Wing/body (both jets)	2, 4, 6	60
Wing/body (both jets) LIDs	2	61

Section IV

x/d_e

Configuration	NPR	Figure number
Delta wing (both jets)	2, 3, 4, 5, 6	62
Delta wing (front jet)	2, 4, 6	63
Delta wing (rear jet)	2, 4, 6	64
Delta wing (OGE)	2, 3, 4, 5, 6	65
Body (both jets)	2, 4, 6	66
Body (both jets) LIDs	2	67
Wing/body (both jets)	2, 4, 6	68
Wing/body (both jets) LIDs	2	69

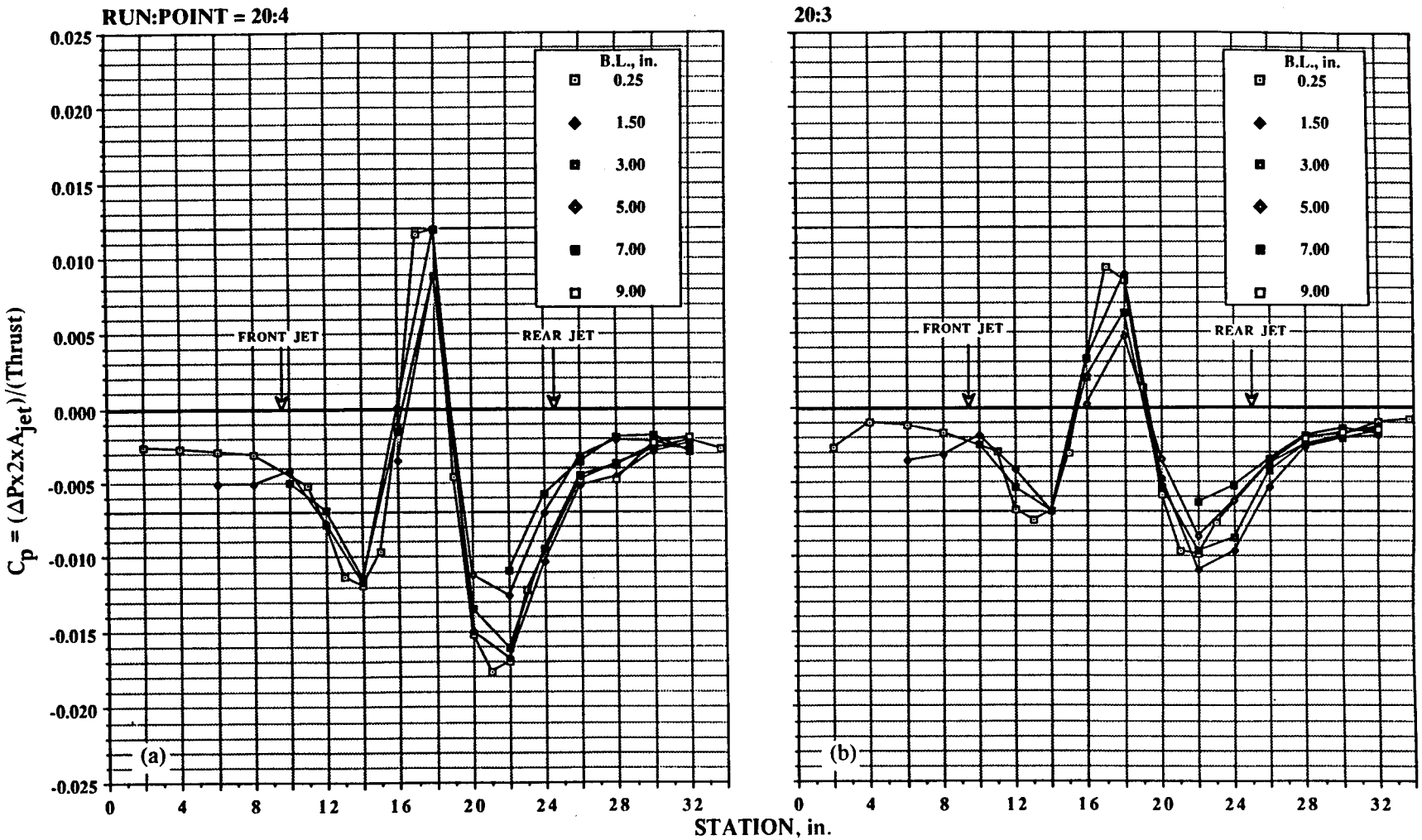

Figure 20. Pressures induced on delta-wing configuration in ground effect; NPR = 2.0, T = 51 lb, both jets, no LIDs. (a) $h/d_e = 2.30$. (b) $h/d_e = 3.45$.

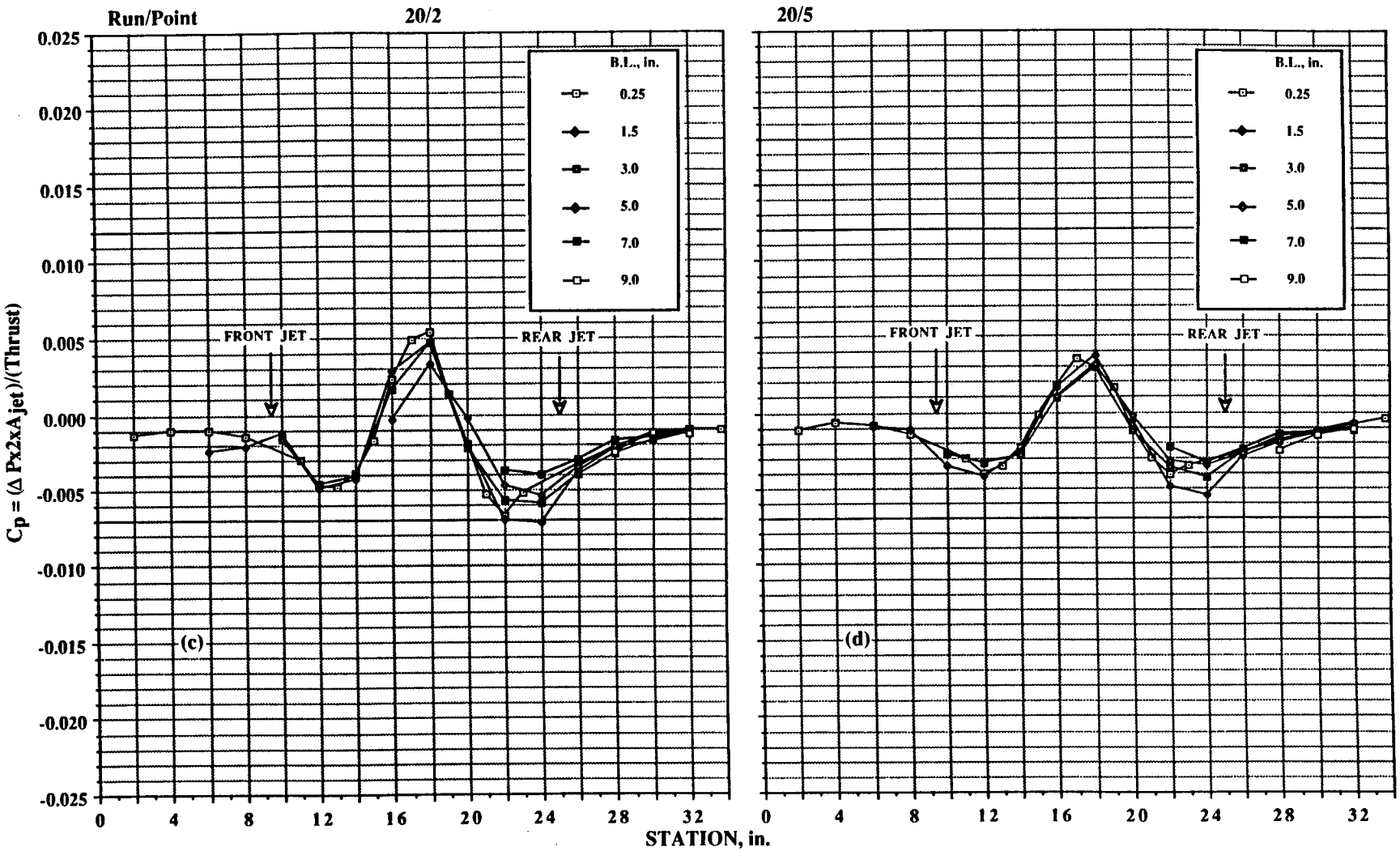

Figure 20. Continued. (c) $h/d_e = 4.6$. (d) $h/d_e = 5.75$.

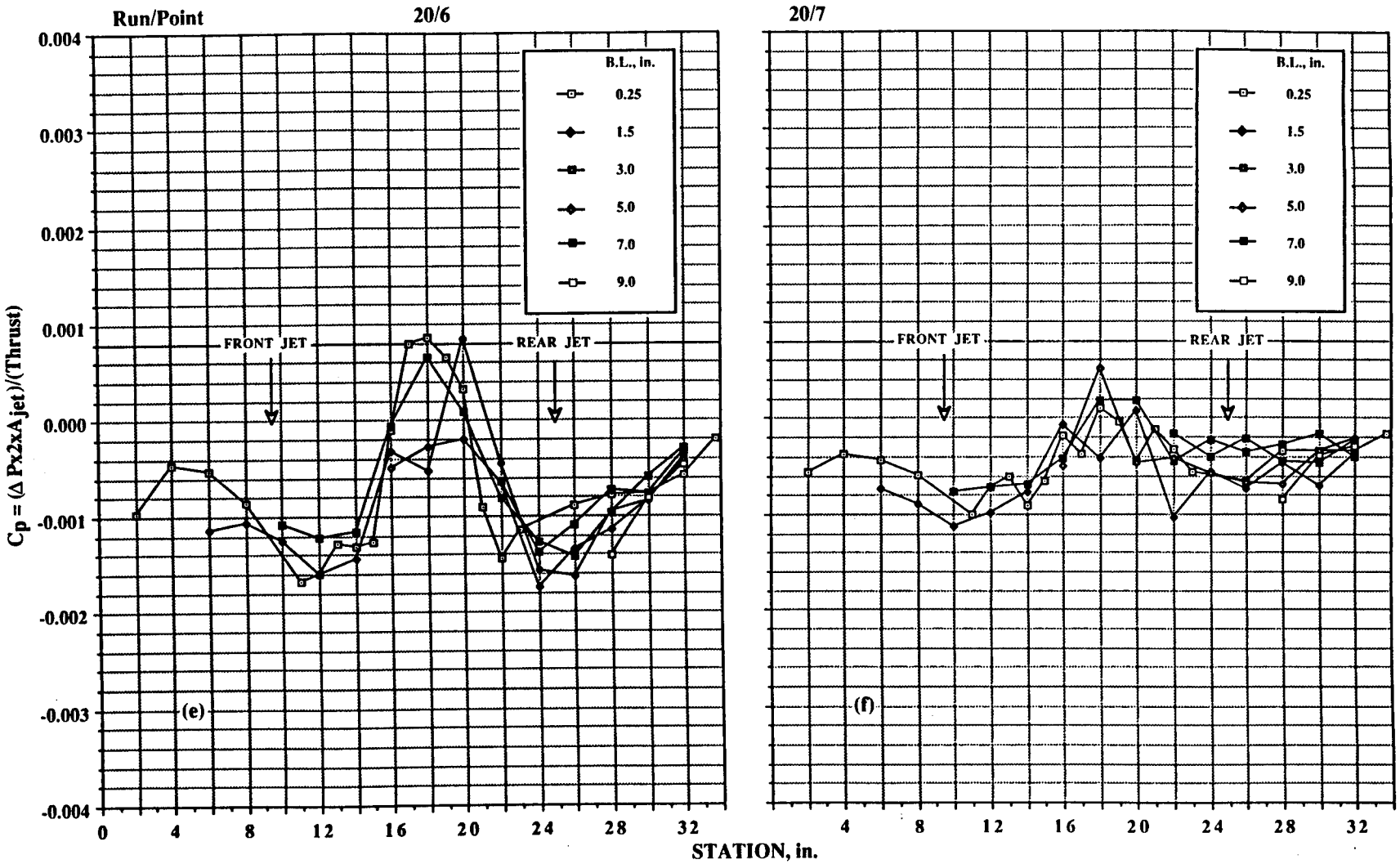

Figure 20. Continued. (e) $h/d_e = 8.62$. (f) $h/d_e = 11.5$.

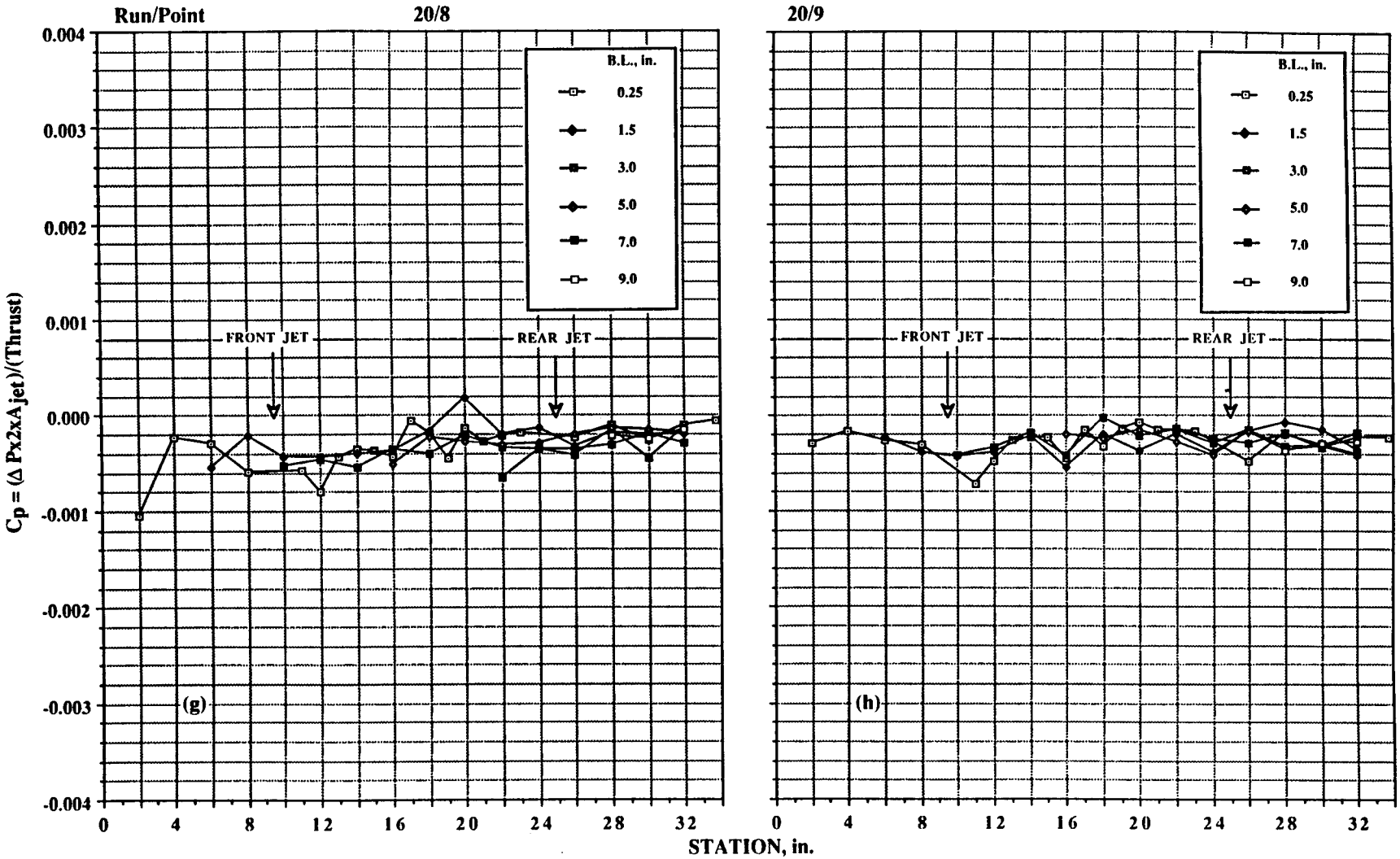

Figure 20. Concluded. (g) $h/d_e = 14.37$. (h) $h/d_e = 23.0$.

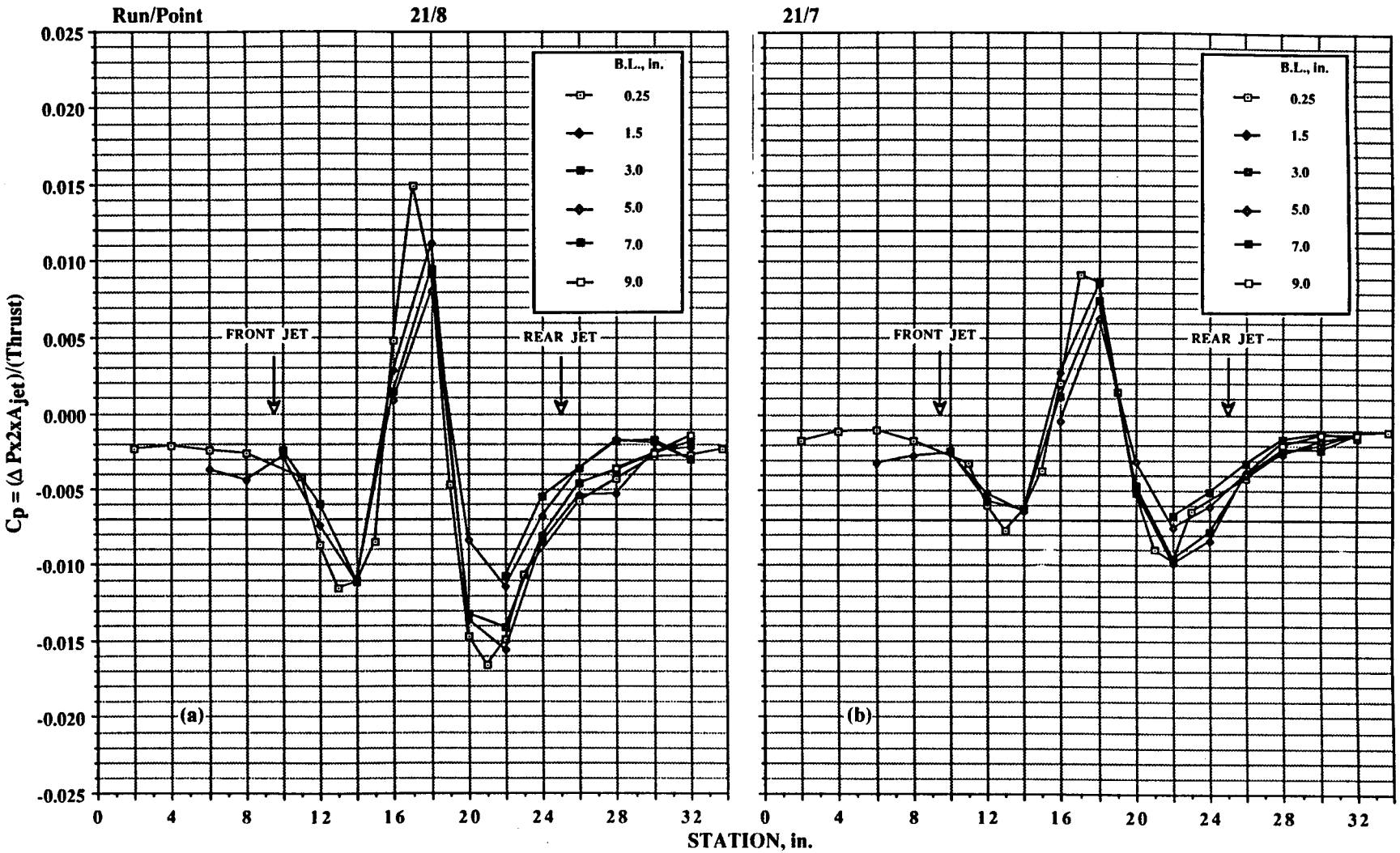

Figure 21. Pressures induced on delta-wing configuration in ground effect; NPR = 3.0, T = 93 lb, both jets, no LIDs. (a) $h/d_e = 2.30$. (b) $h/d_e = 3.45$.

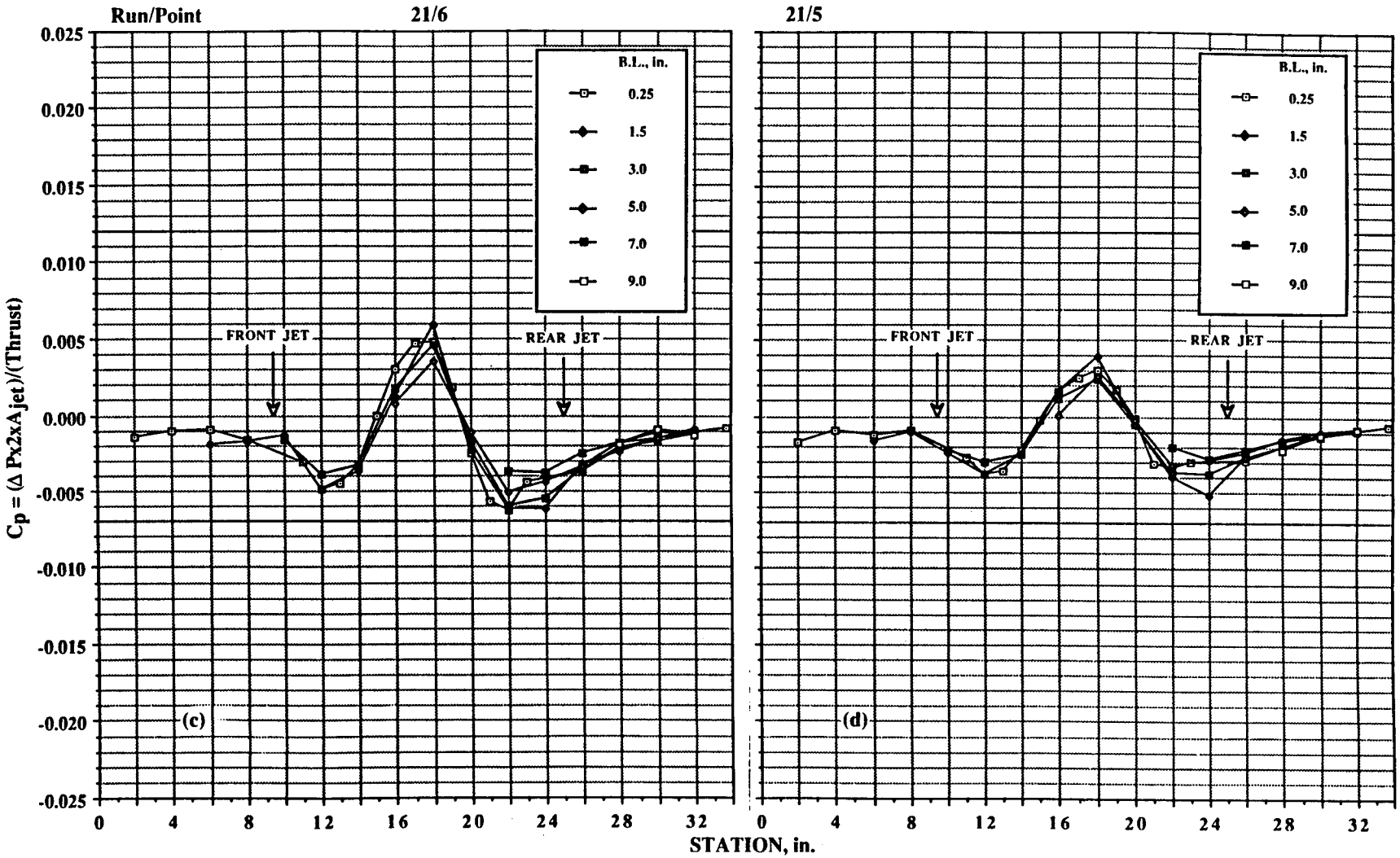

Figure 21. Continued. (c) $h/d_e = 4.6$. (d) $h/d_e = 5.75$.

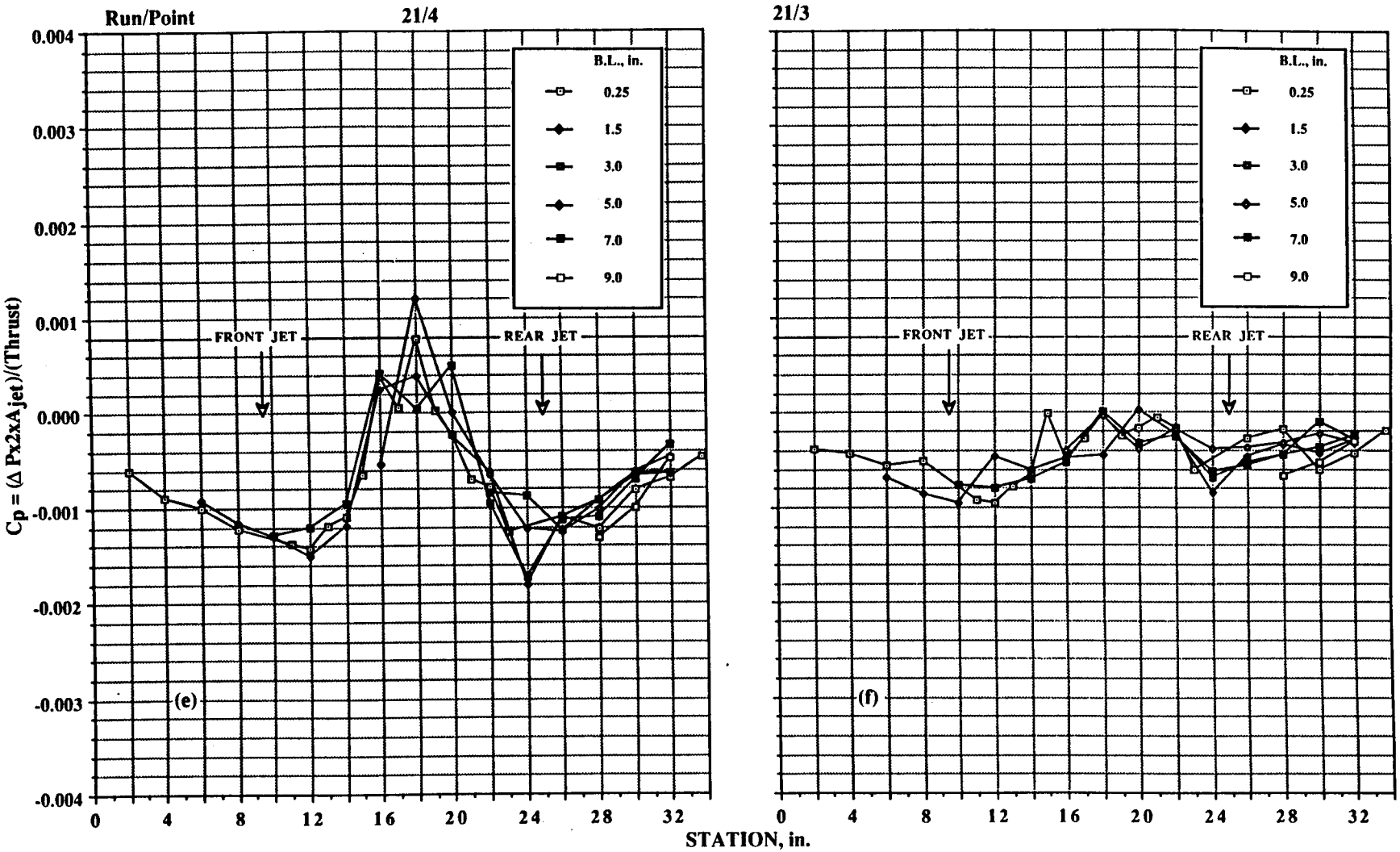

Figure 21. Continued. (e) $h/d_e = 8.62$. (f) $h/d_e = 11.5$.

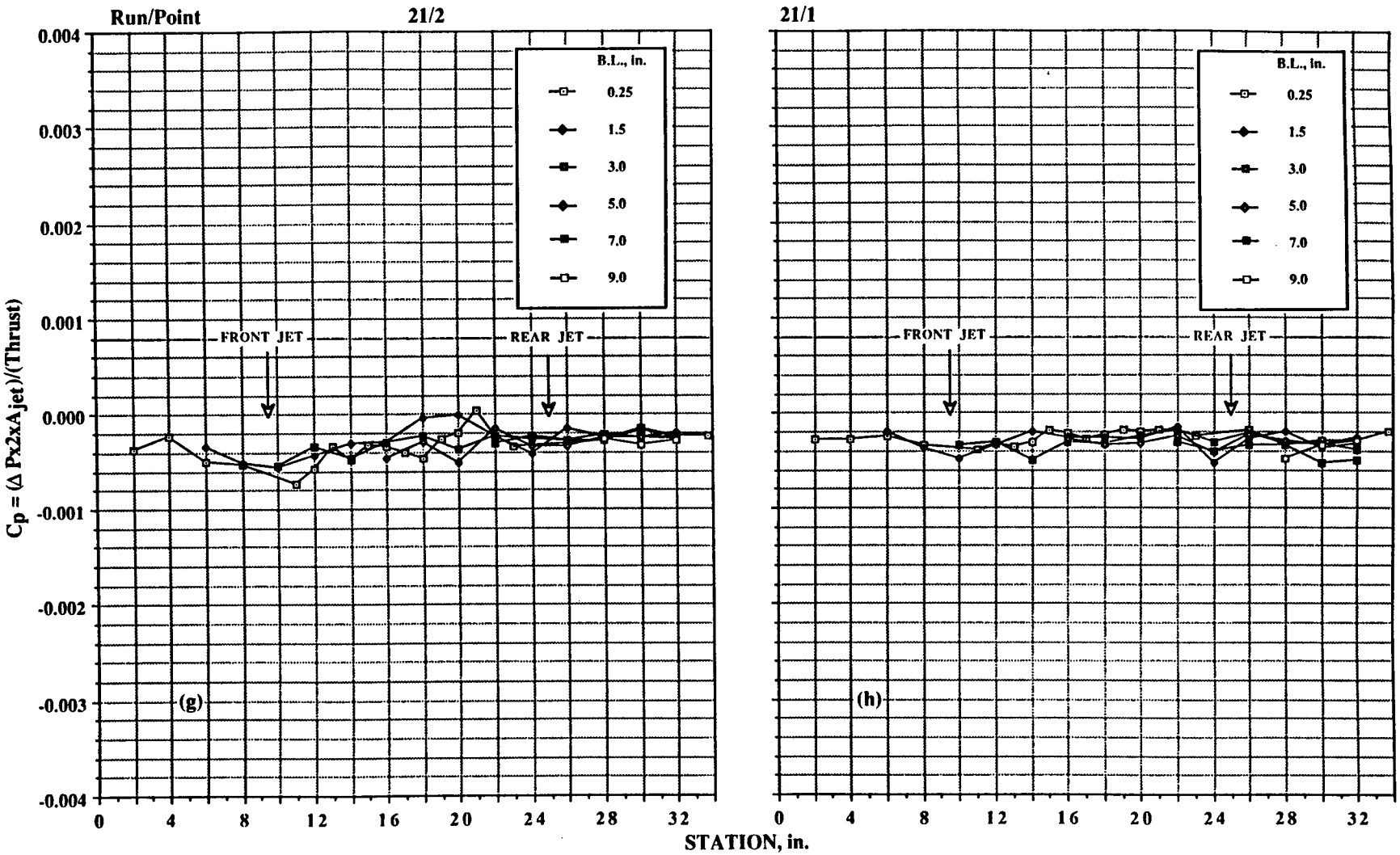

Figure 21. Concluded. (g) $h/d_e = 14.37$. (h) $h/d_e = 23.0$.

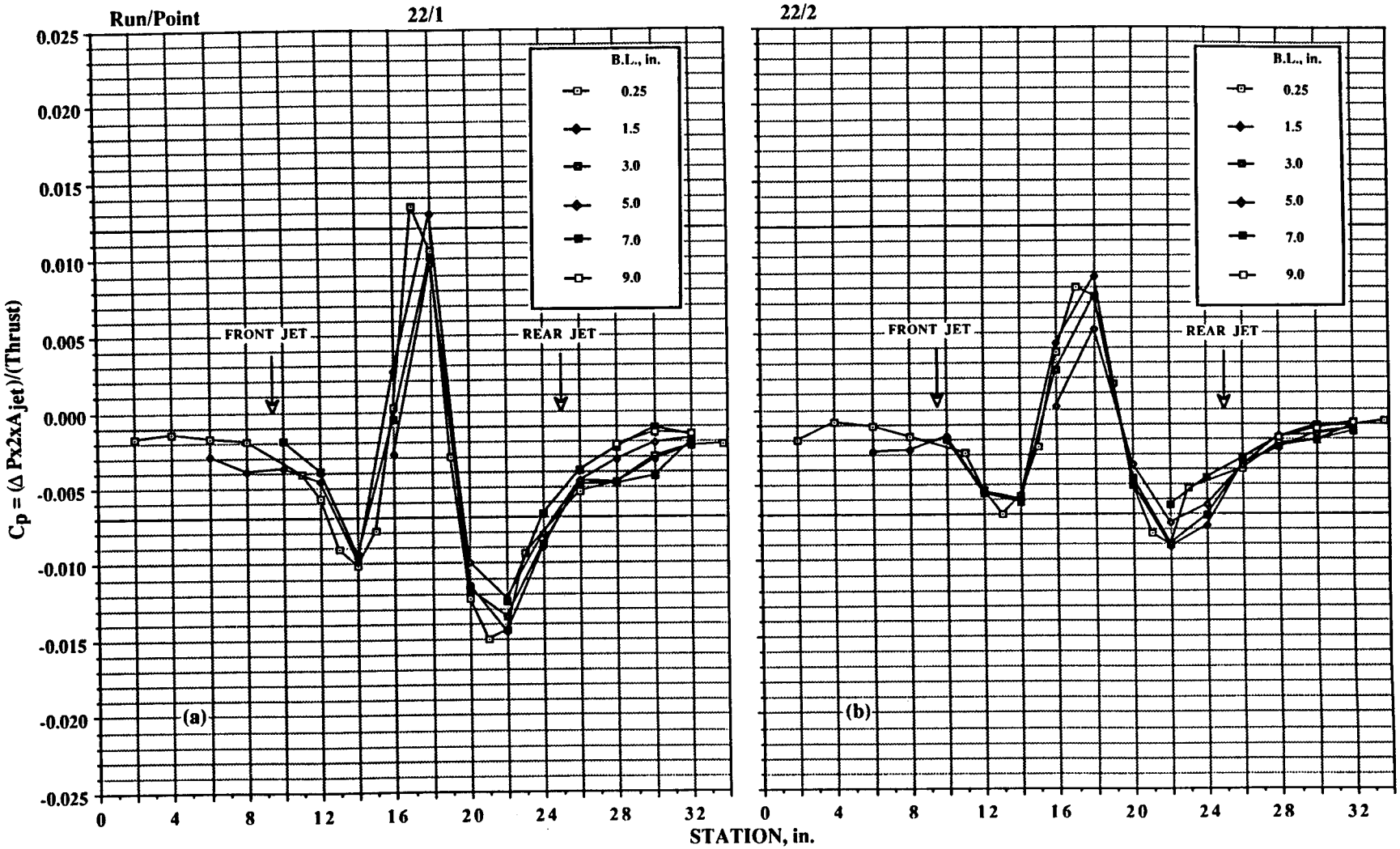

Figure 22. Pressures induced on delta-wing configuration in ground effect; NPR = 4.0, T = 135 lb, both jets, no LIDs. (a) $h/d_e = 2.30$. (b) $h/d_e = 3.45$.

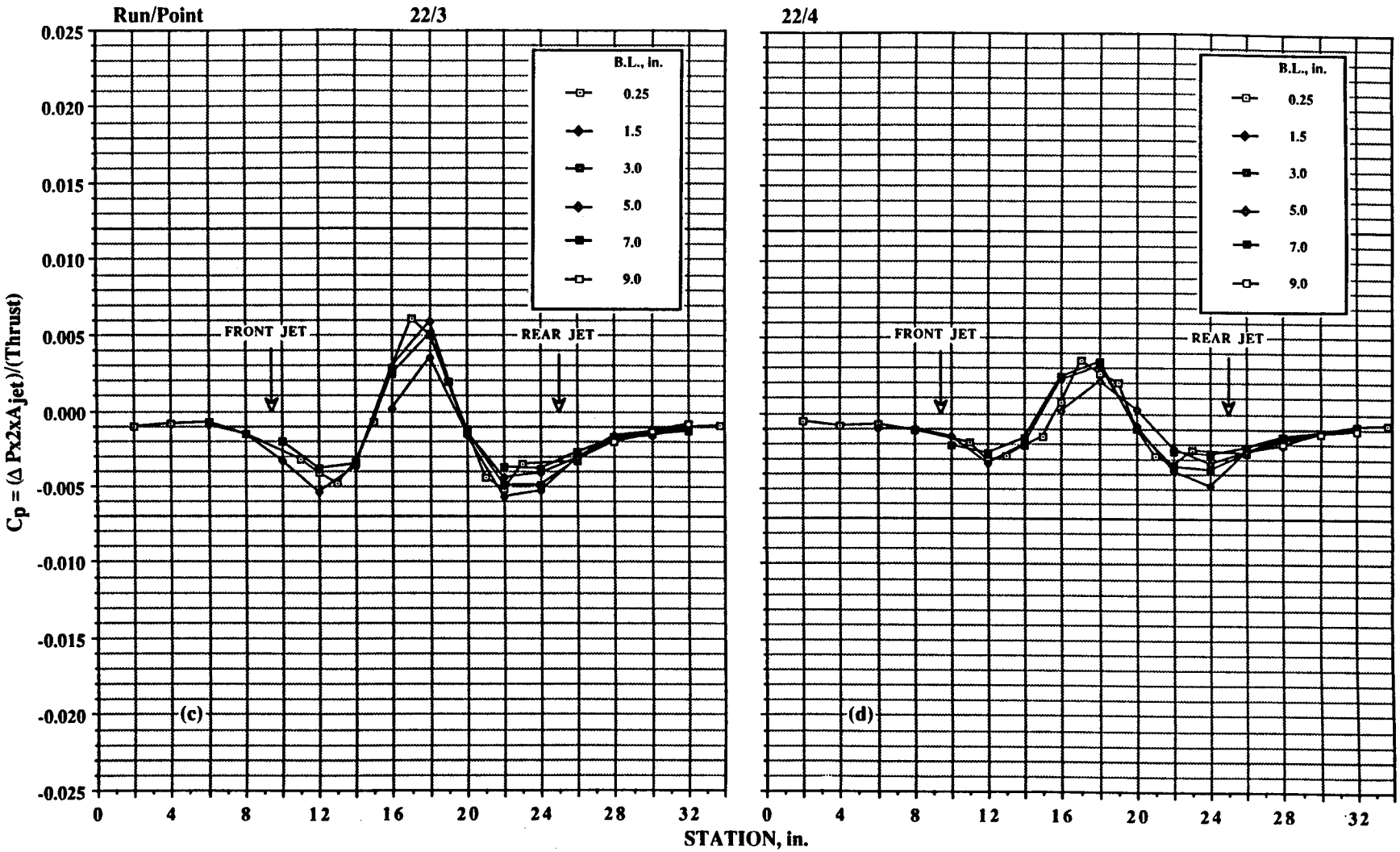

Figure 22. Continued. (c) $h/d_e = 4.6$. (d) $h/d_e = 5.75$.

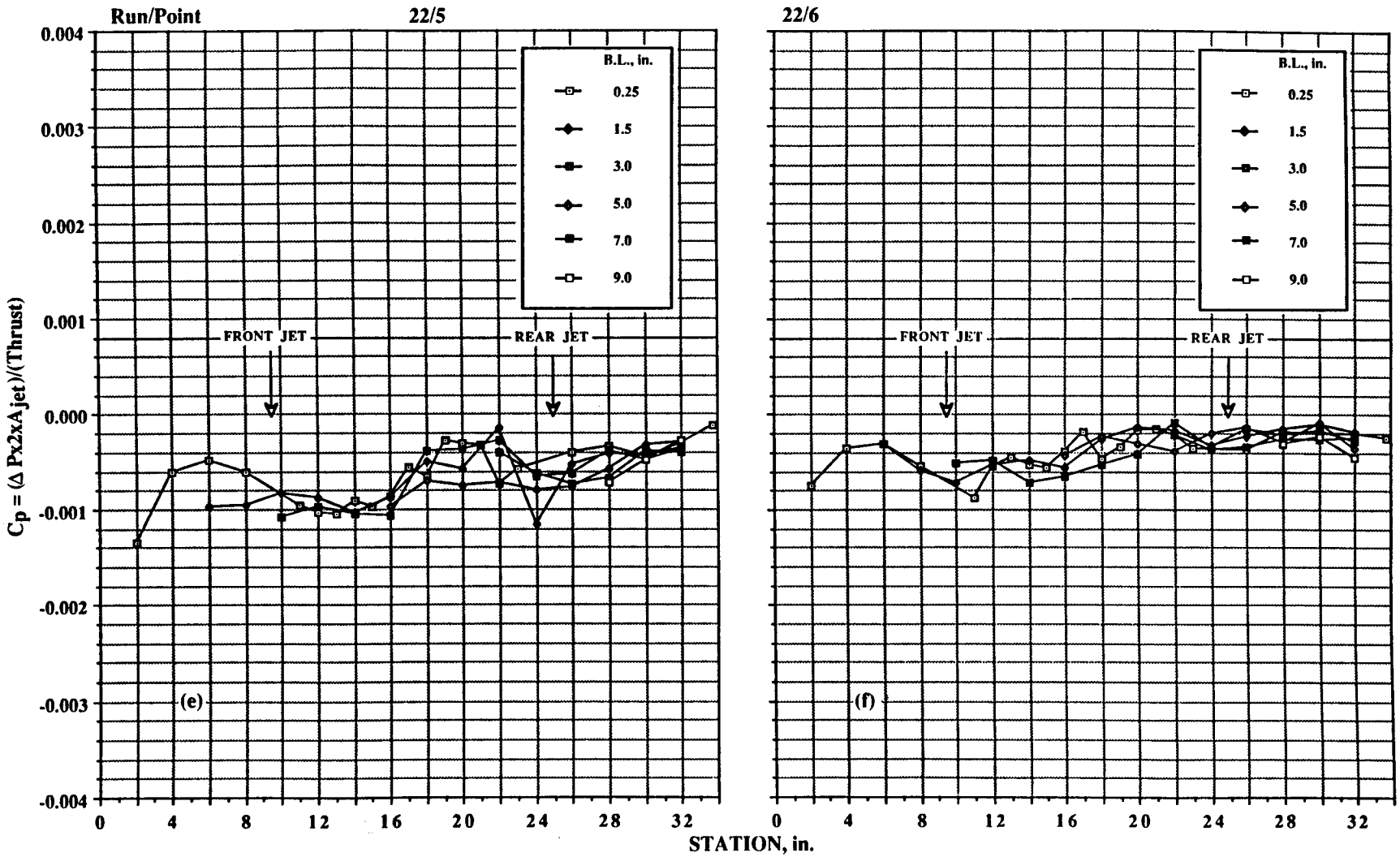

Figure 22. Continued. (e) $h/d_e = 8.62$. (f) $h/d_e = 11.5$.

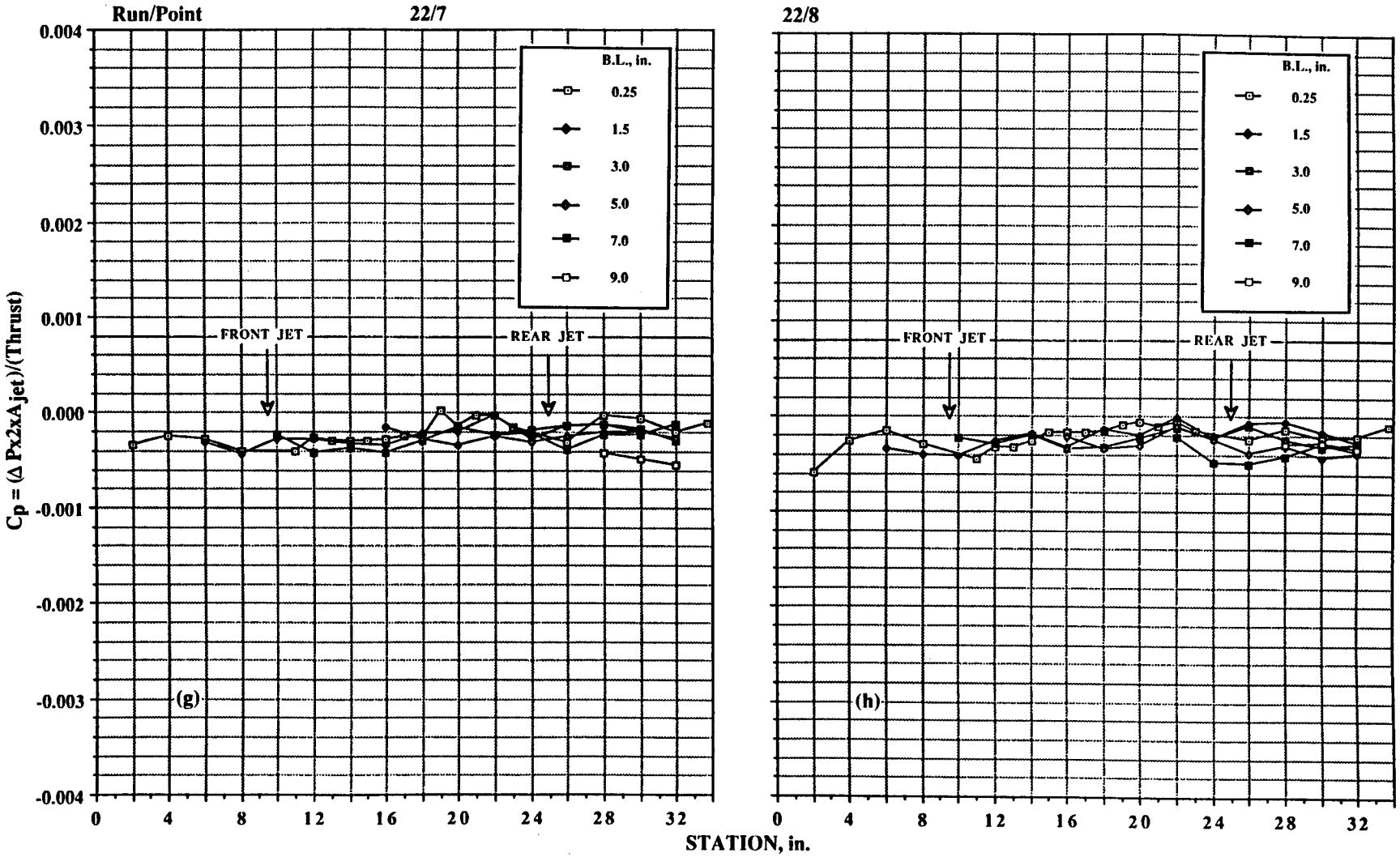

Figure 22. Concluded. (g) $h/d_e = 14.37$. (h) $h/d_e = 23.0$.

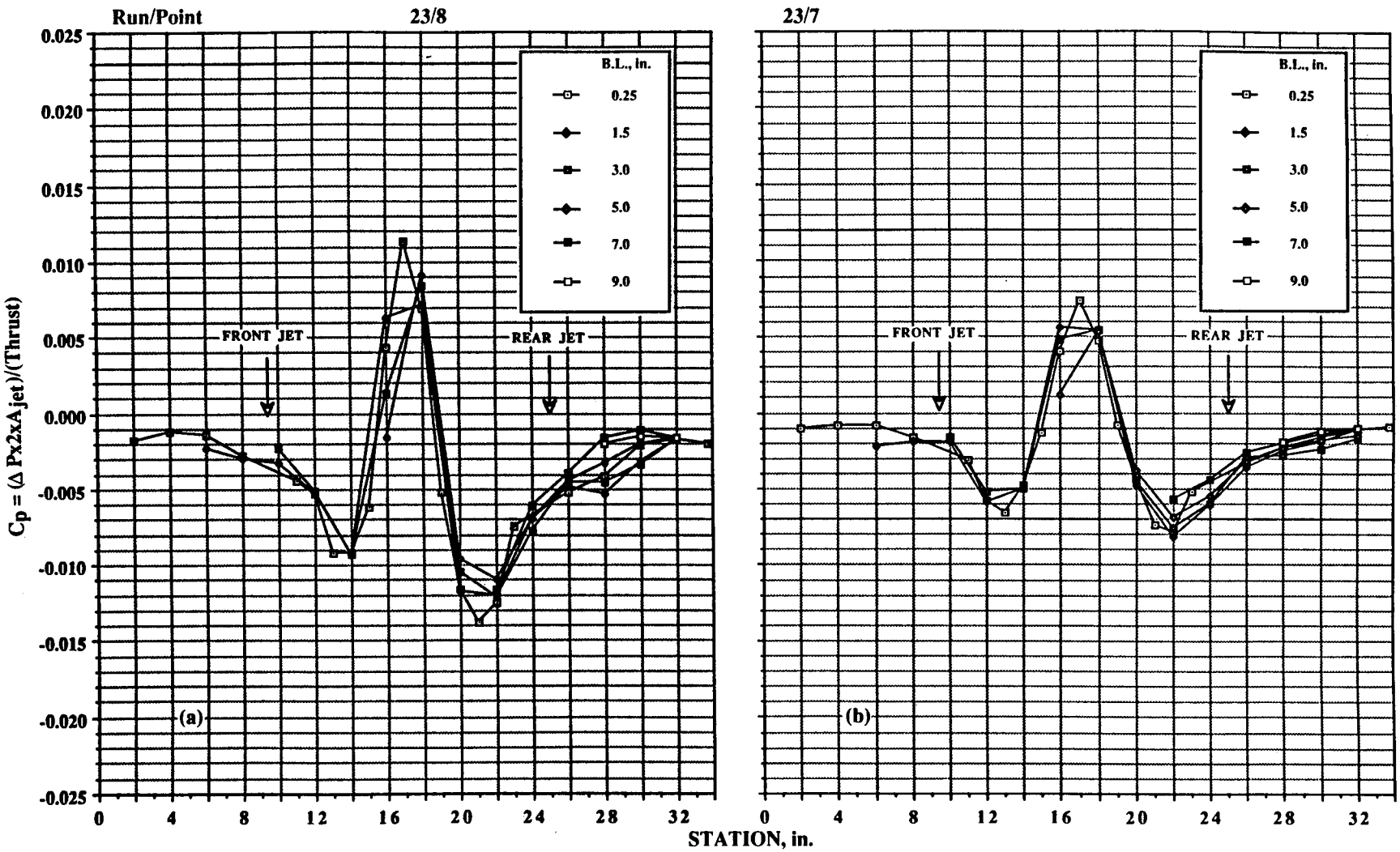

Figure 23. Pressures induced on delta-wing configuration in ground effect; NPR = 5.0, T = 176 lb, both jets, no LIDs. (a) $h/d_e = 2.30$. (b) $h/d_e = 3.45$.

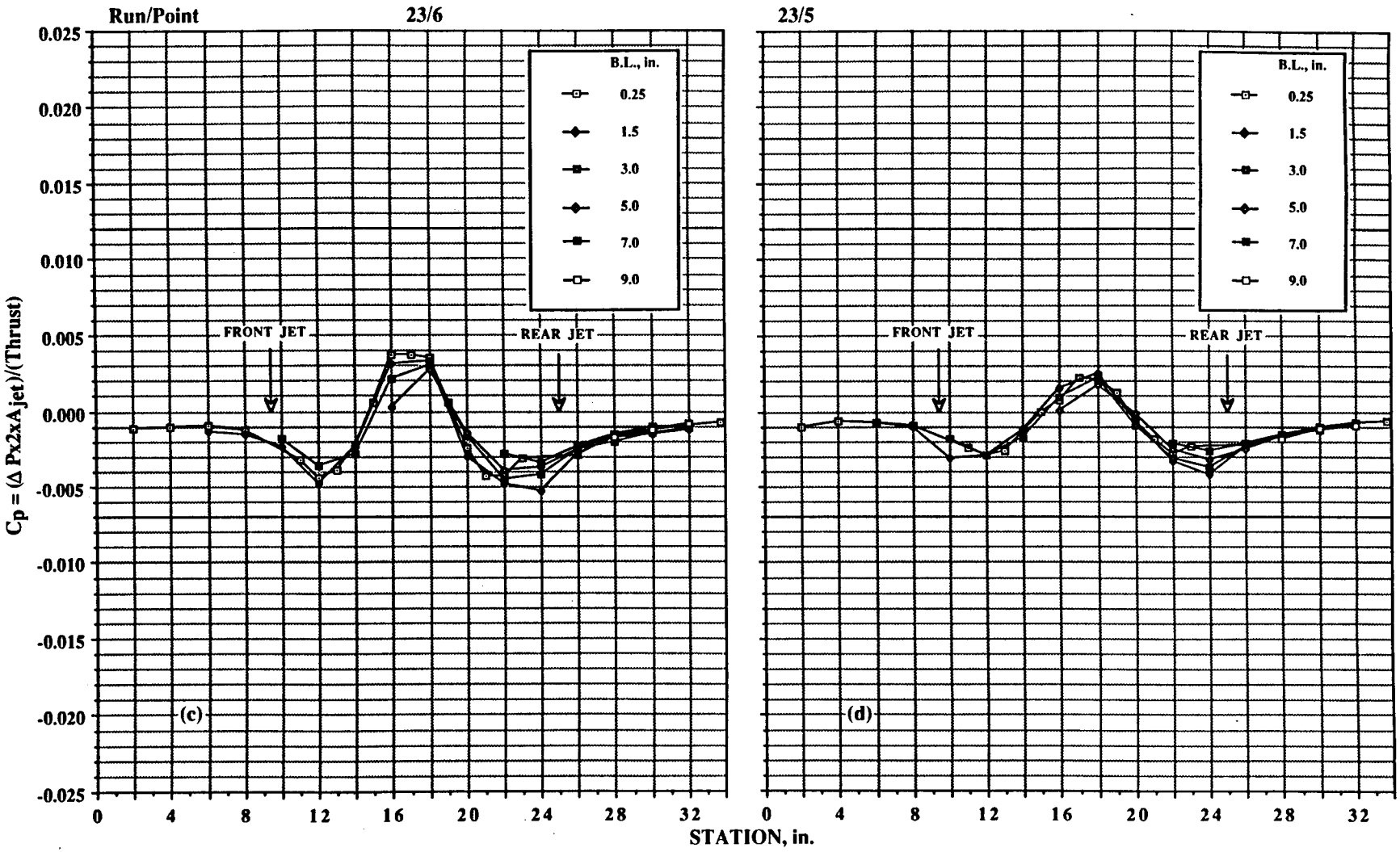

Figure 23. Continued. (c) $h/d_e = 4.6$. (d) $h/d_e = 5.75$.

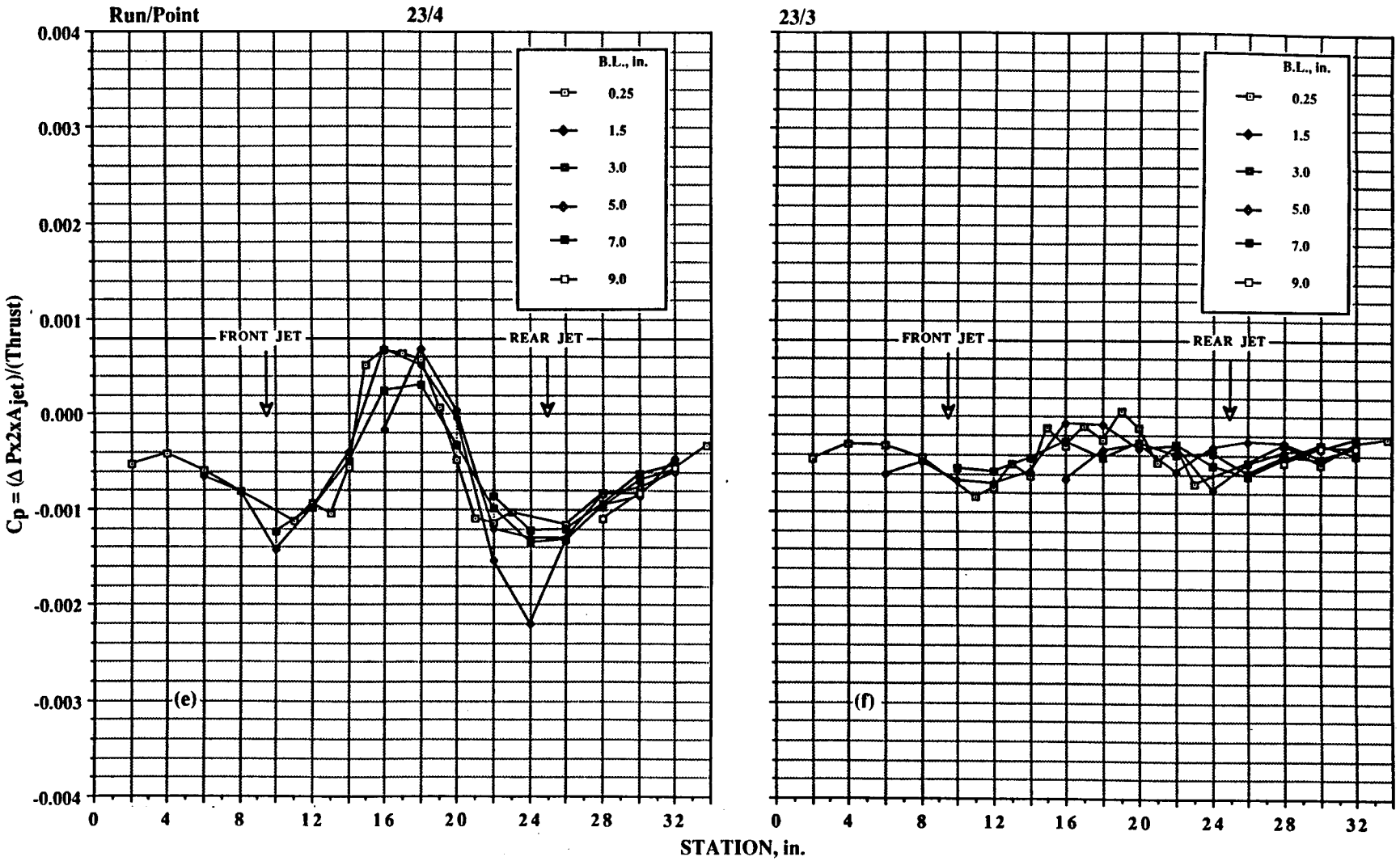

Figure 23. Continued. (e) $h/d_e = 8.62$. (f) $h/d_e = 11.5$.

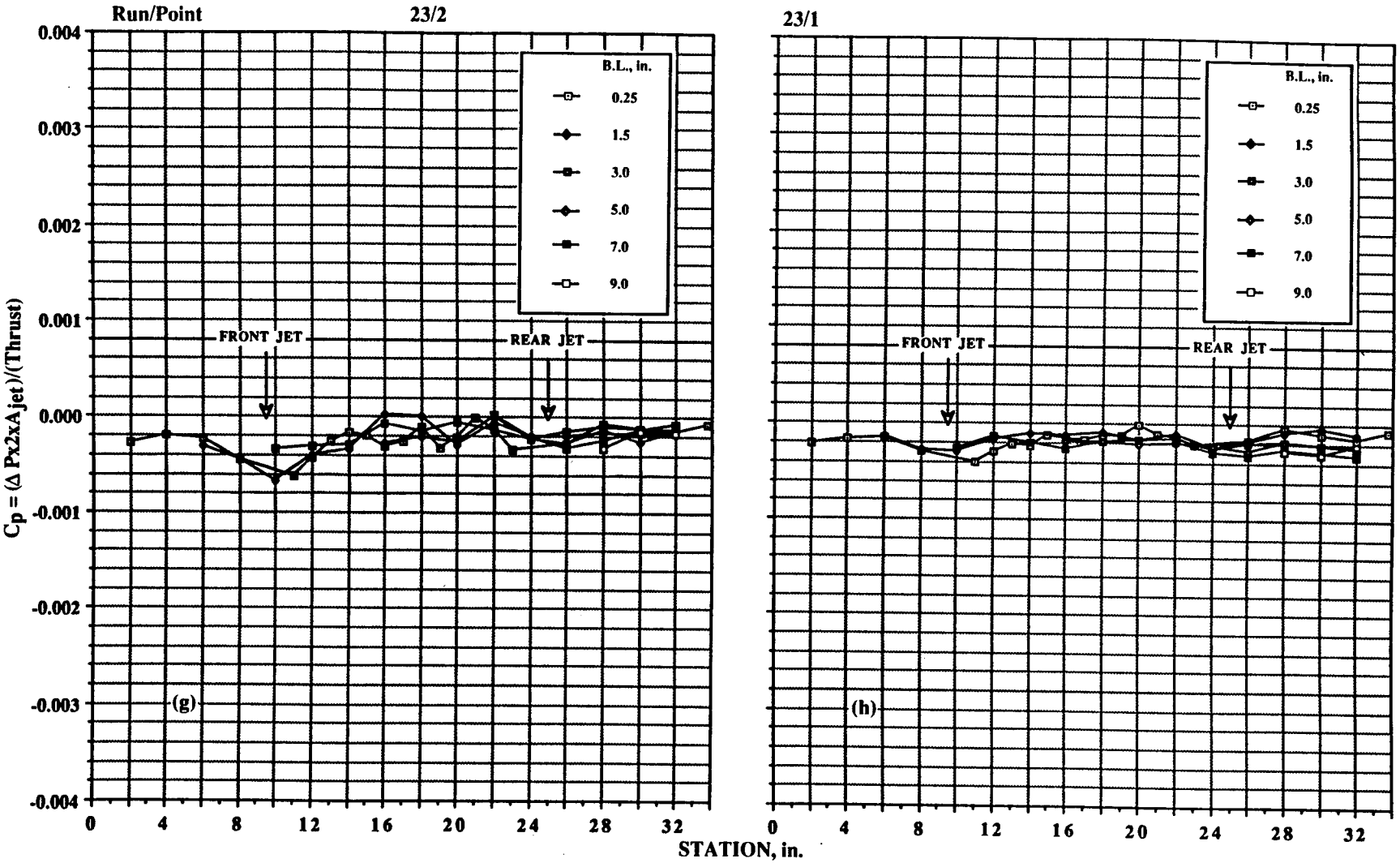

Figure 23. Concluded. (g) $h/d_e = 14.37$. (h) $h/d_e = 23.0$.

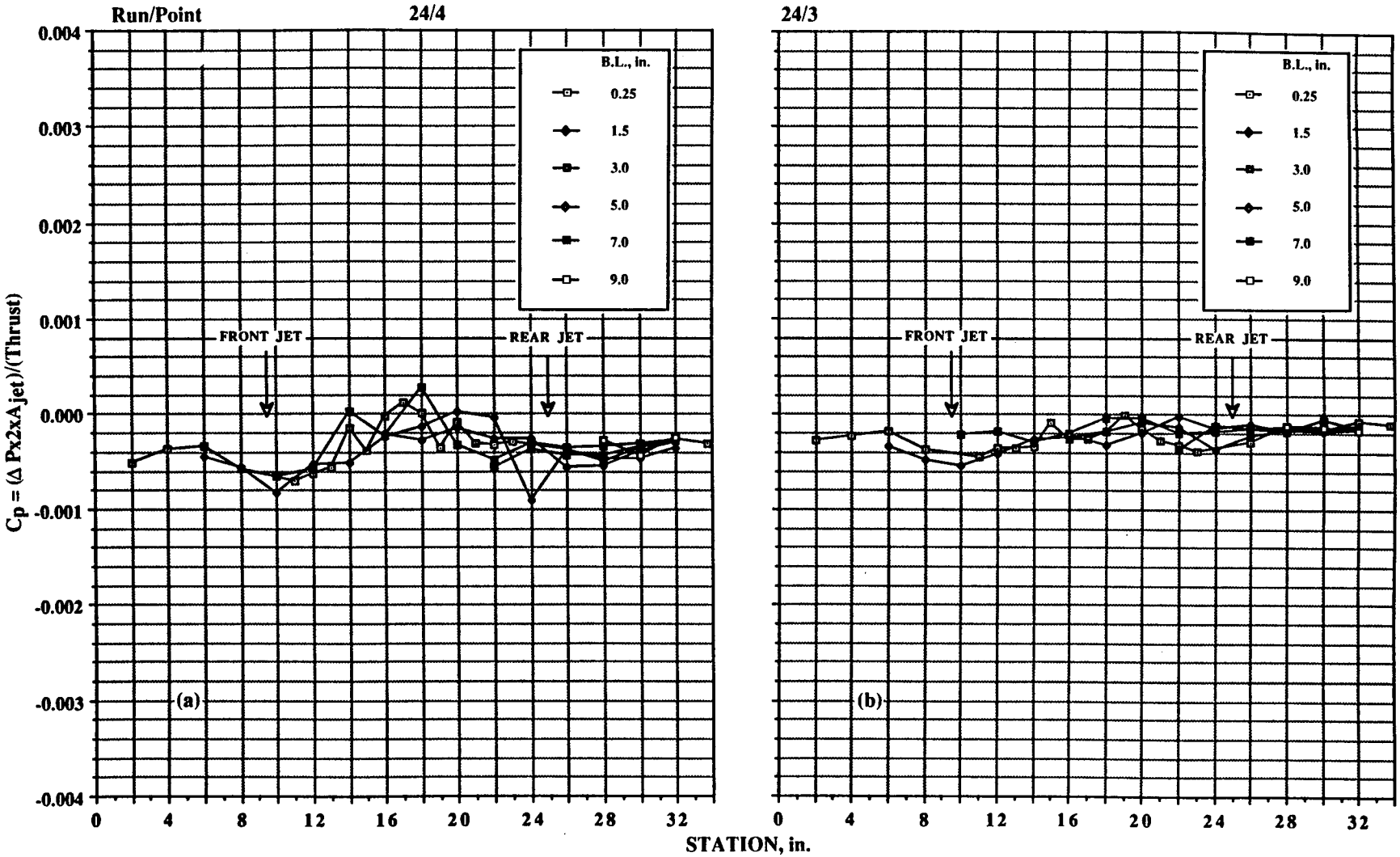

Figure 24. Pressures induced on delta-wing configuration in ground effect; NPR = 6.0, T = 218 lb, both jets, no LIDs. (a) $h/d_e = 11.5$. (b) $h/d_e = 14.37$.

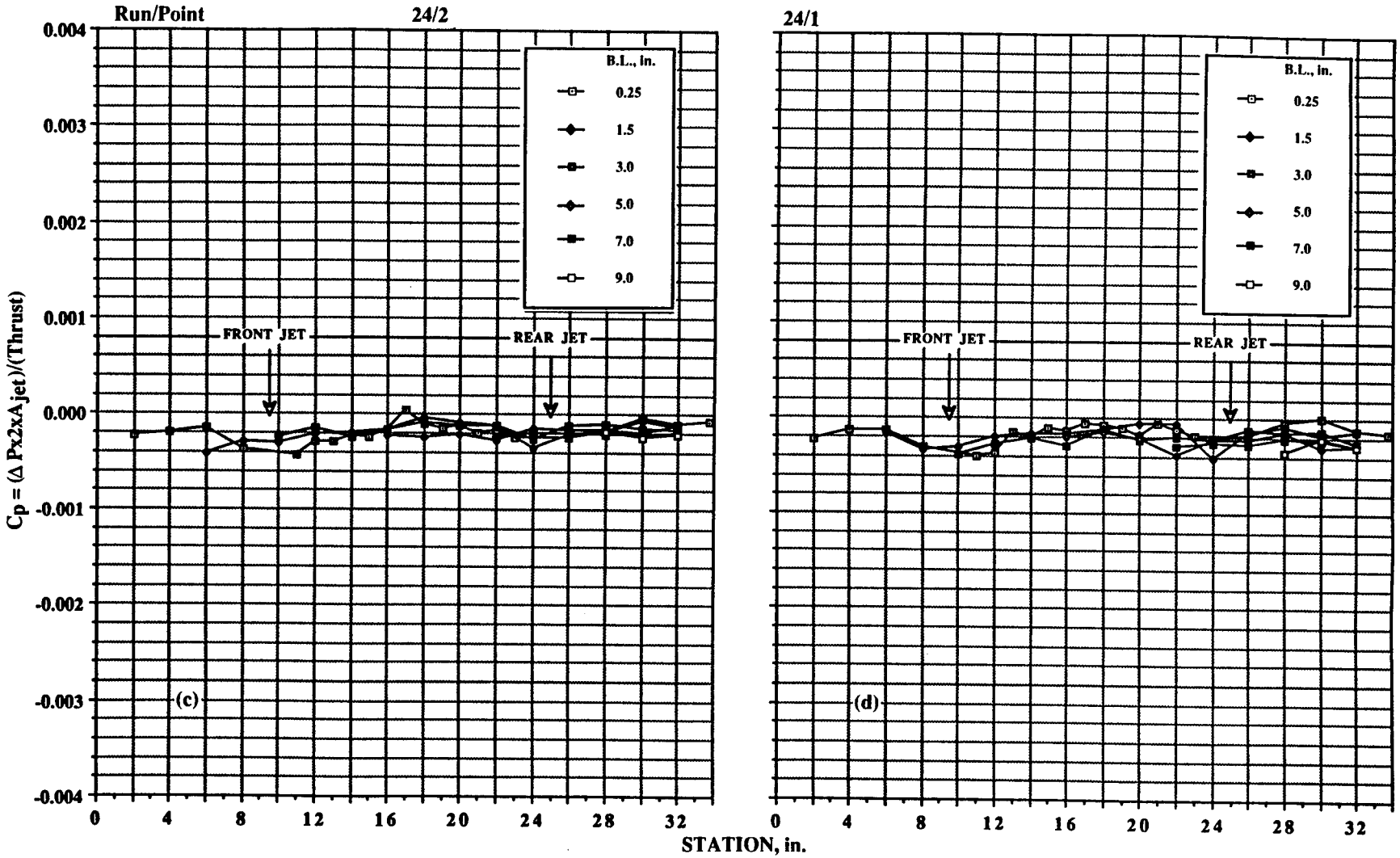

Figure 24. Continued. (c) $h/d_e = 17.24$. (d) $h/d_e = 23.0$.

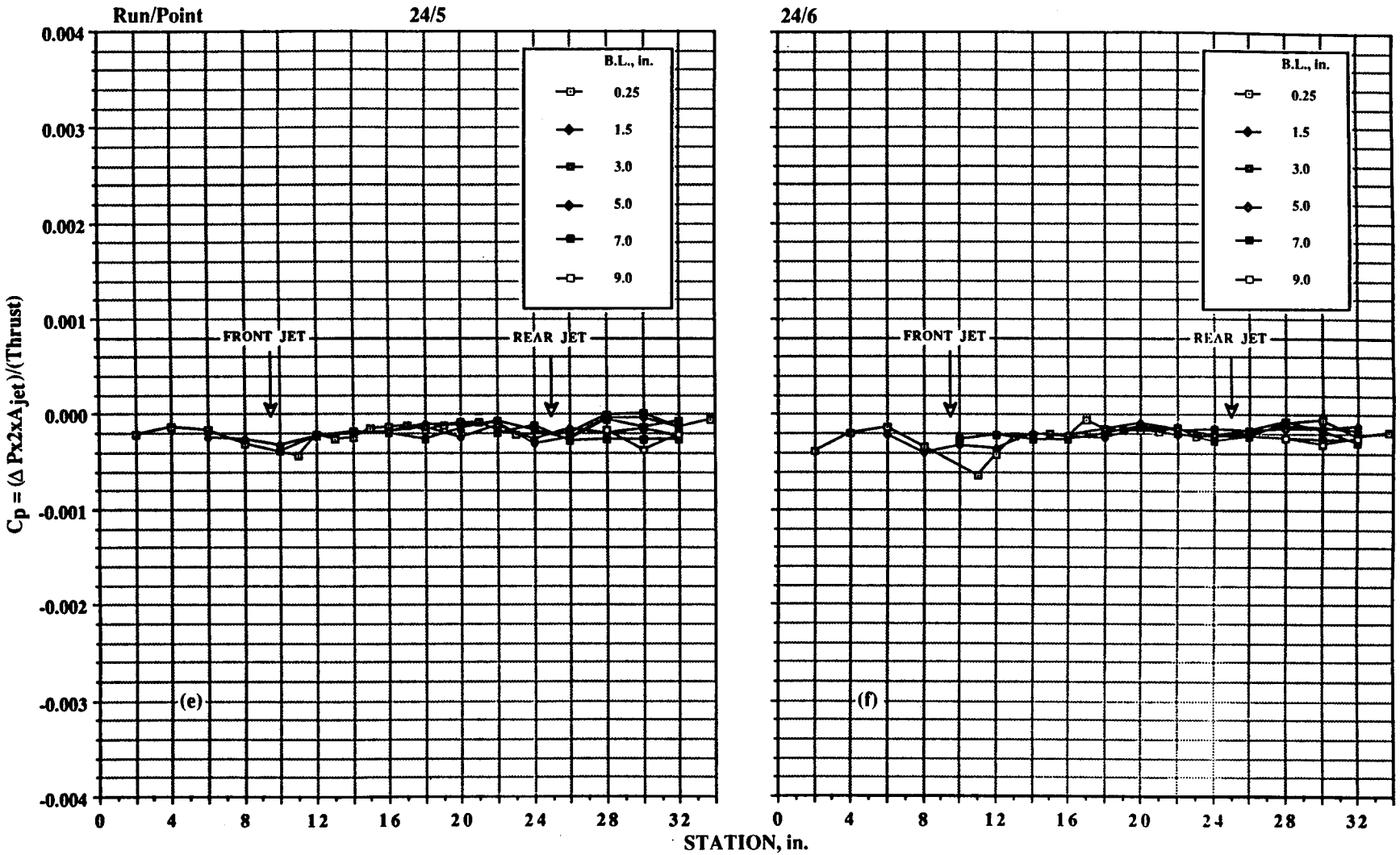

Figure 24. Concluded. (e) $h/d_e = 23.0$ (repeat). (f) $h/d_e = 23.0$ (repeat).

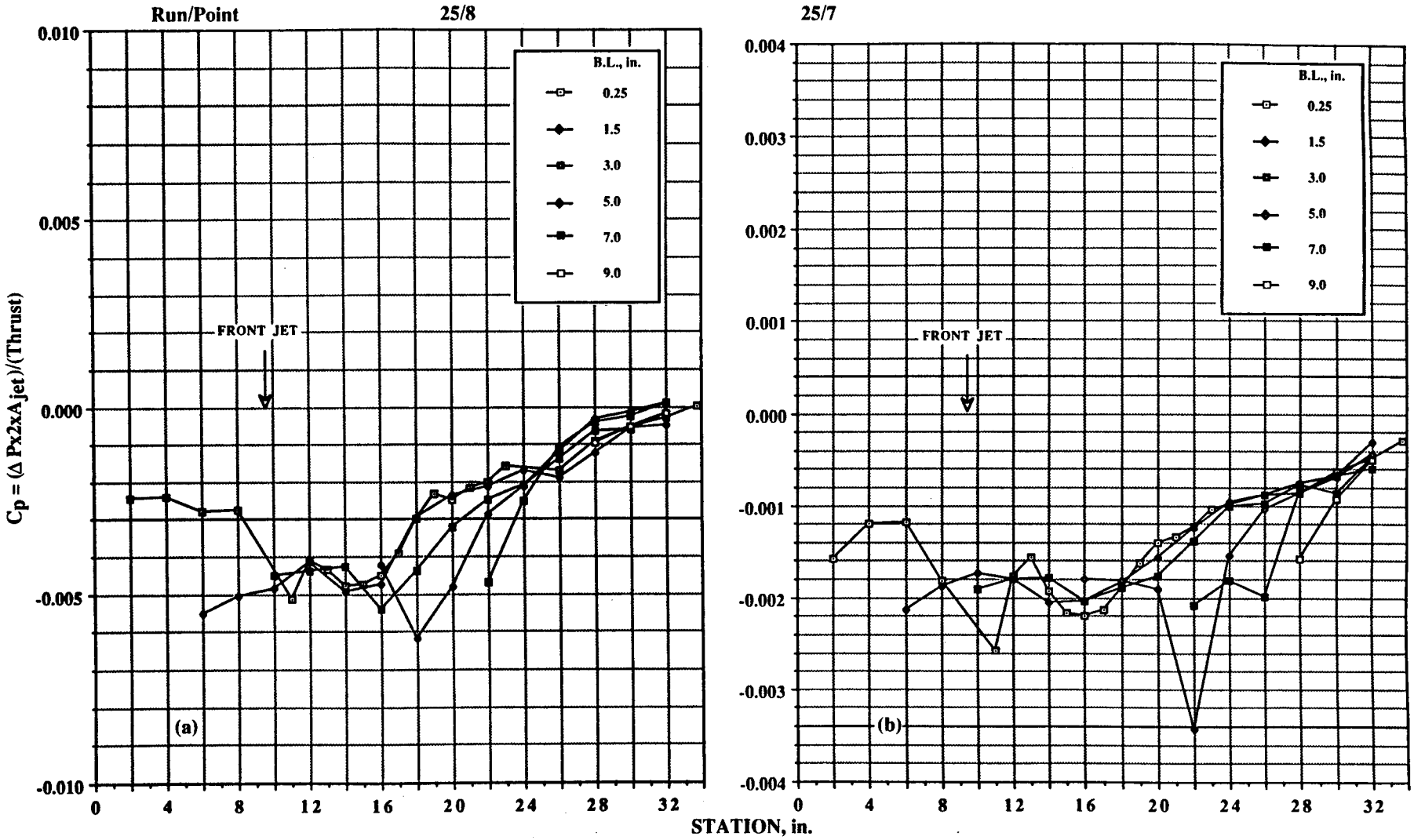

Figure 25. Pressures induced on delta-wing configuration in ground effect; NPR = 2.0, T = 25.5 lb, front jet only, no LIDs. (a) $h/d_e = 3.25$. (b) $h/d_e = 4.87$.

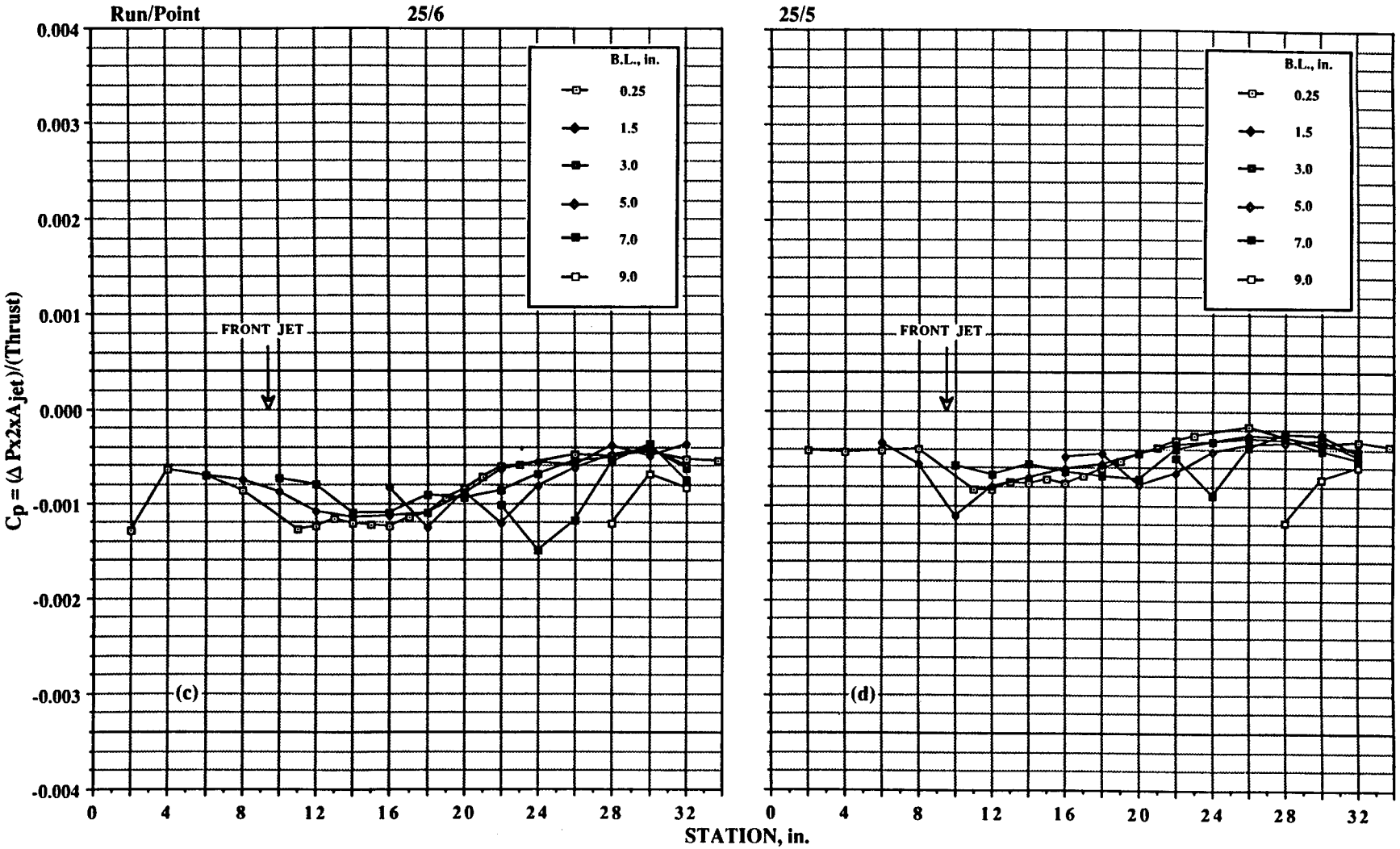

Figure 25. Continued. (c) $h/d_e = 6.50$. (d) $h/d_e = 8.13$.

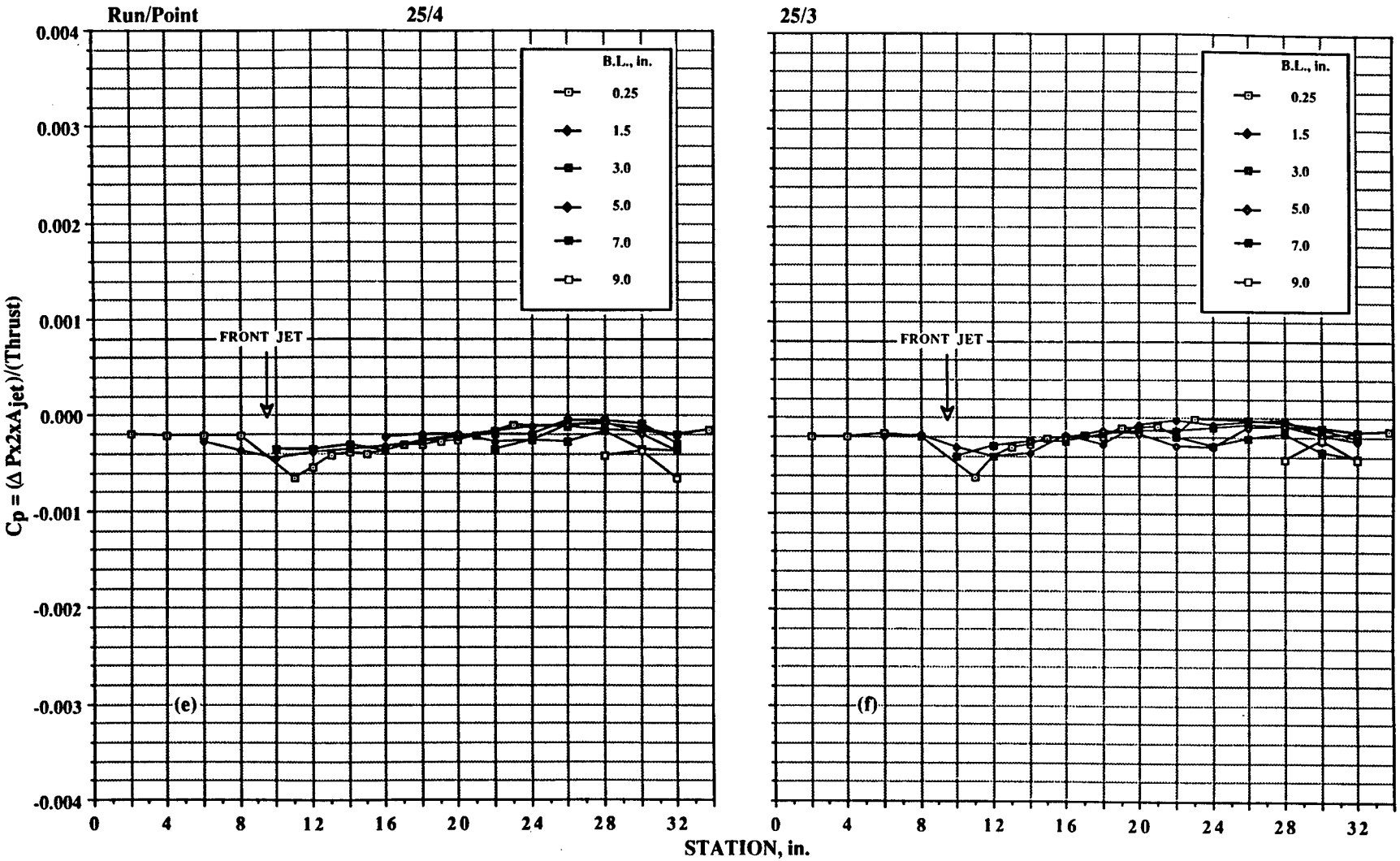

Figure 25. Continued. (e) $h/d_e = 12.20$. (f) $h/d_e = 16.26$.

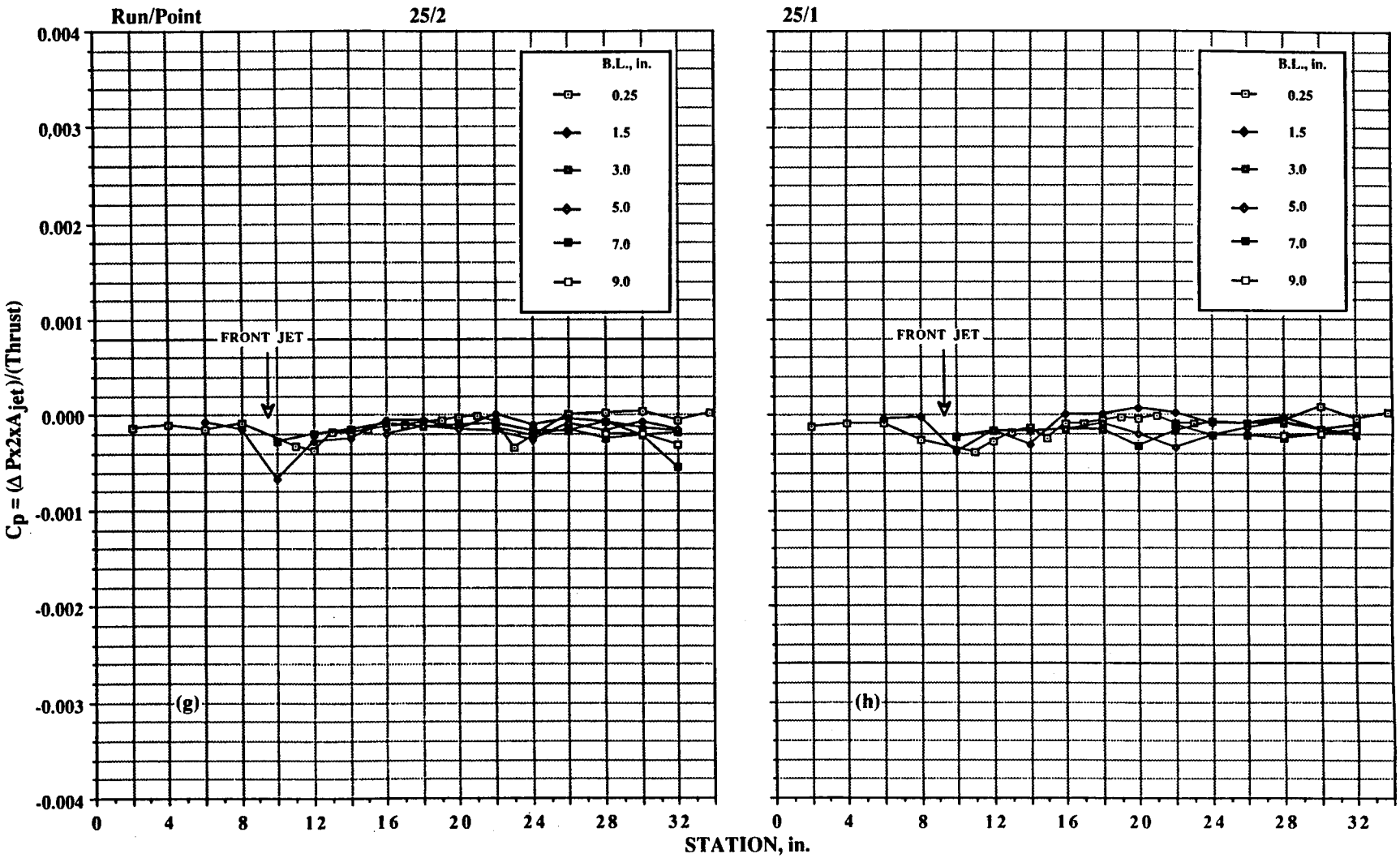

Figure 25. Concluded. (g) $h/d_e = 20.33$. (h) $h/d_e = 32.52$.

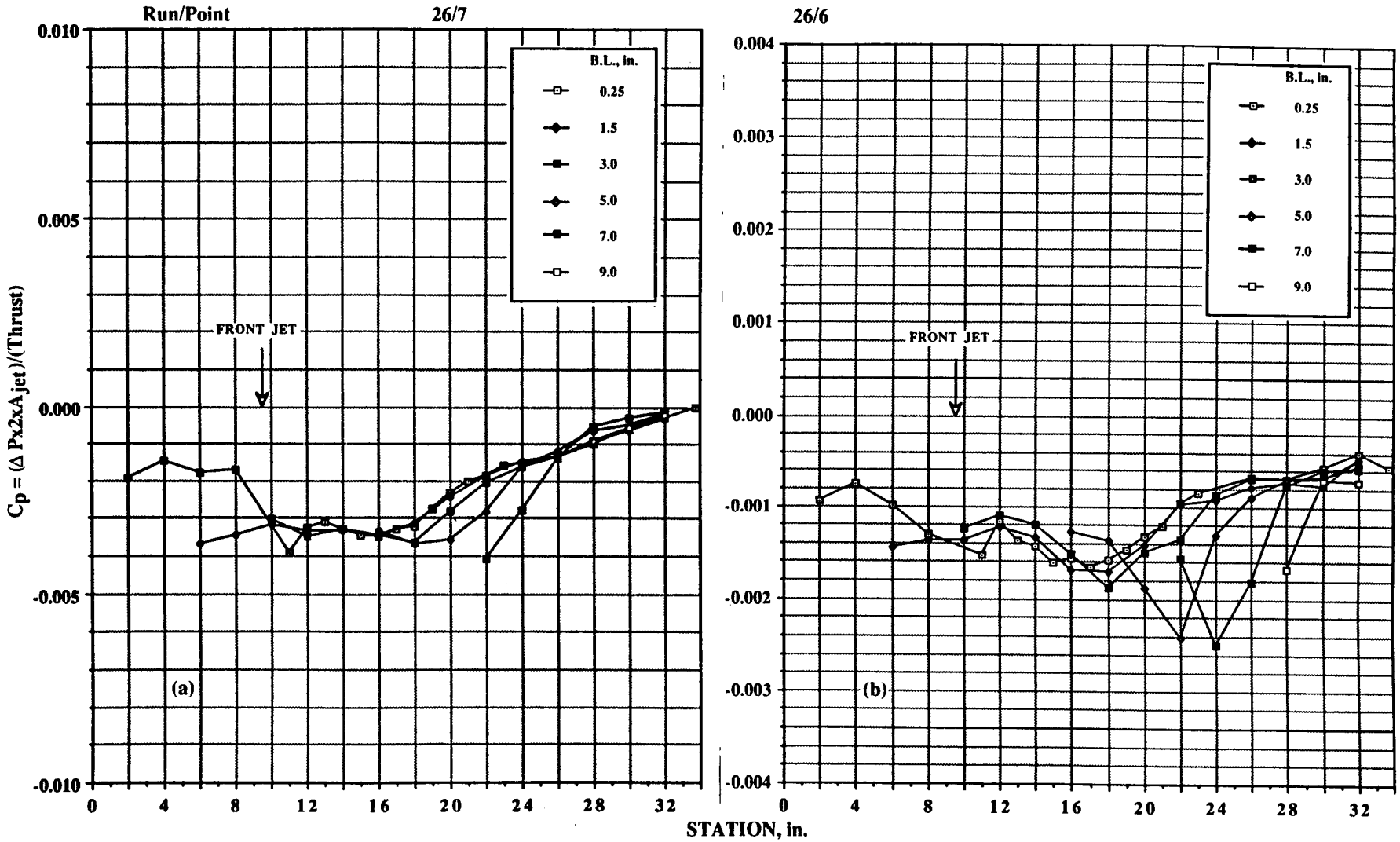

Figure 26. Pressures induced on delta-wing configuration in ground effect; NPR = 4.0, T = 67.5 lb, front jet only, no LIDs. (a) $h/d_e = 3.25$. (b) $h/d_e = 4.87$.

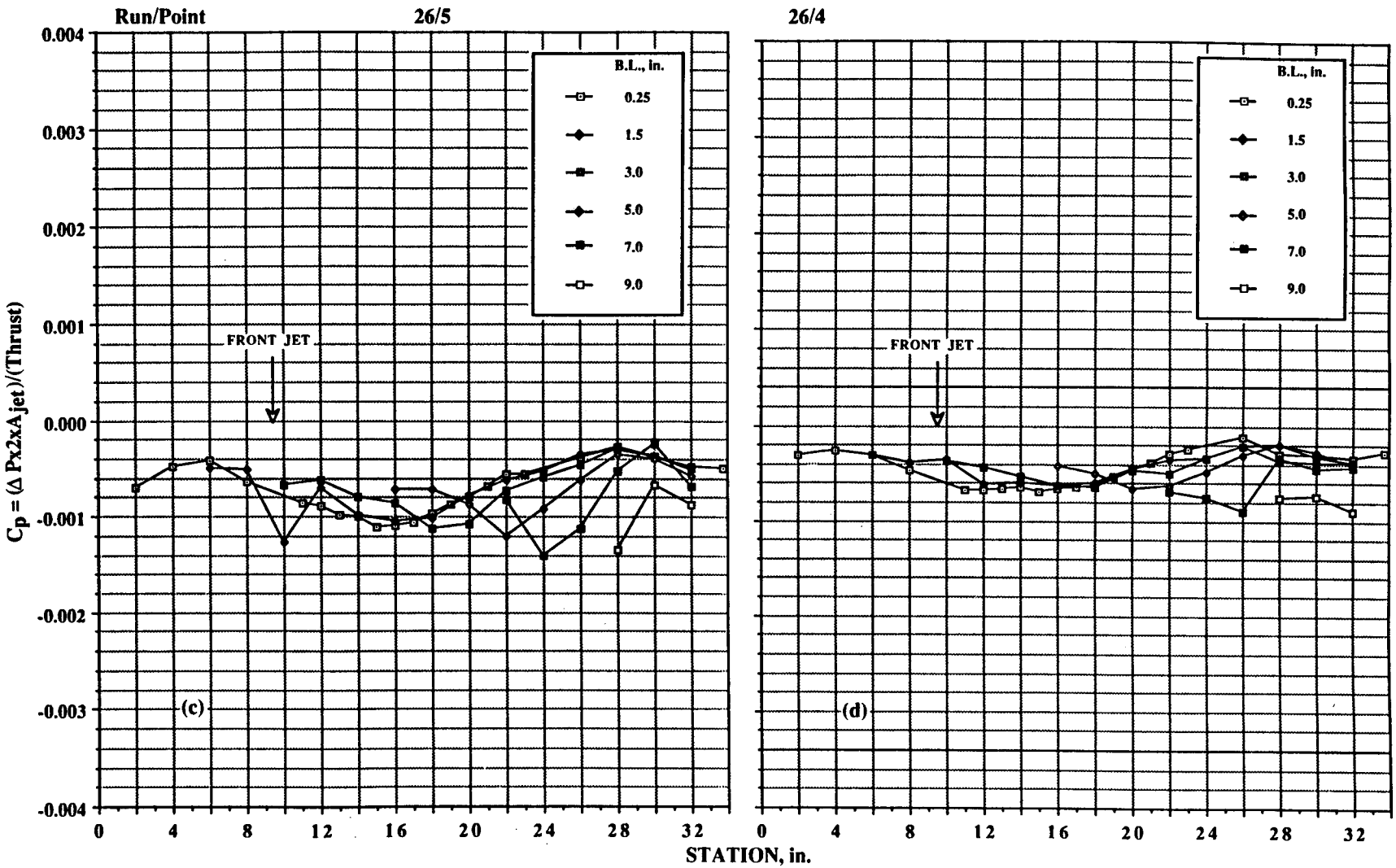

Figure 26. Continued. (c) $h/d_e = 6.50$. (d) $h/d_e = 8.13$.

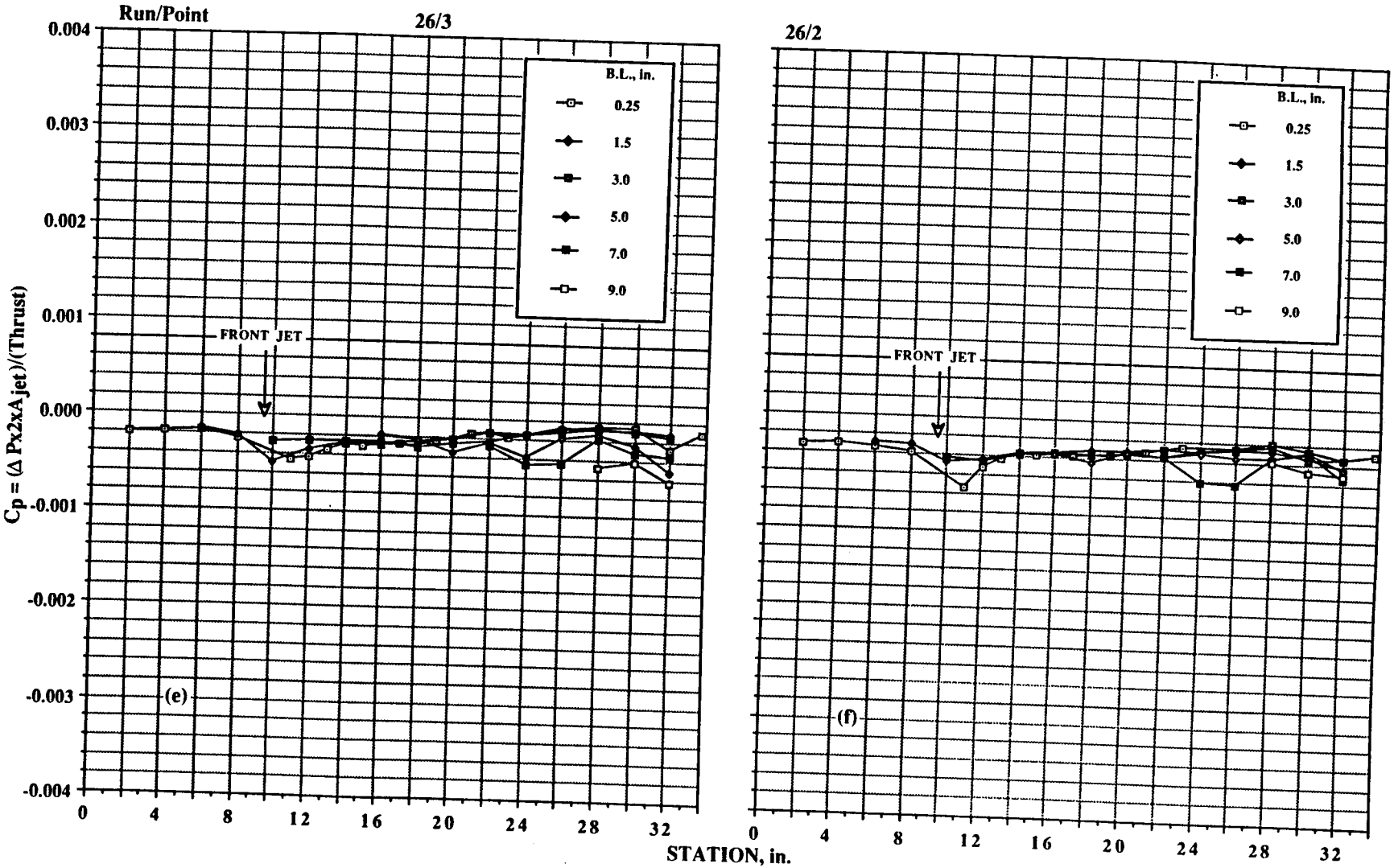

Figure 26. Continued. (e) $h/d_e = 12.20$. (f) $h/d_e = 16.26$.

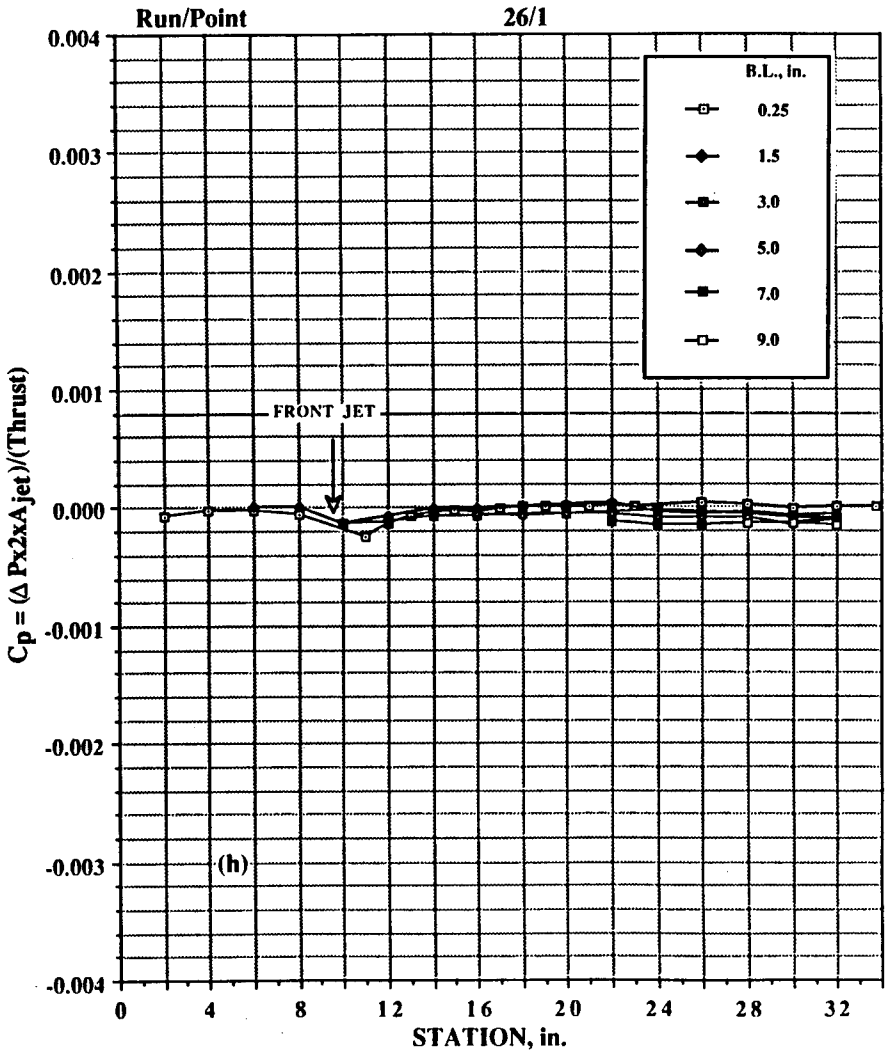

Figure 26. Concluded. (g) $h/d_e = 32.52$.

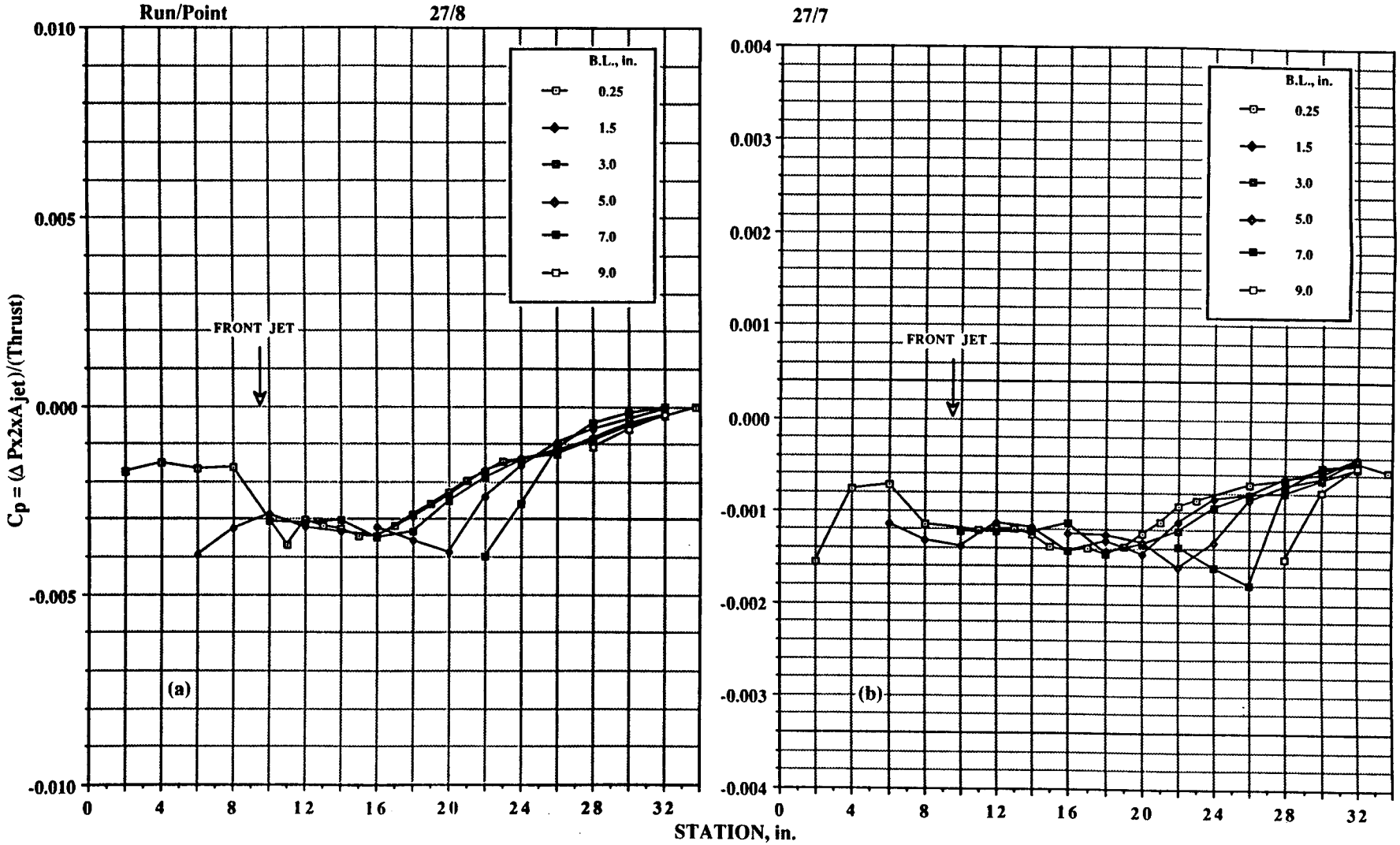

Figure 27. Pressures induced on delta-wing configuration in ground effect; NPR = 6.0, T = 109 lb, front jet only, no LIDs. (a) $h/d_e = 3.25$. (b) $h/d_e = 4.87$.

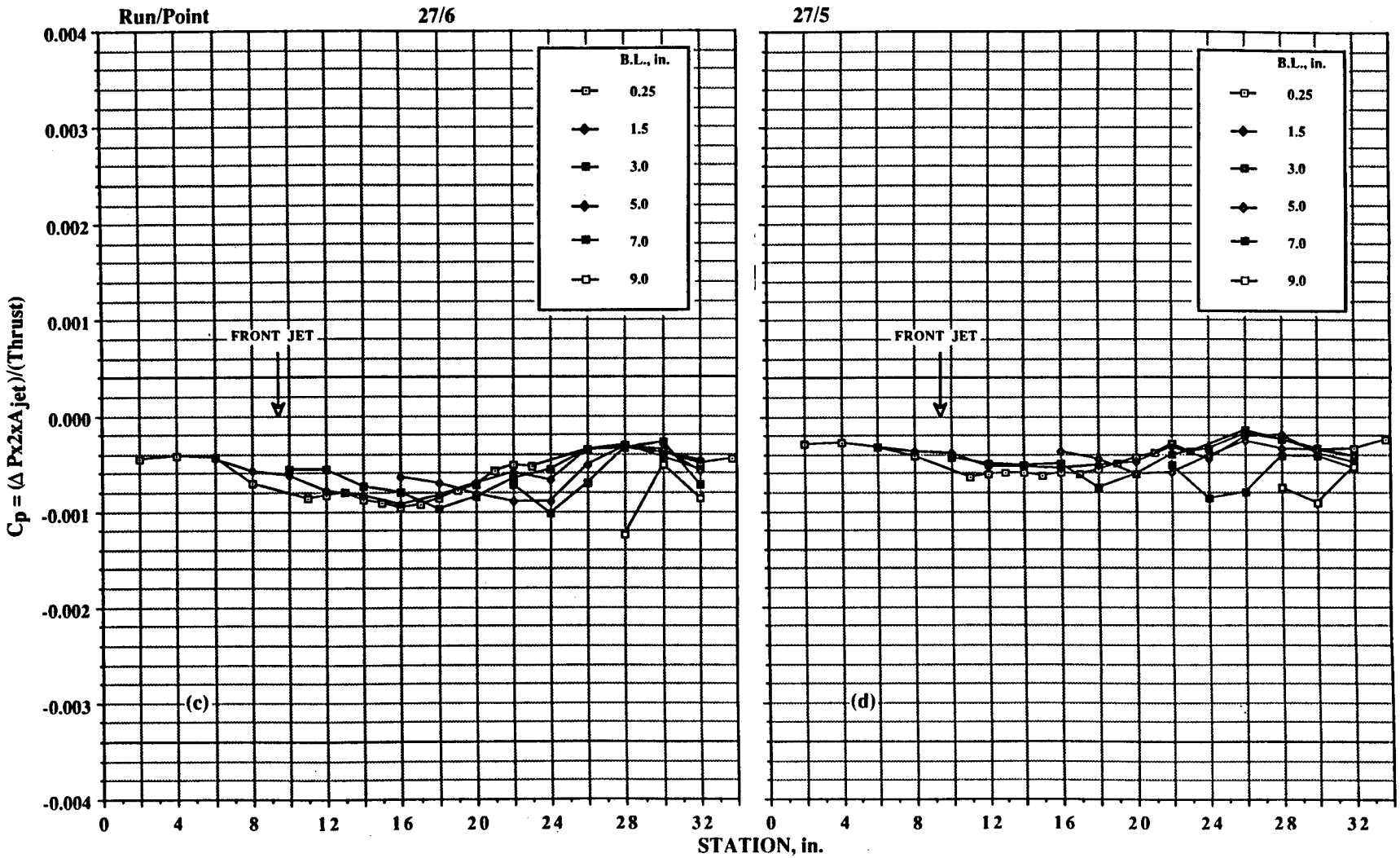

Figure 27. Continued. (c) $h/d_e = 6.50$. (d) $h/d_e = 8.13$.

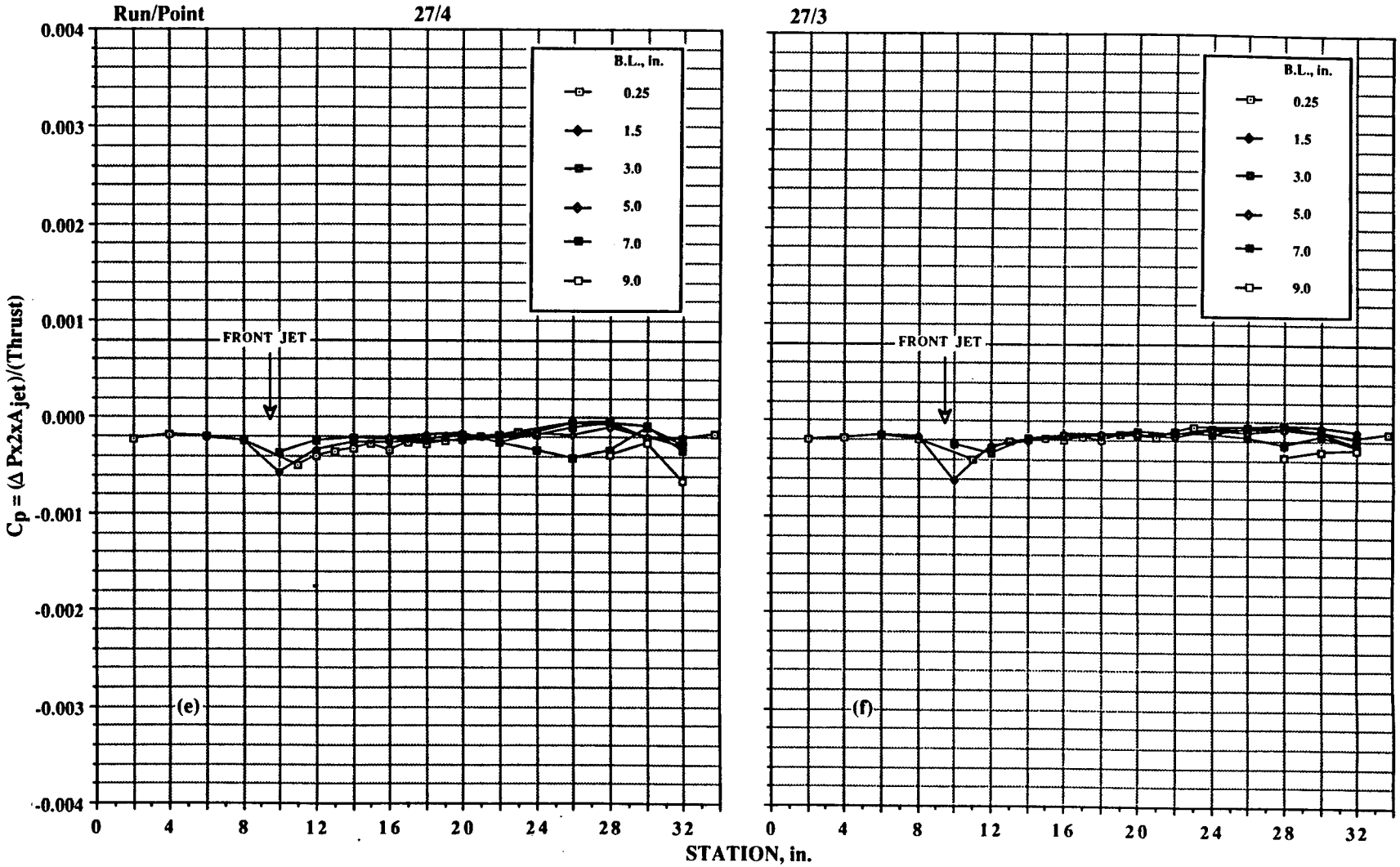

Figure 27. Continued. (e) $h/d_e = 12.20$. (f) $h/d_e = 16.26$.

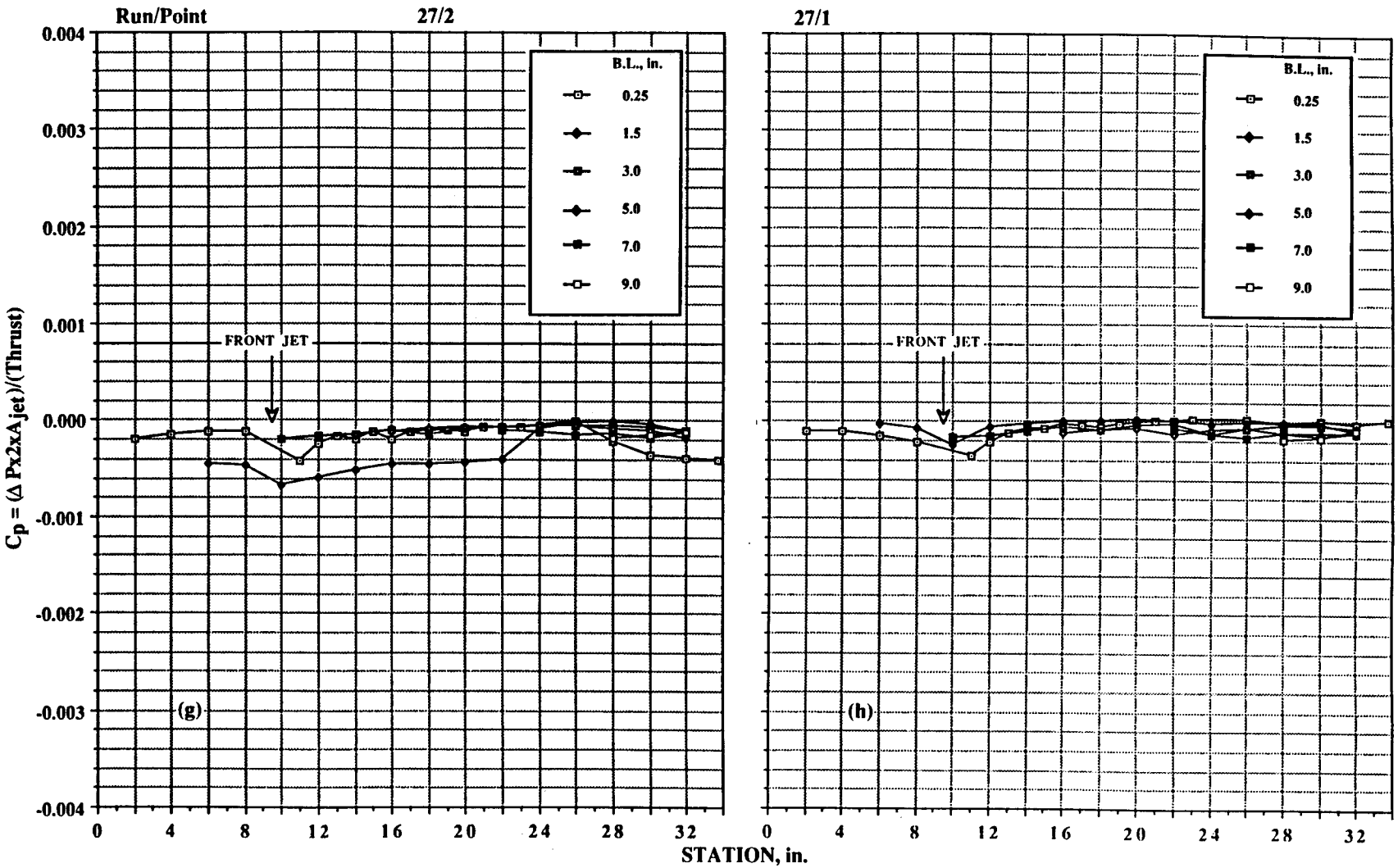

Figure 27. Concluded. (g) $h/d_e = 20.33$. (h) $h/d_e = 32.52$.

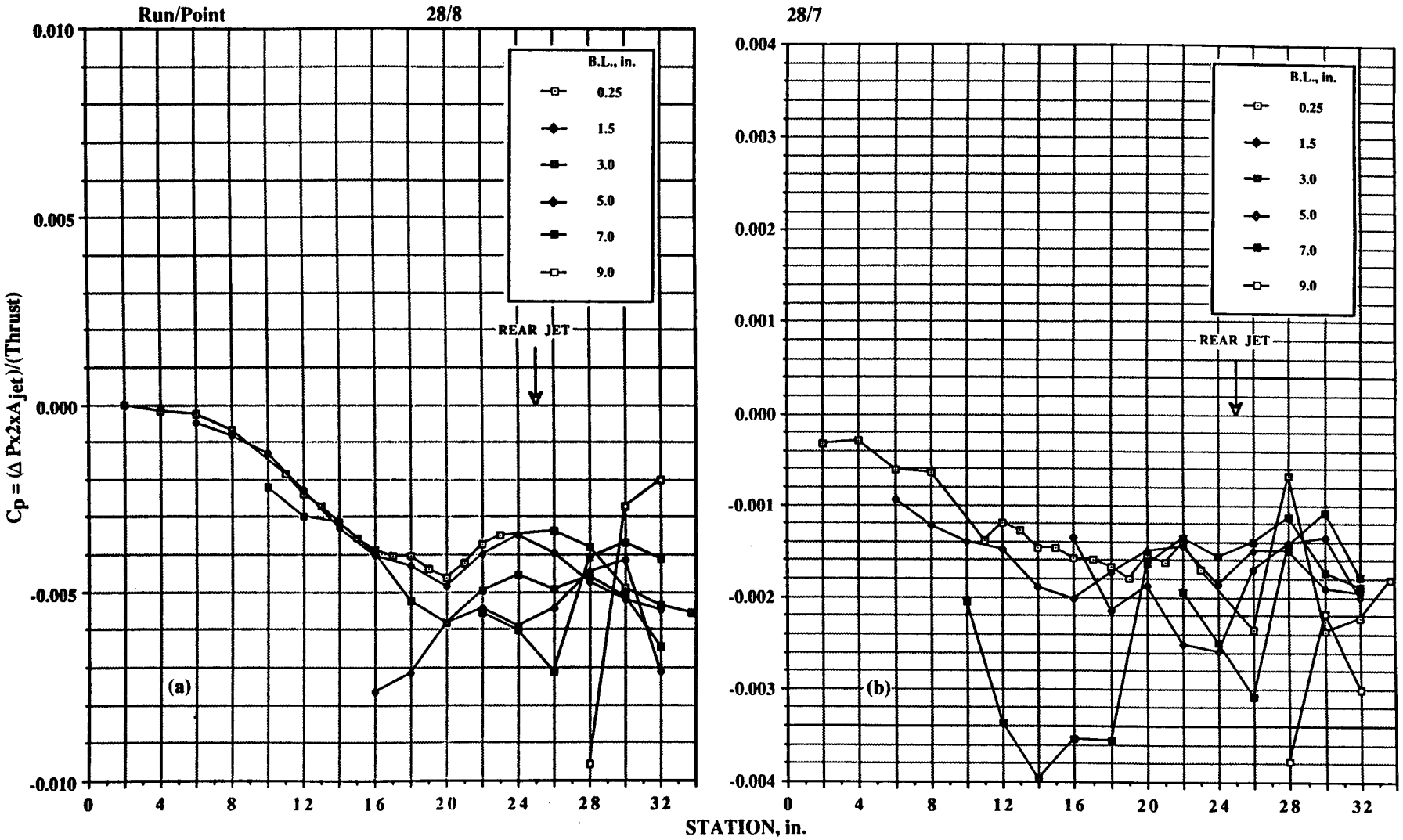

Figure 28. Pressures induced on delta-wing configuration in ground effect; NPR = 2.0, T = 25.5 lb, rear jet only, no LIDs.
(a) $h/d_e = 3.25$. (b) $h/d_e = 4.87$.

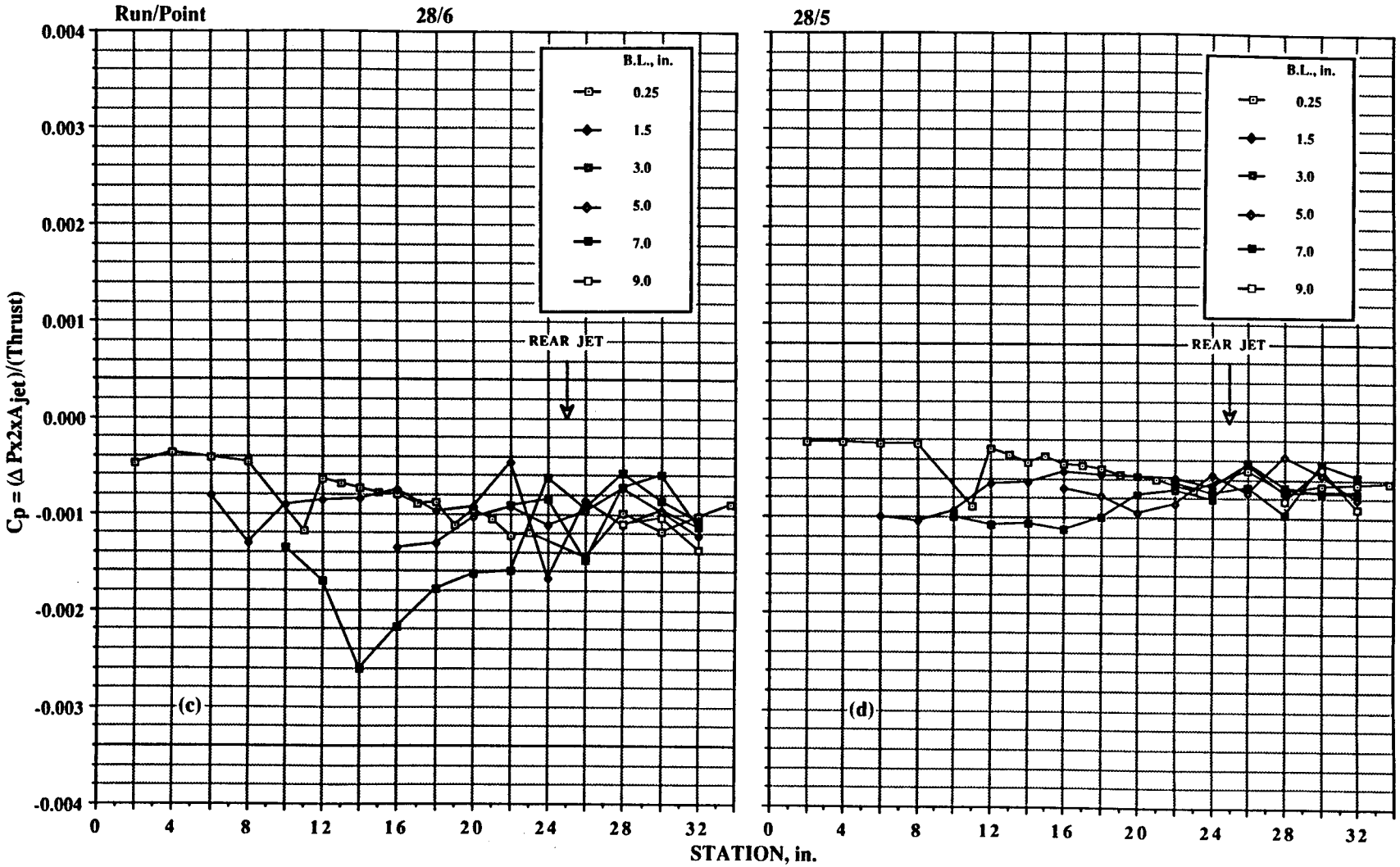

Figure 28. Continued. (c) $h/d_e = 6.50$. (d) $h/d_e = 8.13$.

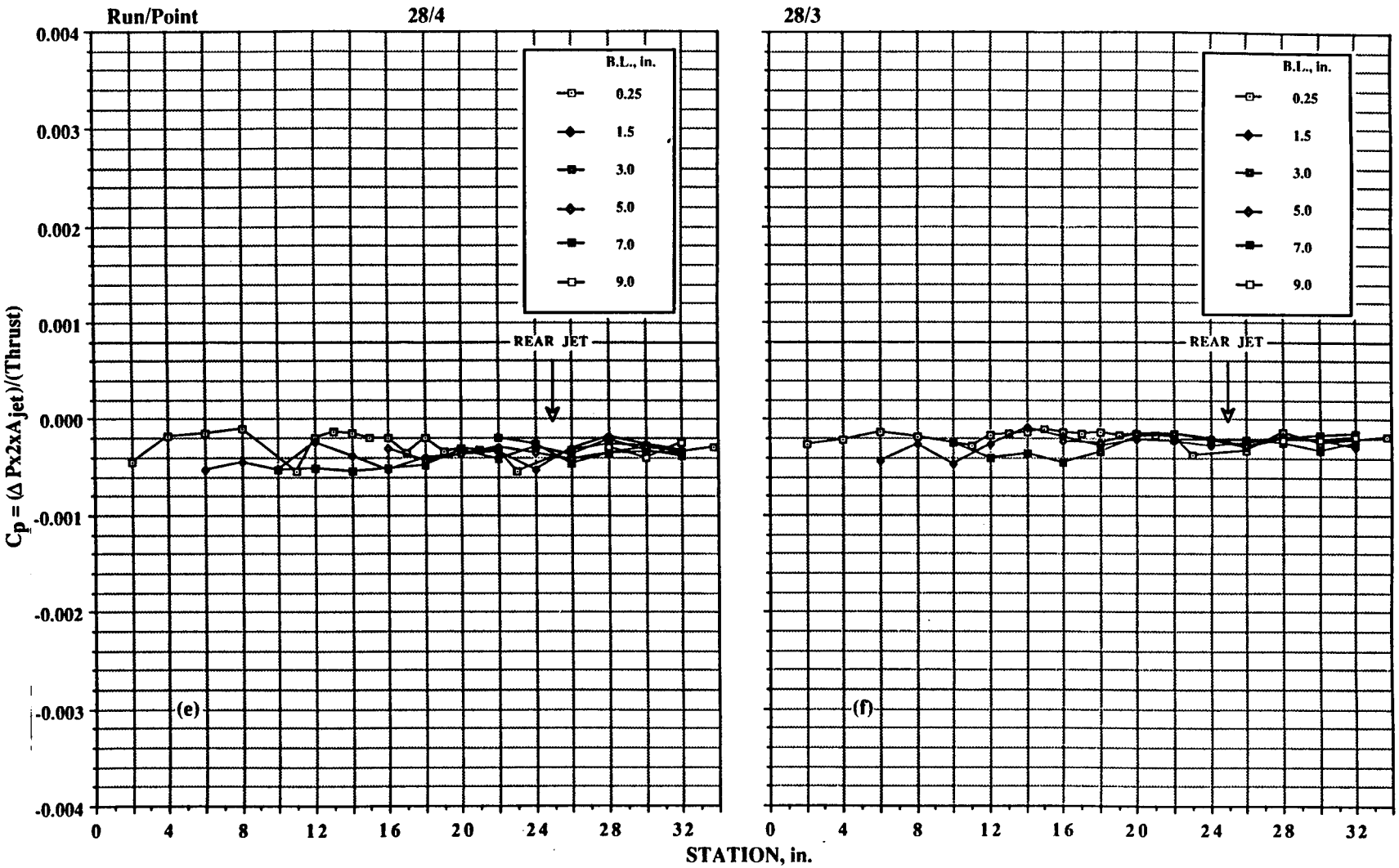

Figure 28. Continued. (e) $h/d_e = 12.20$. (f) $h/d_e = 16.26$.

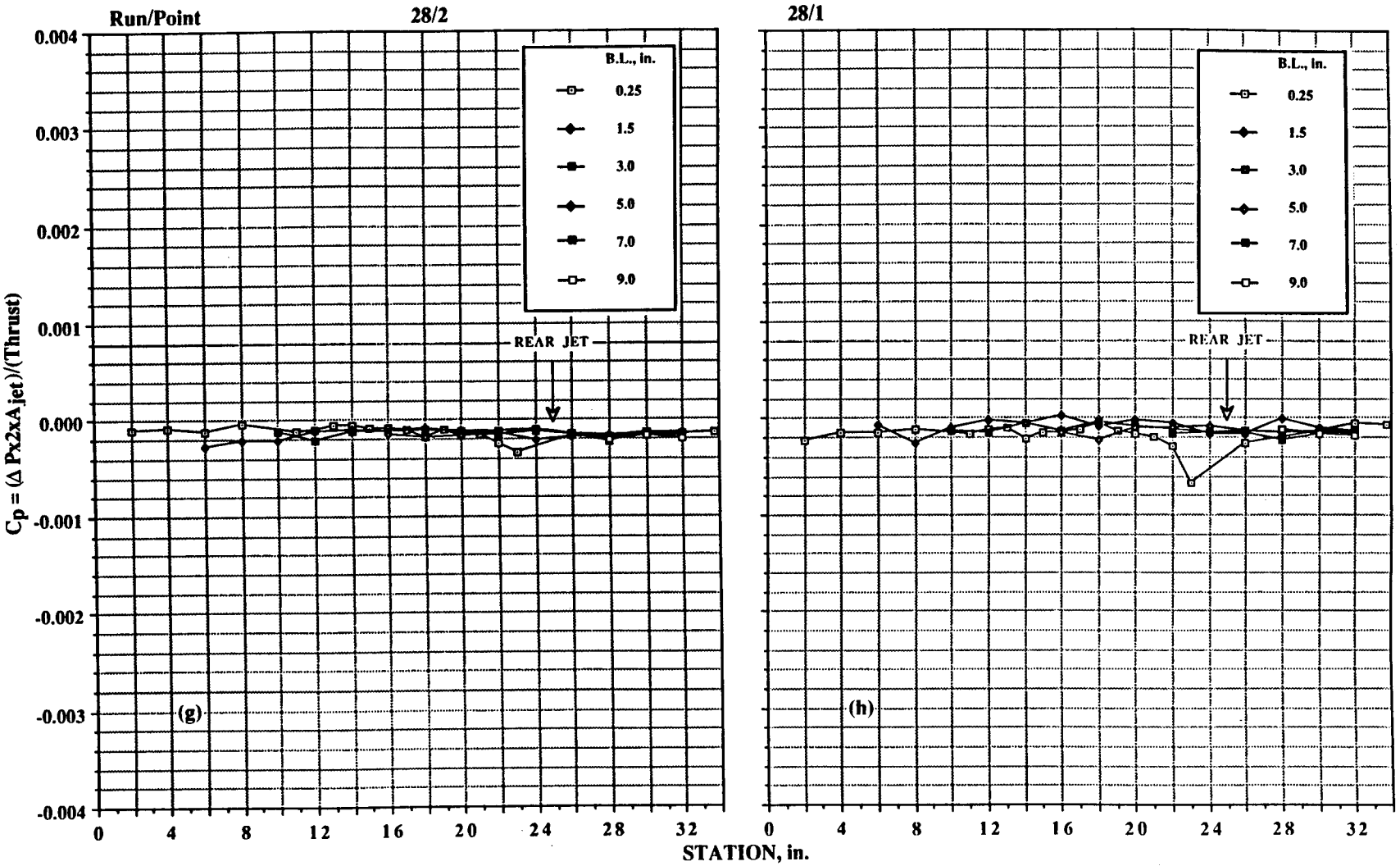

Figure 28. Concluded. (g) $h/d_e = 20.33$. (h) $h/d_e = 32.52$.

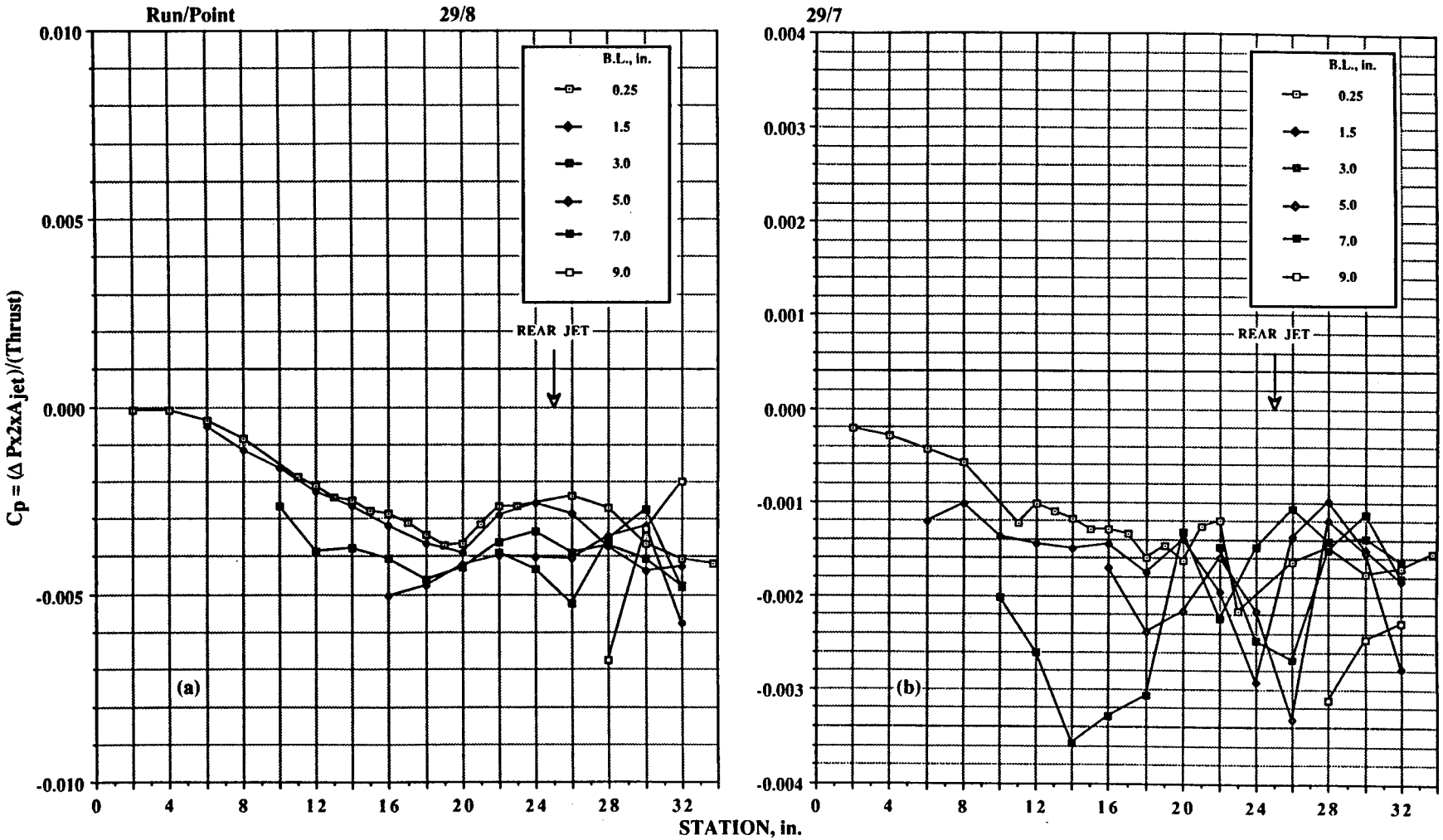

Figure 29. Pressures induced on delta-wing configuration in ground effect; NPR = 4.0, T = 67.5 lb, rear jet only, no LIDs.
(a) $h/d_e = 3.25$. (b) $h/d_e = 4.87$.

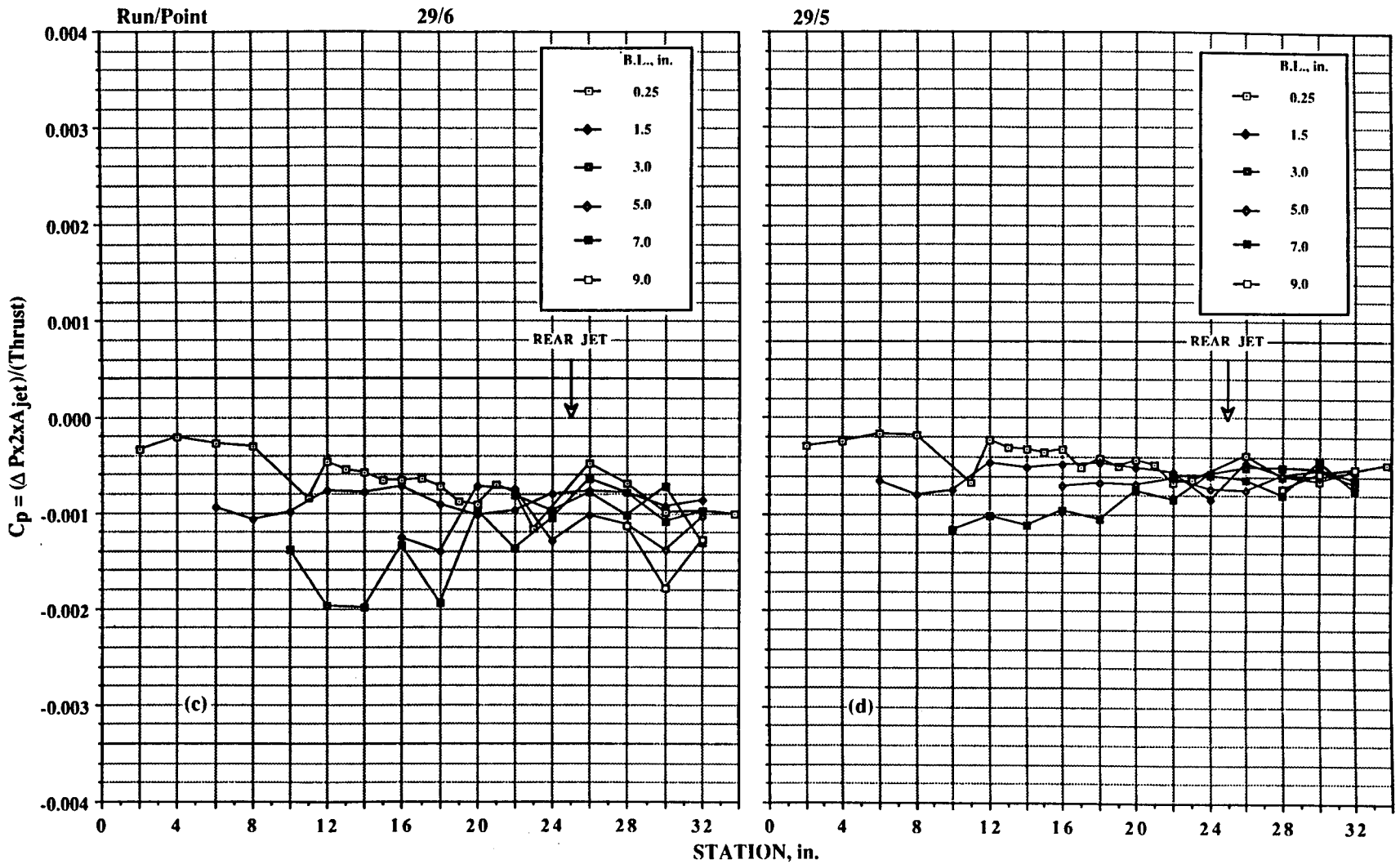

Figure 29. Continued. (c) $h/d_e = 6.50$. (d) $h/d_e = 8.13$.

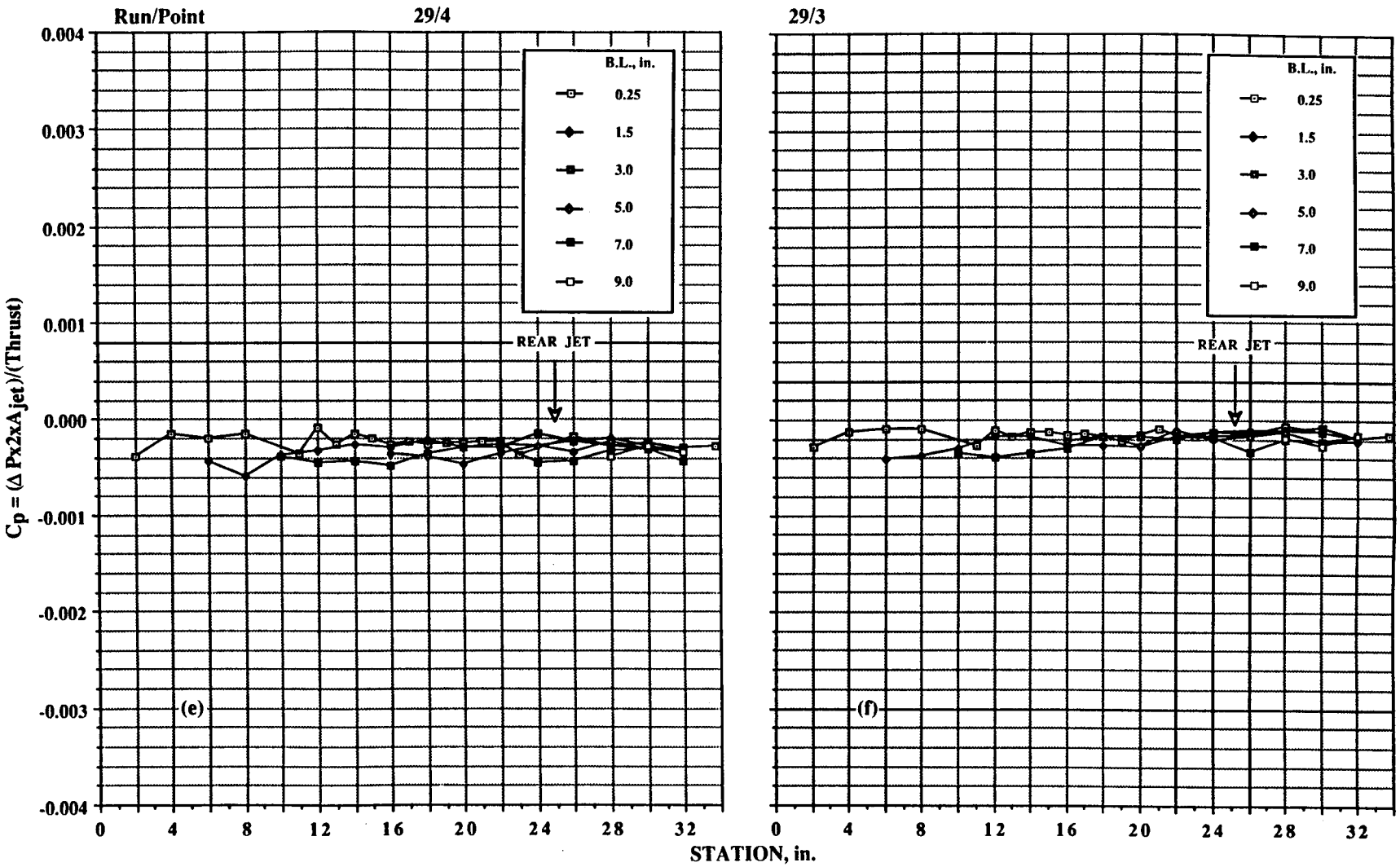

Figure 29. Continued. (e) $h/d_e = 12.20$. (f) $h/d_e = 16.26$.

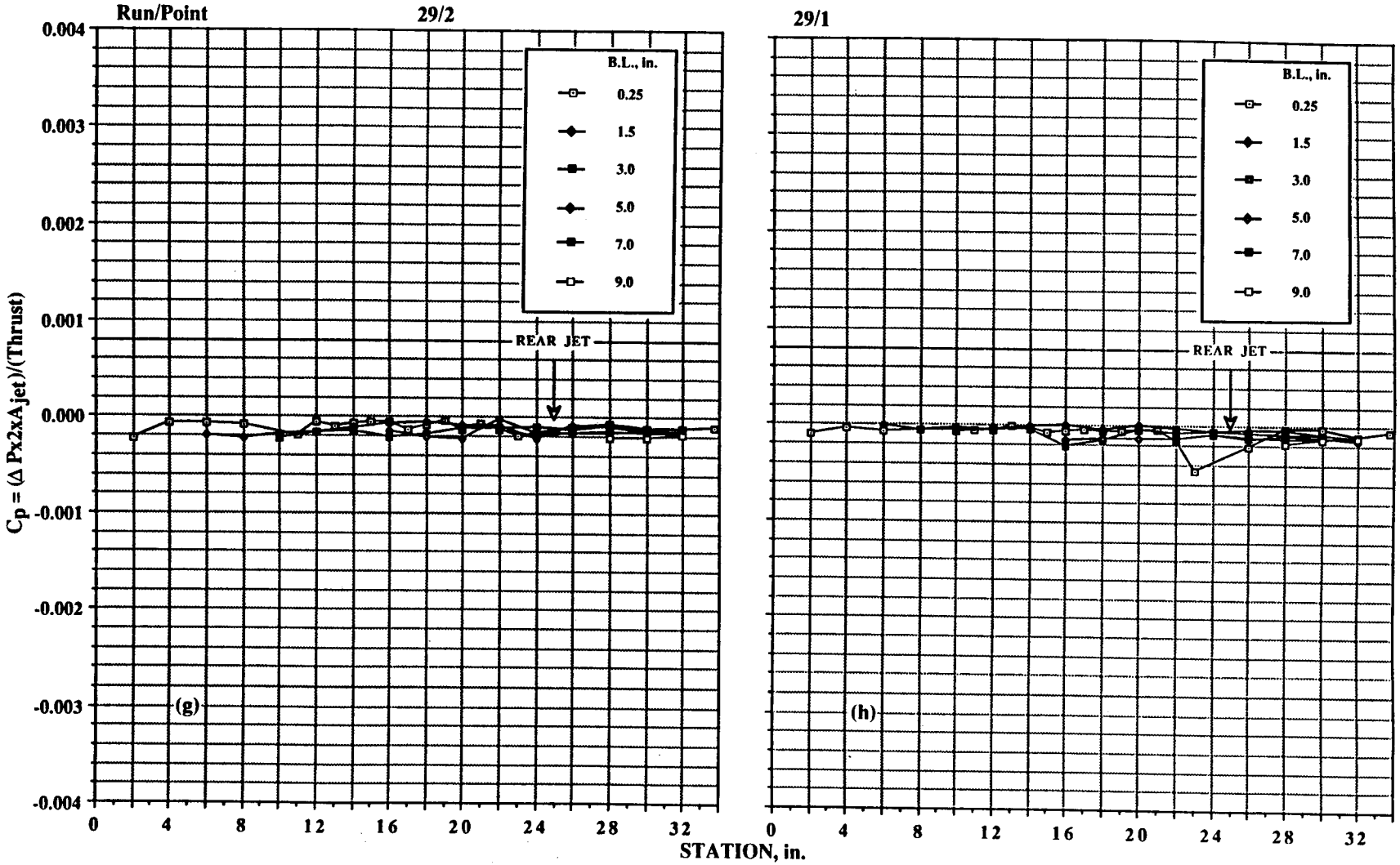

Figure 29. Concluded. (g) $h/d_e = 20.3$. (h) $h/d_e = 32.52$.

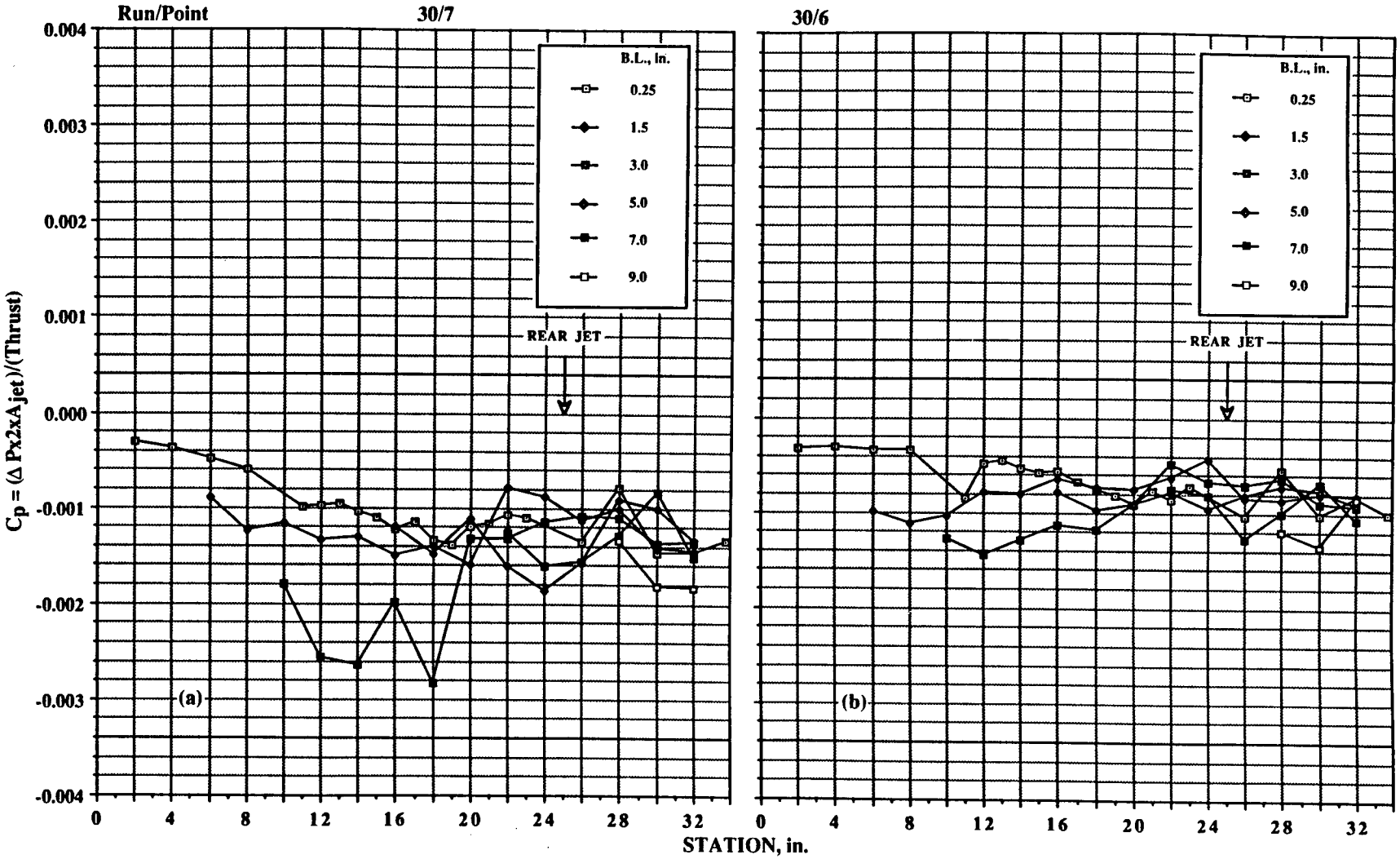

Figure 30. Pressures induced on delta-wing configuration in ground effect; NPR = 6.0, T = 109 lb, rear jet only, no LIDs.
(a) $h/d_e = 4.87$. (b) $h/d_e = 6.50$.

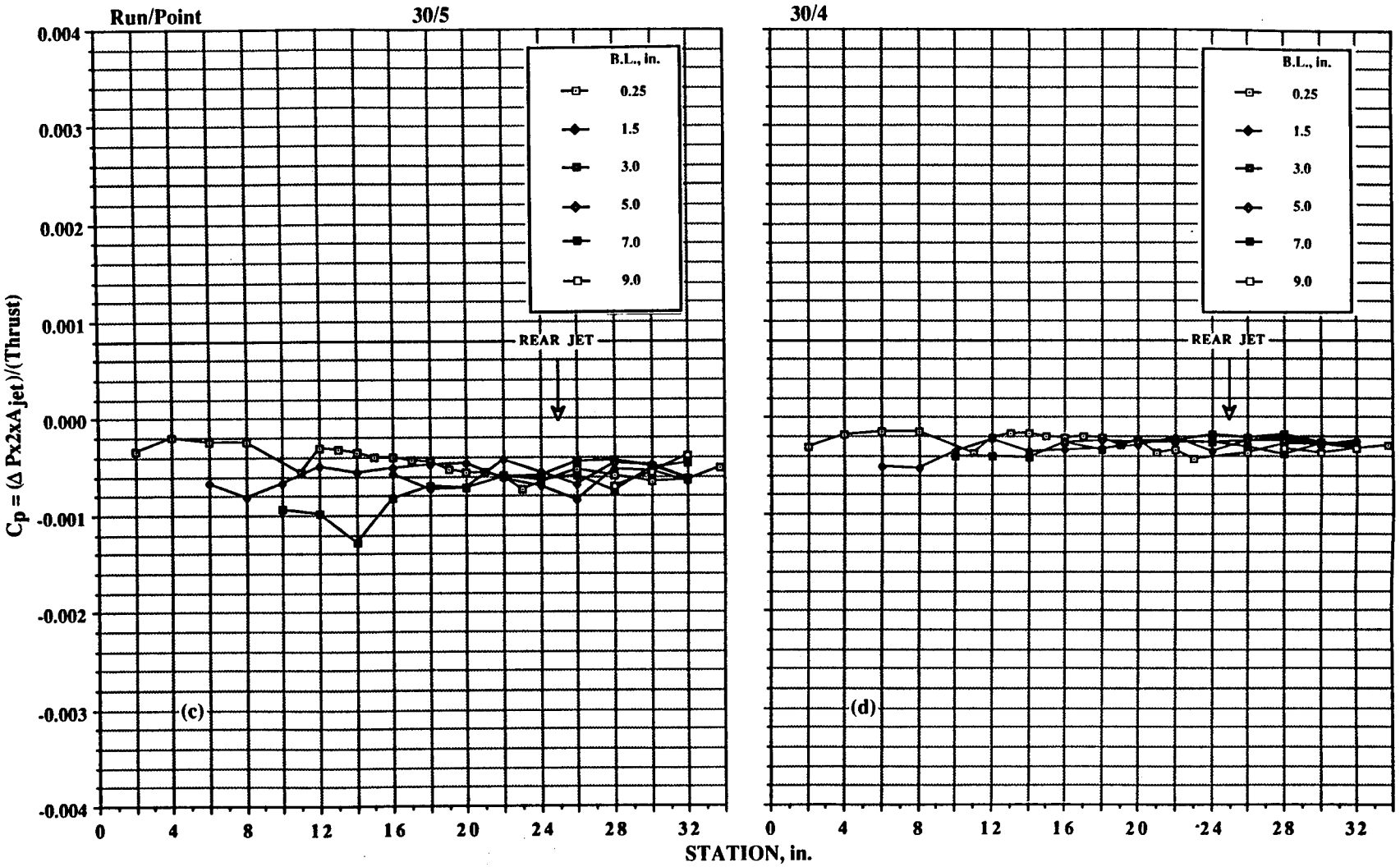

Figure 30. Continued. (c) $h/d_e = 8.13$. (d) $h/d_e = 12.20$.

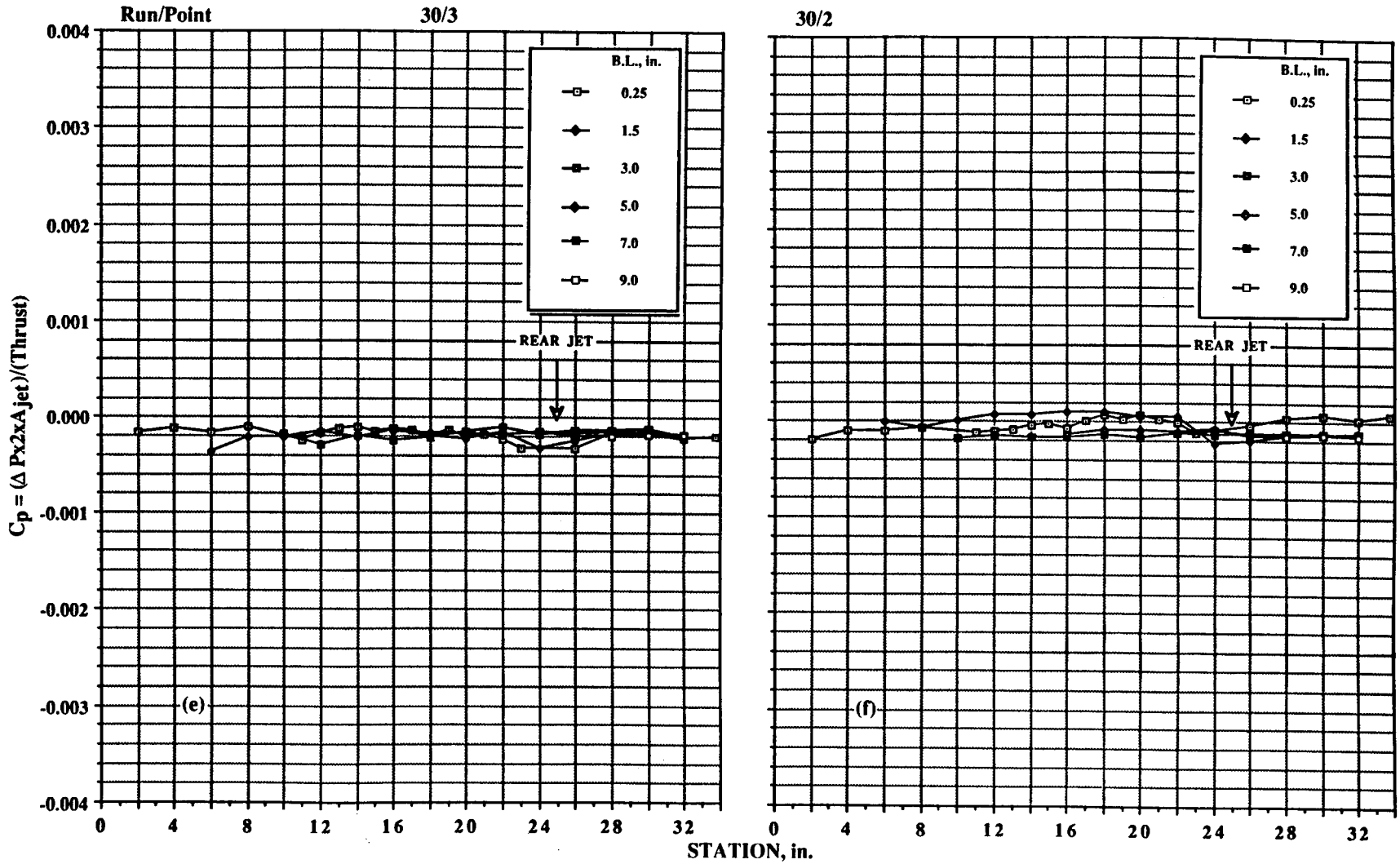

Figure 30. Continued. (e) $h/d_e = 16.26$. (f) $h/d_e = 20.33$.

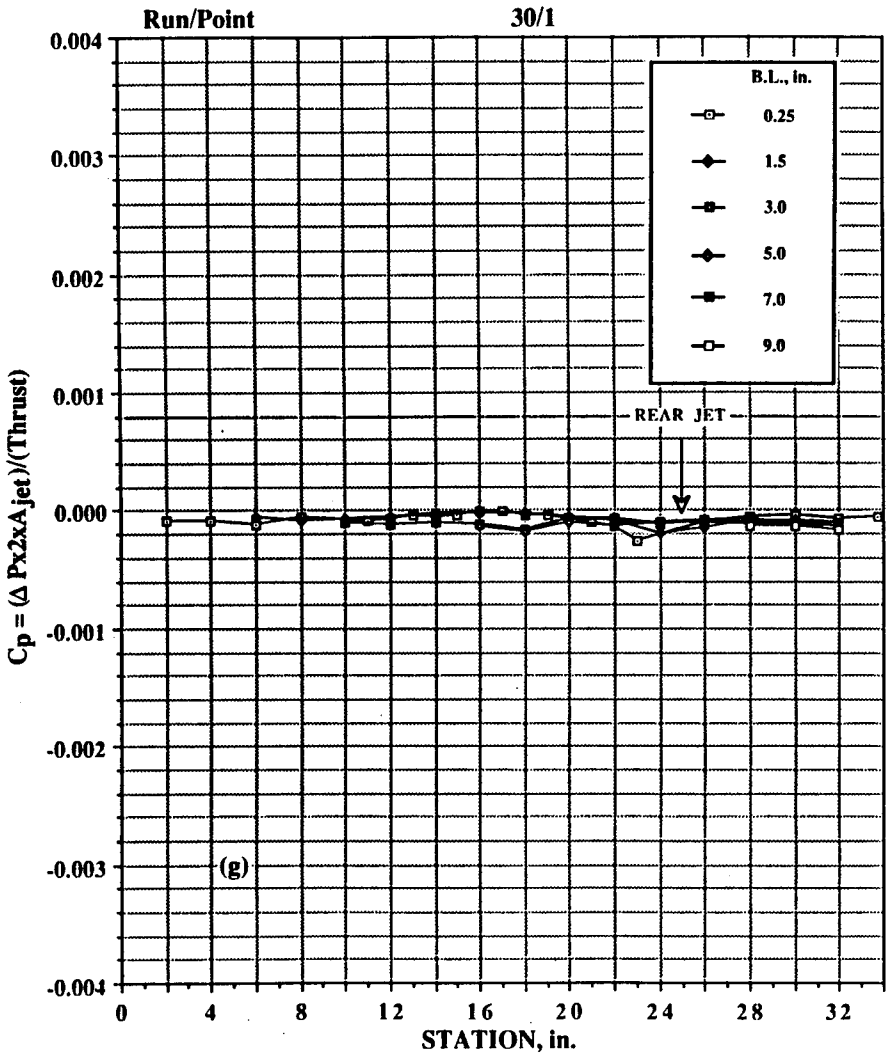

Figure 30. Concluded. (g) $h/d_e = 32.52$.

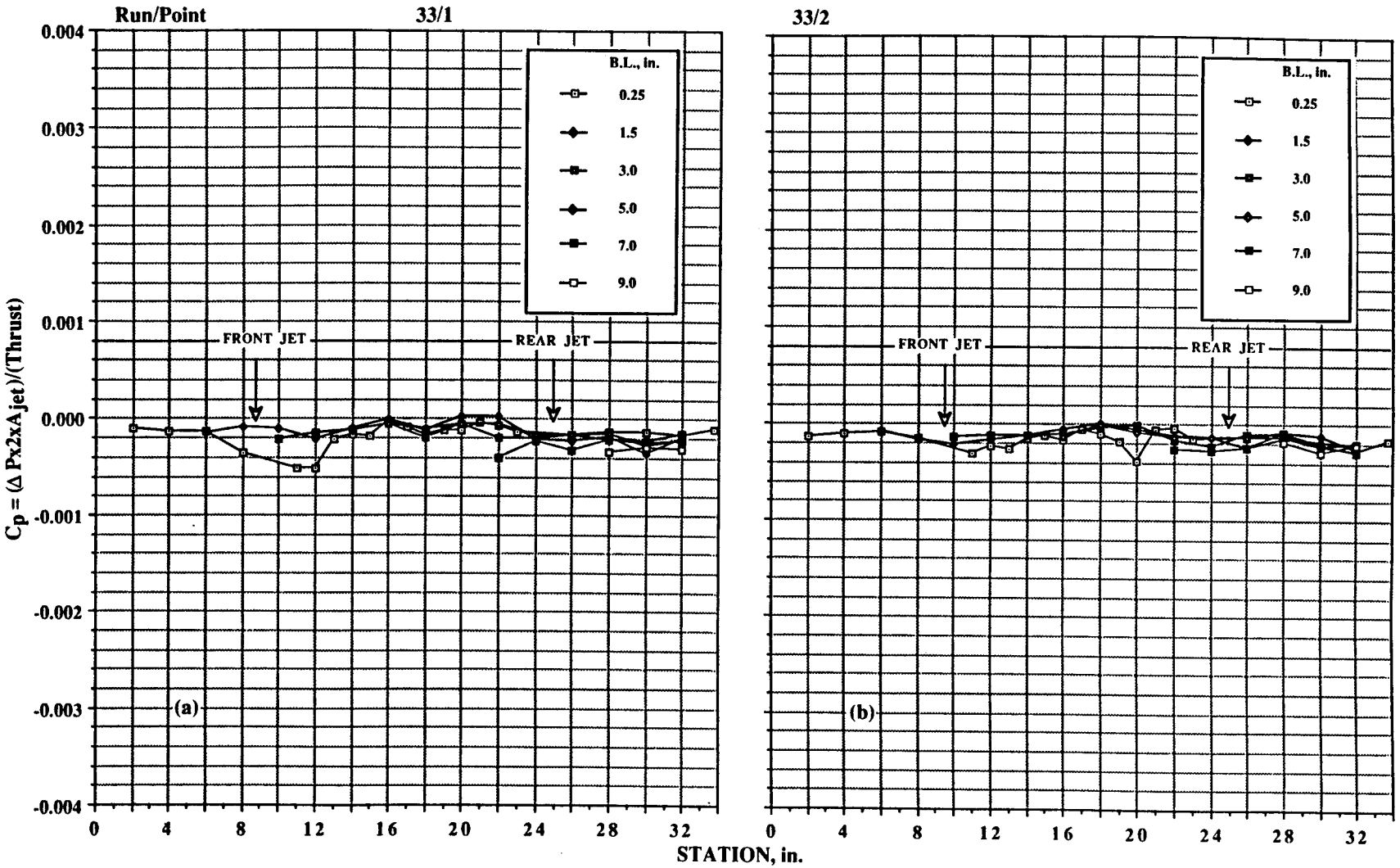

Figure 31. Pressures induced on delta-wing configuration out of ground effect; both jets, no LIDs. (a) NPR = 2. (b) NPR = 3.

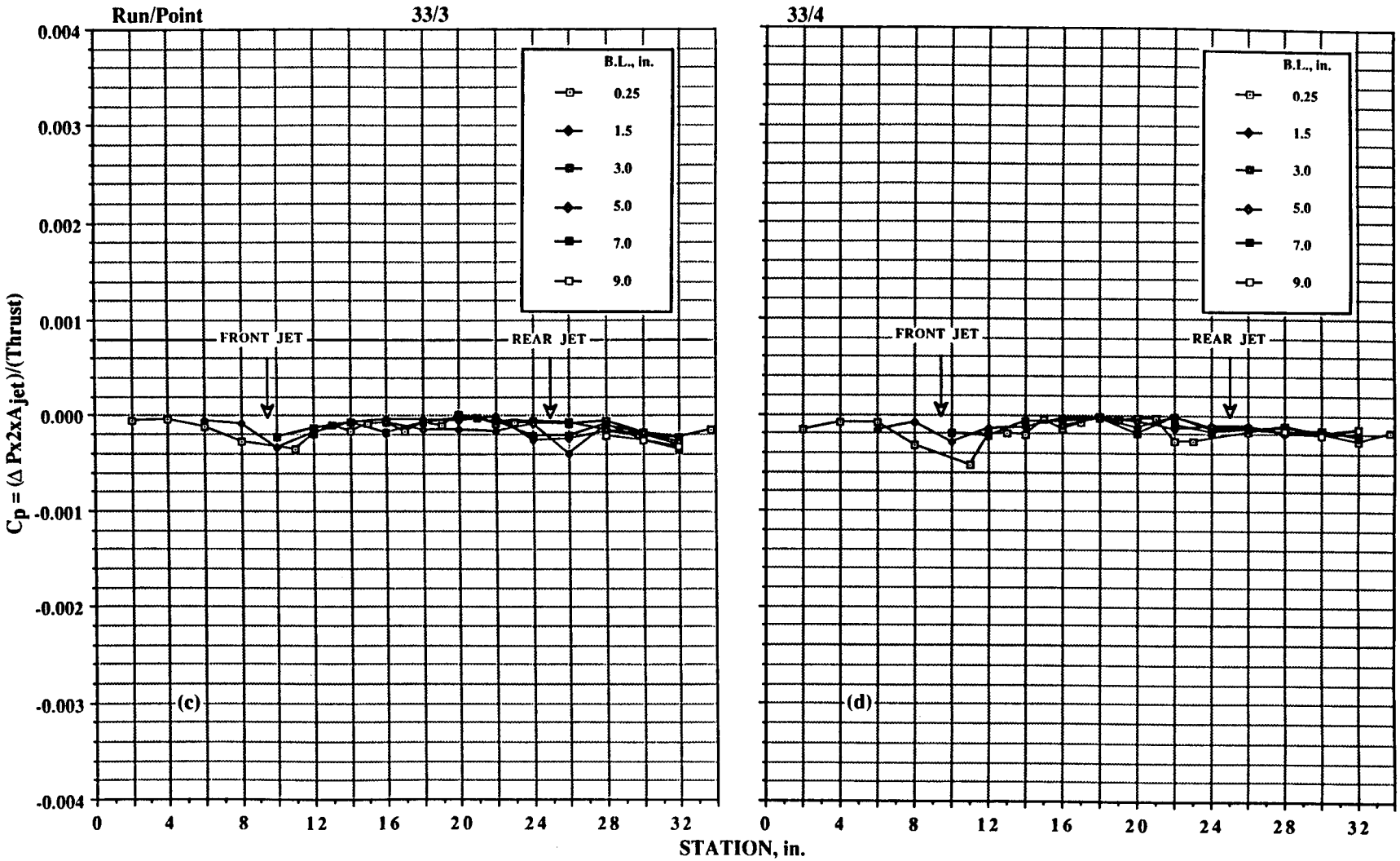

Figure 31. Continued. (c) NPR = 4. (d) NPR = 5.

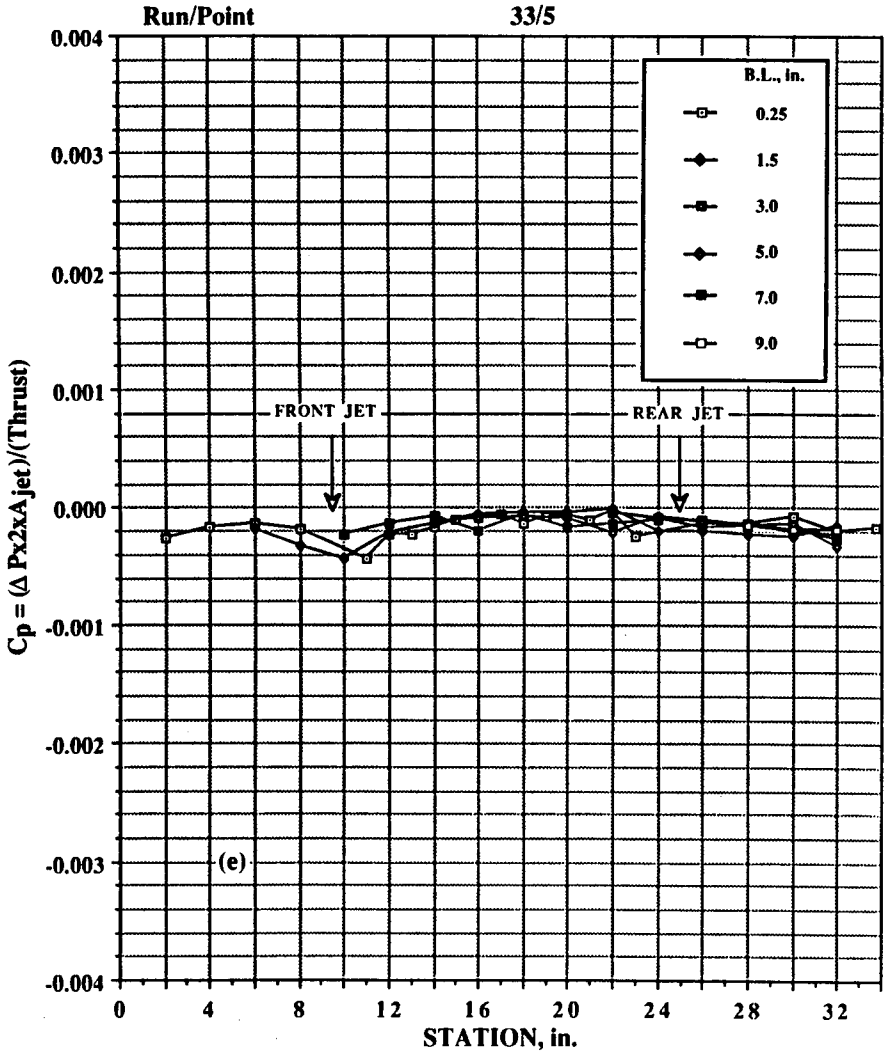

Figure 31. Concluded. (e) NPR = 6.

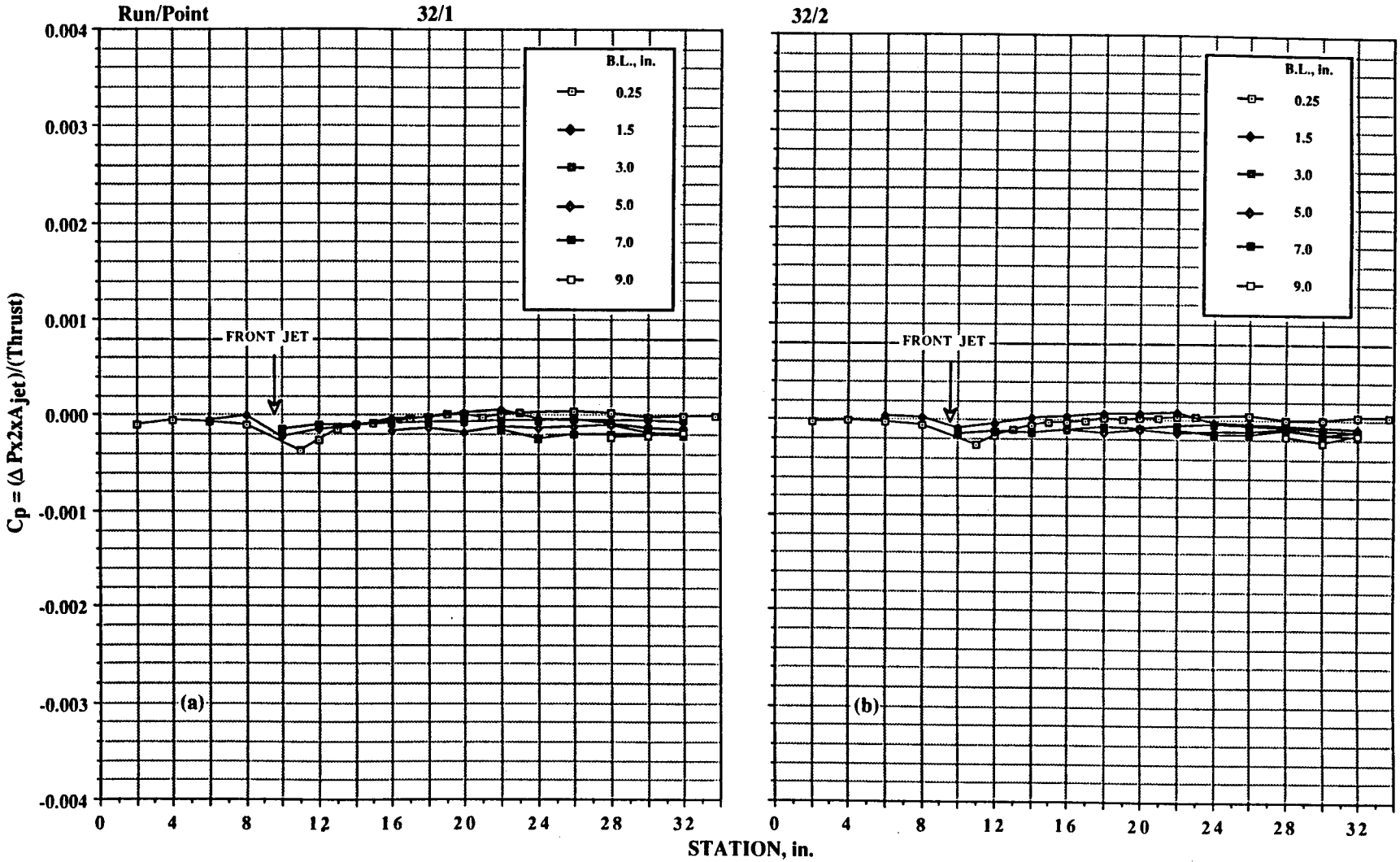

Figure 32. Pressures induced on delta-wing configuration out of ground effect; front jet only, no LIDs. (a) NPR = 2. (b) NPR = 3.

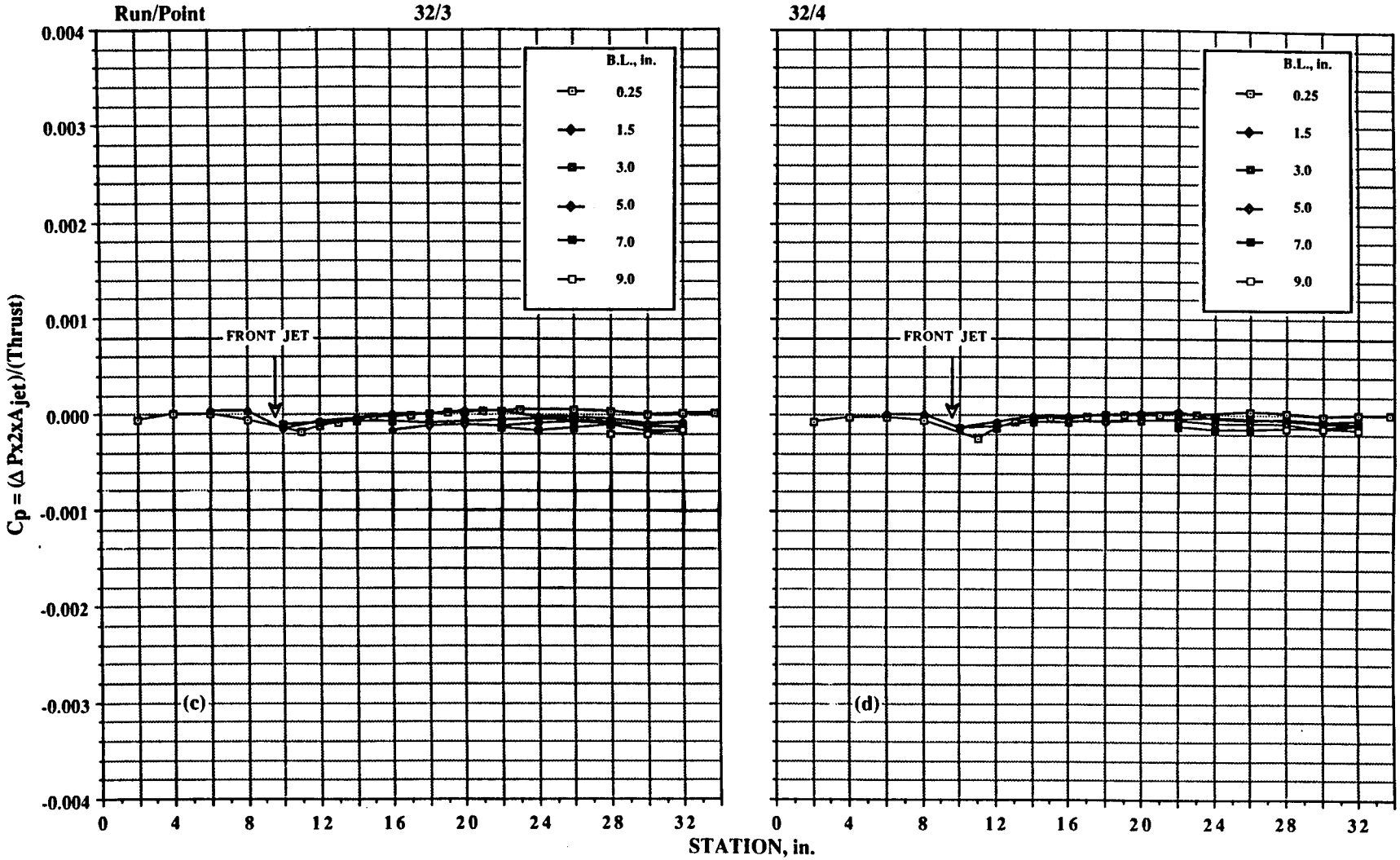

Figure 32. Continued. (c) NPR = 4. (d) NPR = 5.

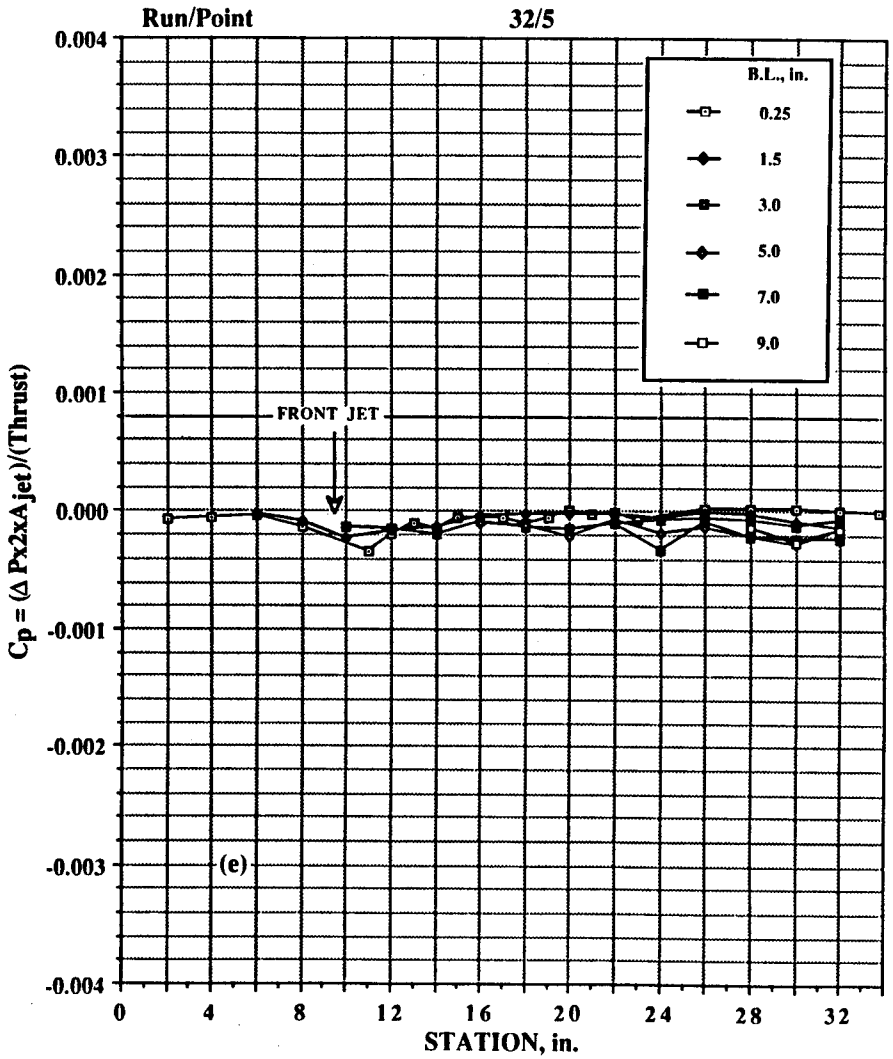

Figure 32. Concluded. (e) NPR = 6.

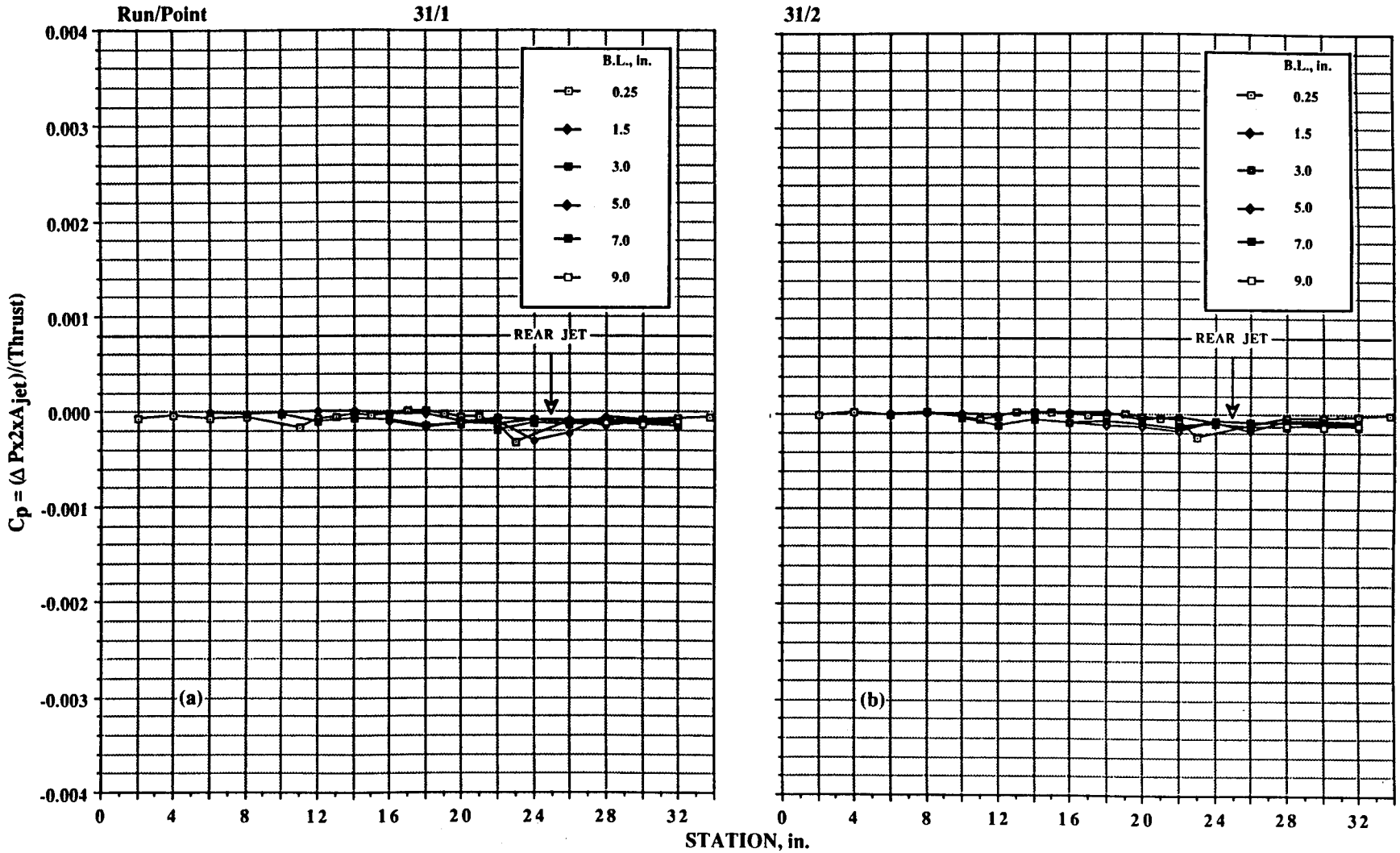

Figure 33. Pressures induced on delta-wing configuration out of ground effect; rear jet alone, no LIDs. (a) NPR = 2. (b) NPR = 3.

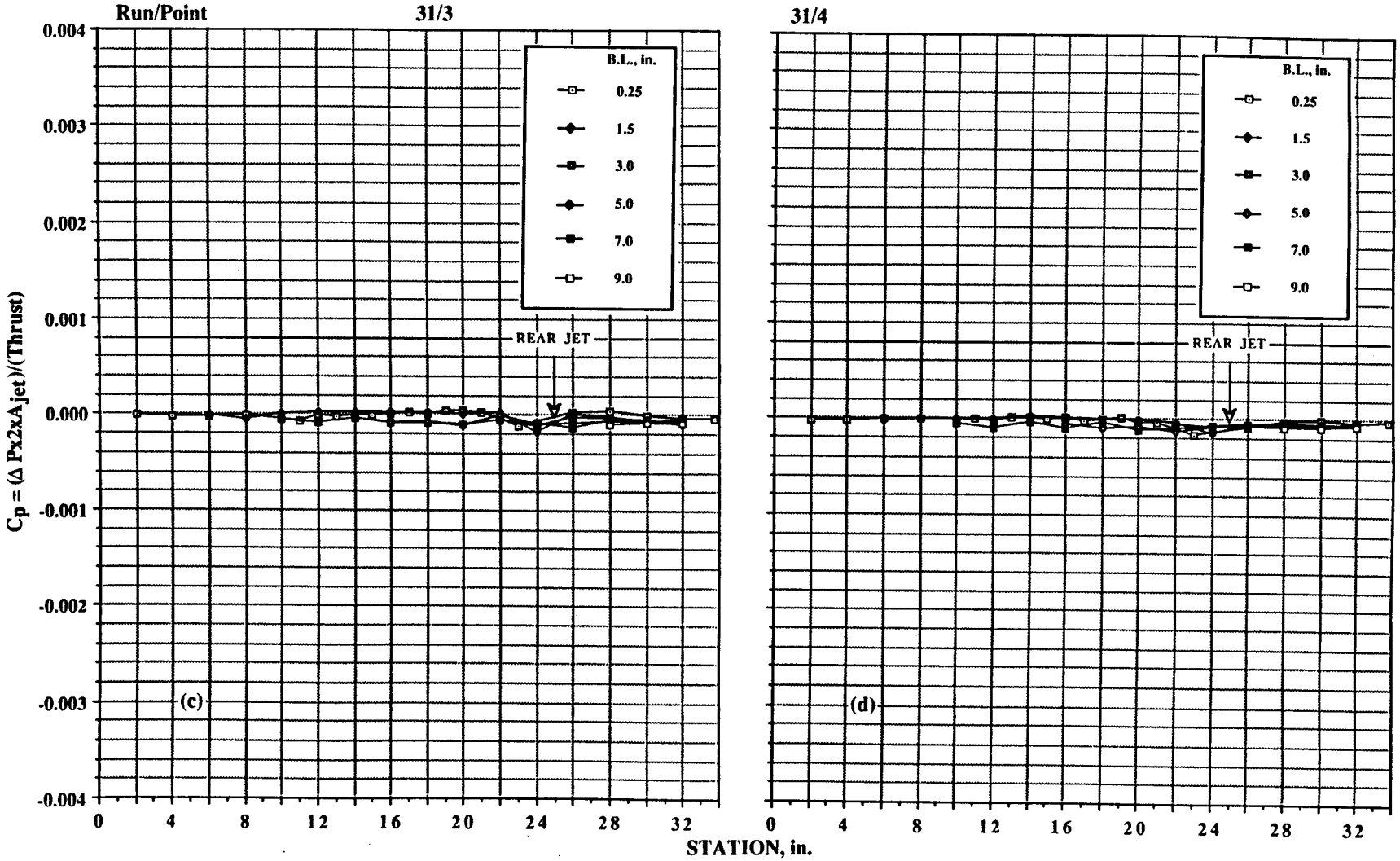

Figure 33. Continued. (c) NPR = 4. (d) NPR = 5.

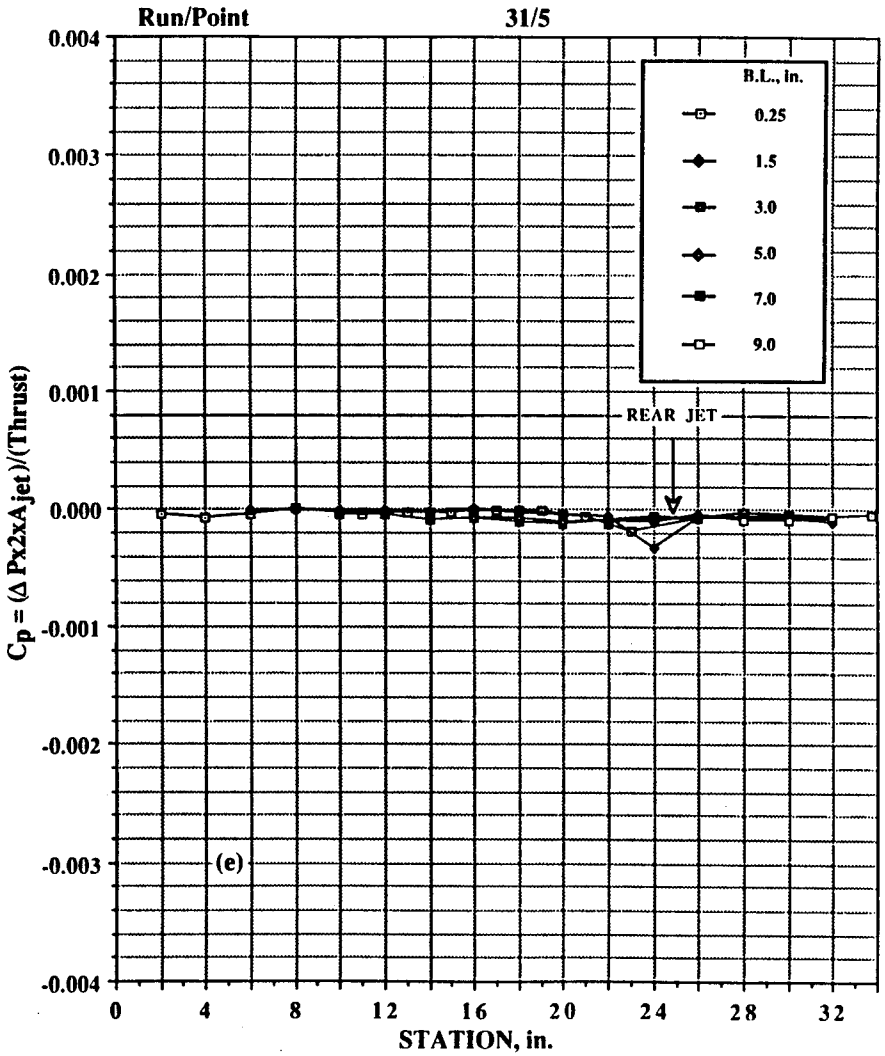

Figure 33. Concluded. (e) NPR = 6.

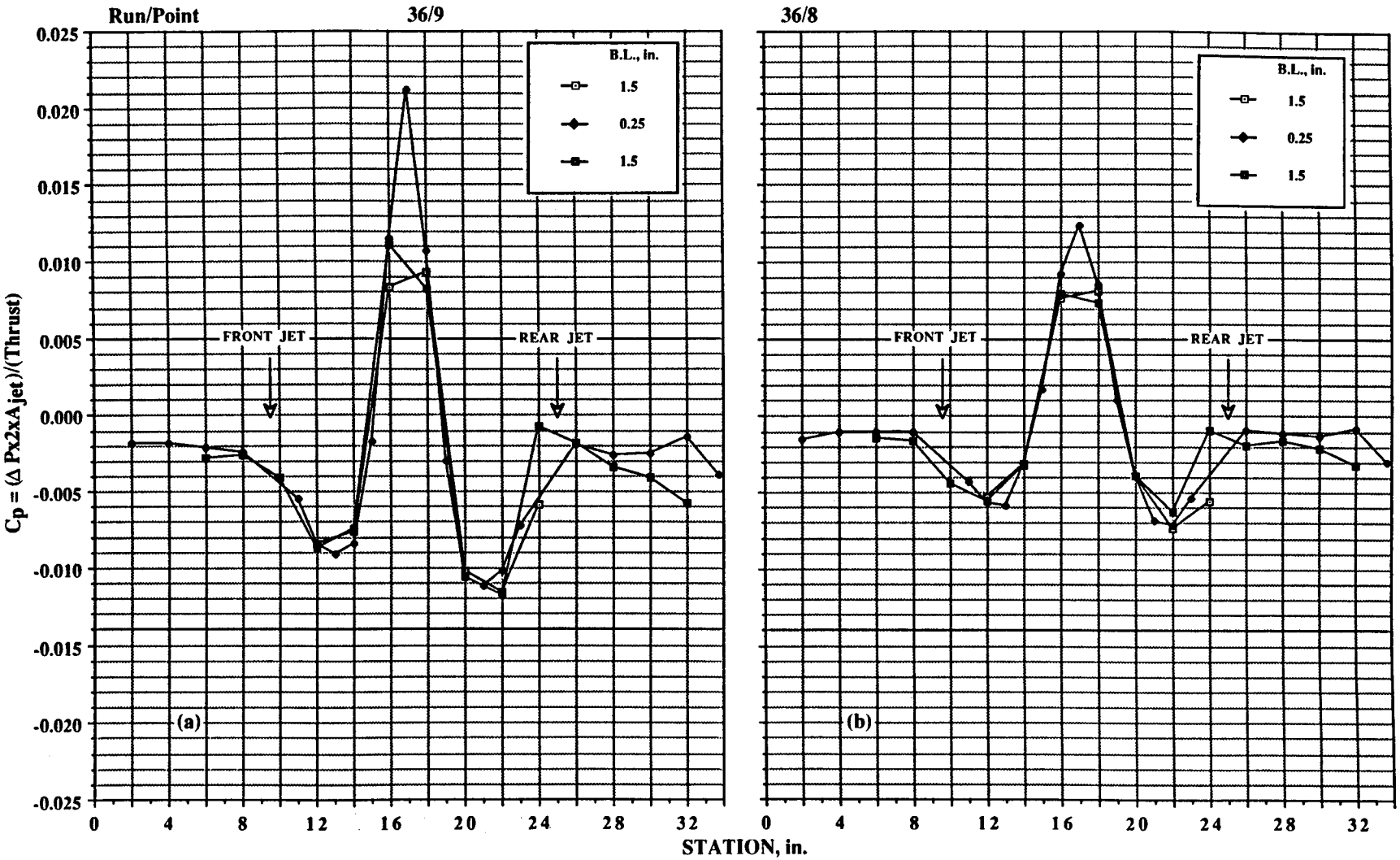

Figure 34. Pressures induced on body-alone configuration in ground effect; NPR = 2.0, T = 51 lb, both jets, no LIDs. (a) $h/d_e = 2.3$. (b) $h/d_e = 3.45$.

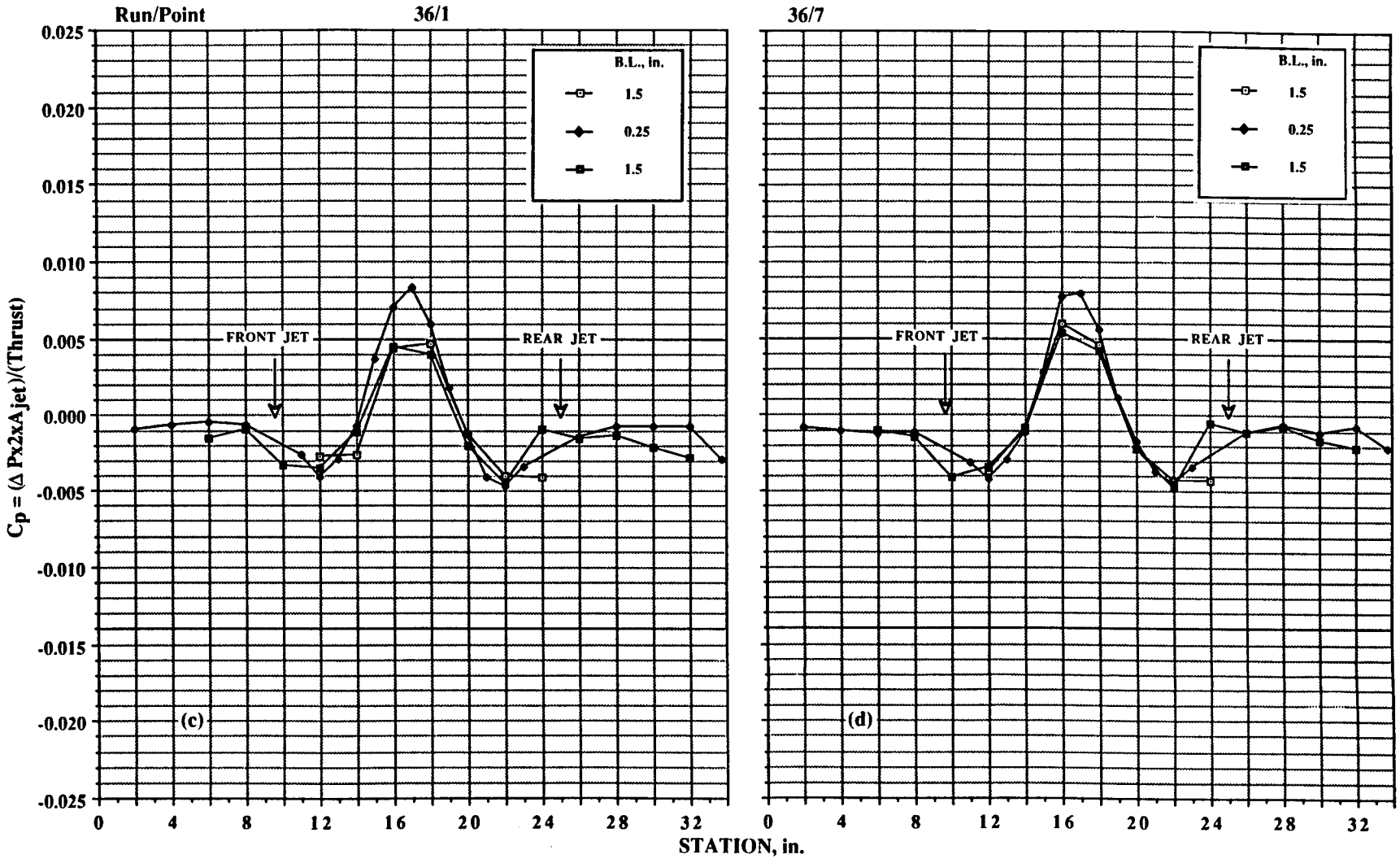

Figure 34. Continued. (c) $h/d_e = 4.6$. (d) $h/d_e = 4.6$ (repeat).

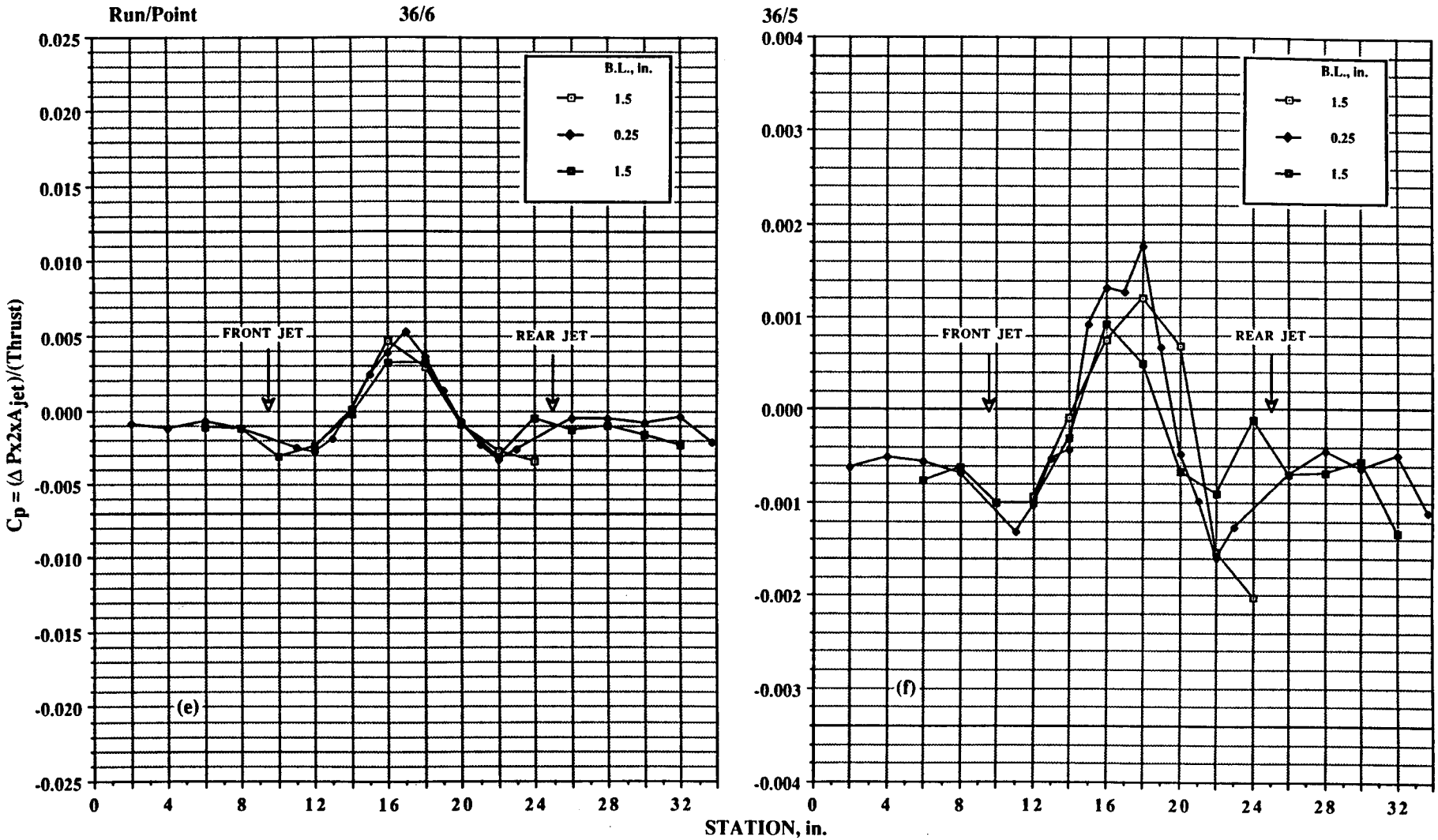

Figure 34. Continued. (e) $h/d_e = 5.75$. (f) $h/d_e = 8.62$.

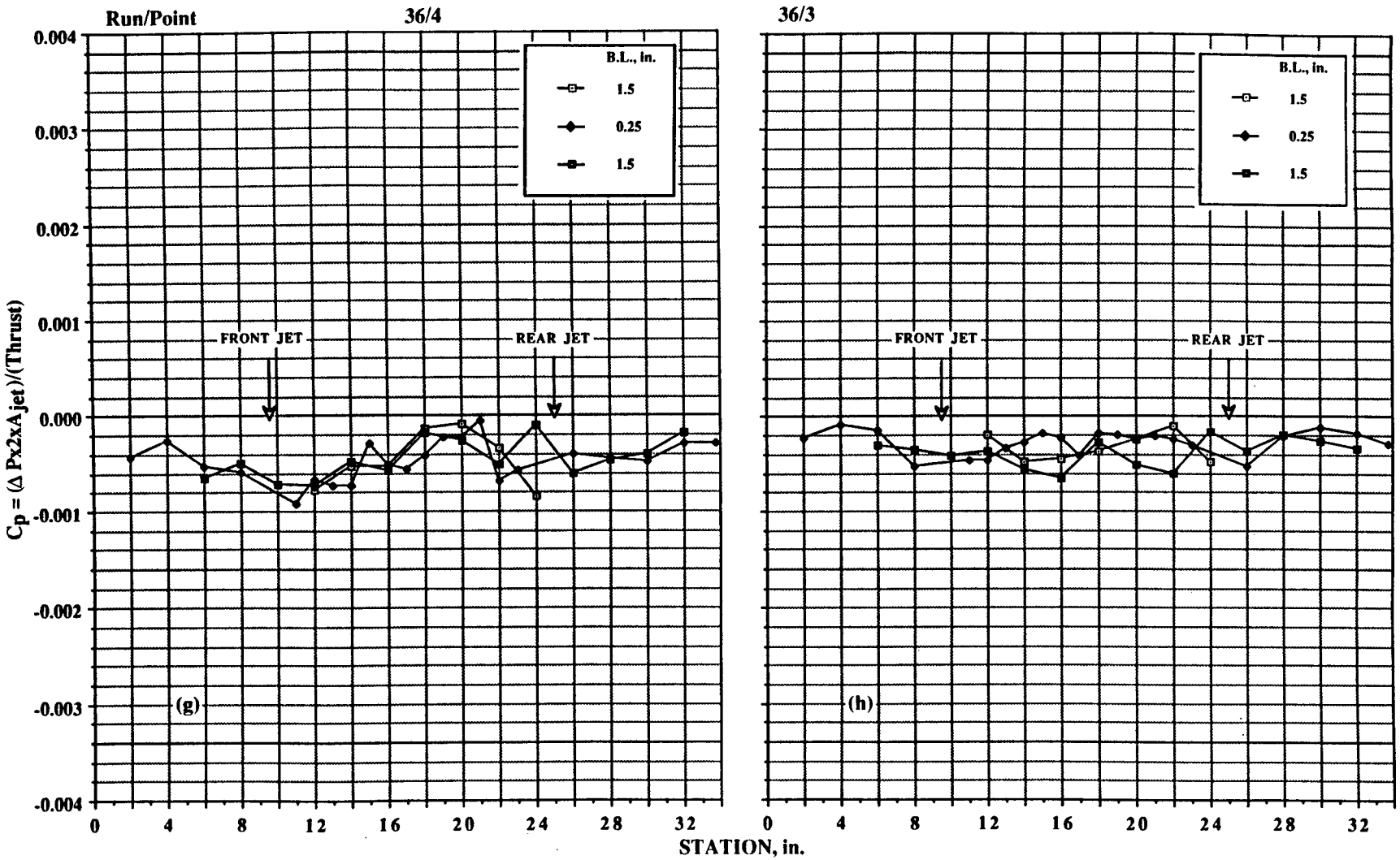

Figure 34. Continued. (g) $h/d_e = 11.5$. (h) $h/d_e = 14.37$.

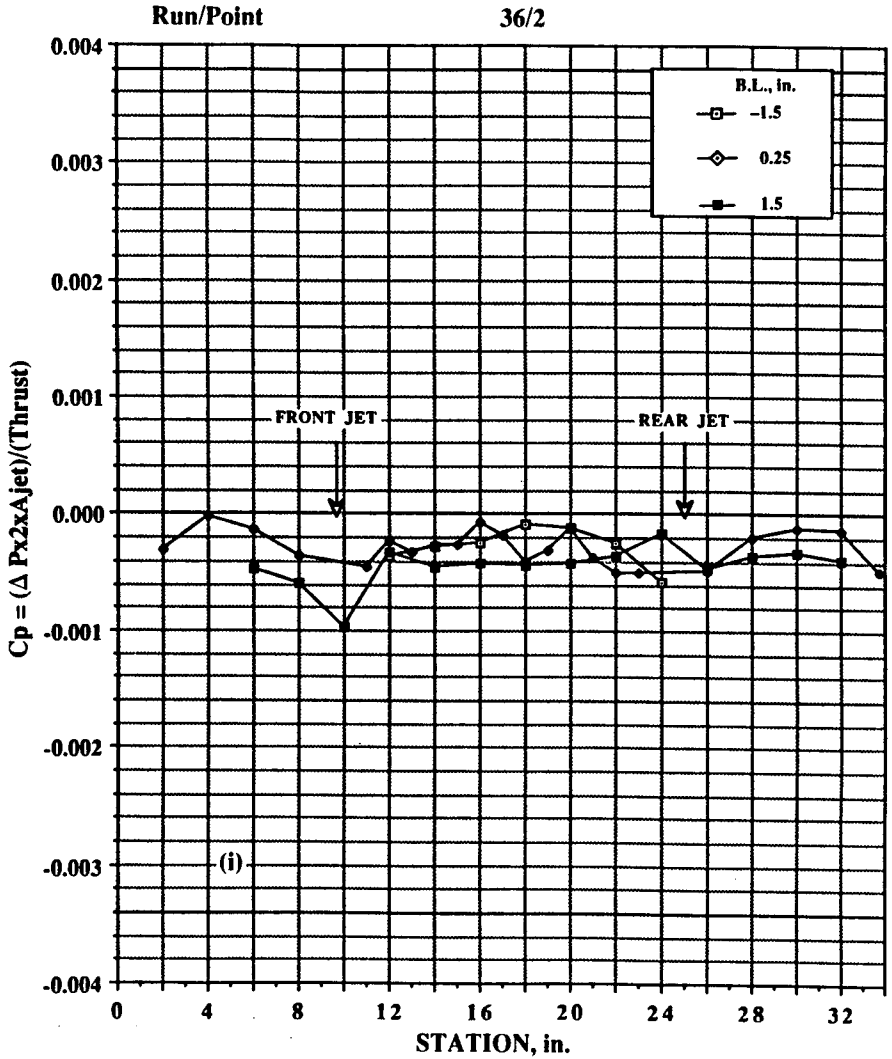

Figure 34. Concluded. (i) $h/d_e = 23.0$.

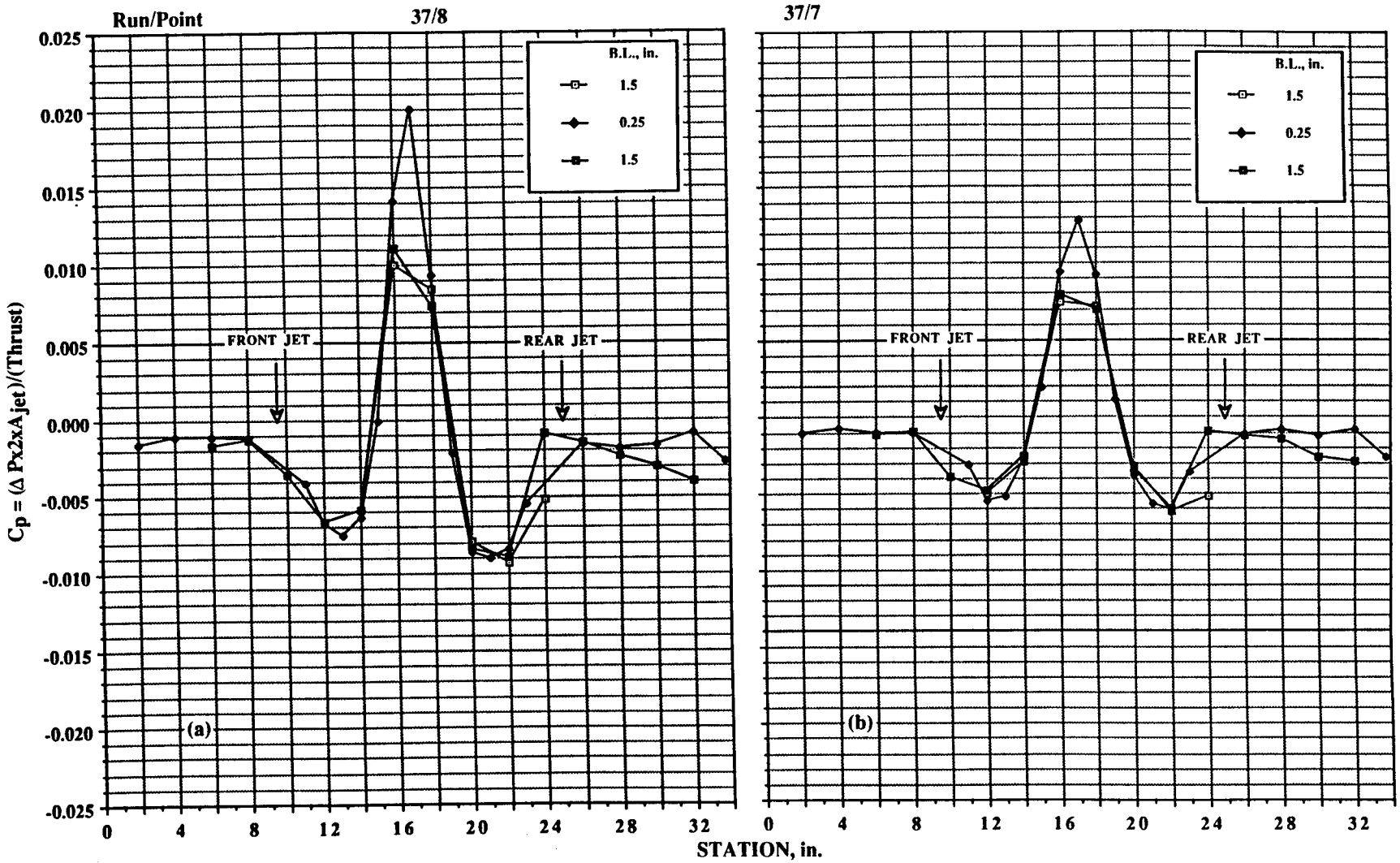

Figure 35. Pressures induced on body-alone configuration in ground effect; NPR = 4.0, T = 135 lb, both jets, no LIDs. (a) $h/d_e = 2.3$. (b) $h/d_e = 3.45$.

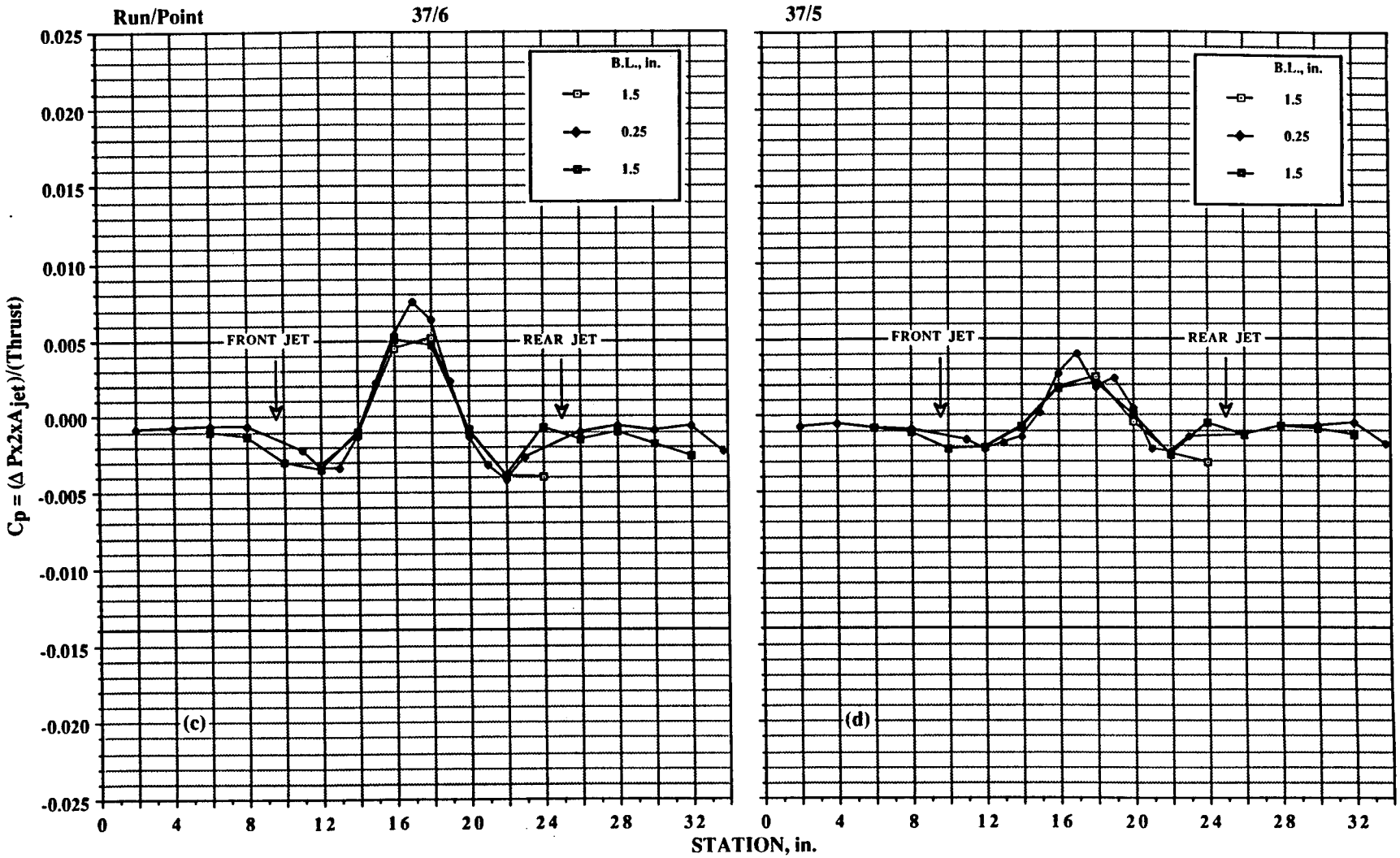

Figure 35. Continued. (c) $h/d_e = 4.6$. (d) $h/d_e = 5.75$.

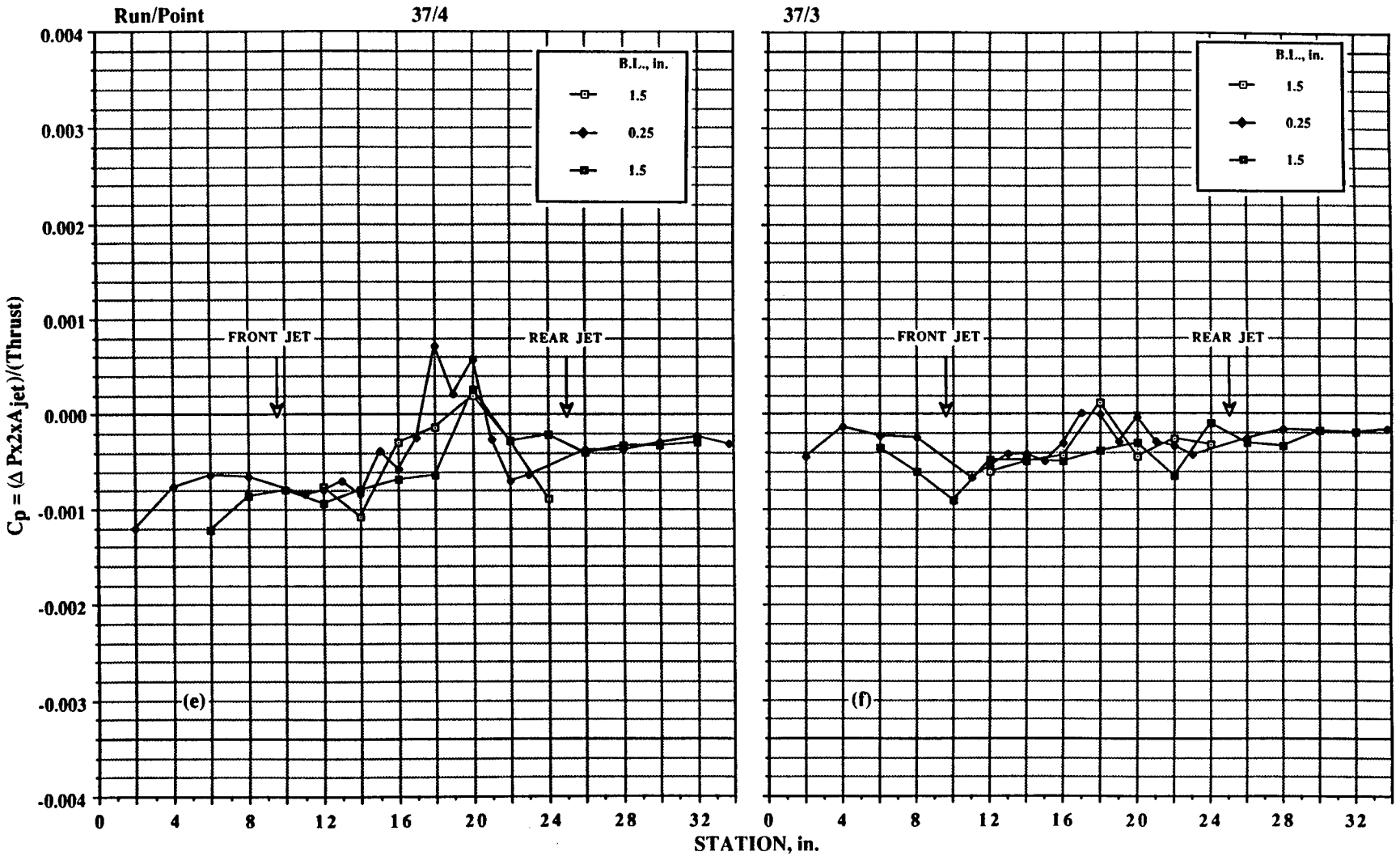

Figure 35. Continued. (e) $h/d_e = 8.62$. (f) $h/d_e = 11.5$.

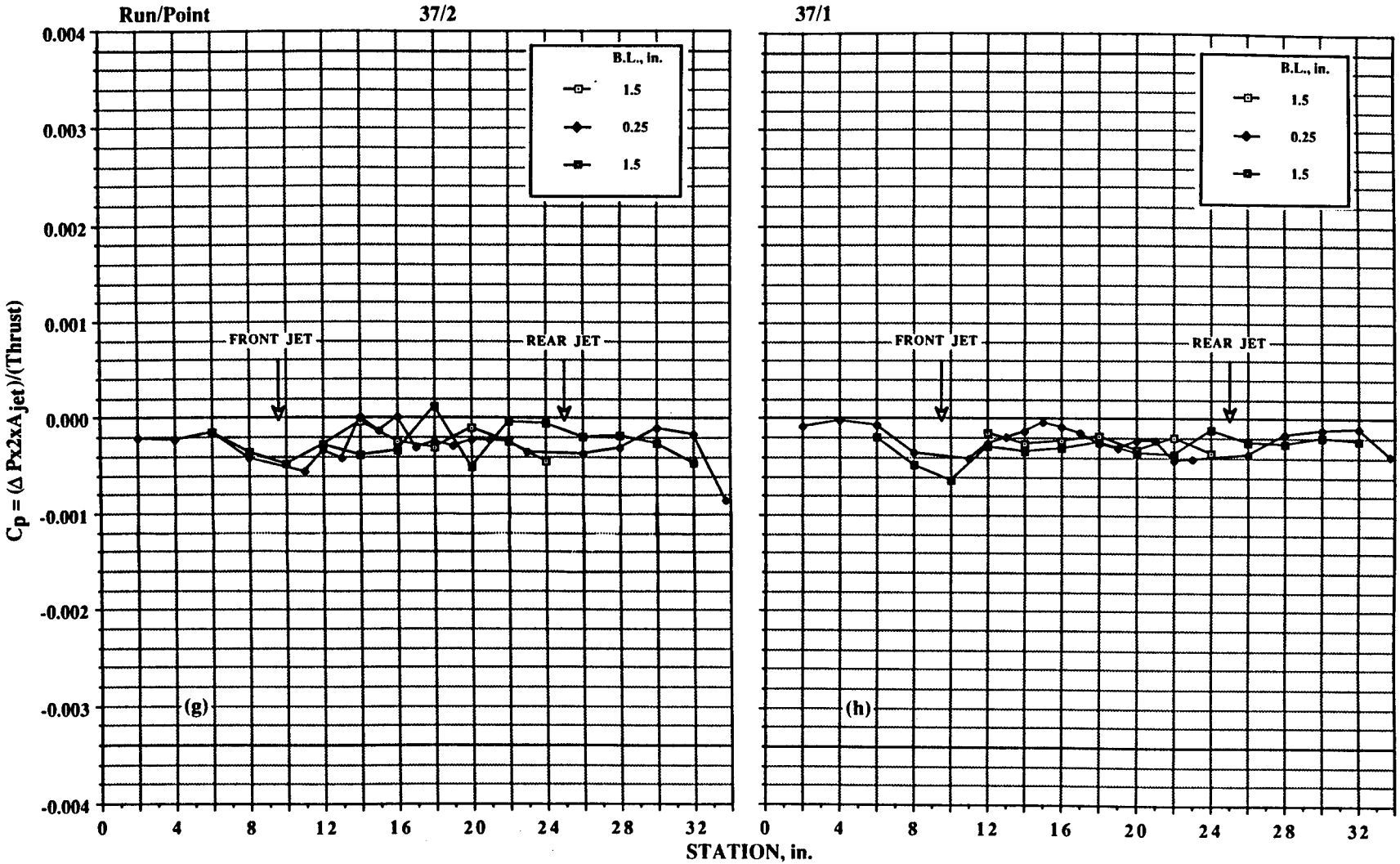

Figure 35. Concluded. (g) $h/d_e = 14.37$. (h) $h/d_e = 23.0$.

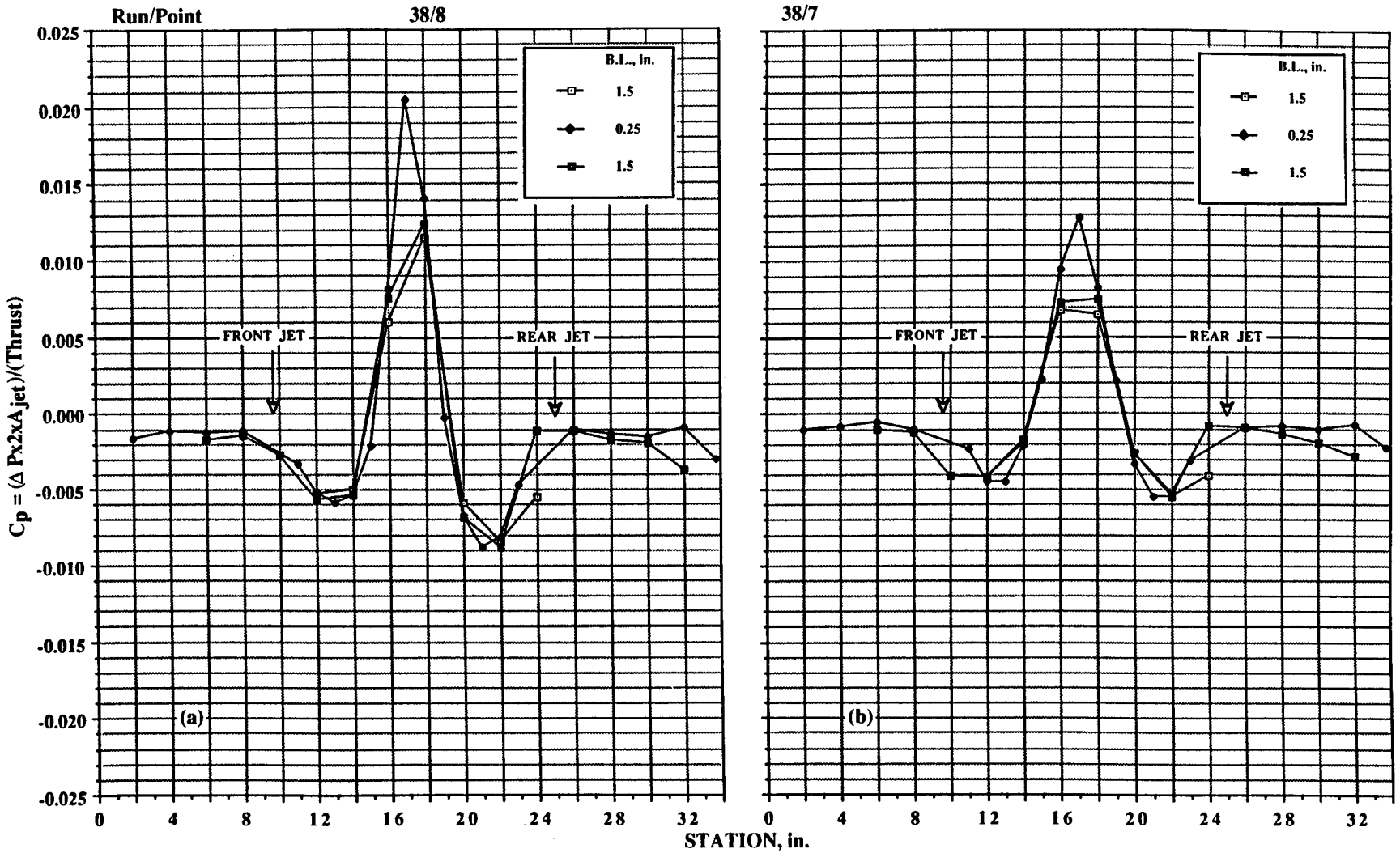

Figure 36. Pressures induced on body-alone configuration in ground effect; NPR = 6.0, T = 218 lb, both jets, no LIDs. (a) $h/d_e = 2.3$. (b) $h/d_e = 3.45$.

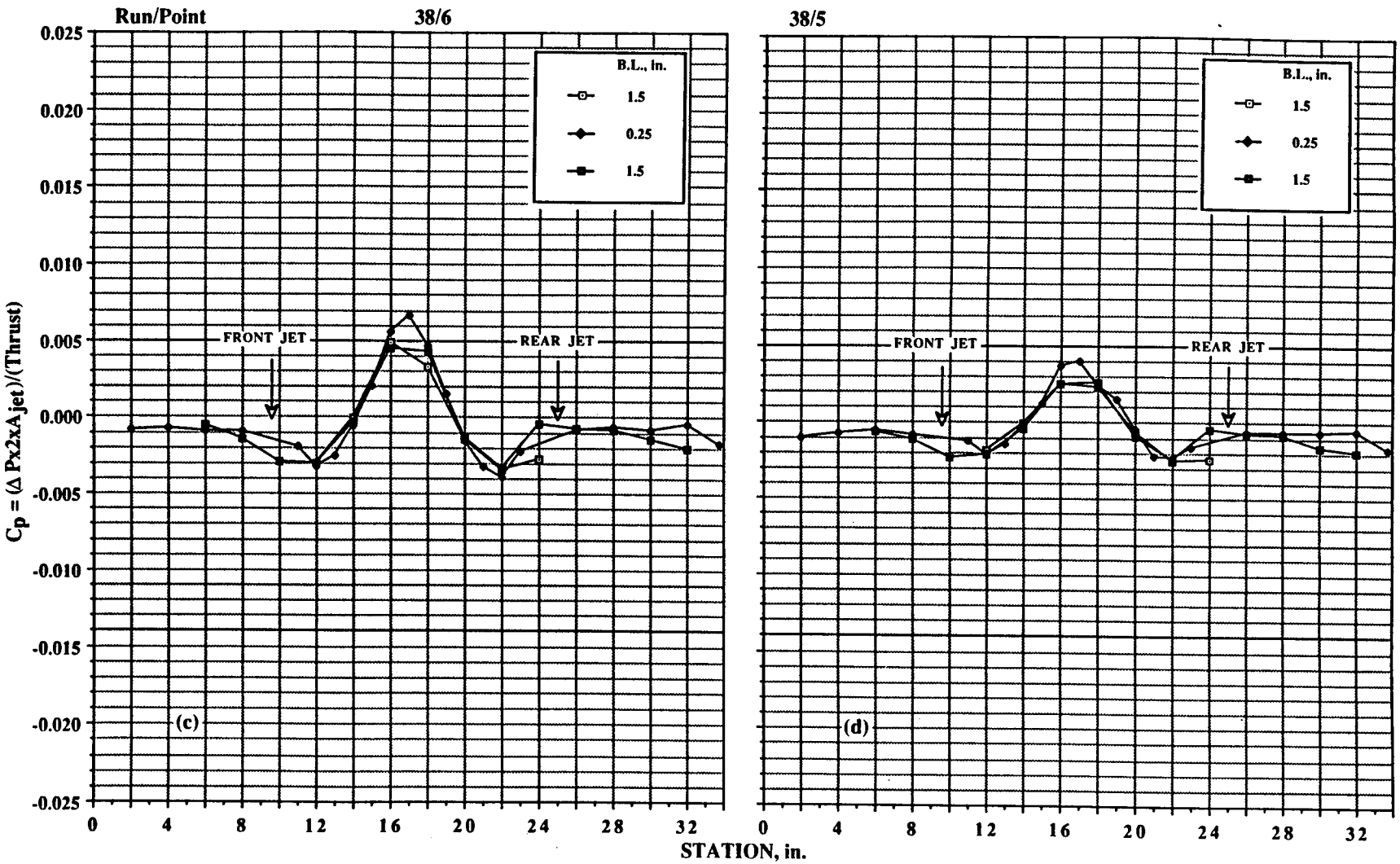

Figure 36. Continued. (c) $h/d_e = 4.6$. (d) $h/d_e = 5.75$.

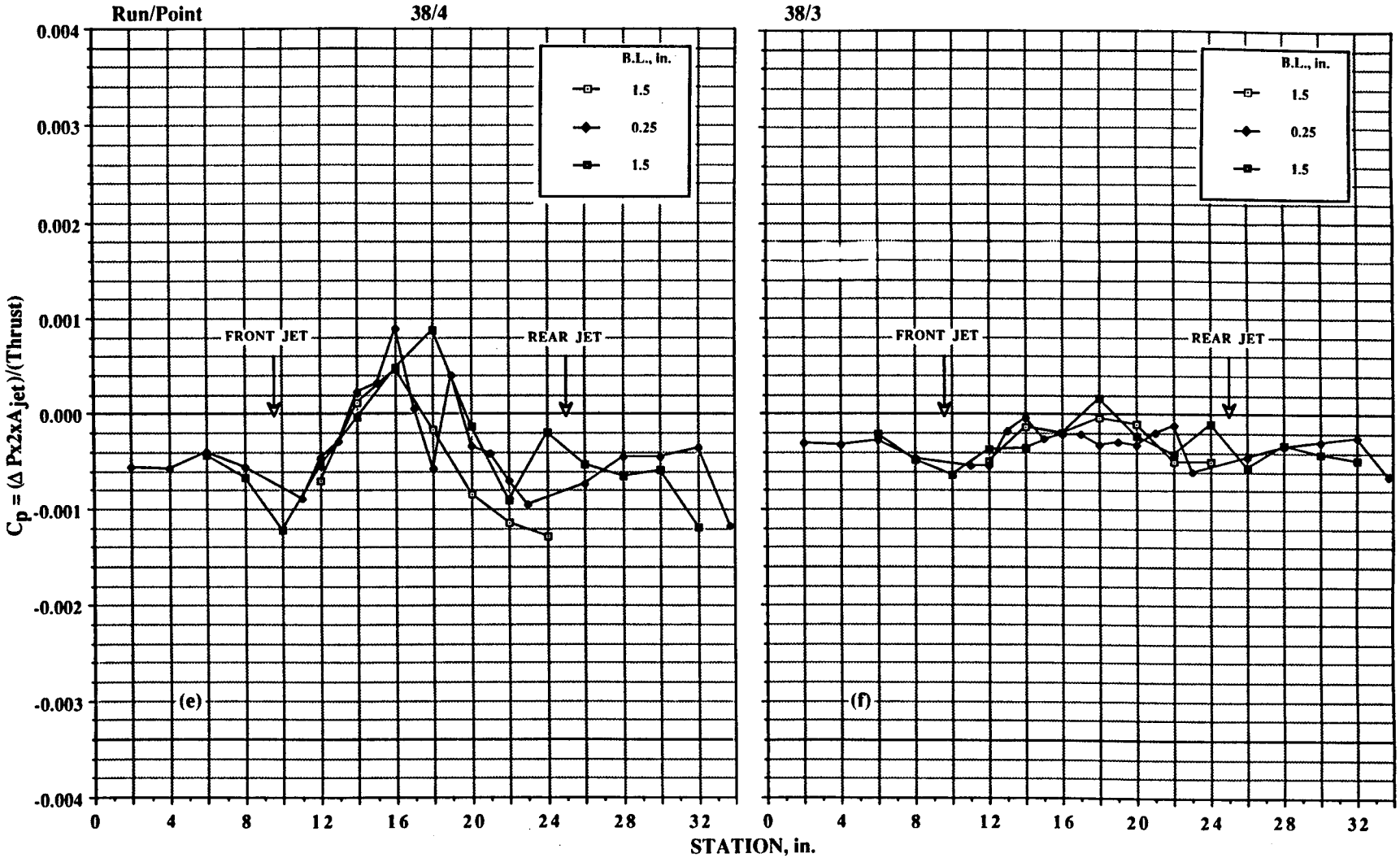

Figure 36. Continued. (e) $h/d_e = 8.62$. (f) $h/d_e = 11.5$.

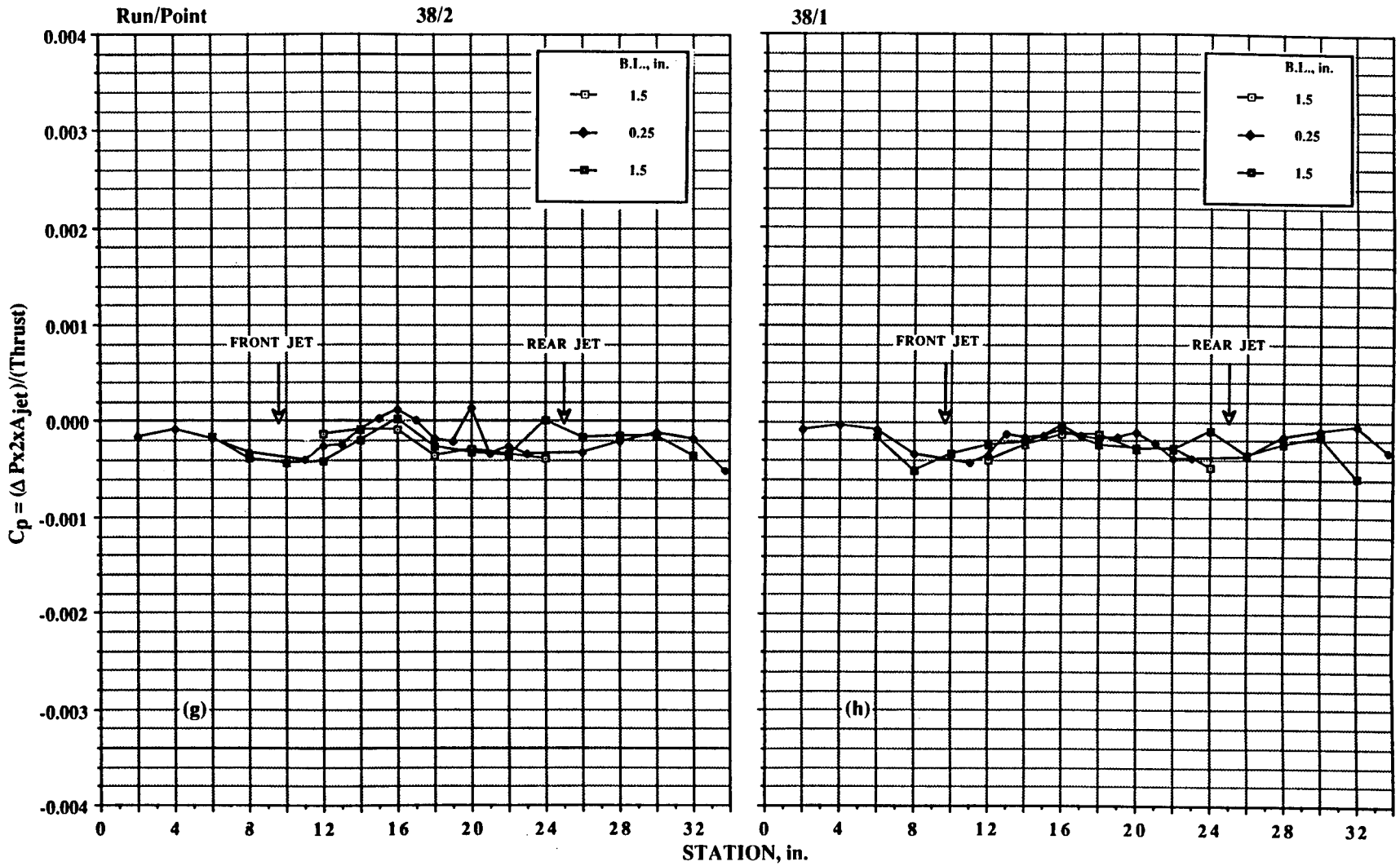

Figure 36. Concluded. (g) $h/d_e = 14.37$. (h) $h/d_e = 23.0$.

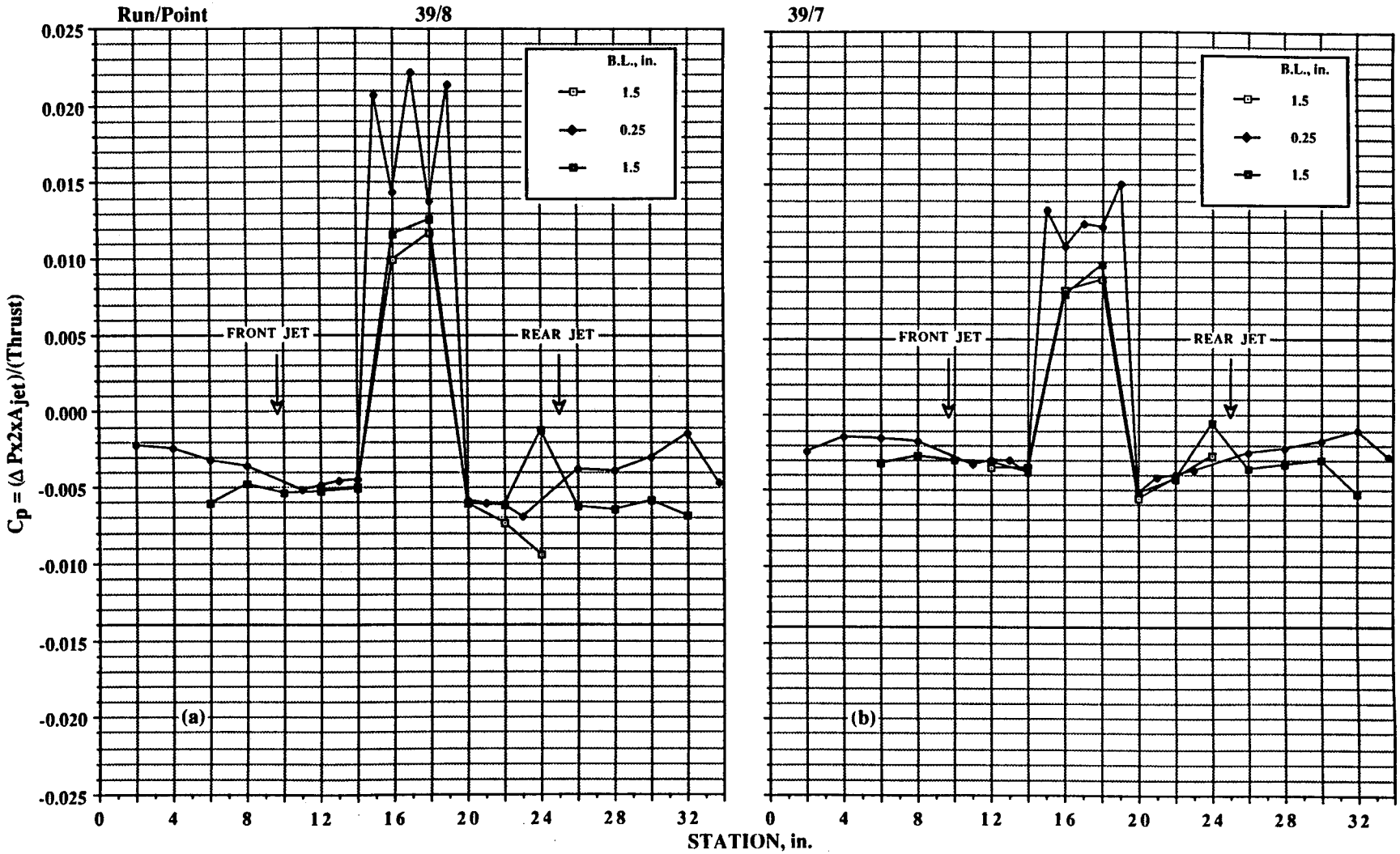

Figure 37. Pressures induced on body-alone configuration in ground effect; NPR = 2.0, T = 51 lb, both jets, LIDs at 15 in./19 in. (a) $h/d_e = 2.3$. (b) $h/d_e = 3.45$.

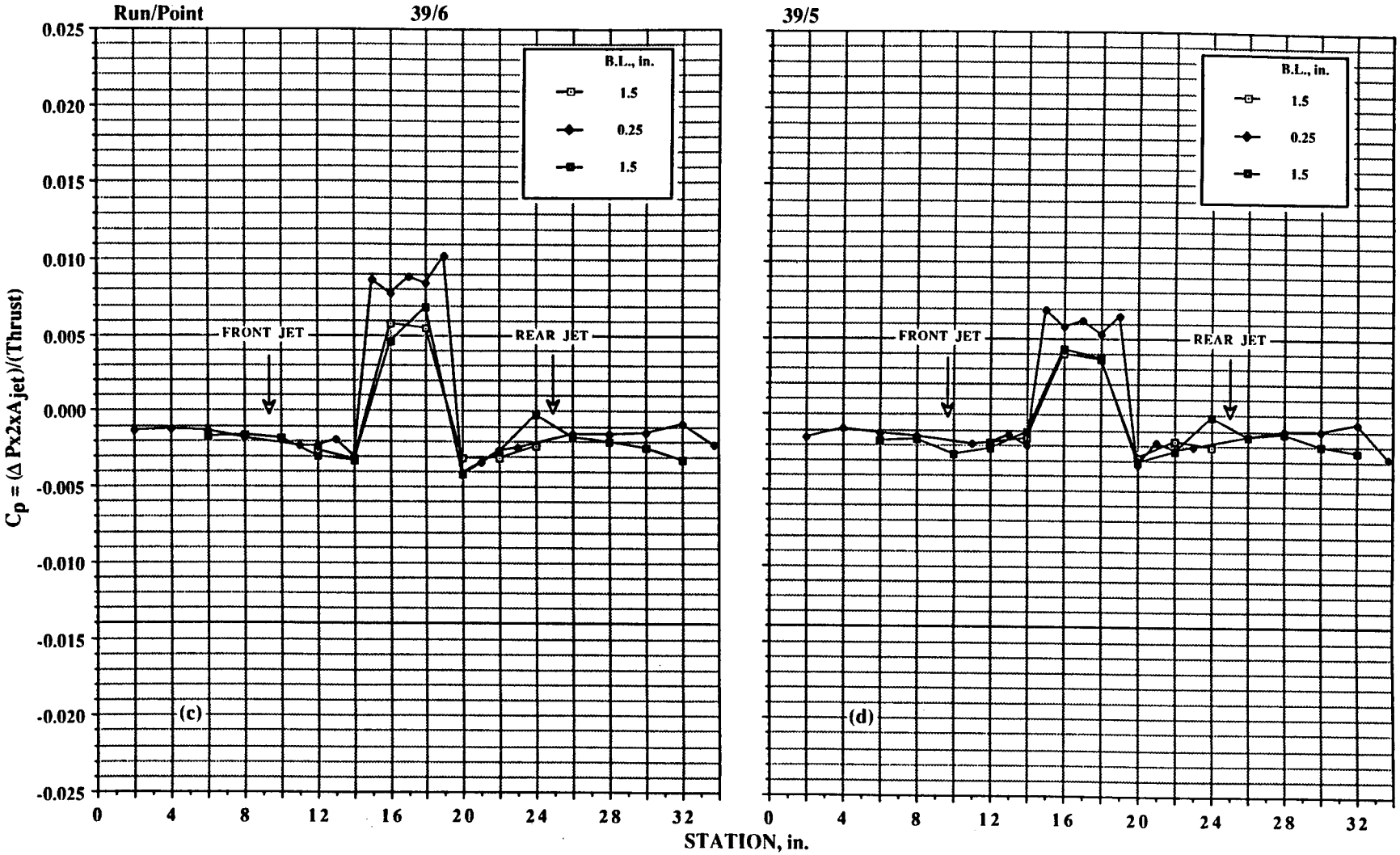

Figure 37. Continued. (c) $h/d_e = 4.6$. (d) $h/d_e = 5.75$.

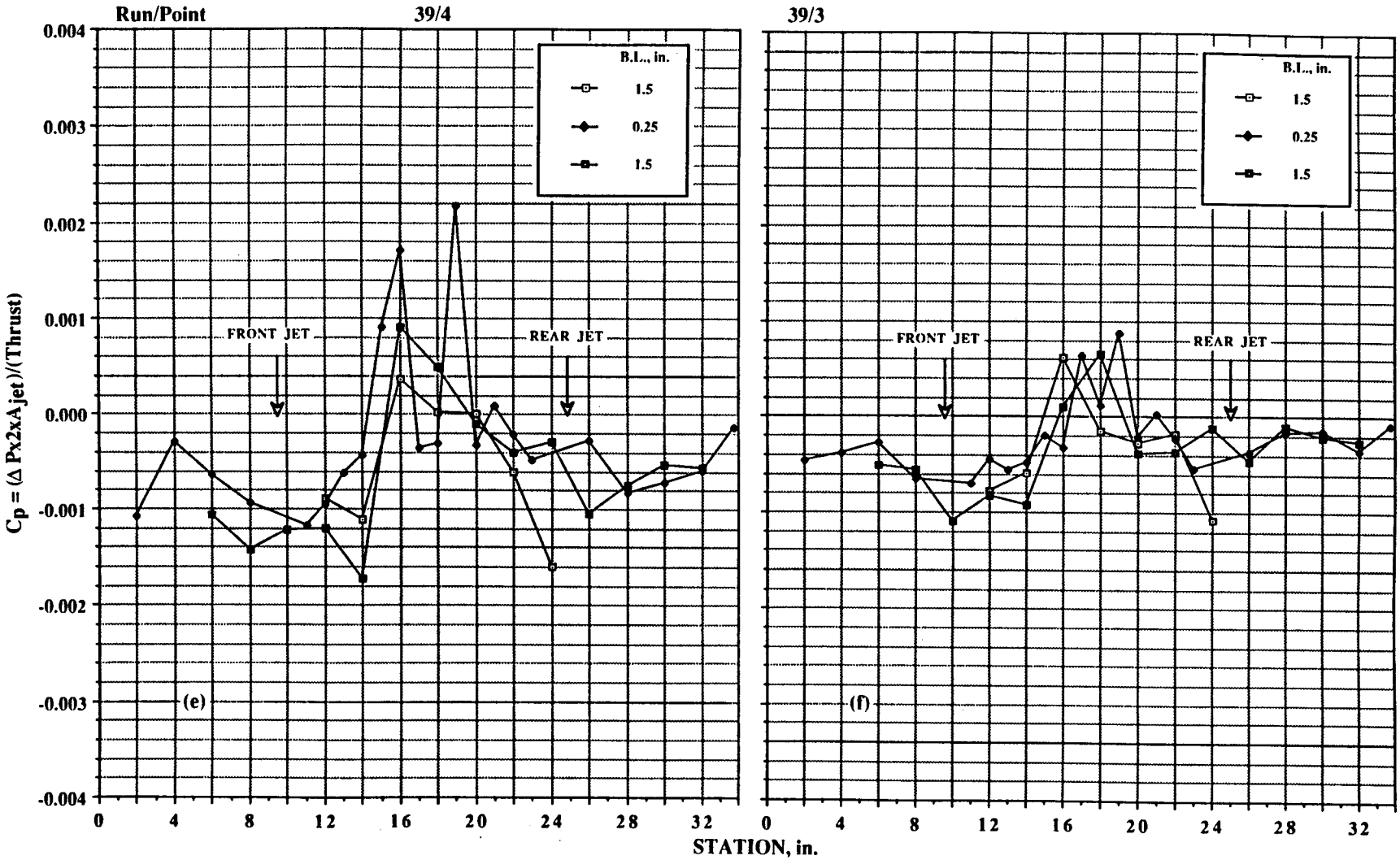

Figure 37. Continued. (e) $h/d_e = 8.62$. (f) $h/d_e = 11.5$.

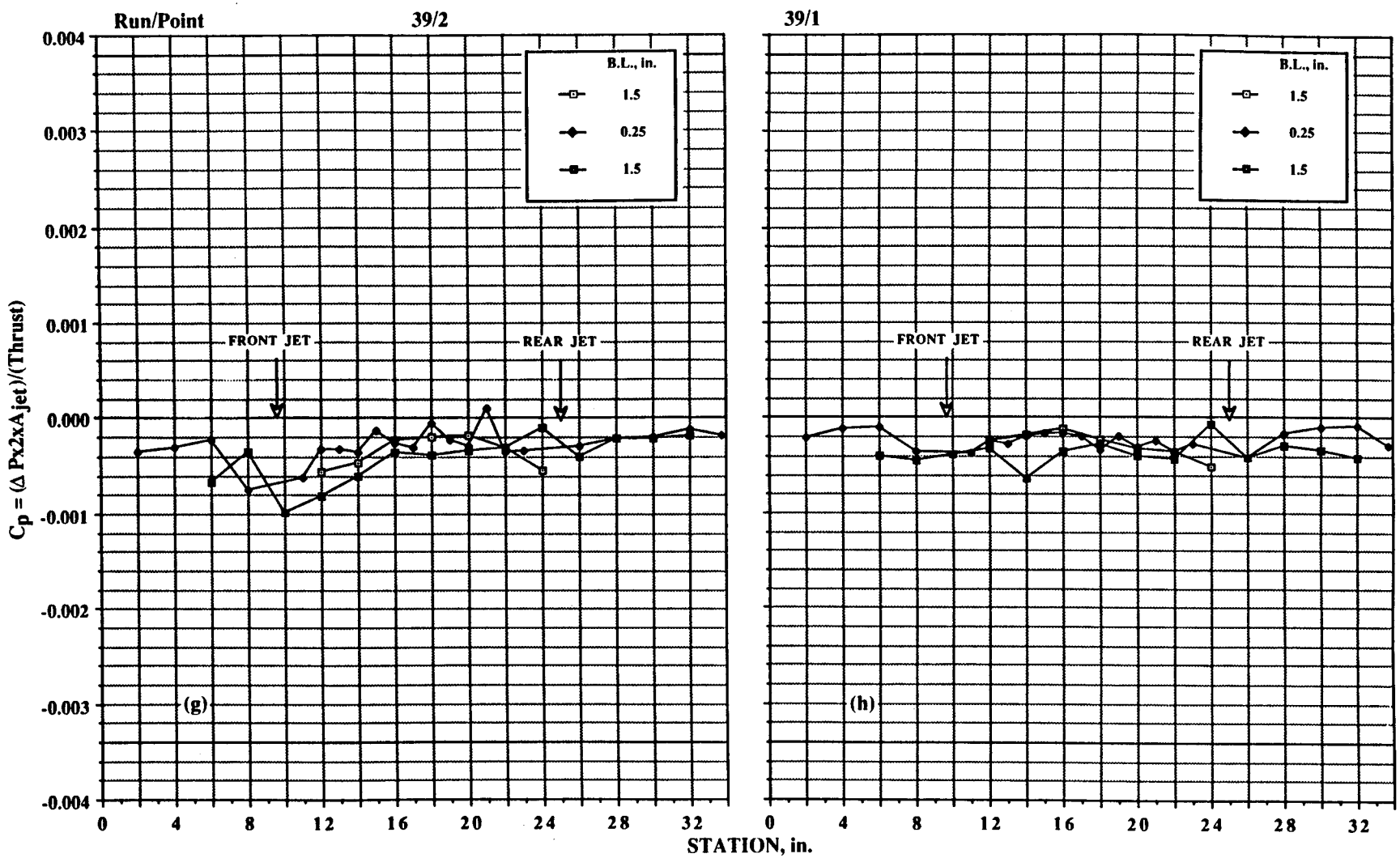

Figure 37. Concluded. (g) $h/d_e = 14.37$. (h) $h/d_e = 23.0$.

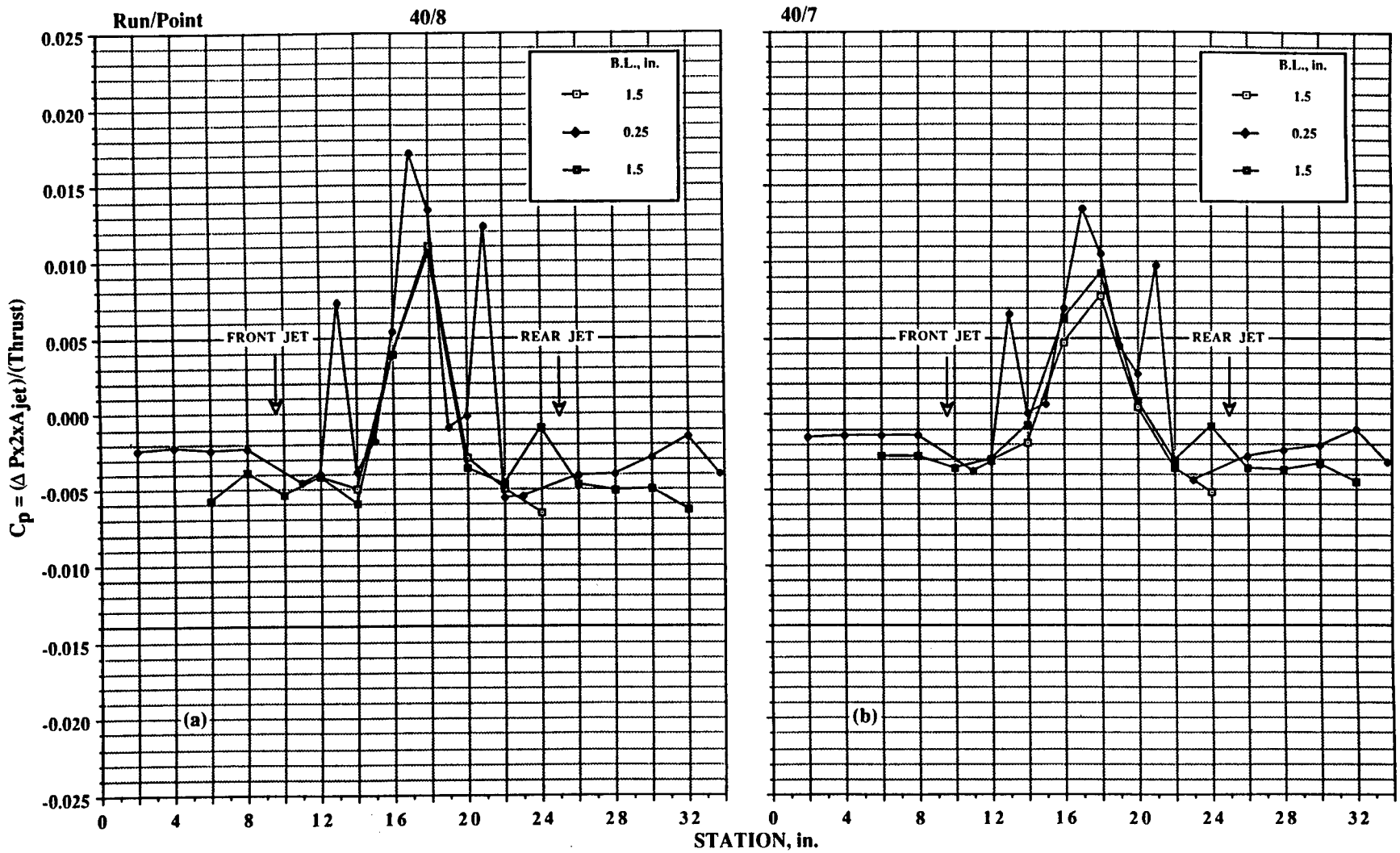

Figure 38. Pressures induced on body-alone configuration in ground effect; NPR = 2.0, T = 51 lb, both jets, LIDs at 13 in./21 in. (a) $h/d_e = 2.3$. (b) $h/d_e = 3.45$.

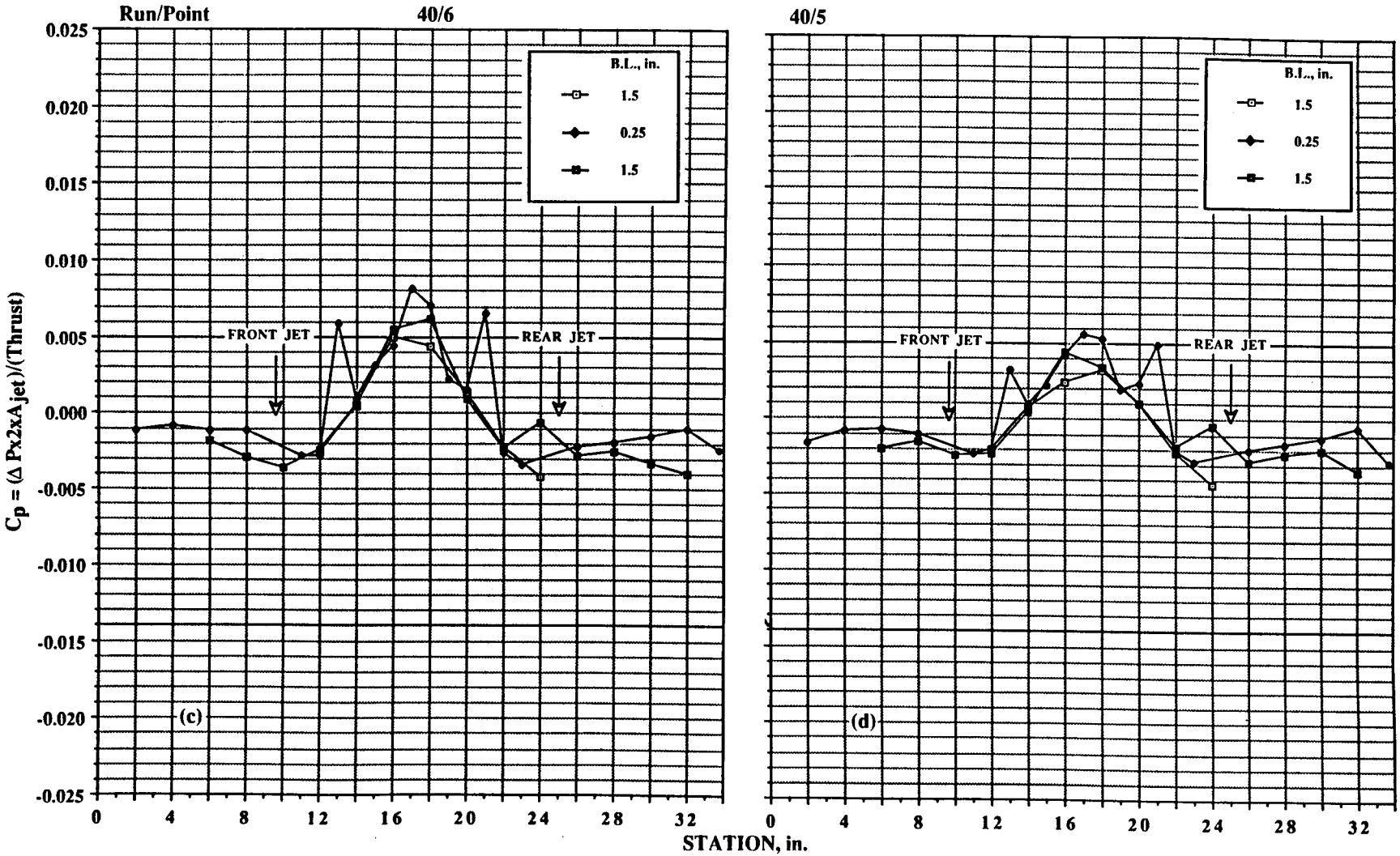

Figure 38. Continued. (c) $h/d_e = 4.6$. (d) $h/d_e = 5.75$.

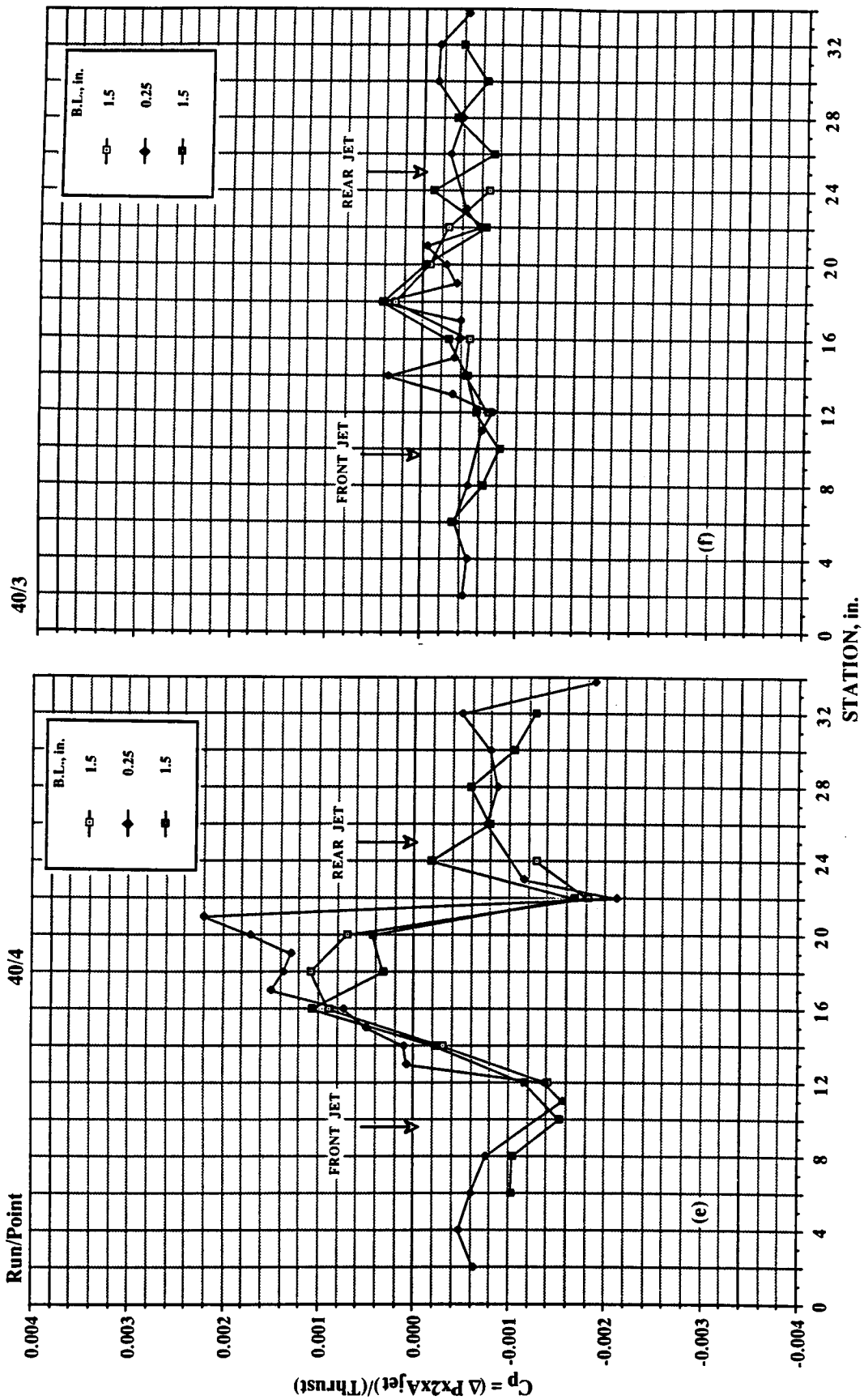

Figure 38. Continued. (e) $h/d_e = 8.62$. (f) $h/d_e = 11.5$.

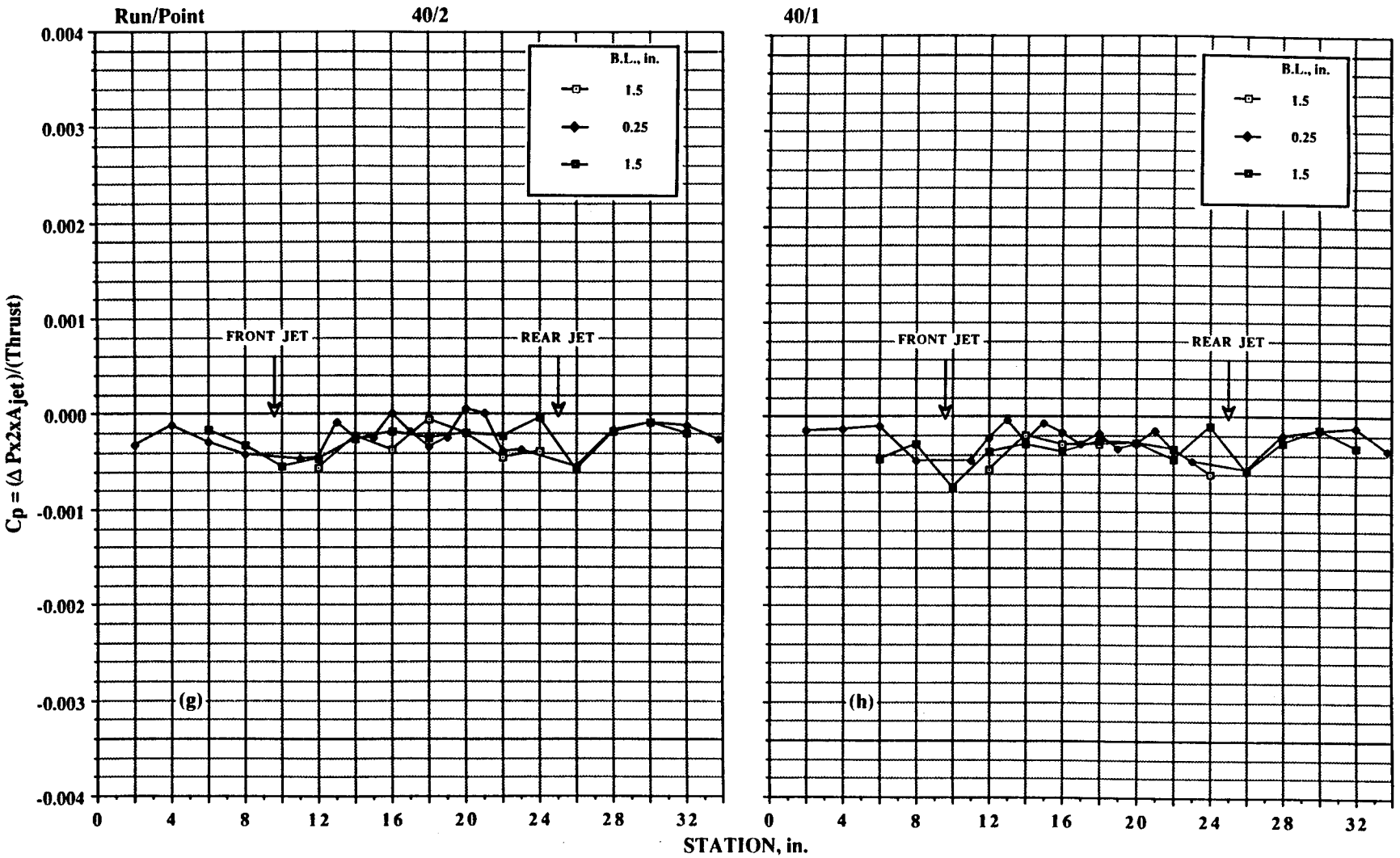

Figure 38. Continued. (g) $h/d_e = 14.37$. (h) $h/d_e = 23.0$.

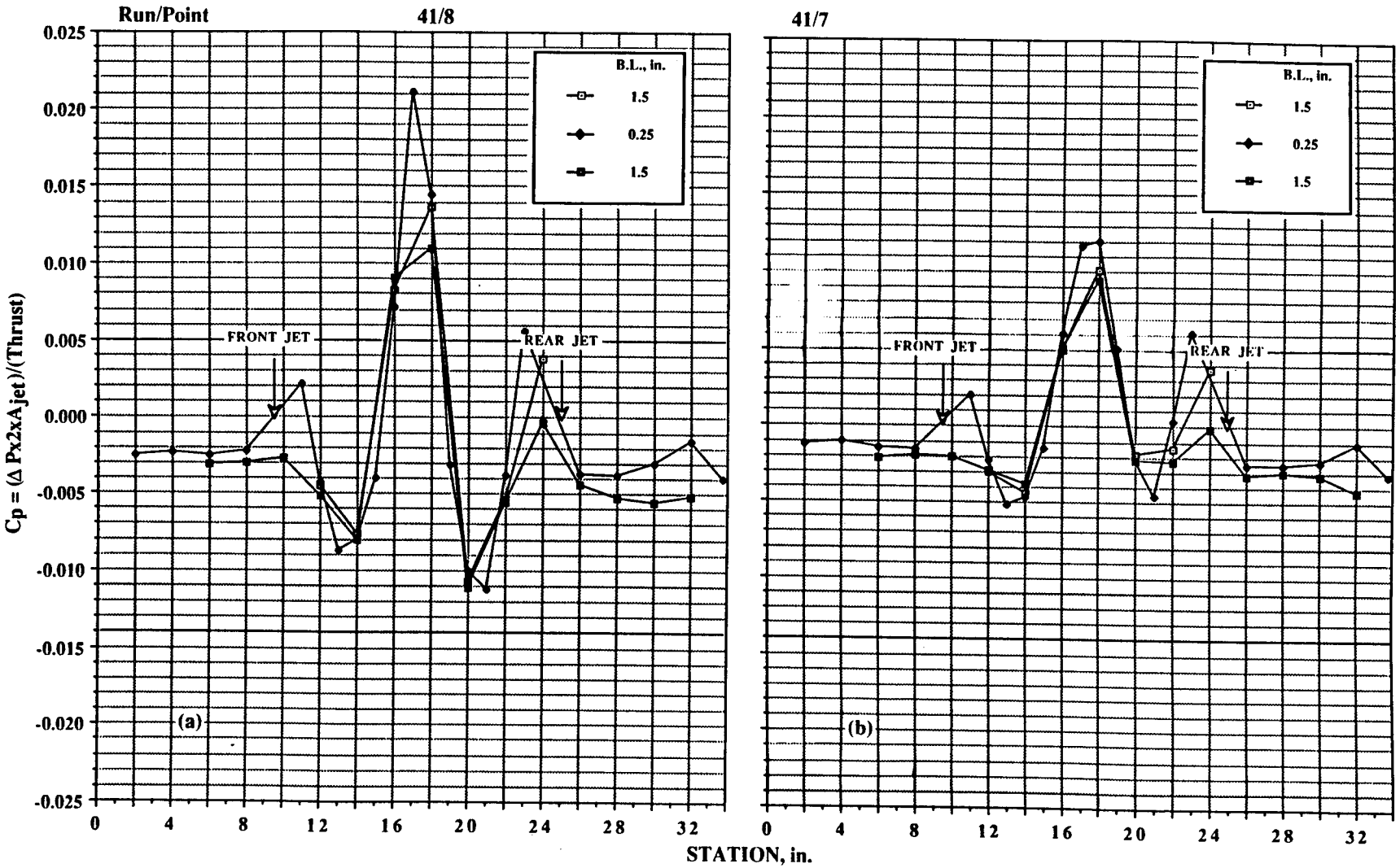

Figure 39. Pressures induced on body-alone configuration in ground effect; NPR = 2.0, T = 51 lb, both jets, LIDs at 11 in./23 in. (a) $h/d_e = 2.3$. (b) $h/d_e = 3.45$.

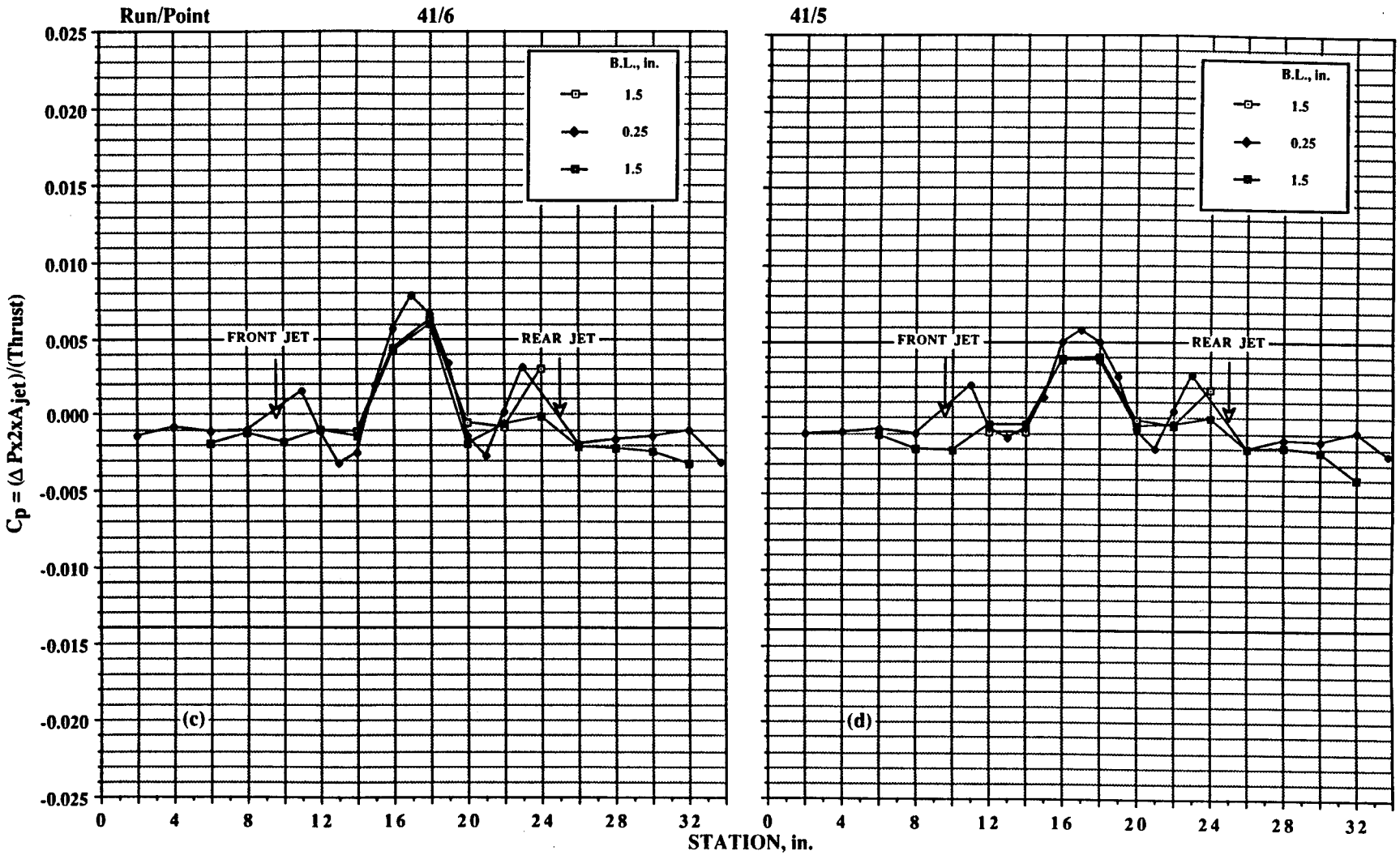

Figure 39. Continued. (c) $h/d_e = 4.6$. (d) $h/d_e = 5.75$.

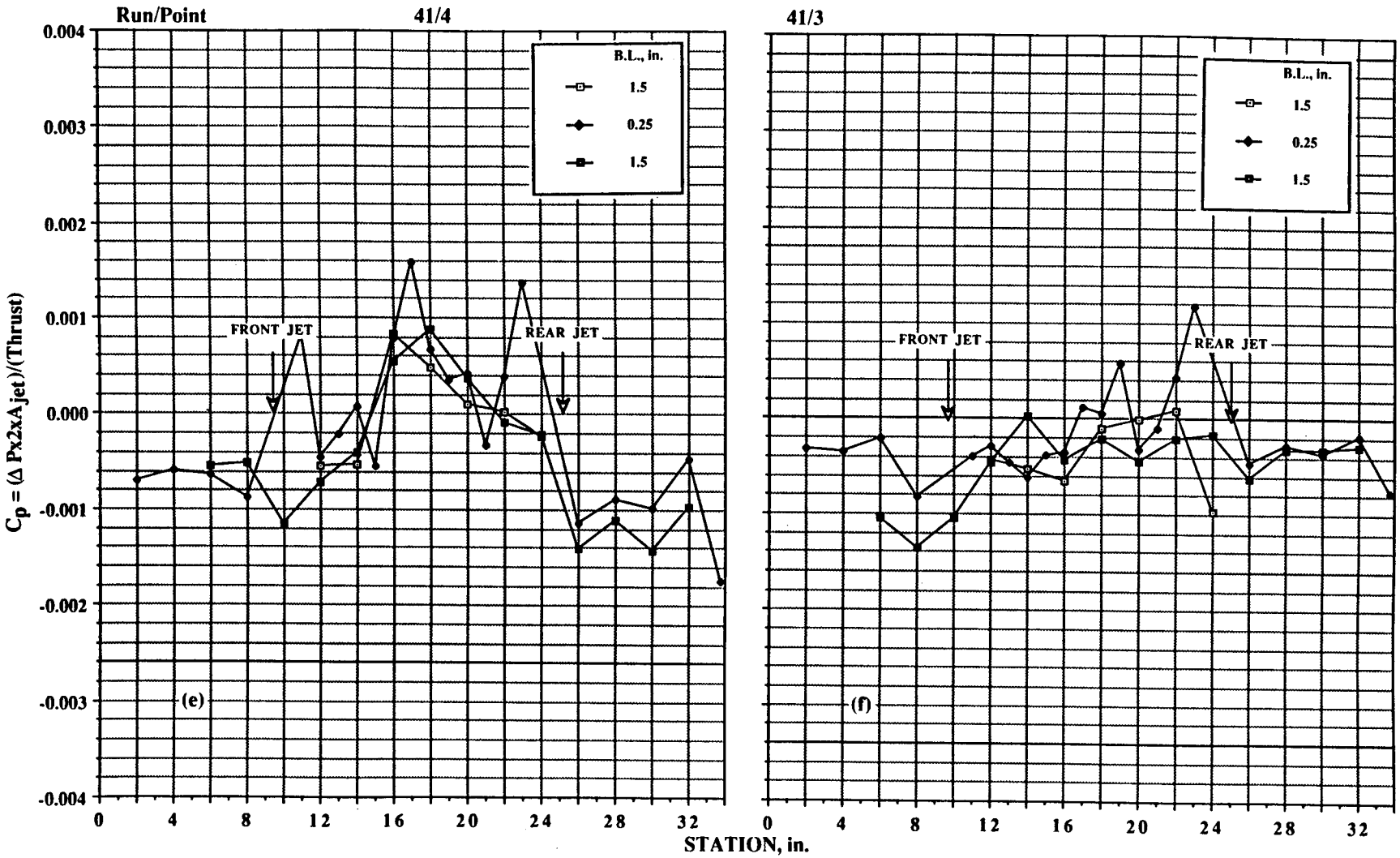

Figure 39. Continued. (e) $h/d_e = 8.62$. (f) $h/d_e = 11.5$.

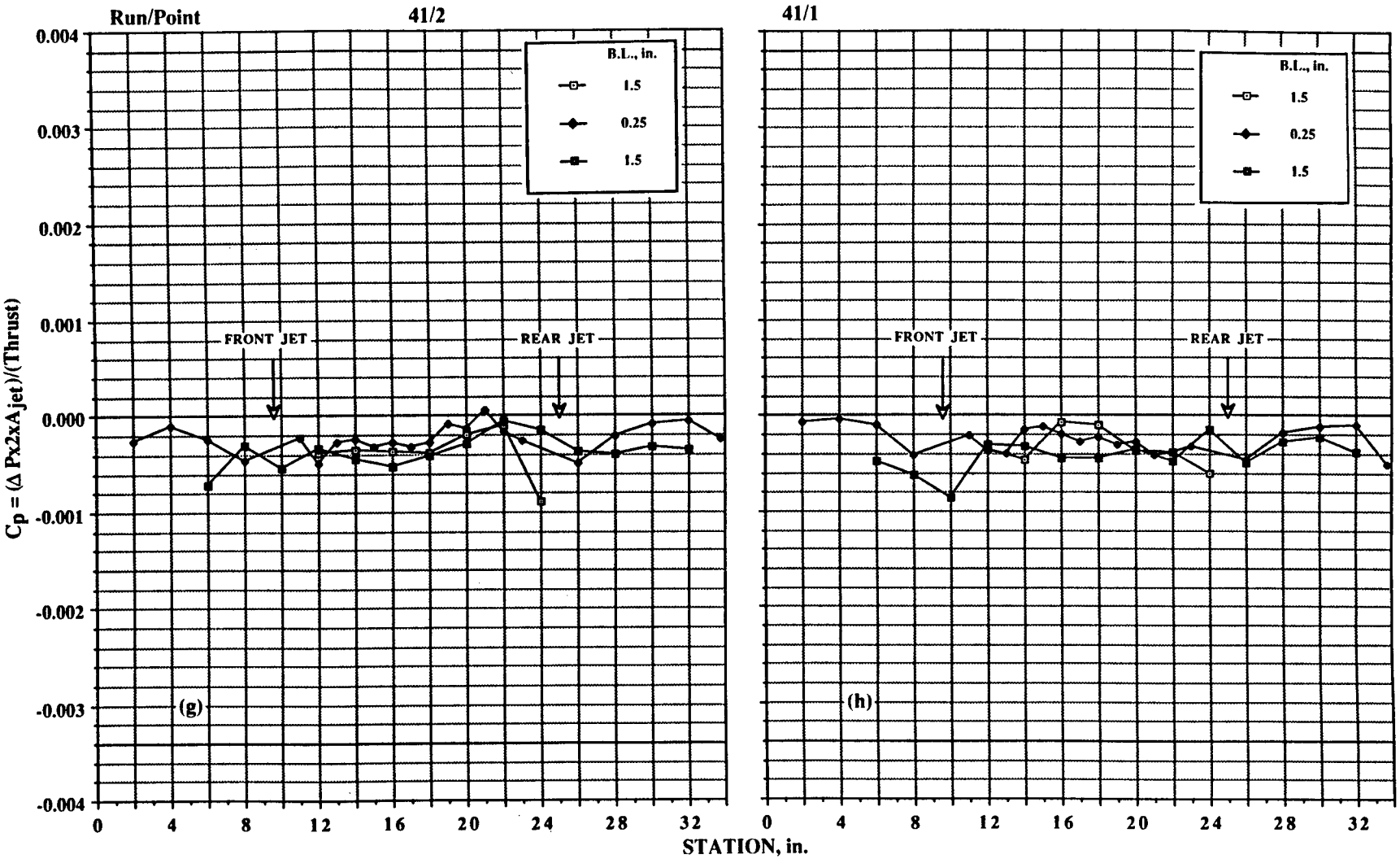

Figure 39. Concluded. (g) $h/d_e = 14.37$. (h) $h/d_e = 23.0$.

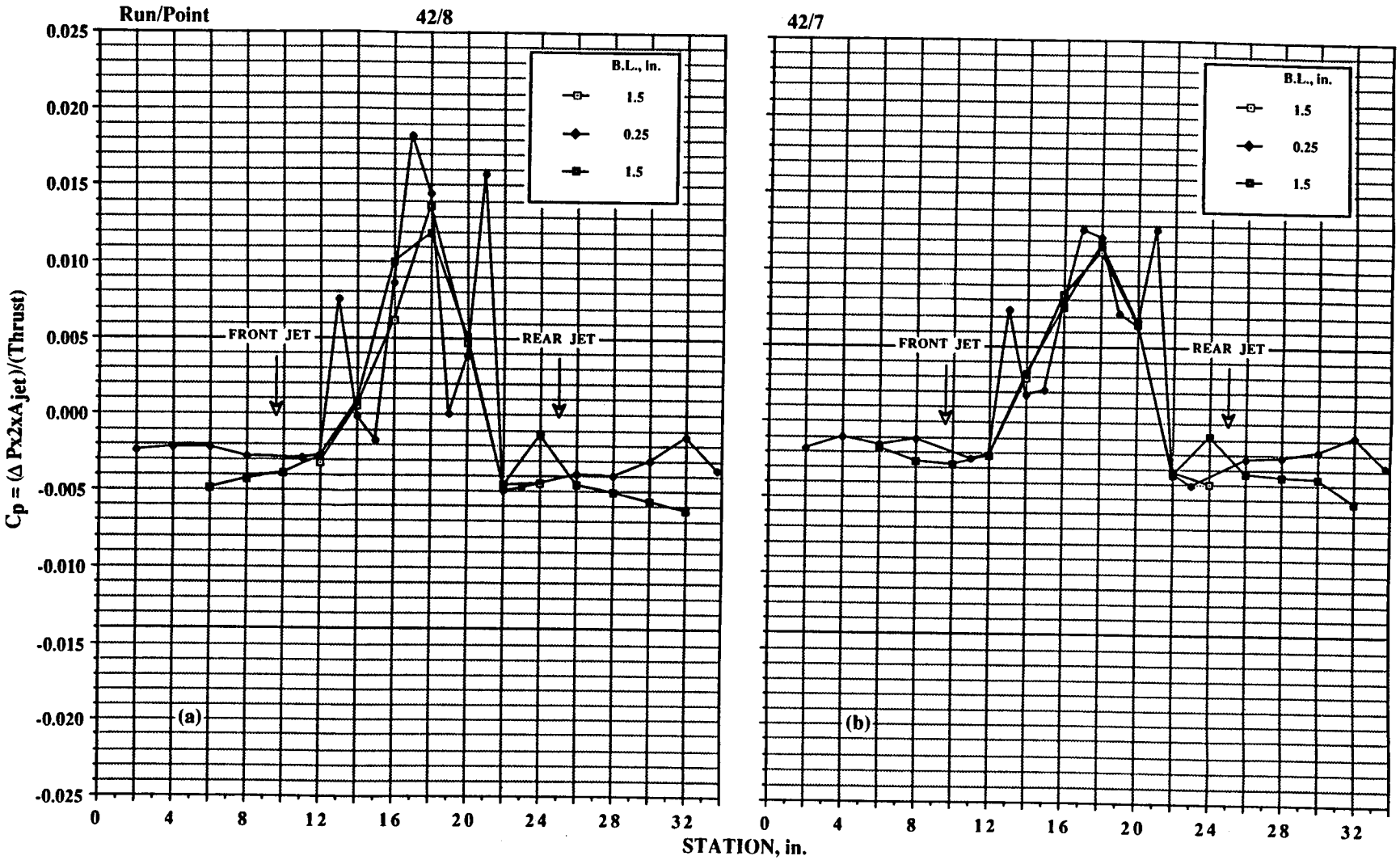

Figure 40. Pressures induced on body-alone configuration in ground effect; NPR = 2.0, T = 51 lb, both jets, LIDs at 13 in./21 in. (box). (a) $h/d_e = 2.3$. (b) $h/d_e = 3.45$.

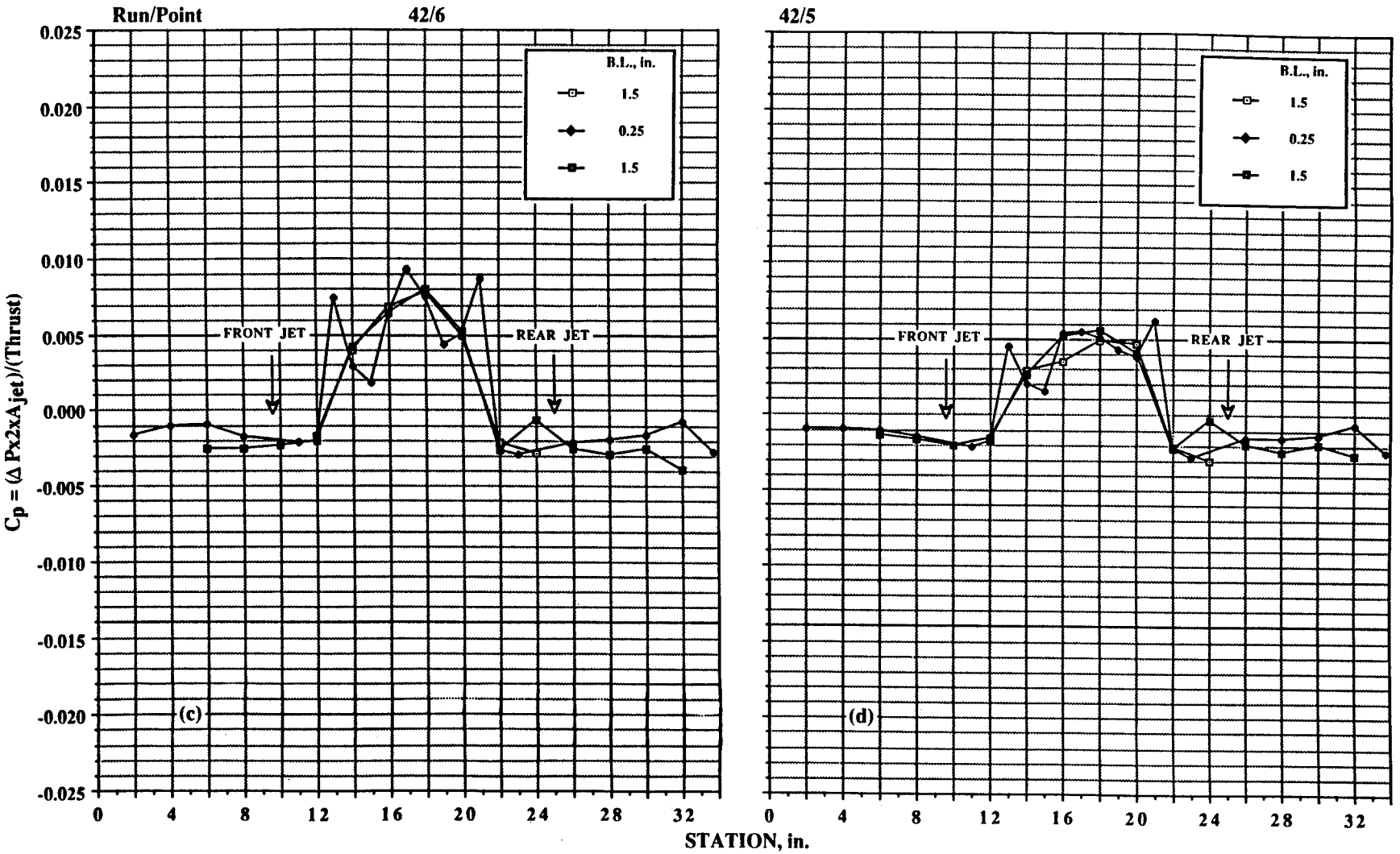

Figure 40. Continued. (c) $h/d_e = 4.6$. (d) $h/d_e = 5.75$.

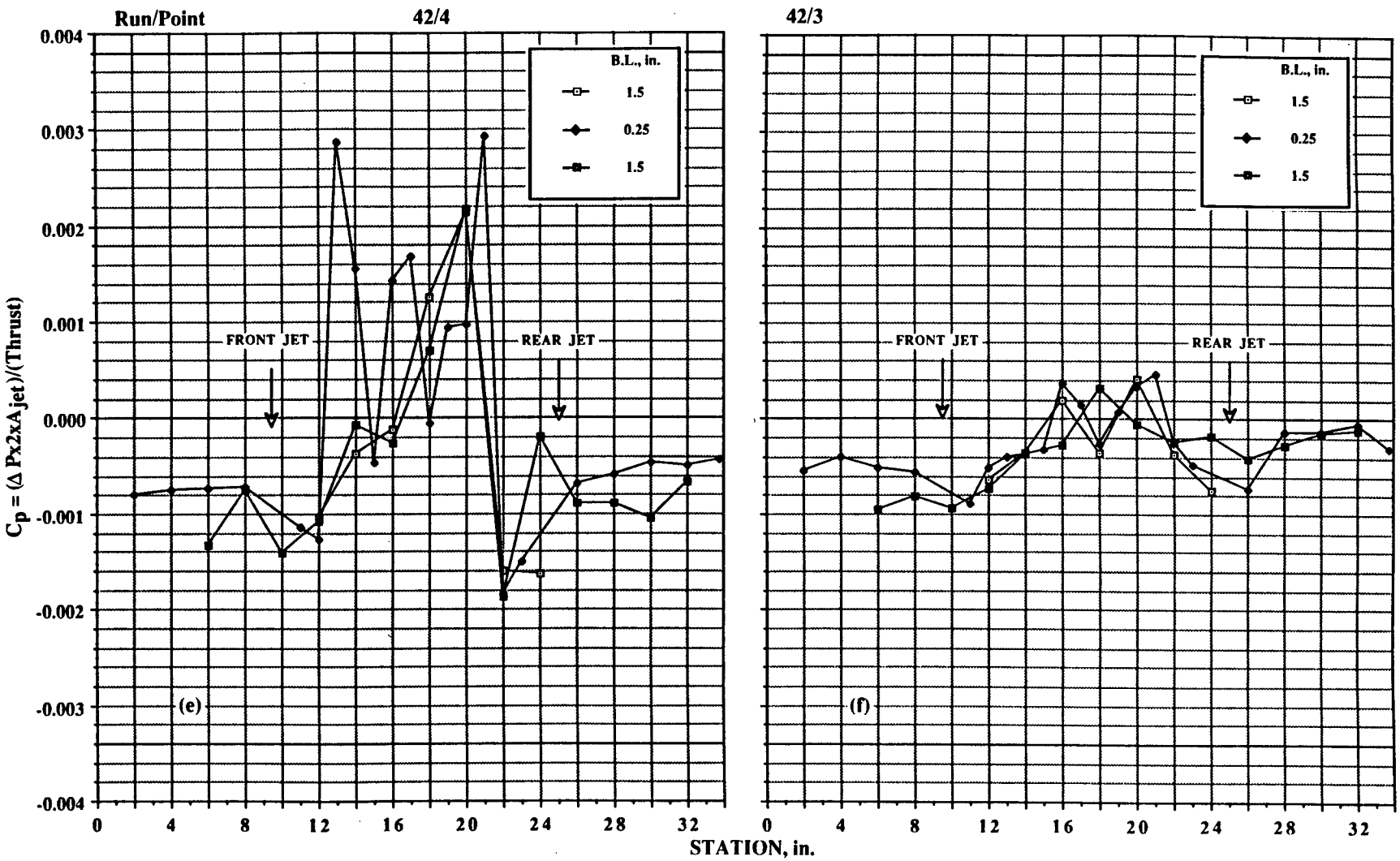

Figure 40. Continued. (e) $h/d_e = 8.62$. (f) $h/d_e = 11.5$.

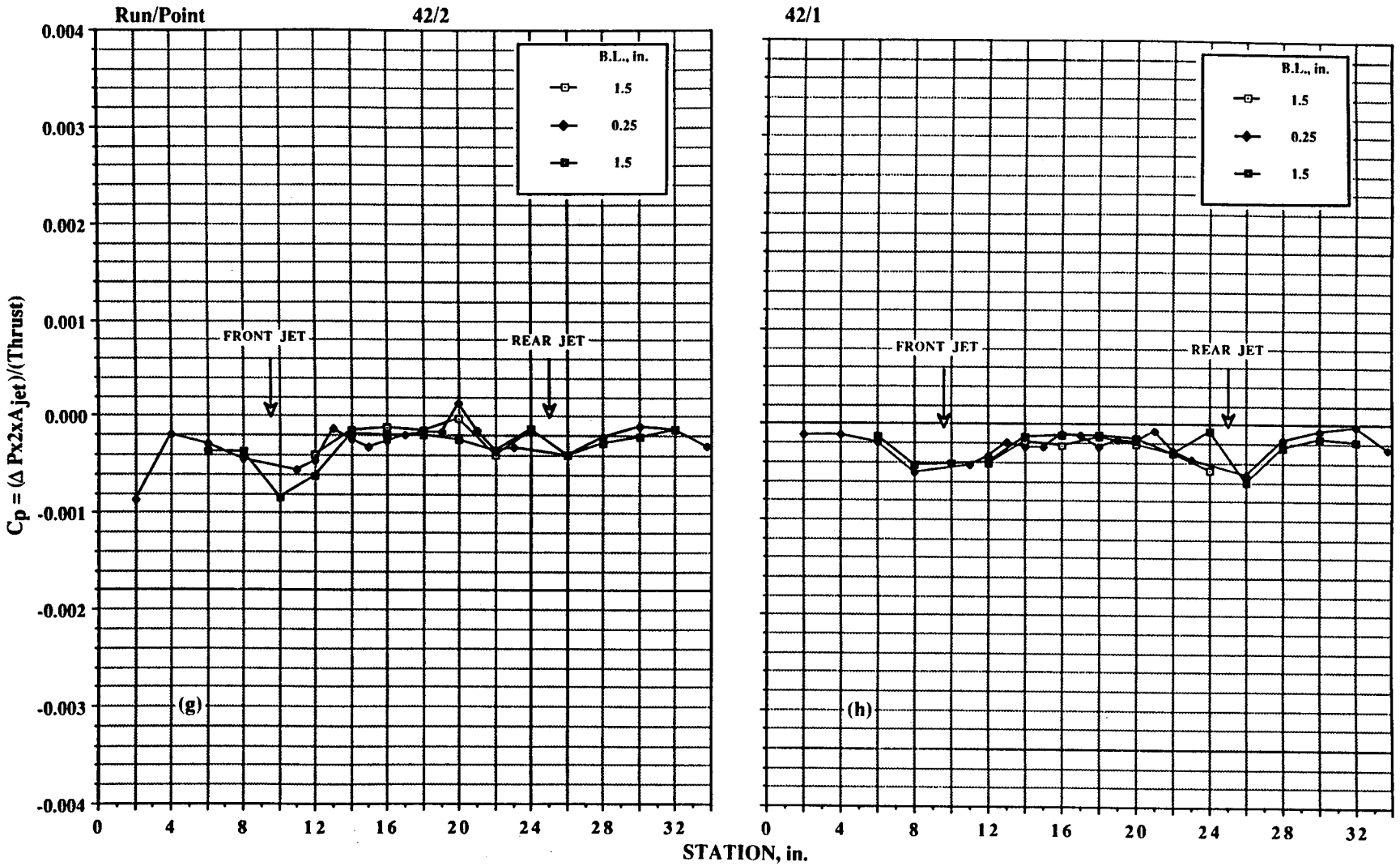

Figure 40. Continued. (g) $h/d_e = 14.37$. (h) $h/d_e = 23.0$.

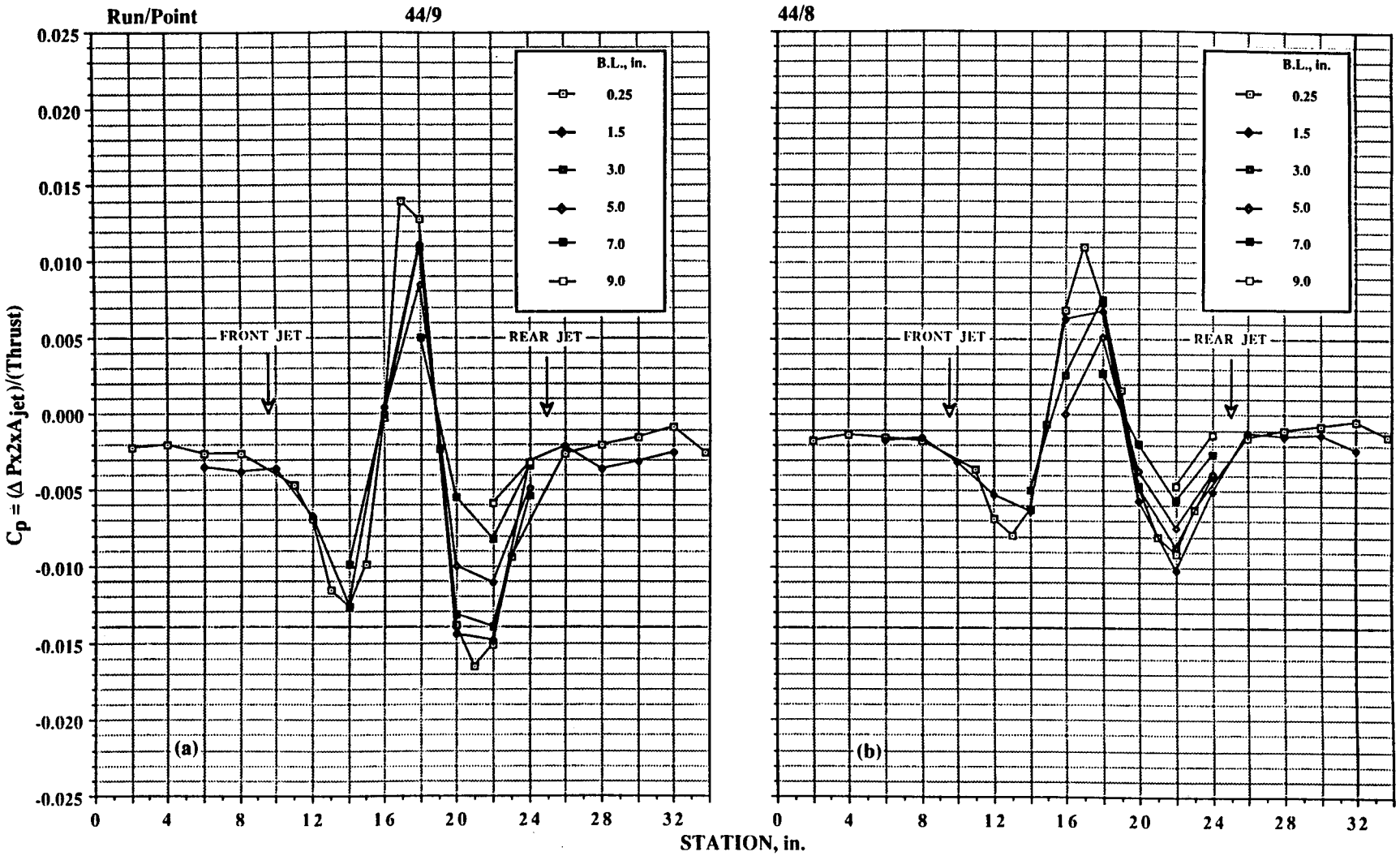

Figure 41. Pressures induced on wing/body configuration in ground effect; NPR = 2.0, T = 51 lb, both jets, no LIDs. (a) $h/d_e = 2.30$. (b) $h/d_e = 3.45$.

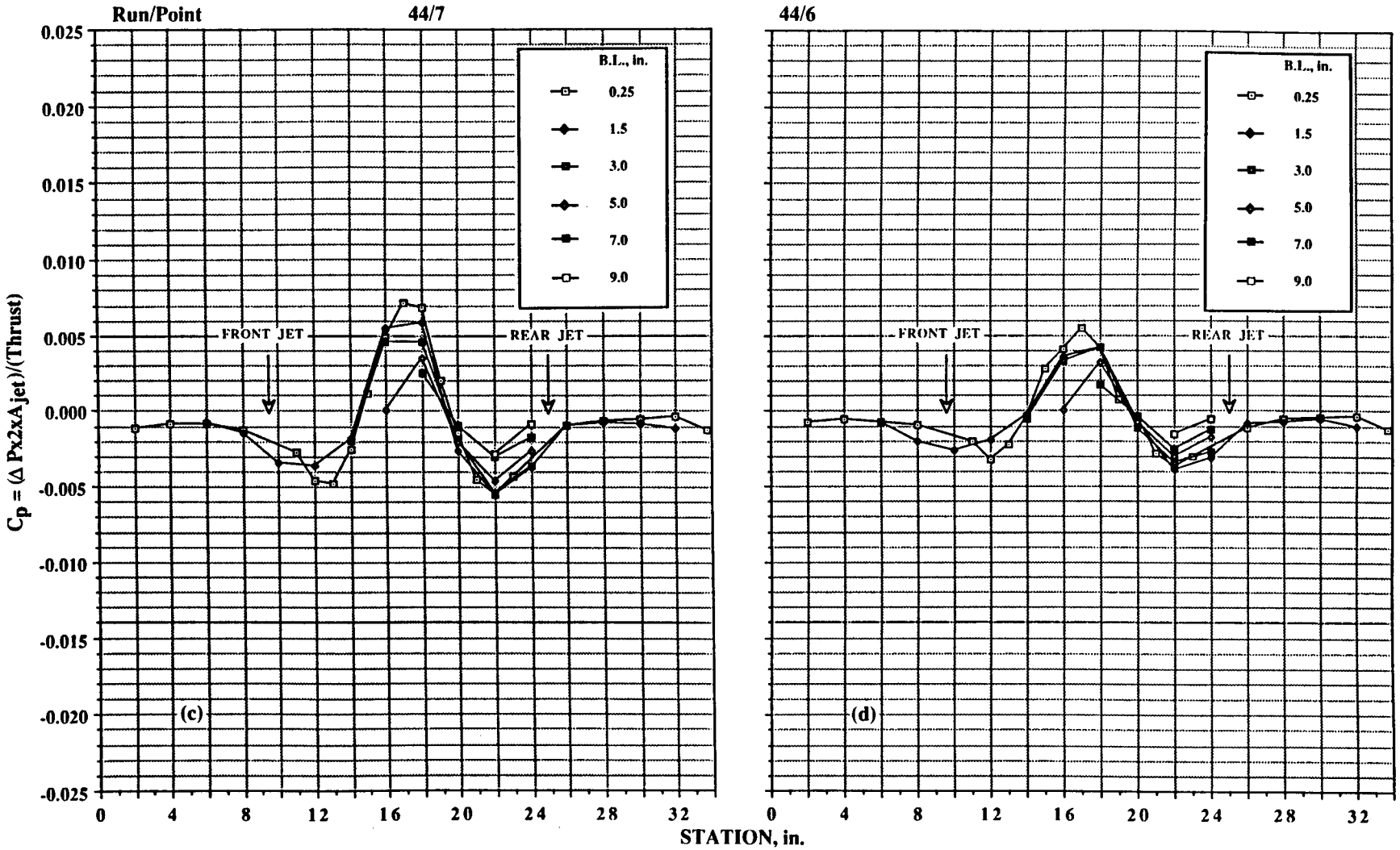

Figure 41. Continued. (c) $h/d_e = 4.6$. (d) $h/d_e = 5.75$.

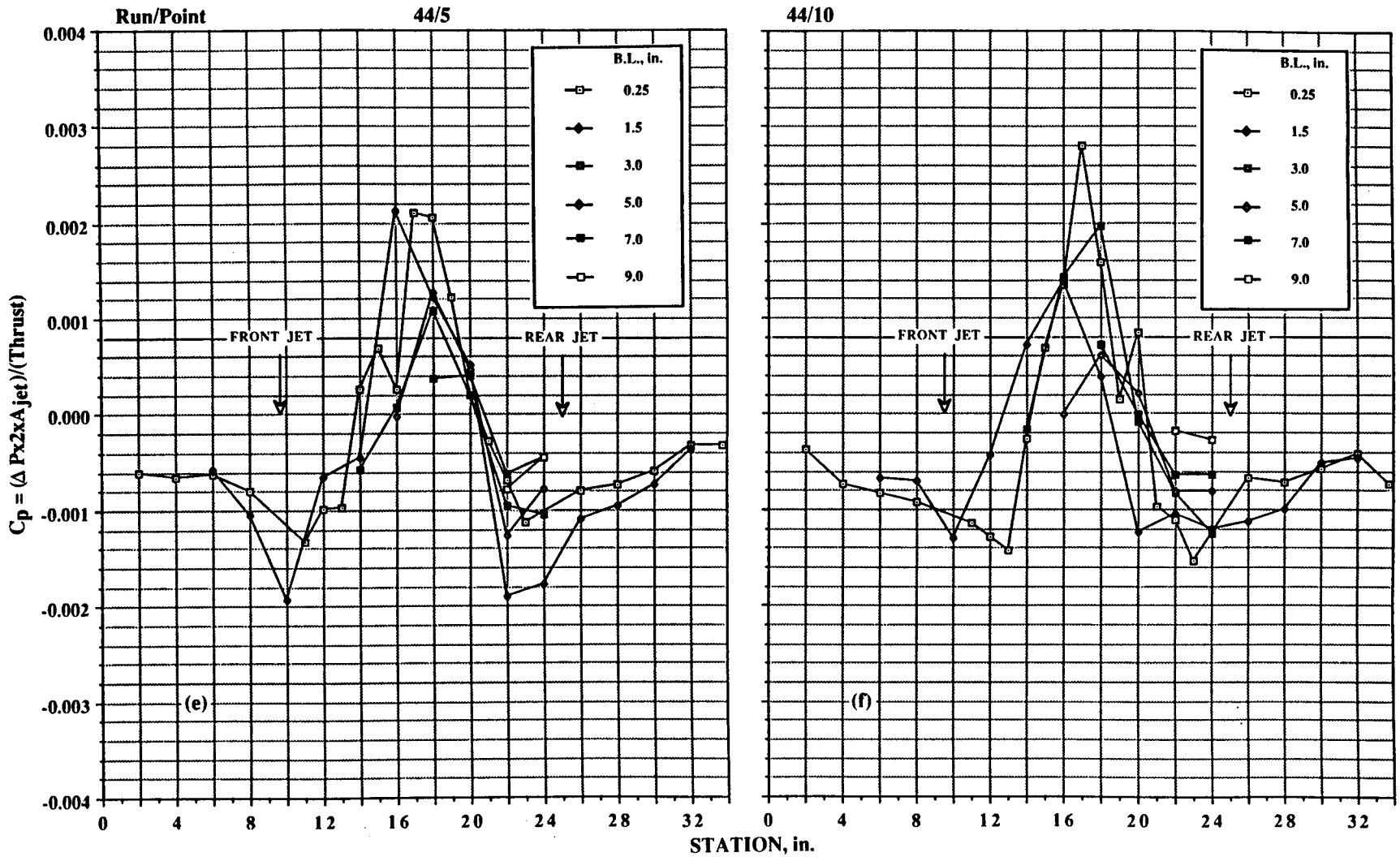

Figure 41. Continued. (e) $h/d_e = 8.62$. (f) $h/d_e = 8.62$ (repeat).

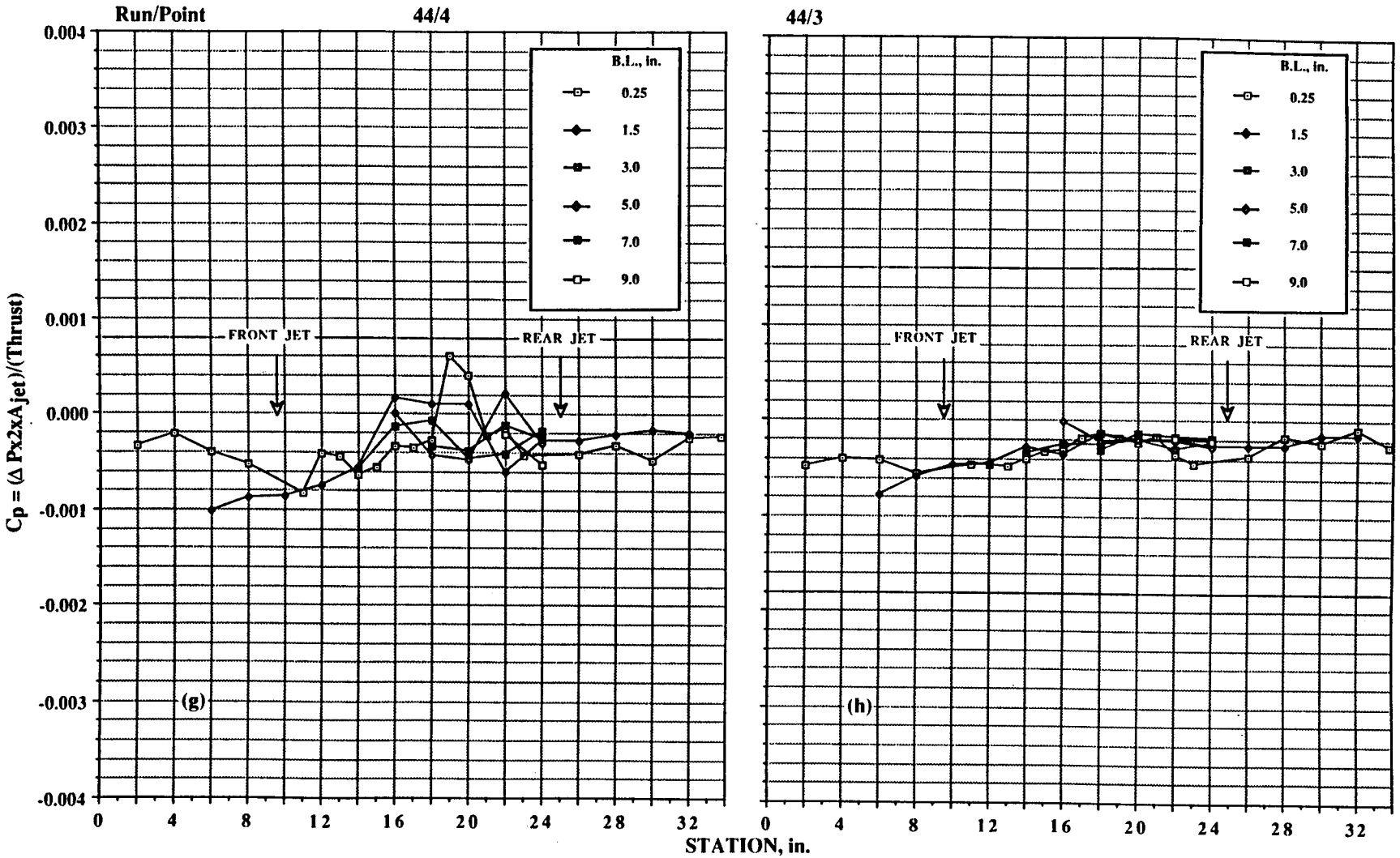

Figure 41. Continued. (g) $h/d_e = 11.5$. (h) $h/d_e = 14.37$.

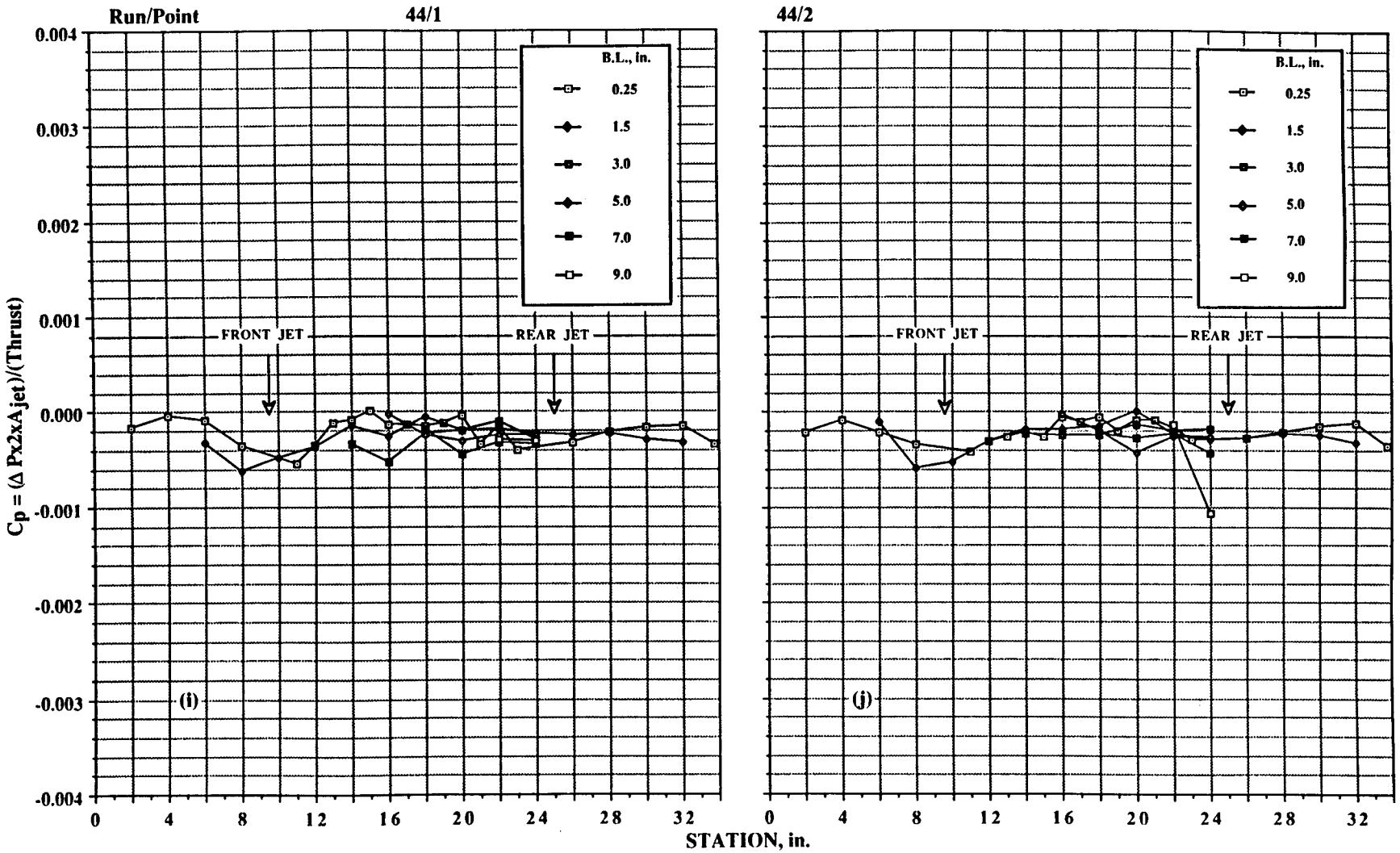

Figure 41. Concluded. (i) $h/d_e = 23.0$. (j) $h/d_e = 23.0$ (repeat).

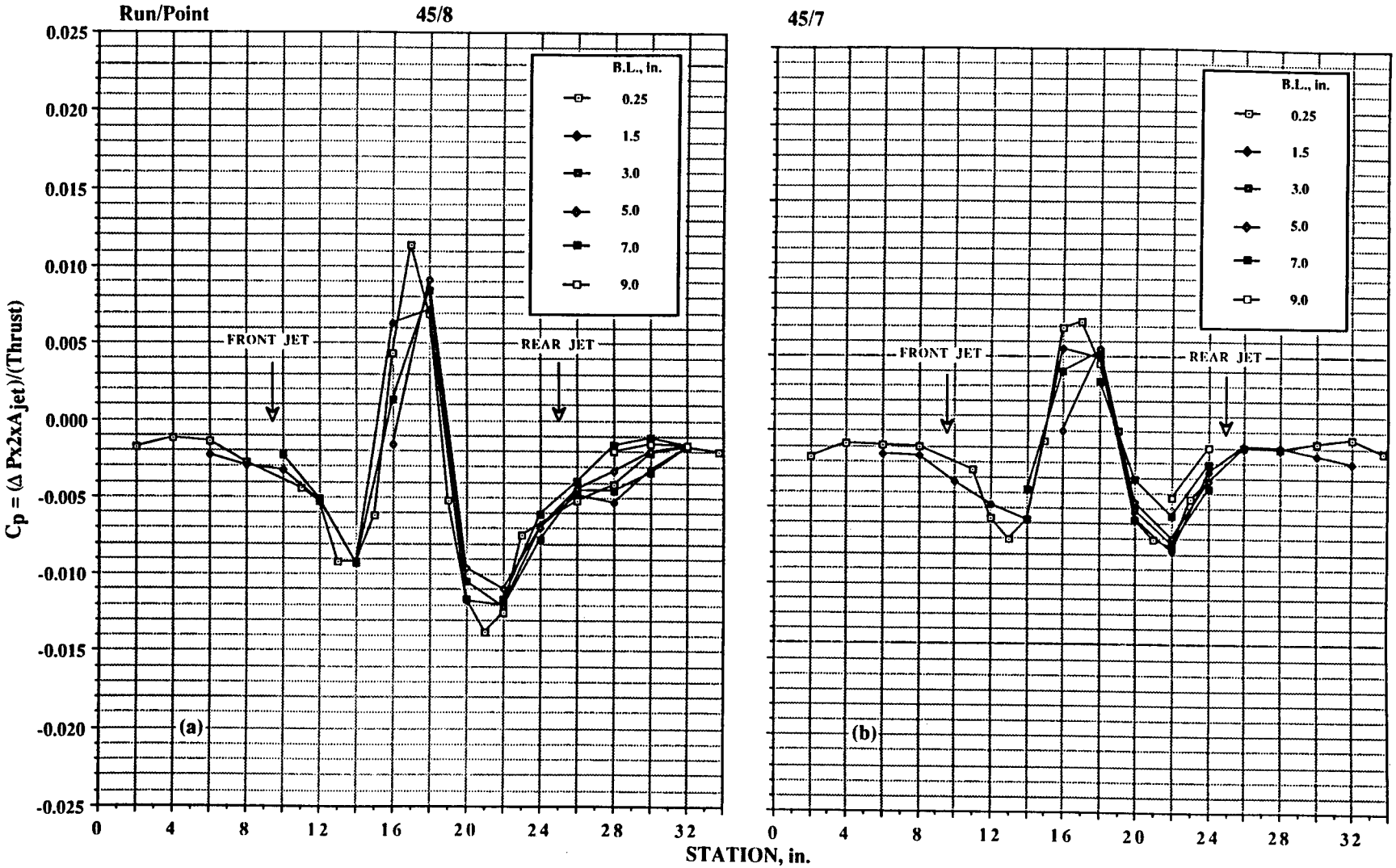

Figure 42. Pressures induced on wing/body configuration in ground effect; NPR = 4.0, T = 135 lb, both jets, no LIDs. (a) $h/d_e = 2.30$. (b) $h/d_e = 3.45$.

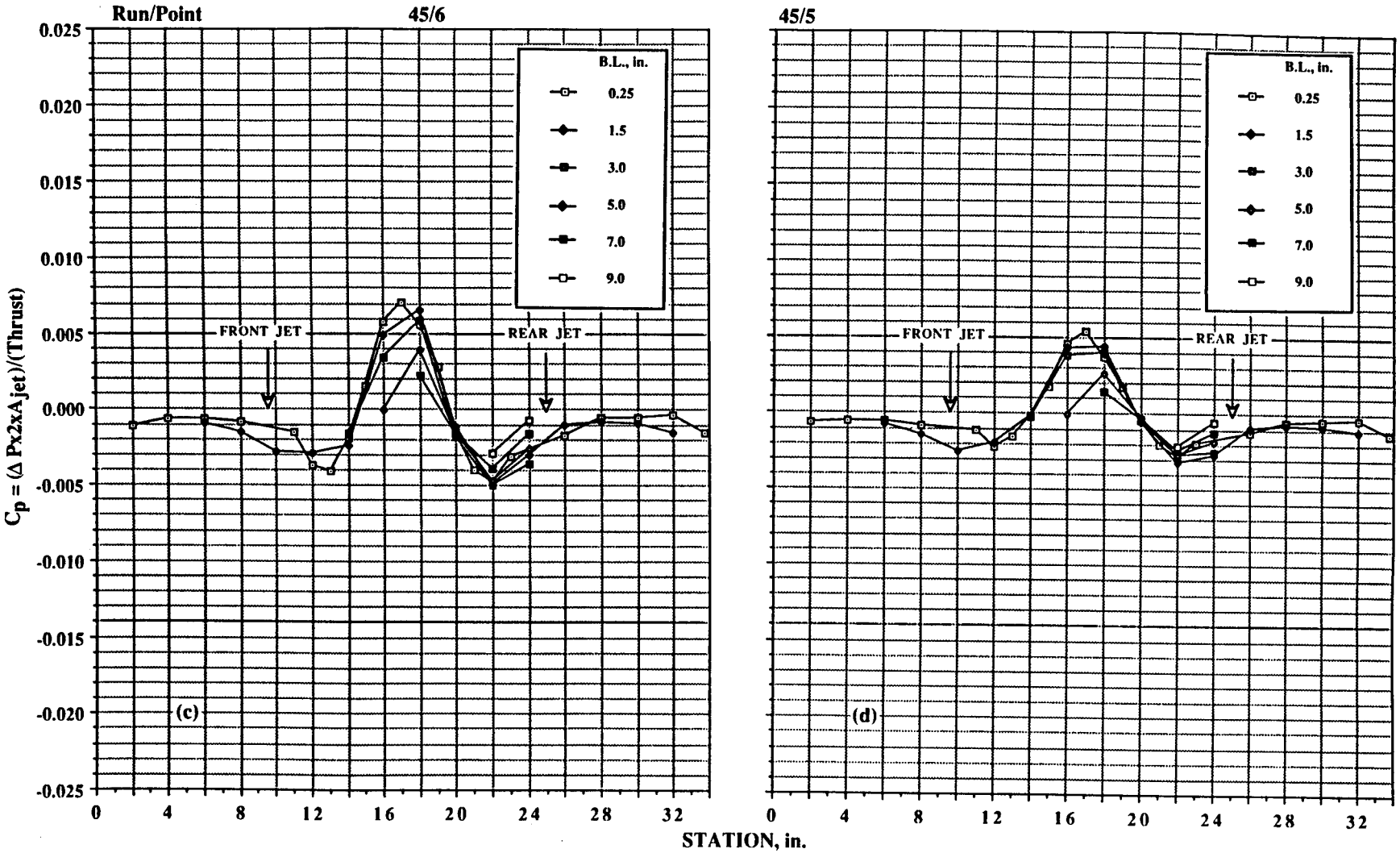

Figure 42. Continued. (c) $h/d_e = 4.6$. (d) $h/d_e = 5.75$.

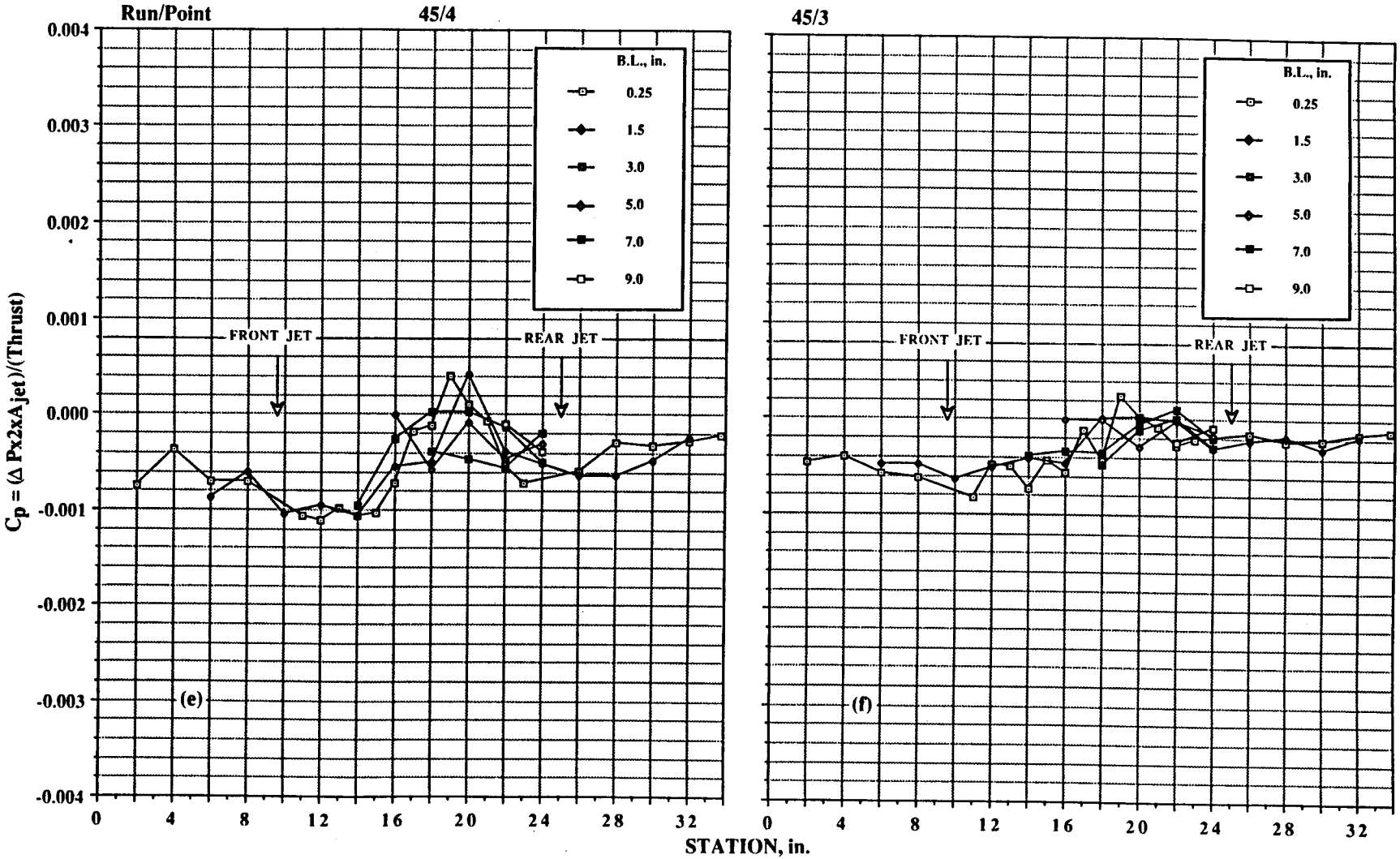

Figure 42. Continued. (e) $h/d_e = 8.62$. (f) $h/d_e = 11.5$.

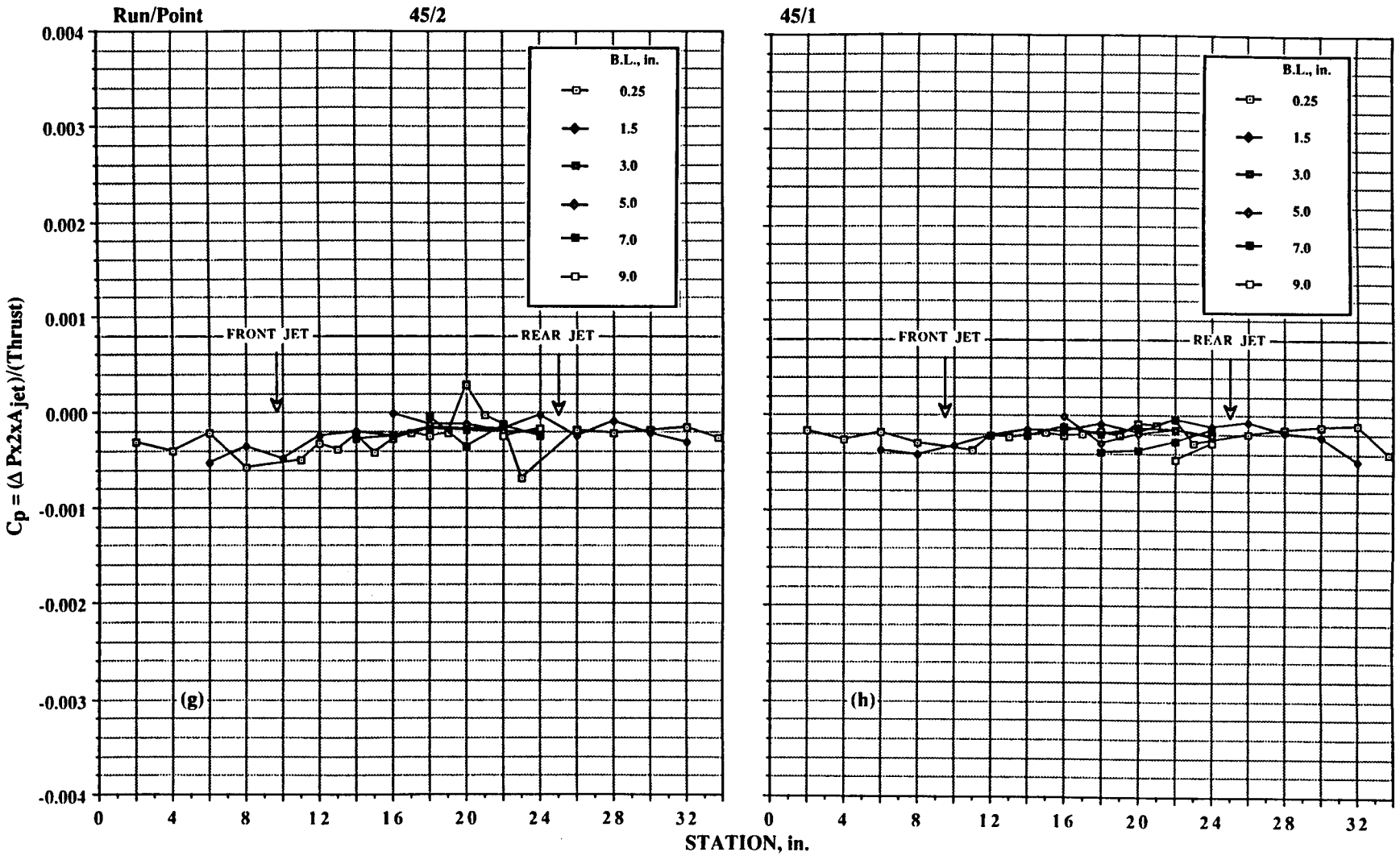

Figure 42. Continued. (g) $h/d_e = 14.37$. (h) $h/d_e = 23.0$.

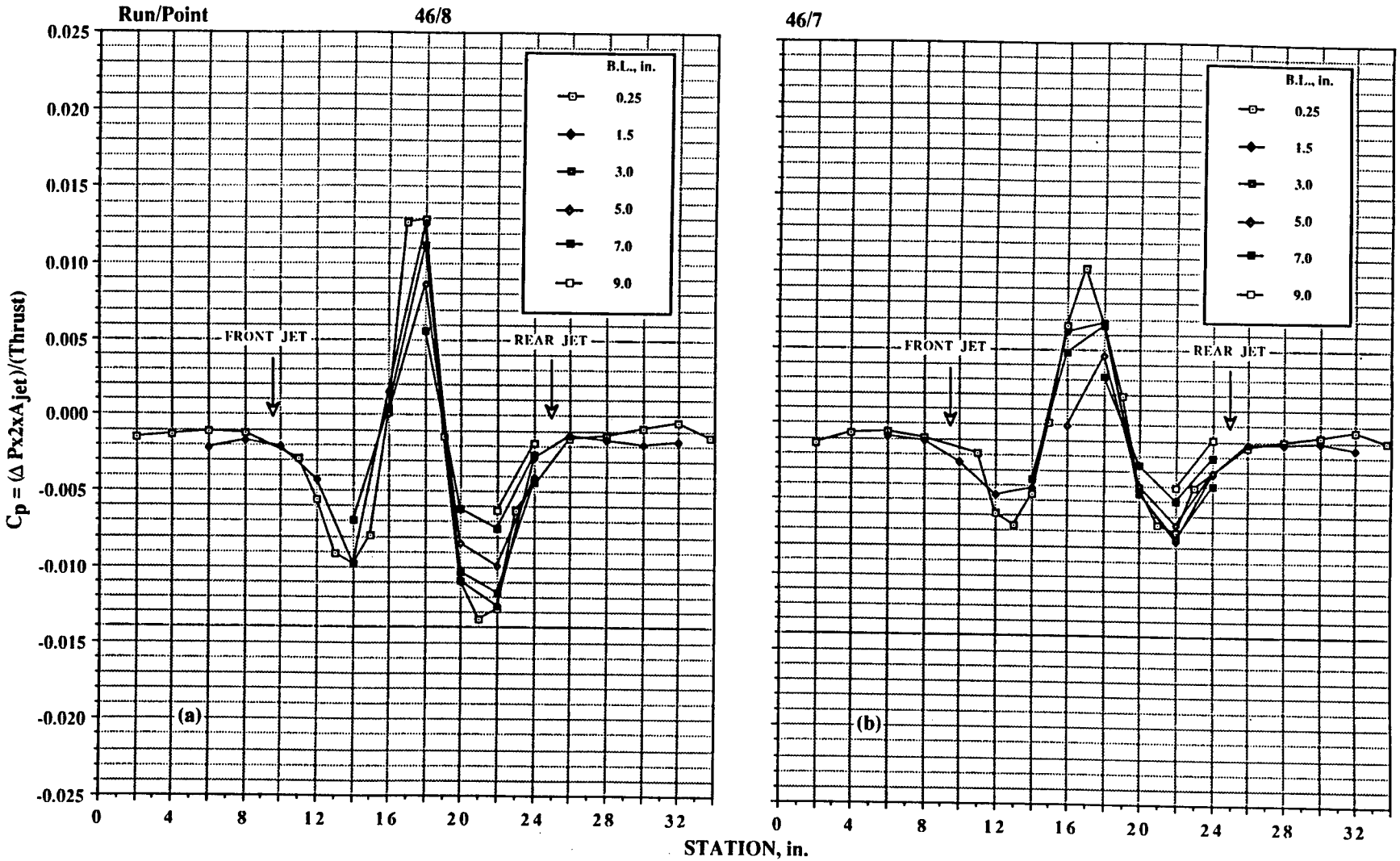

Figure 43. Pressures induced on wing/body configuration in ground effect; NPR = 6.0, T = 218 lb, both jets, no LIDs. (a) $h/d_e = 2.30$. (b) $h/d_e = 3.45$.

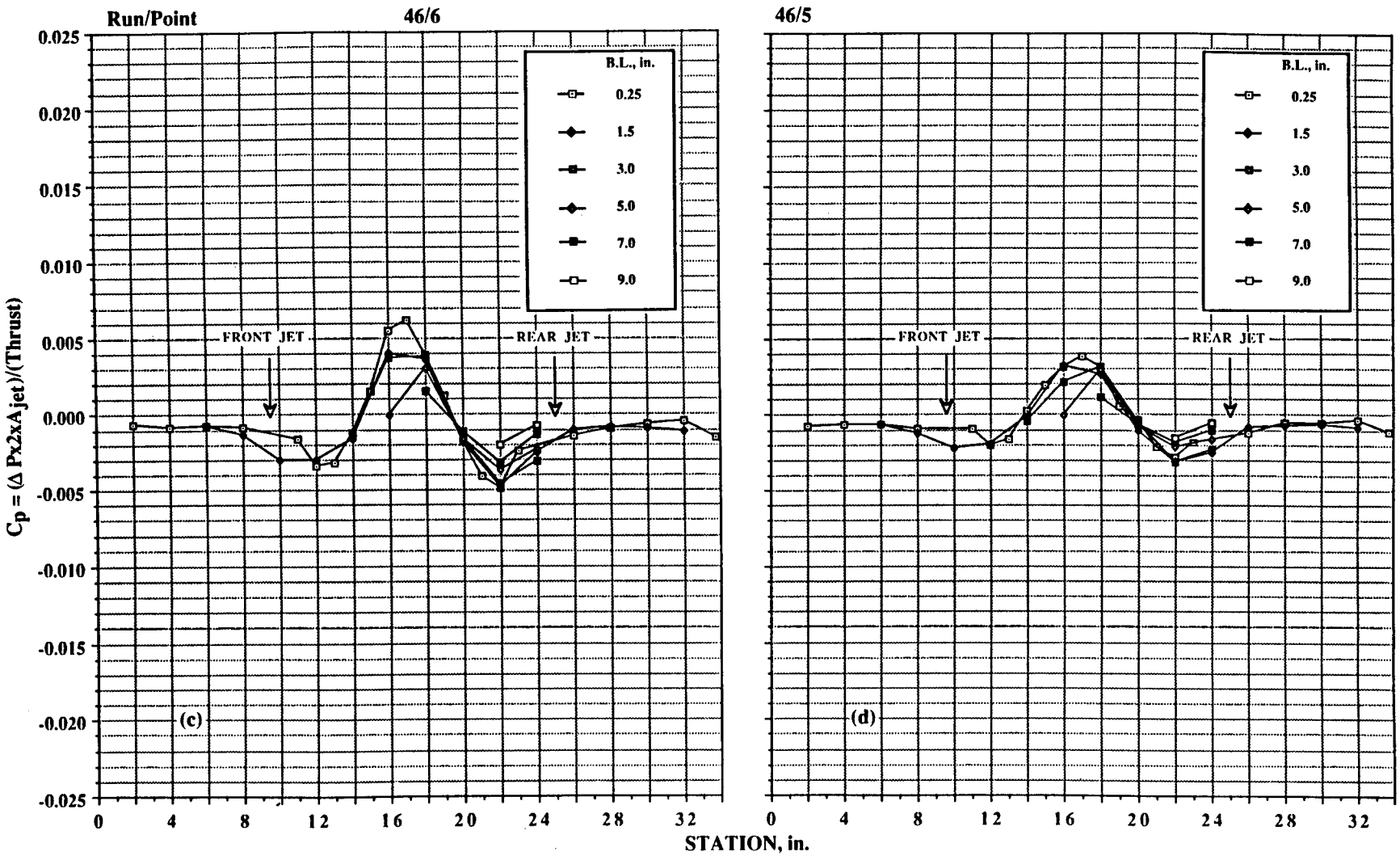

Figure 43. Continued. (c) $h/d_e = 4.6$. (d) $h/d_e = 5.75$.

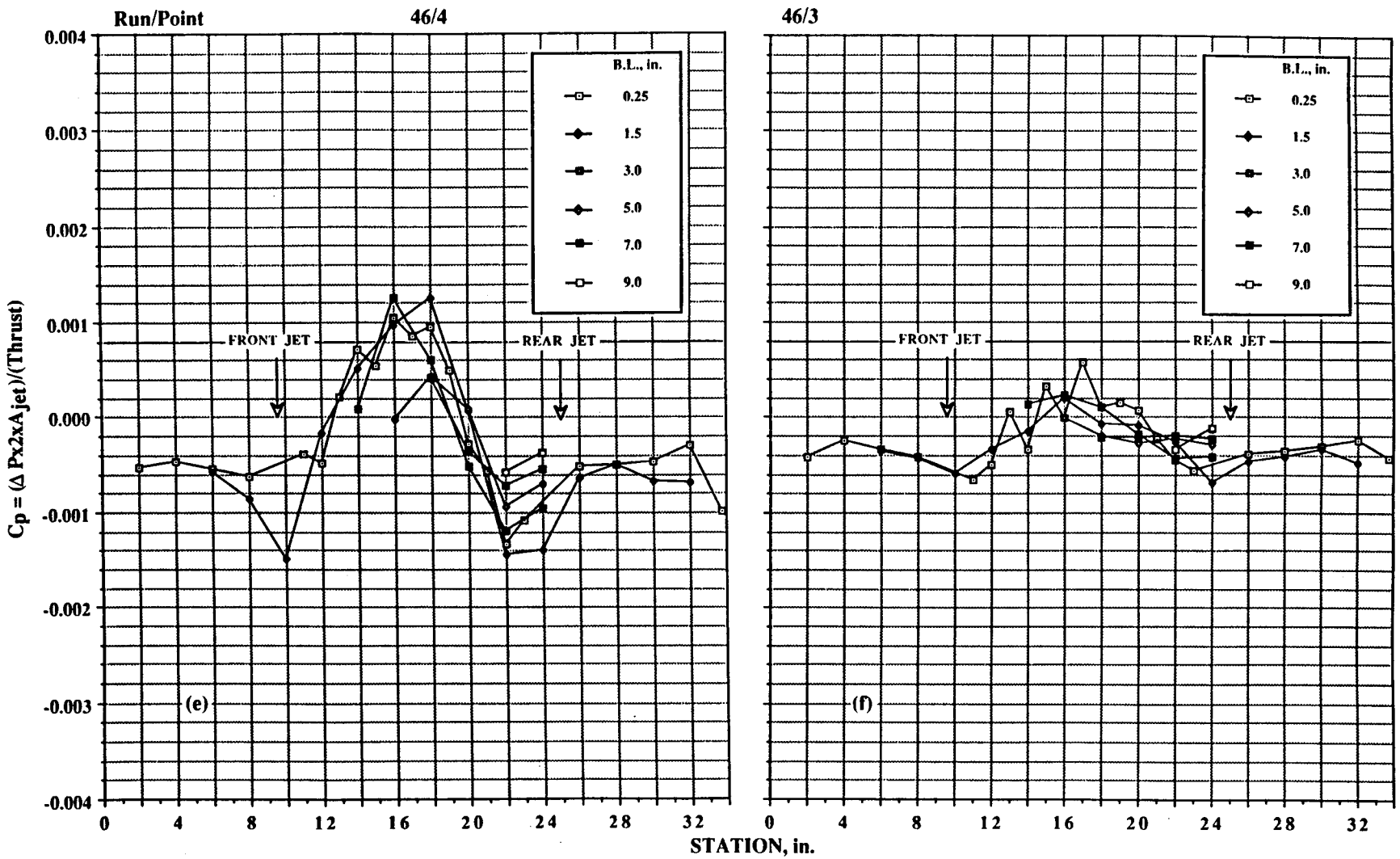

Figure 43. Continued. (e) $h/d_e = 8.62$. (f) $h/d_e = 11.5$.

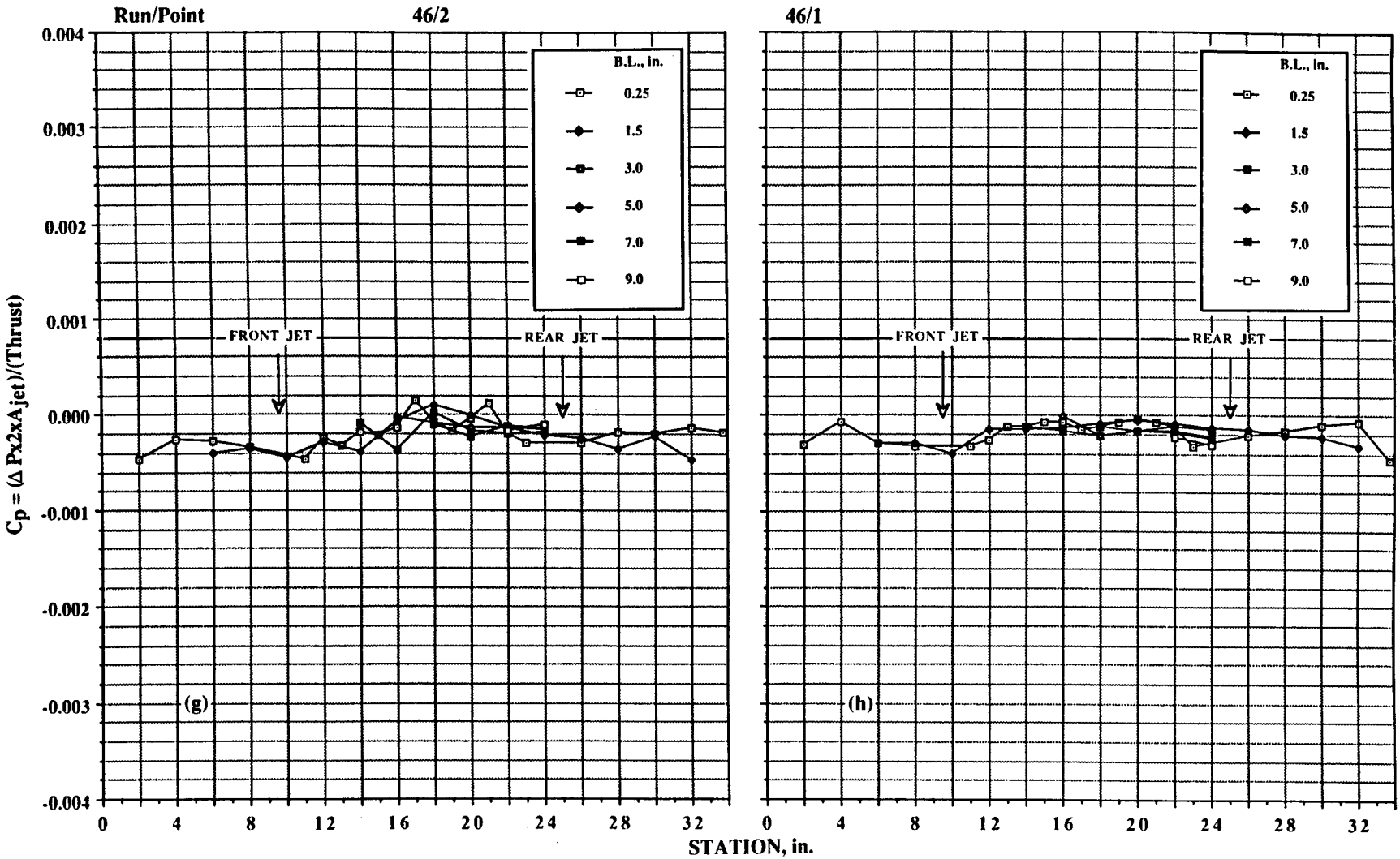

Figure 43. Concluded. (g) $h/d_e = 14.37$. (h) $h/d_e = 23.0$.

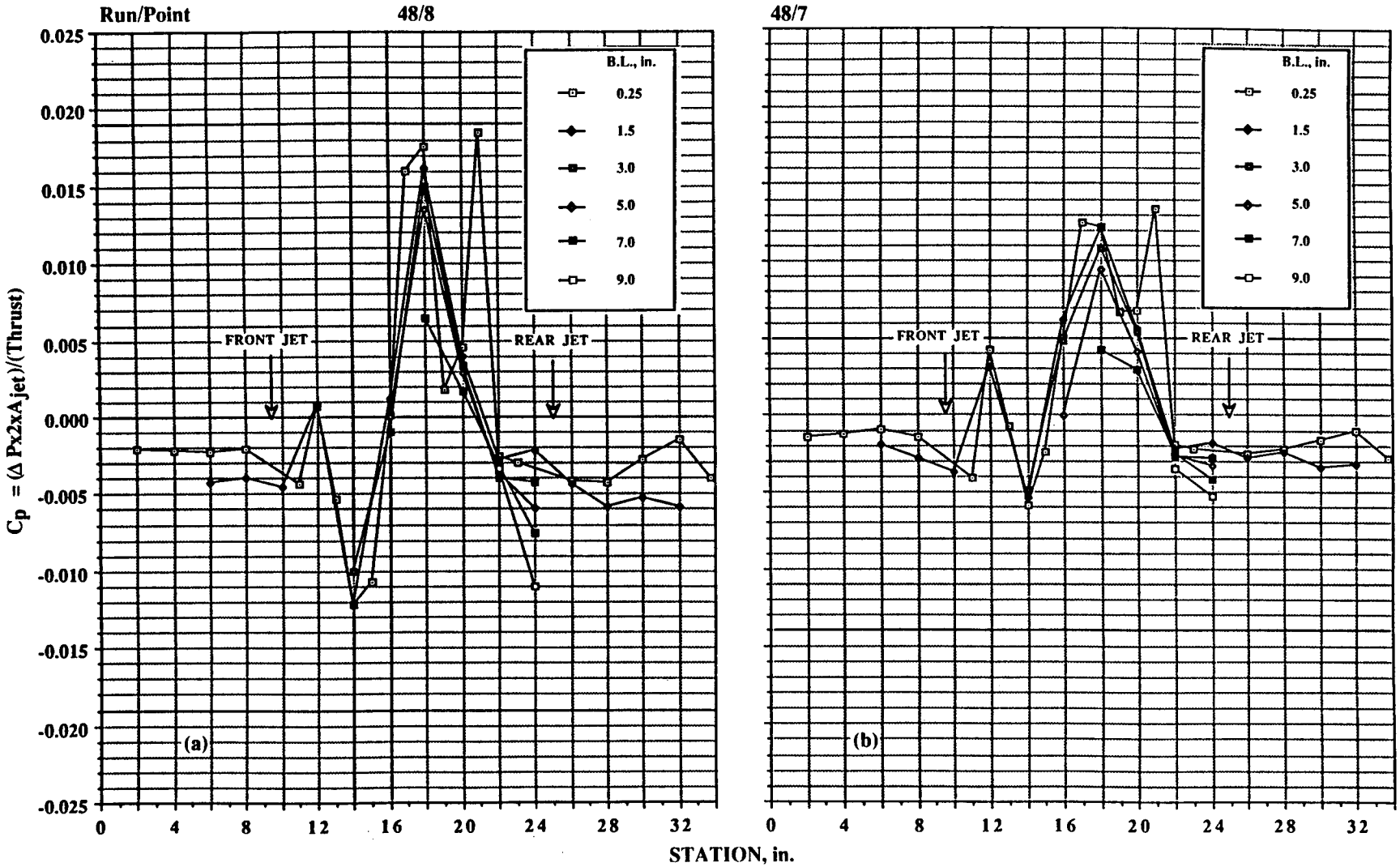

Figure 44. Pressures induced on wing/body configuration in ground effect; NPR = 2.0, T = 51 lb, both jets, LIDs at 12 in./21 in. (wing). (a) $h/d_e = 2.30$. (b) $h/d_e = 3.45$.

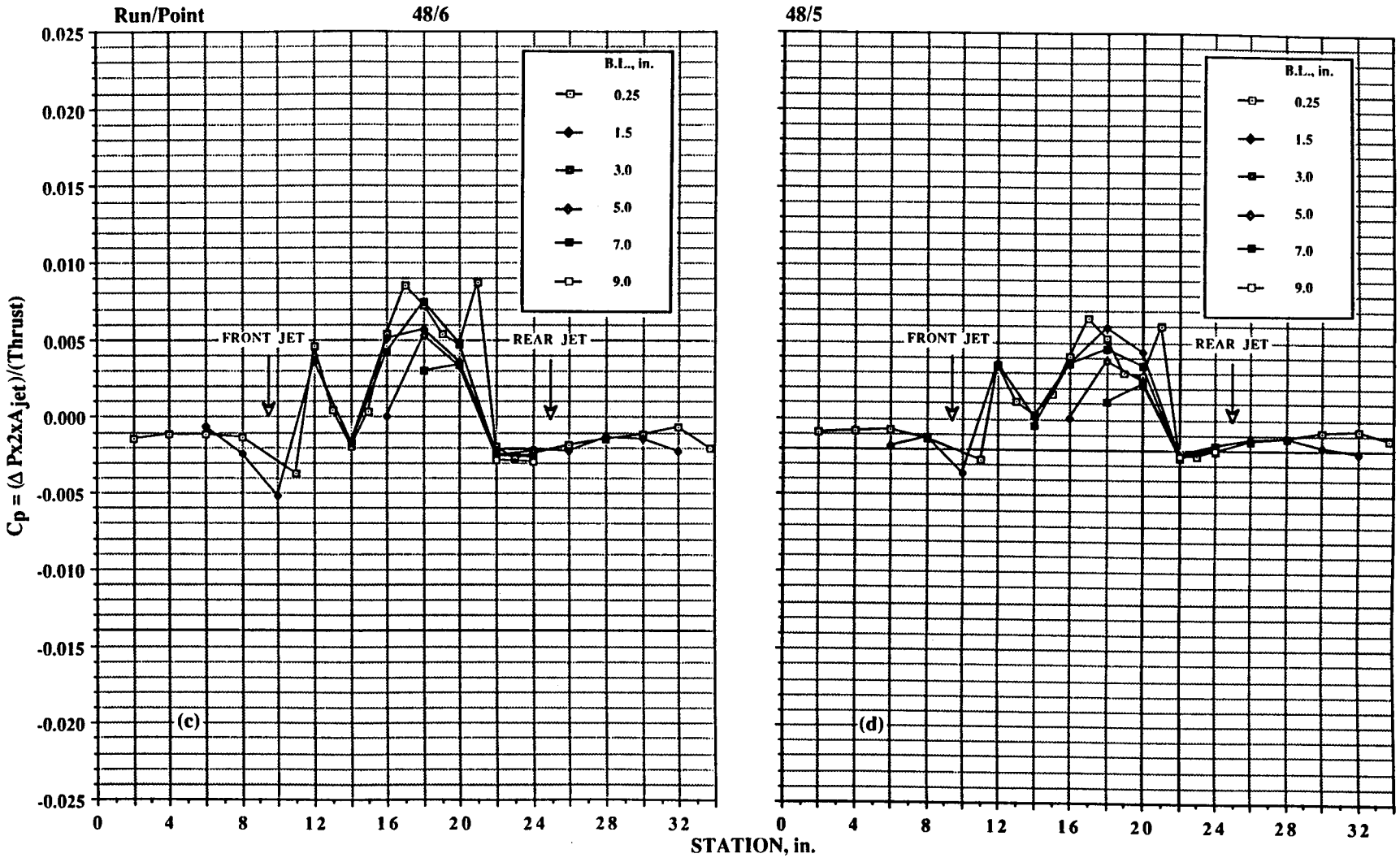

Figure 44. Continued. (c) $h/d_e = 4.6$. (d) $h/d_e = 5.75$.

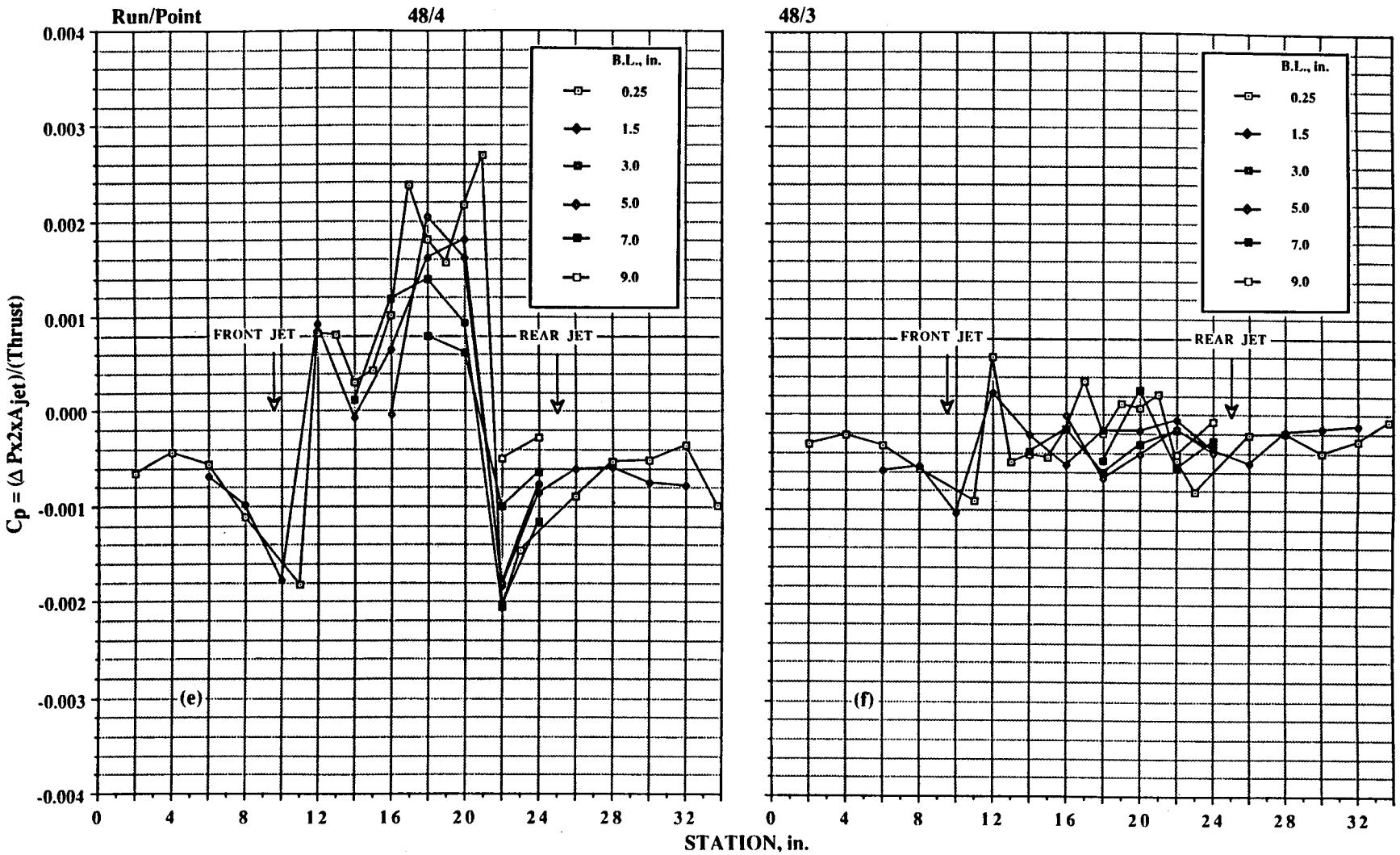

Figure 44. Continued. (e) $h/d_e = 8.62$. (f) $h/d_e = 11.5$.

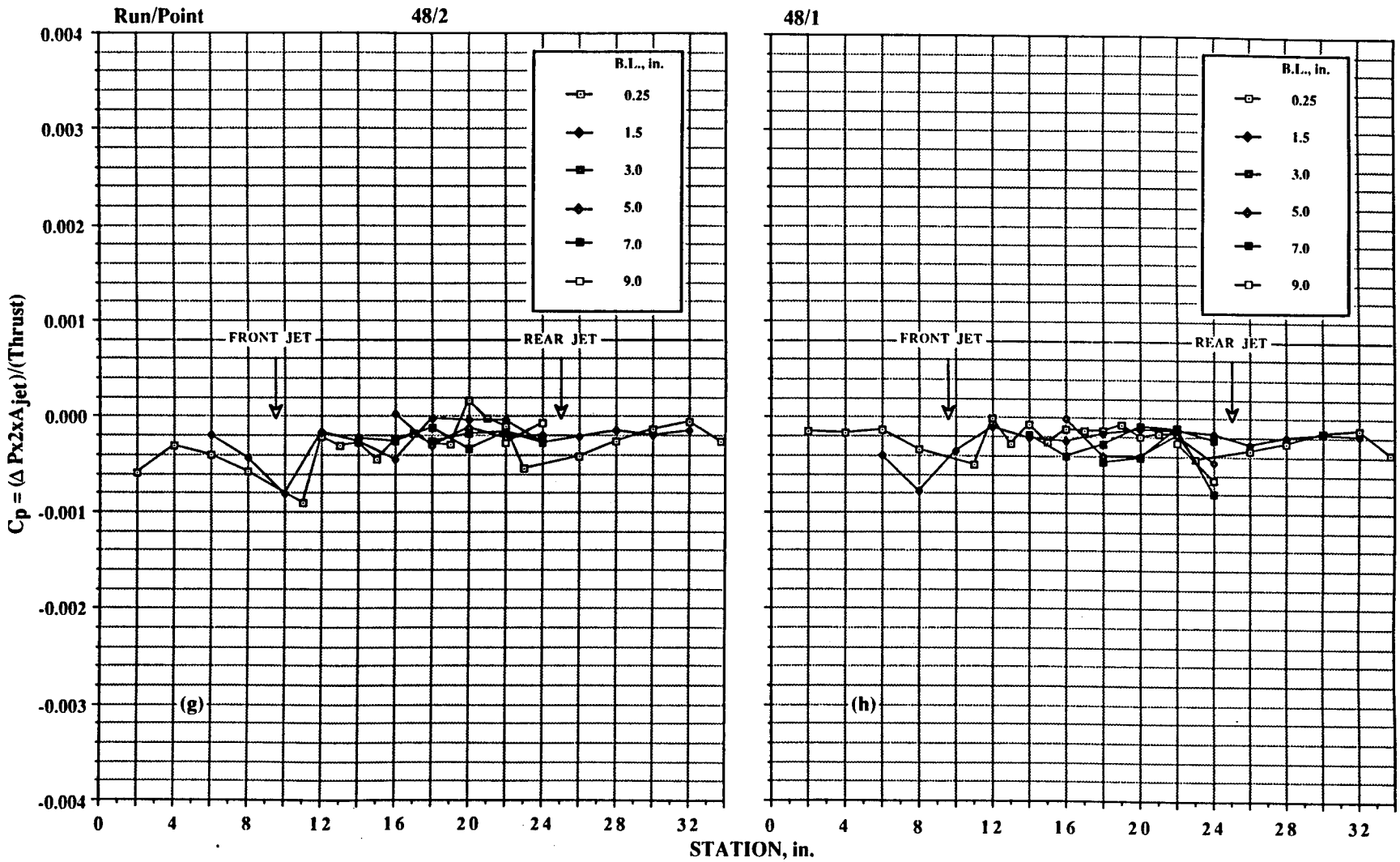

Figure 44. Concluded. (g) $h/d_e = 14.37$. (h) $h/d_e = 23.0$.

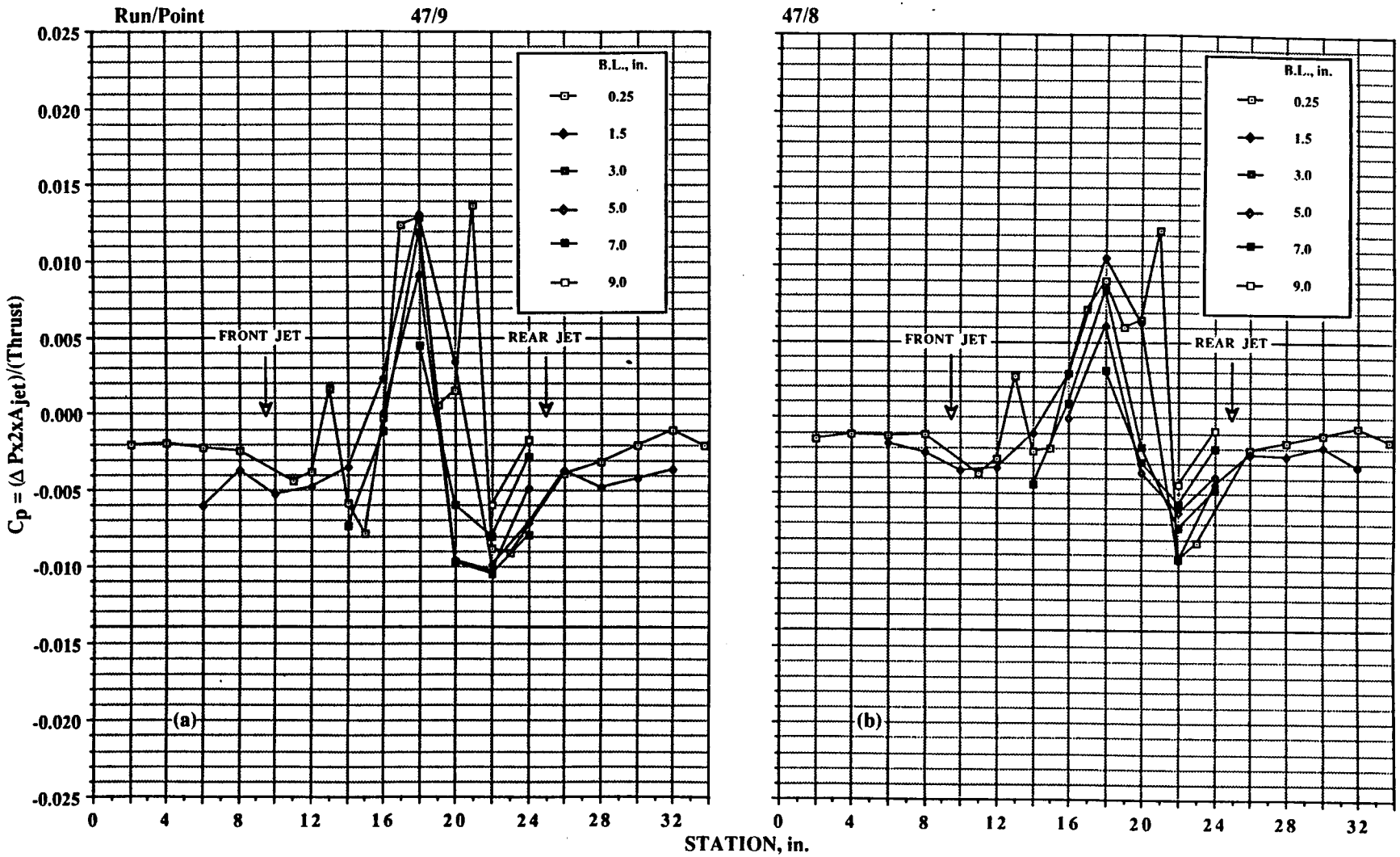

Figure 45. Pressures induced on wing/body configuration in ground effect; NPR = 2.0, T = 51 lb, both jets, LIDs at 13 in./21 in. (box). (a) $h/d_e = 2.30$. (b) $h/d_e = 3.45$.

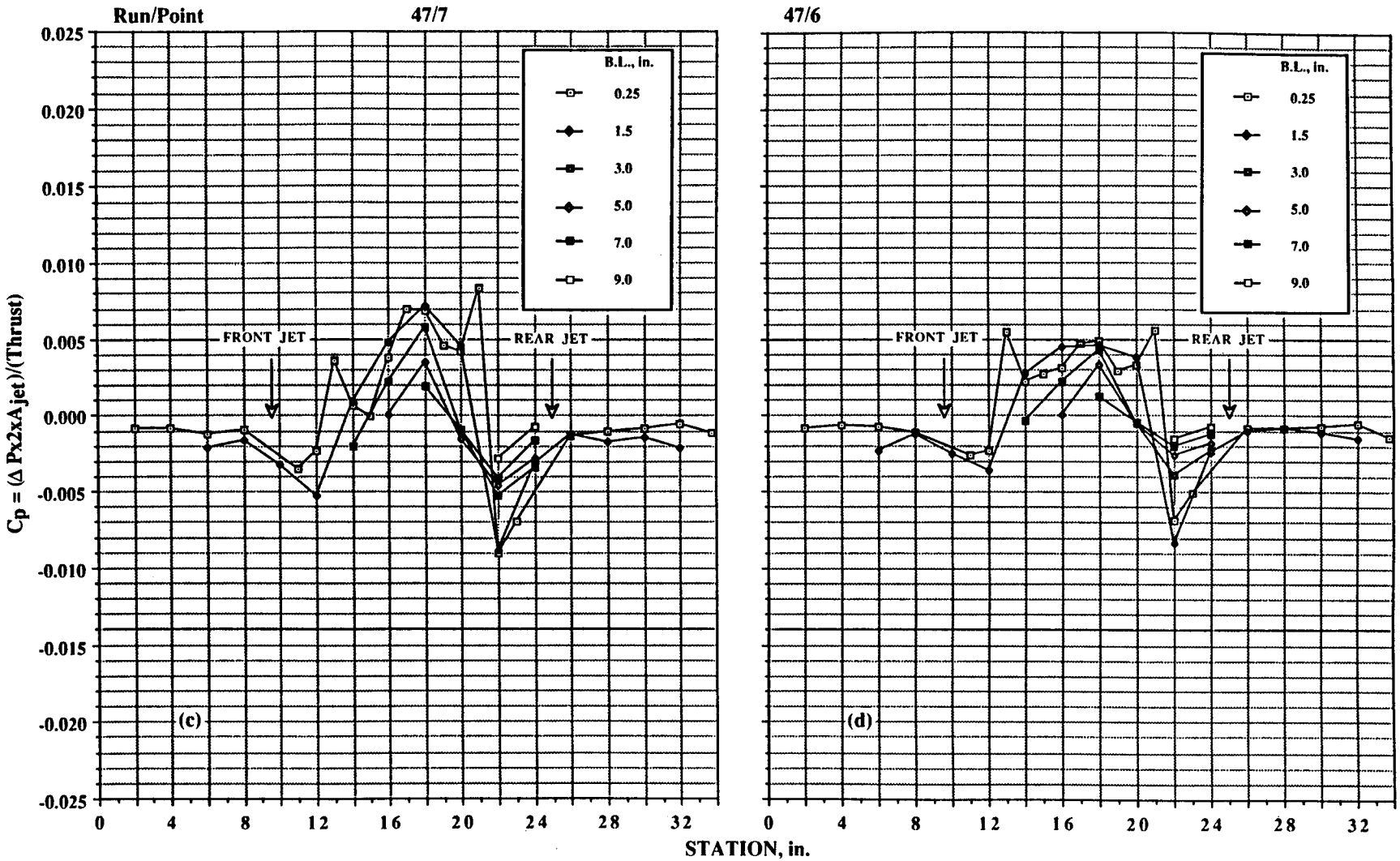

Figure 45. Continued. (c) $h/d_e = 4.6$. (d) $h/d_e = 5.75$.

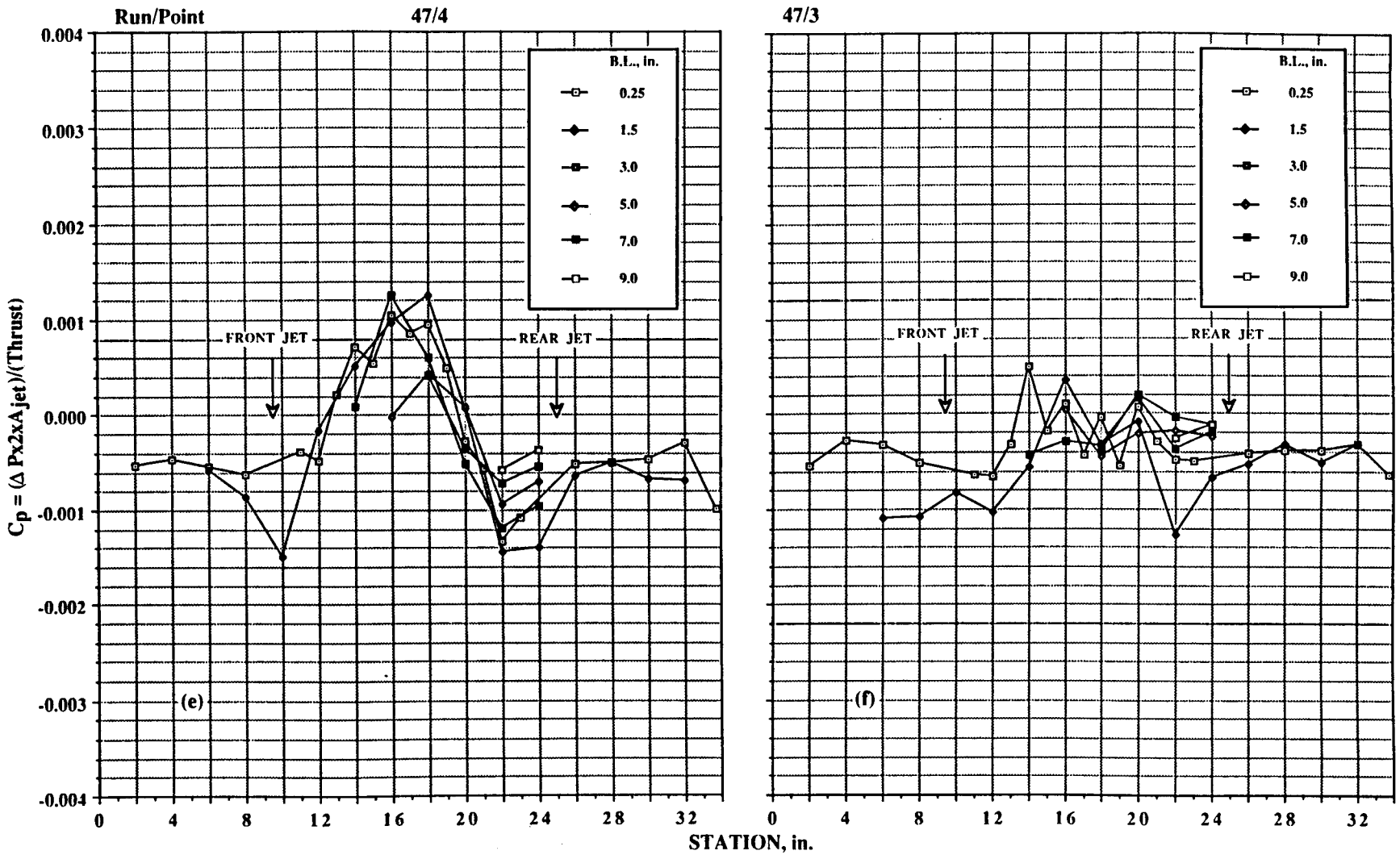

Figure 45. Continued. (e) $h/d_e = 8.62$. (f) $h/d_e = 11.5$.

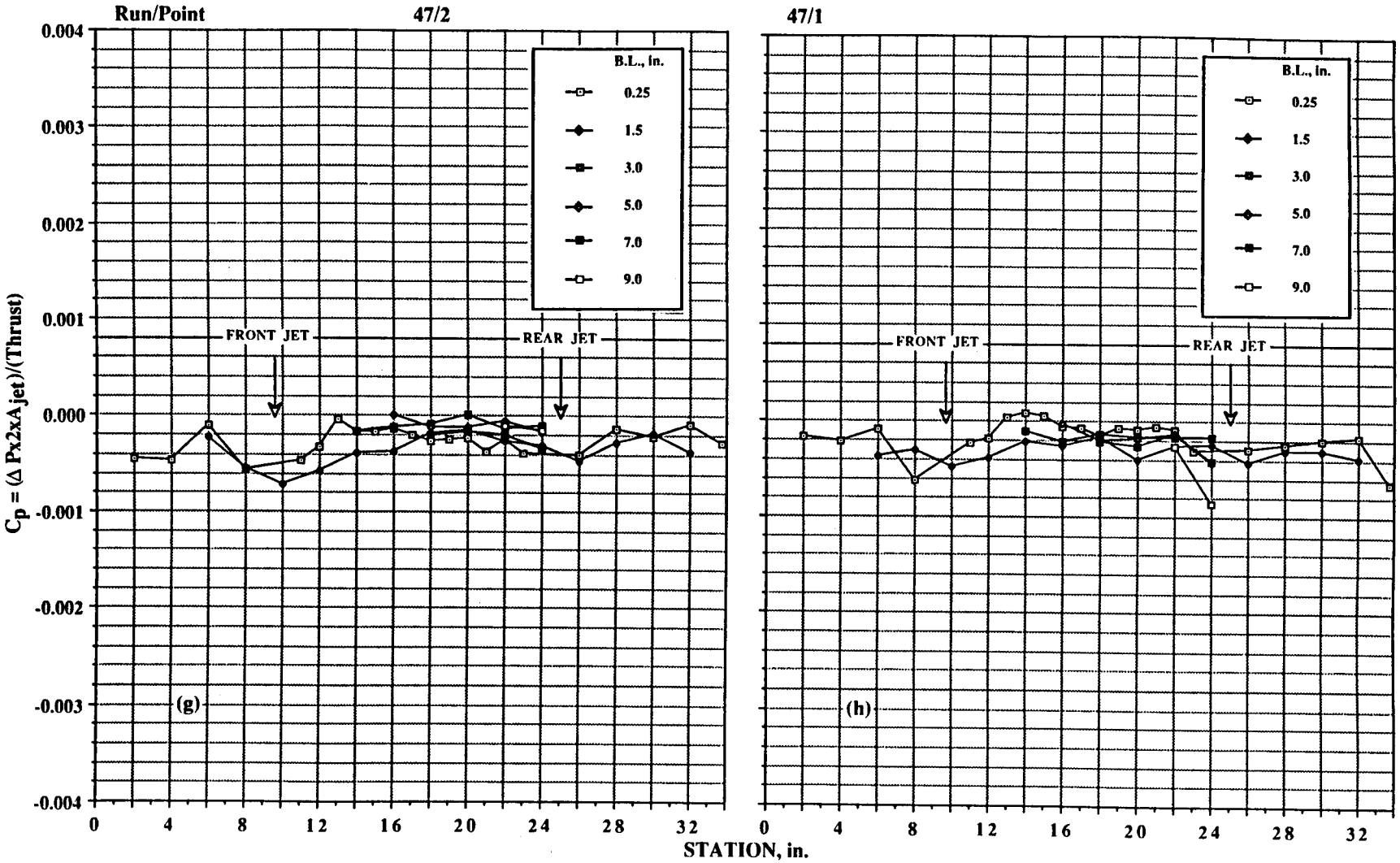

Figure 45. Concluded. (g) $h/d_e = 14.37$. (h) $h/d_e = 23.0$.

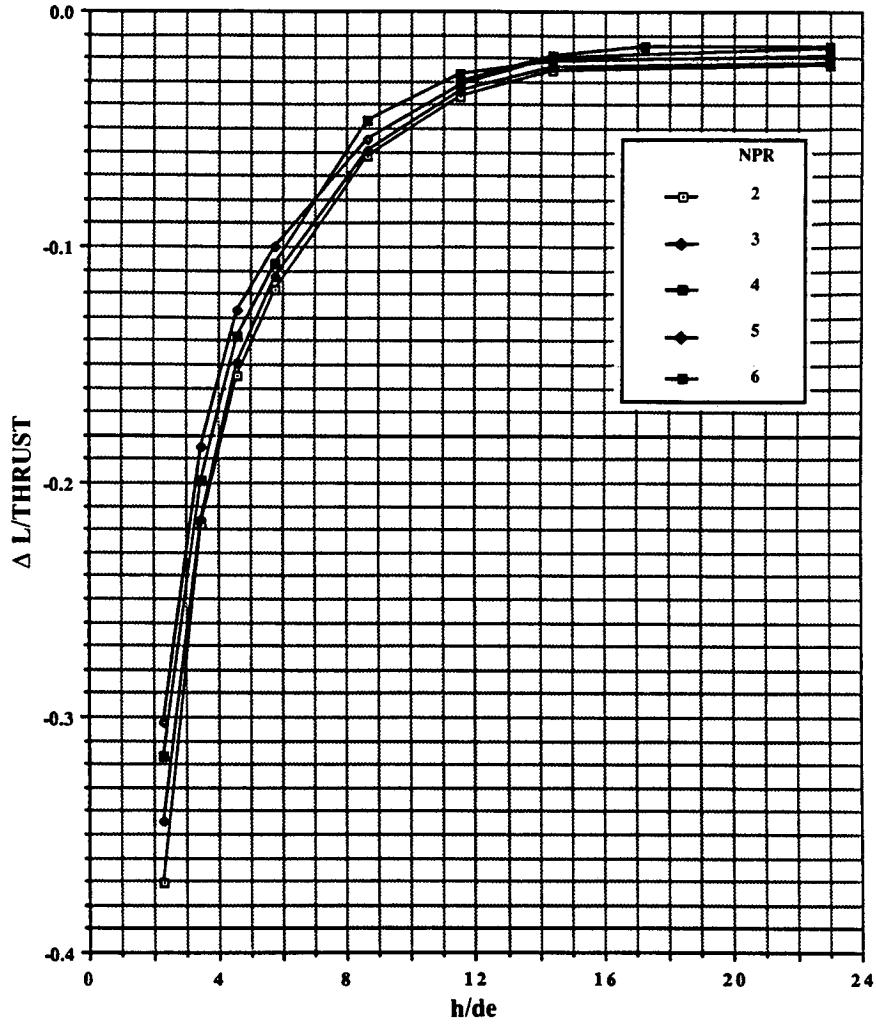

Figure 46. Effect of pressure ratio on jet-induced lift on delta-wing configuration in ground effect, both jets, no LIDs.

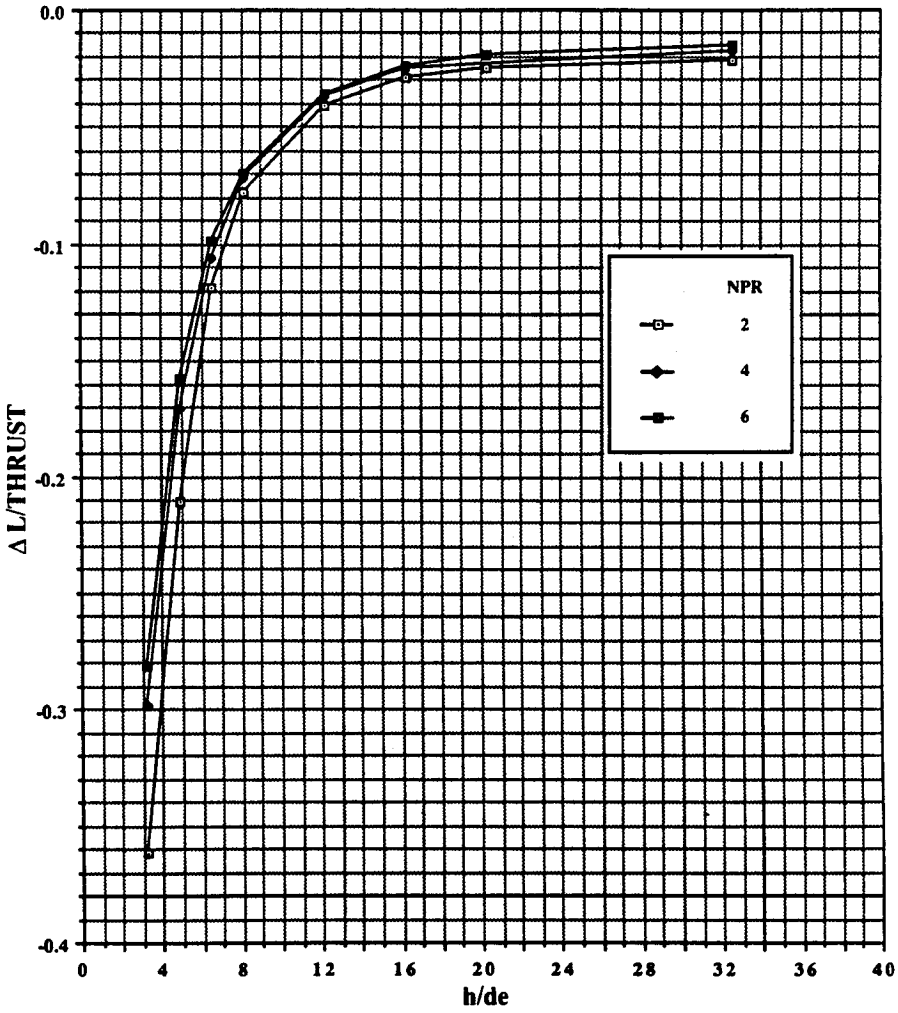

Figure 47. Effect of pressure ratio on jet-induced lift on delta-wing configuration in ground effect, front jet only, no LIDs.

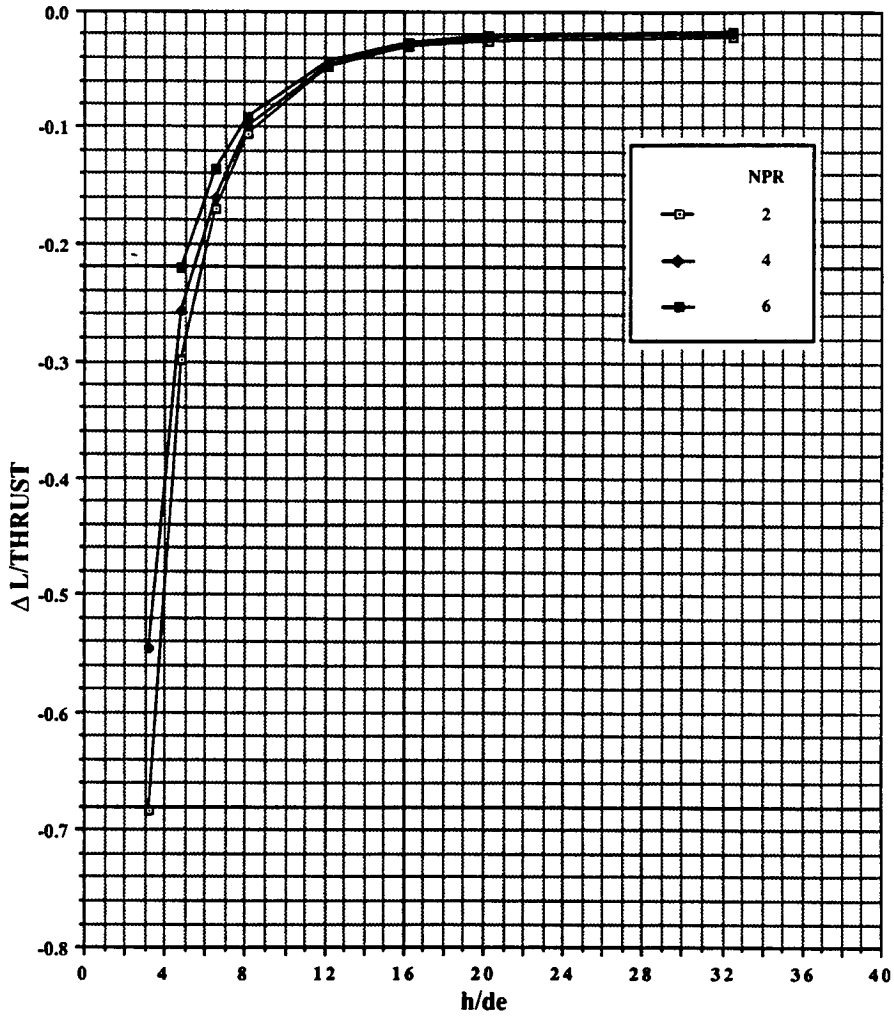

Figure 48. Effect of pressure ratio on jet-induced lift on delta-wing configuration in ground effect, rear jet only, no LIDs.

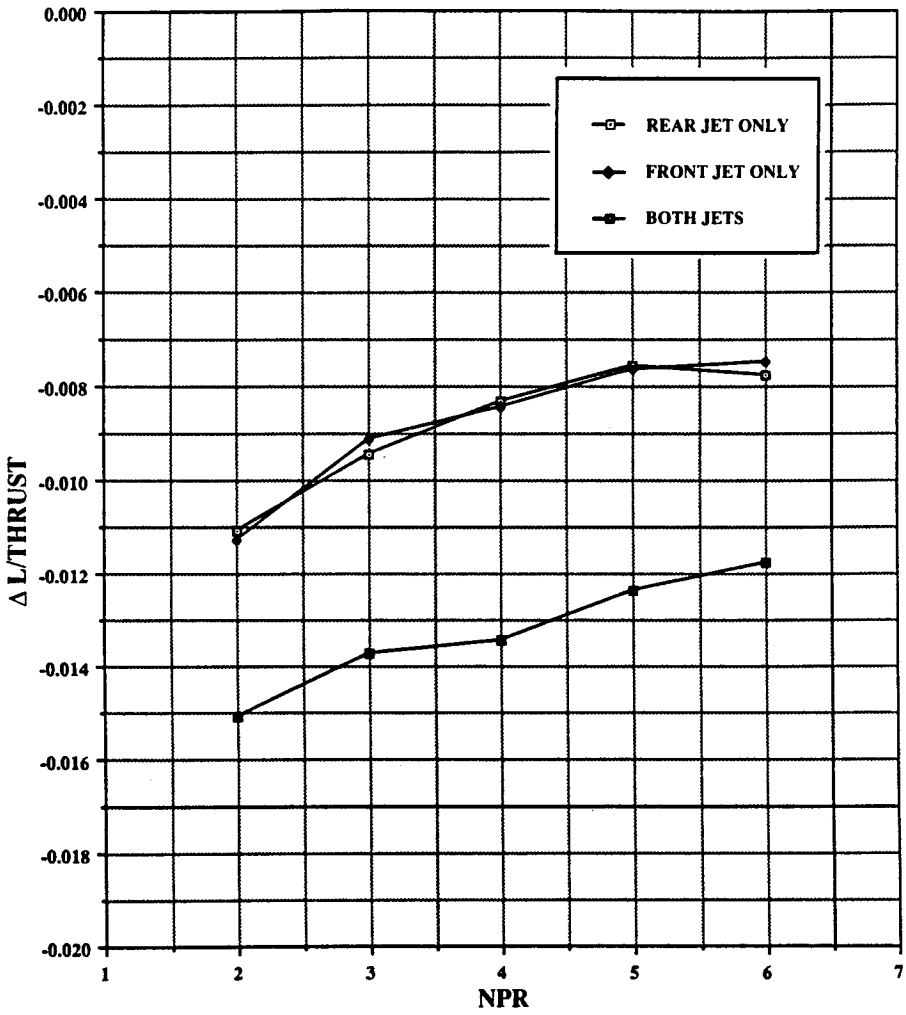

Figure 49. Jet-induced lift on delta-wing configuration out of ground effect, no LIDs.

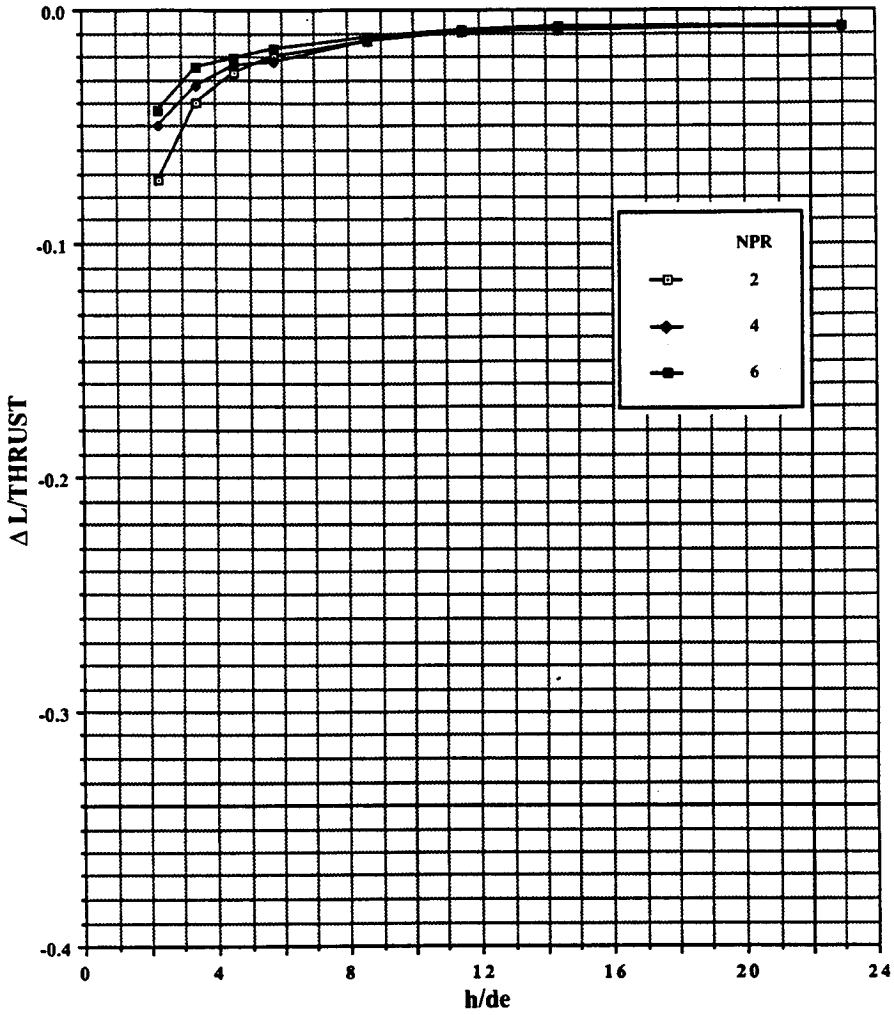

Figure 50. Effect of pressure ratio on jet-induced lift on body-alone configuration in ground effect, both jets, no LIDs.

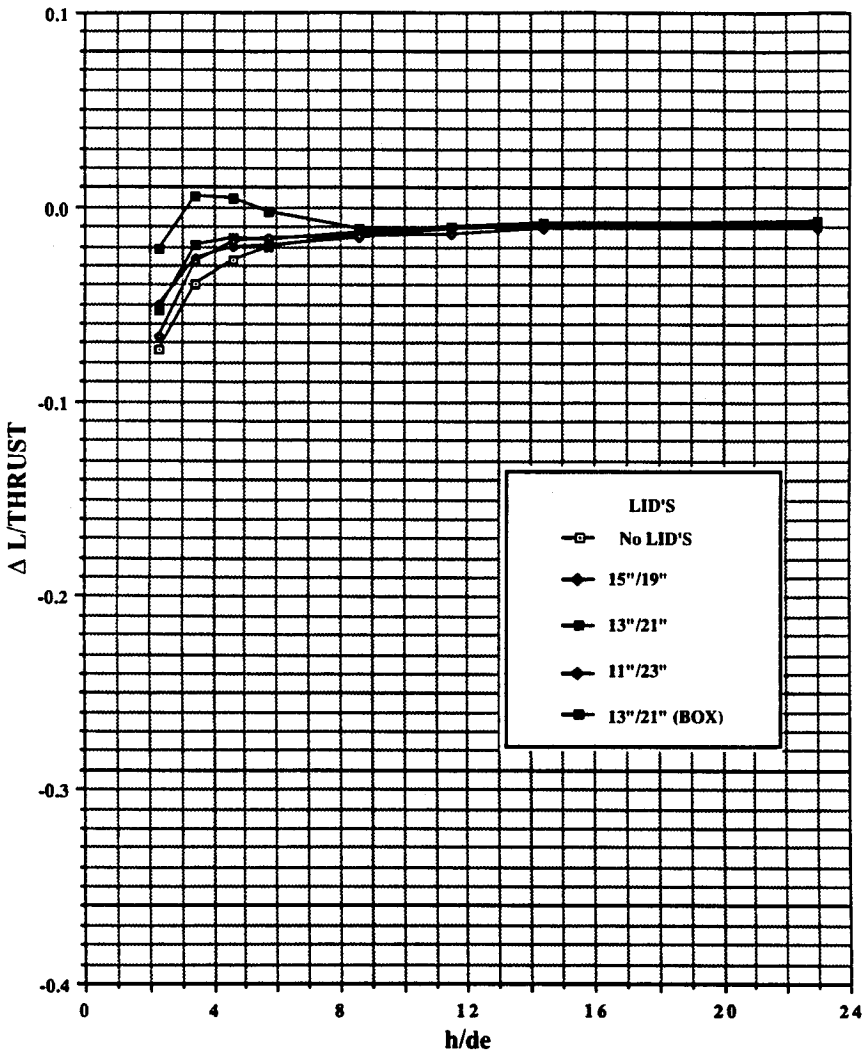

Figure 51. Effect of LIDs on jet-induced lift on body-alone configuration in ground effect, NPR = 2.0, both jets.

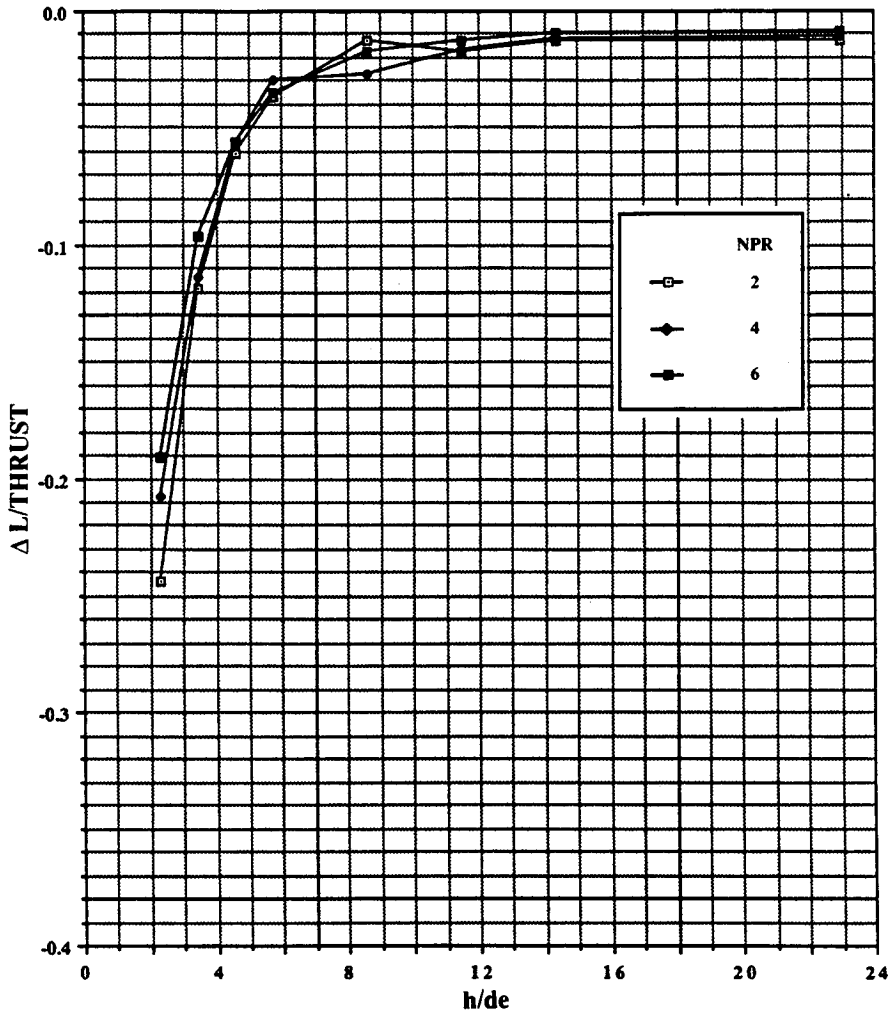

Figure 52. Effect of pressure ratio on jet-induced lift on wing/body configuration in ground effect, both jets, no LIDs.

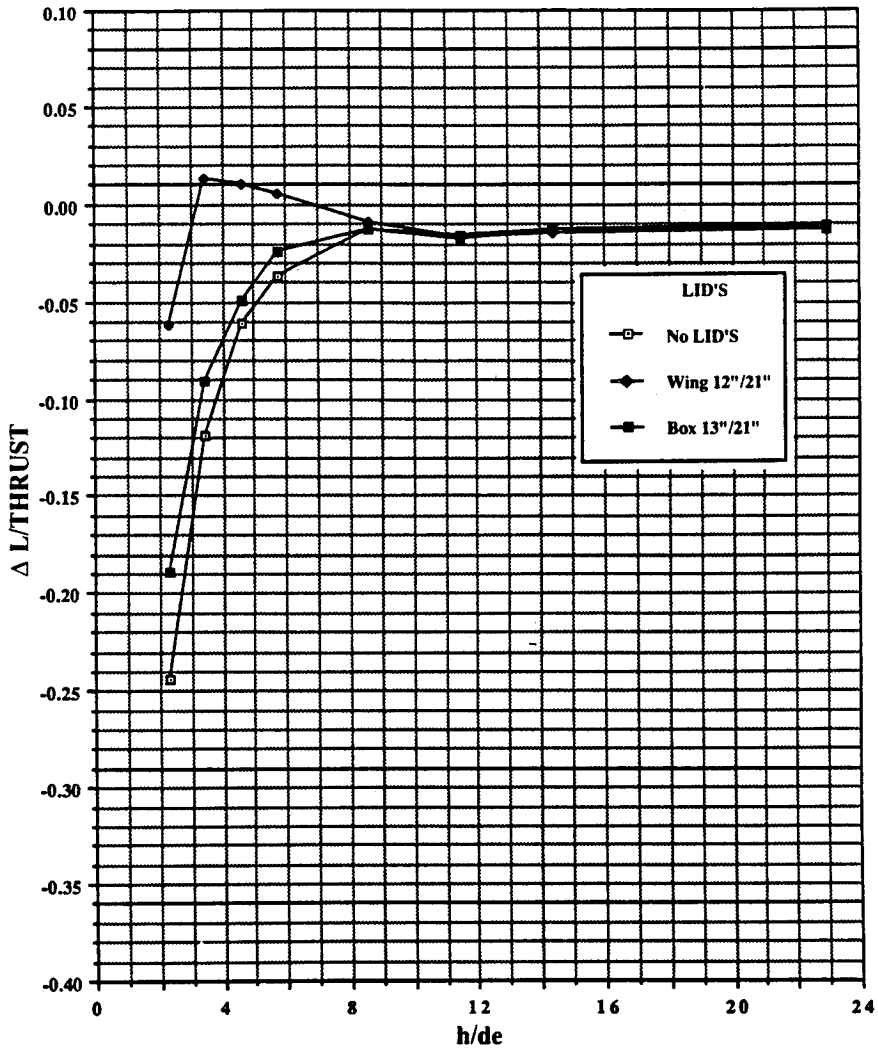

Figure 53. Effect of LIDs on jet-induced lift on wing/body configuration in ground effect, both jets, NPR = 2.0.

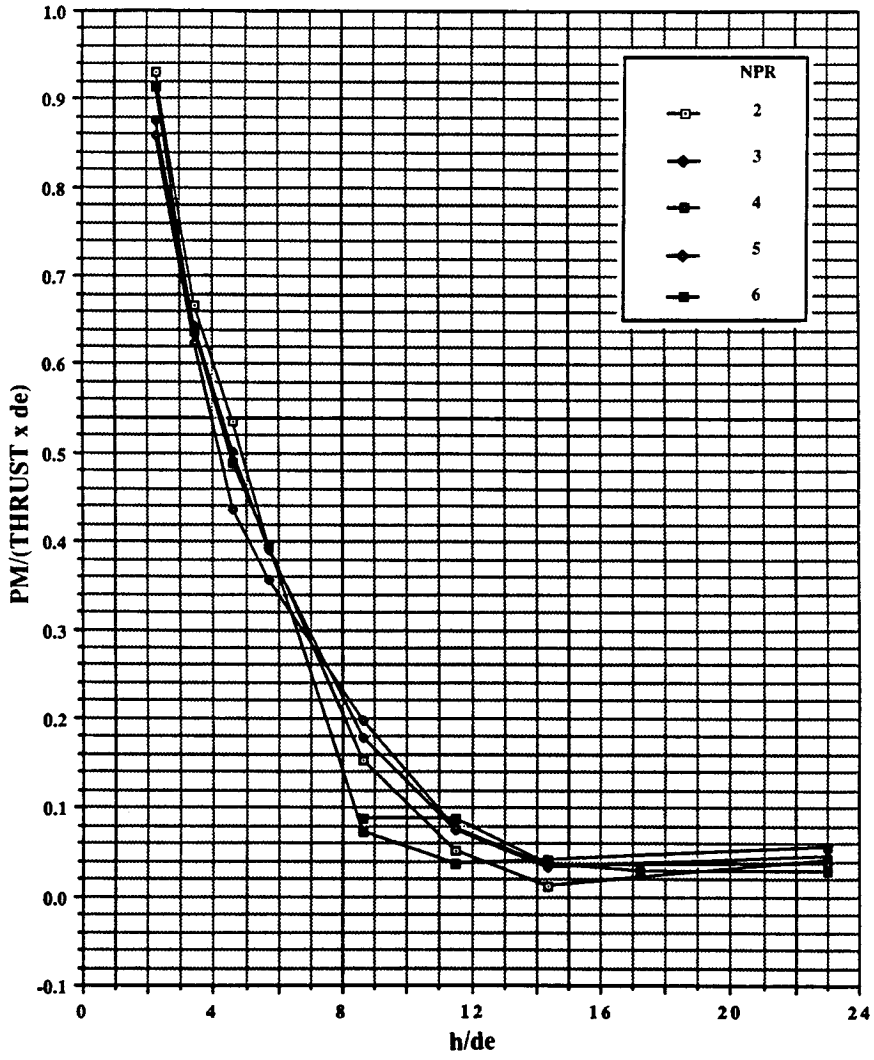

Figure 54. Effect of pressure ratio on jet-induced pitching moment on delta-wing configuration in ground effect, both jets, no LIDs.

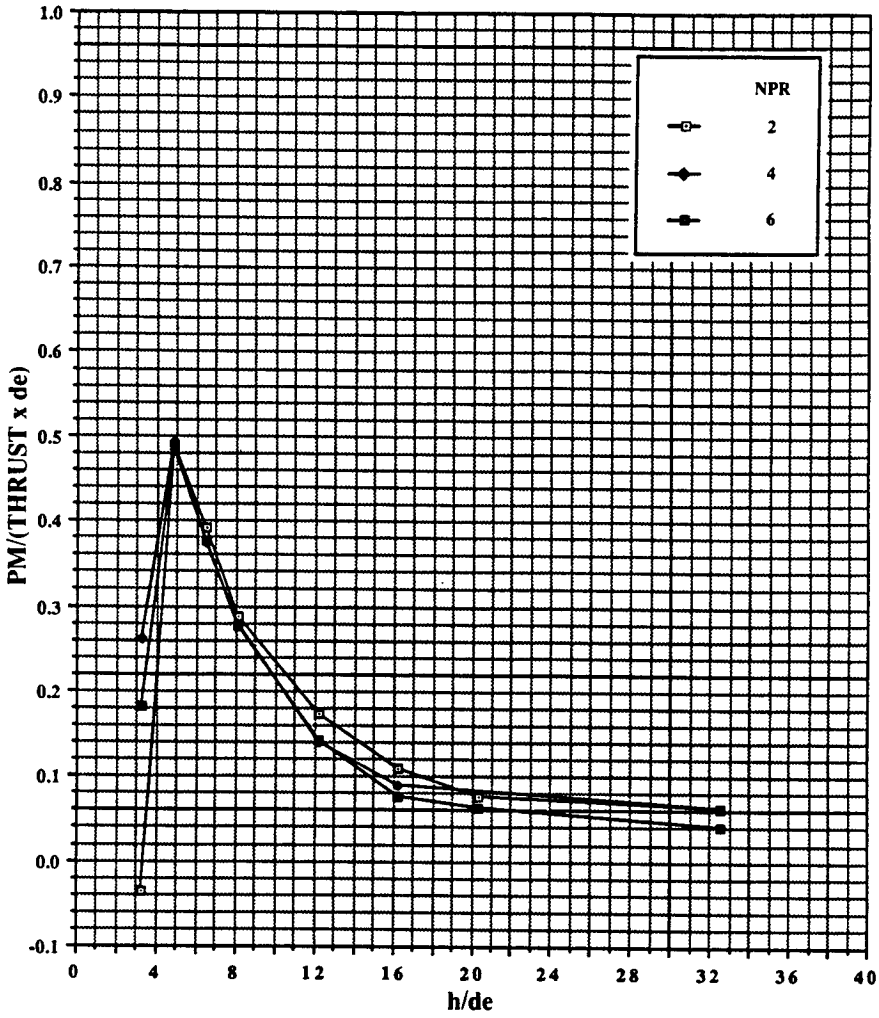

Figure 55. Effect of pressure ratio on jet-induced pitching moment on delta-wing configuration in ground effect, front jet only, no LIDs.

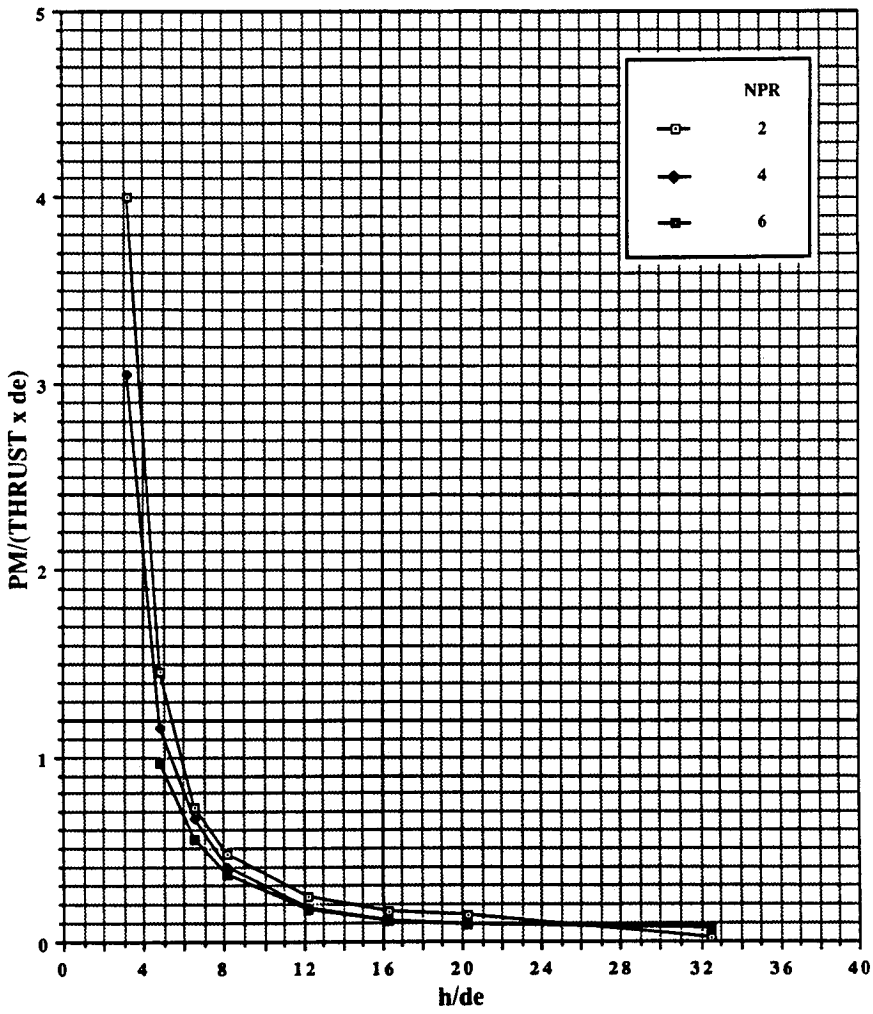

Figure 56. Effect of pressure ratio on jet-induced pitching moment on delta-wing configuration in ground effect, rear jet only, no LIDs.

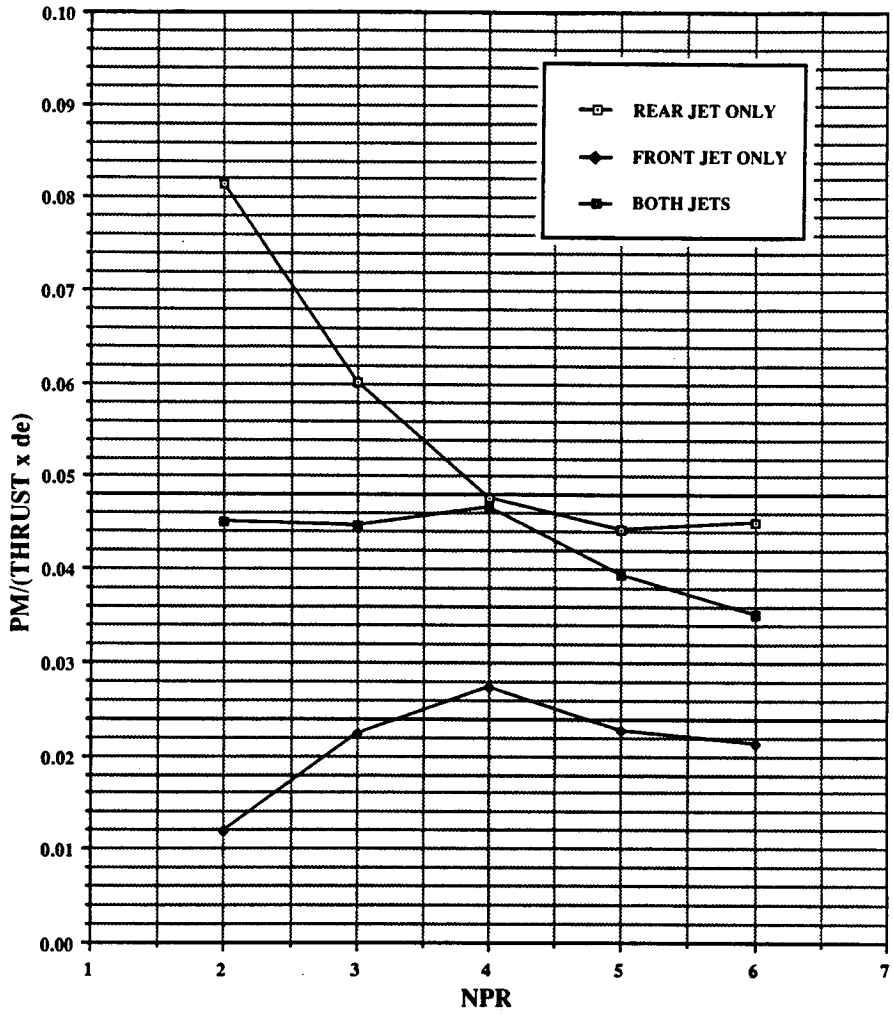

Figure 57. Jet-induced pitching moment on delta-wing configuration out of ground effect, no LIDs.

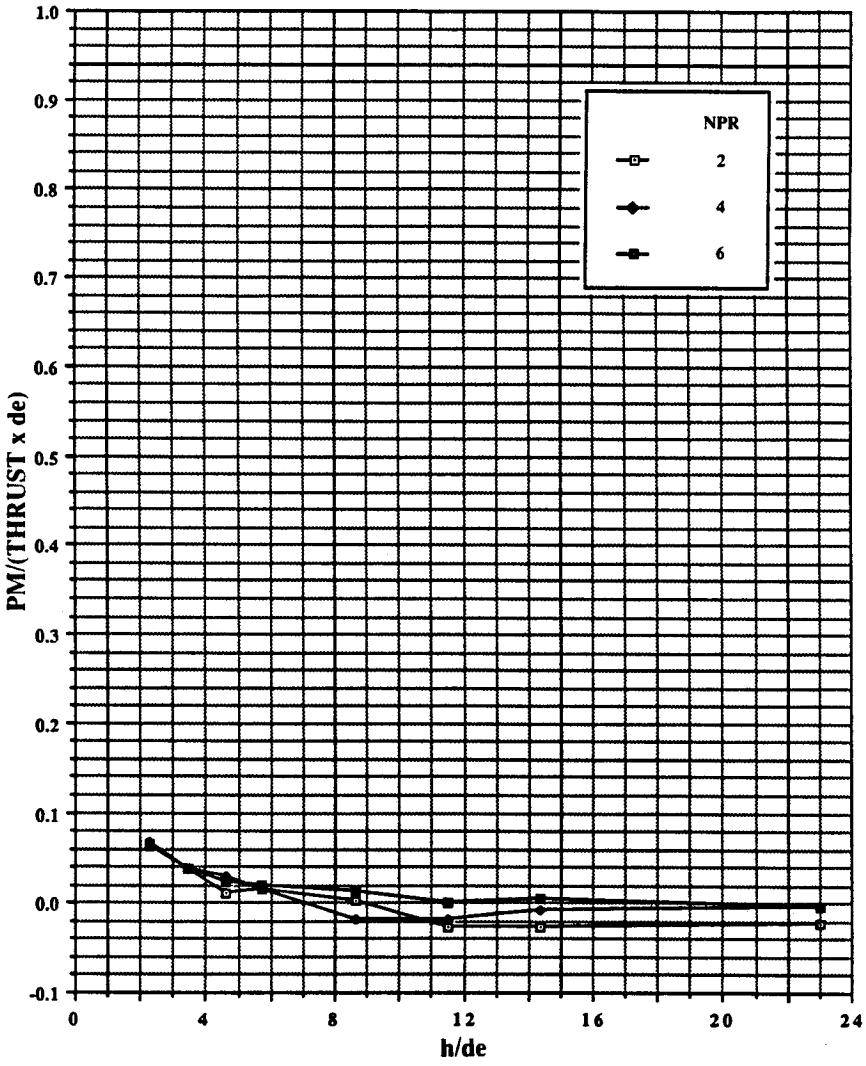

Figure 58. Effect of pressure ratio on jet-induced pitching moment on body-alone configuration in ground effect, both jets, no LIDs.

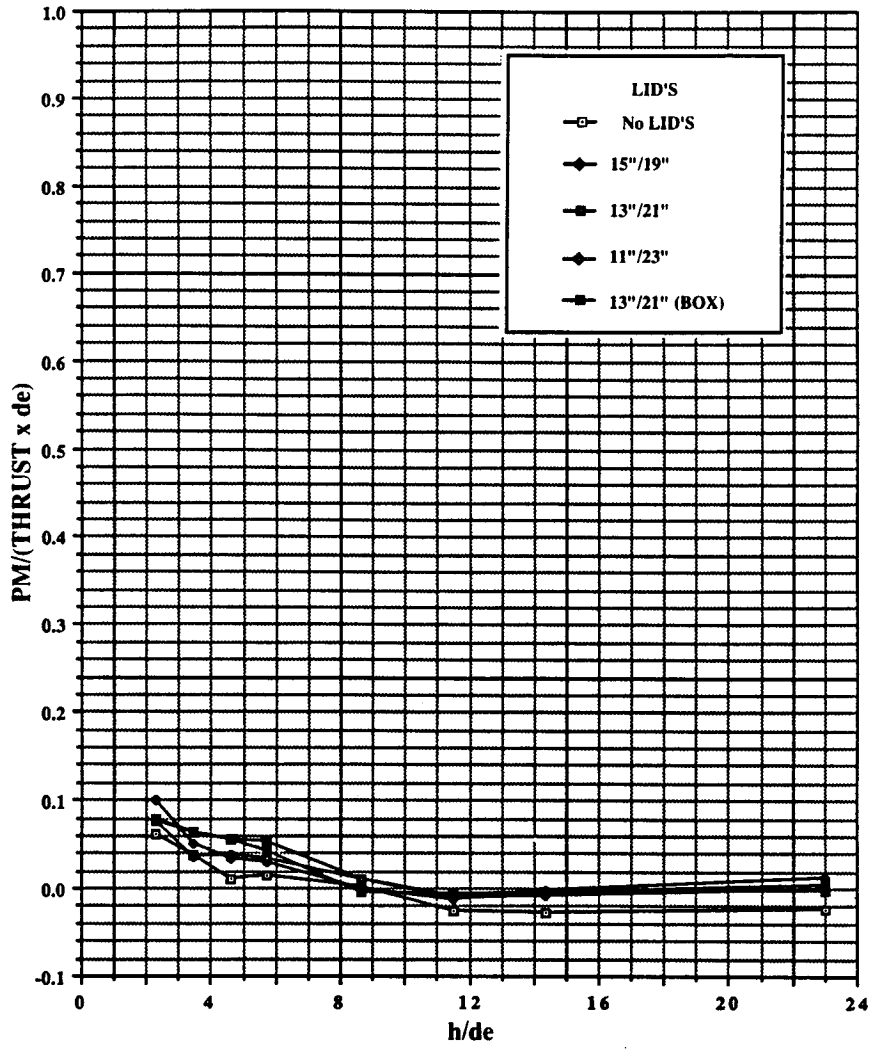

Figure 59. Effect of LIDs on jet-induced pitching moment on body-alone configuration in ground effect, NPR = 2.0, both jets.

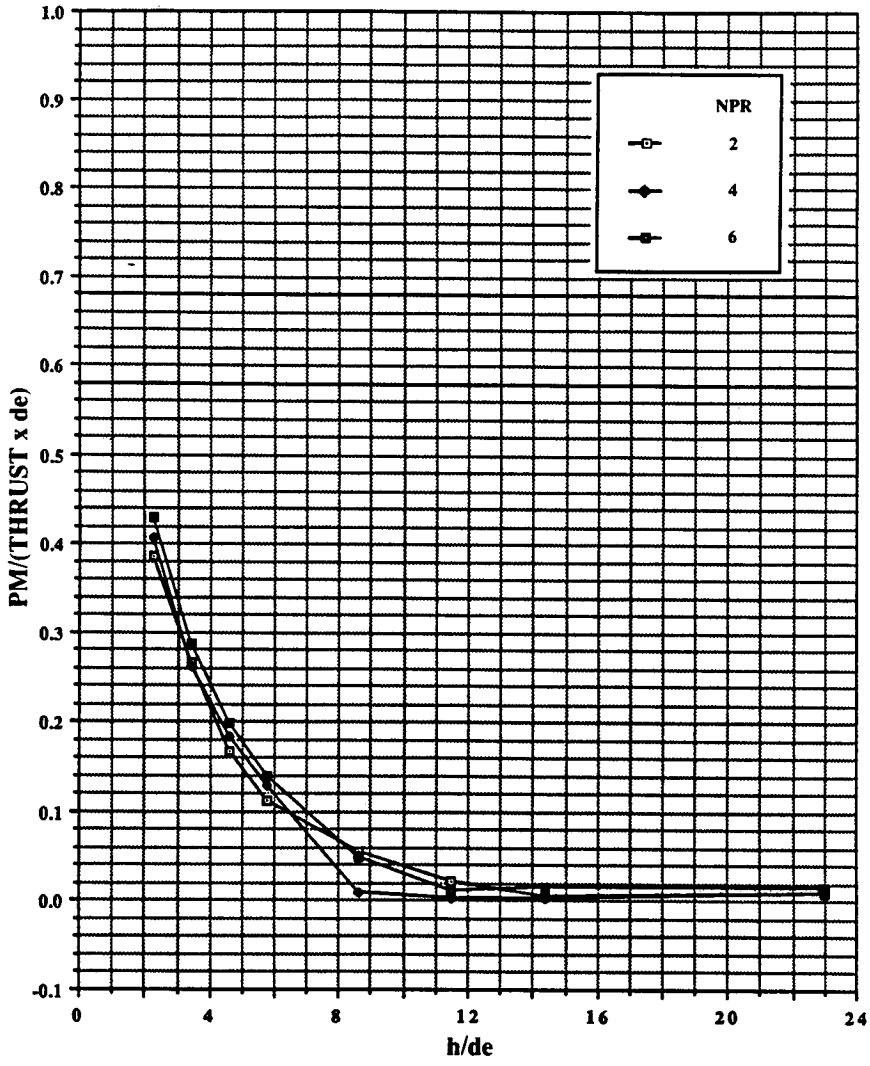

Figure 60. Effect of pressure ratio on jet-induced pitching moment on wing/body configuration in ground effect, both jets, no LIDs.

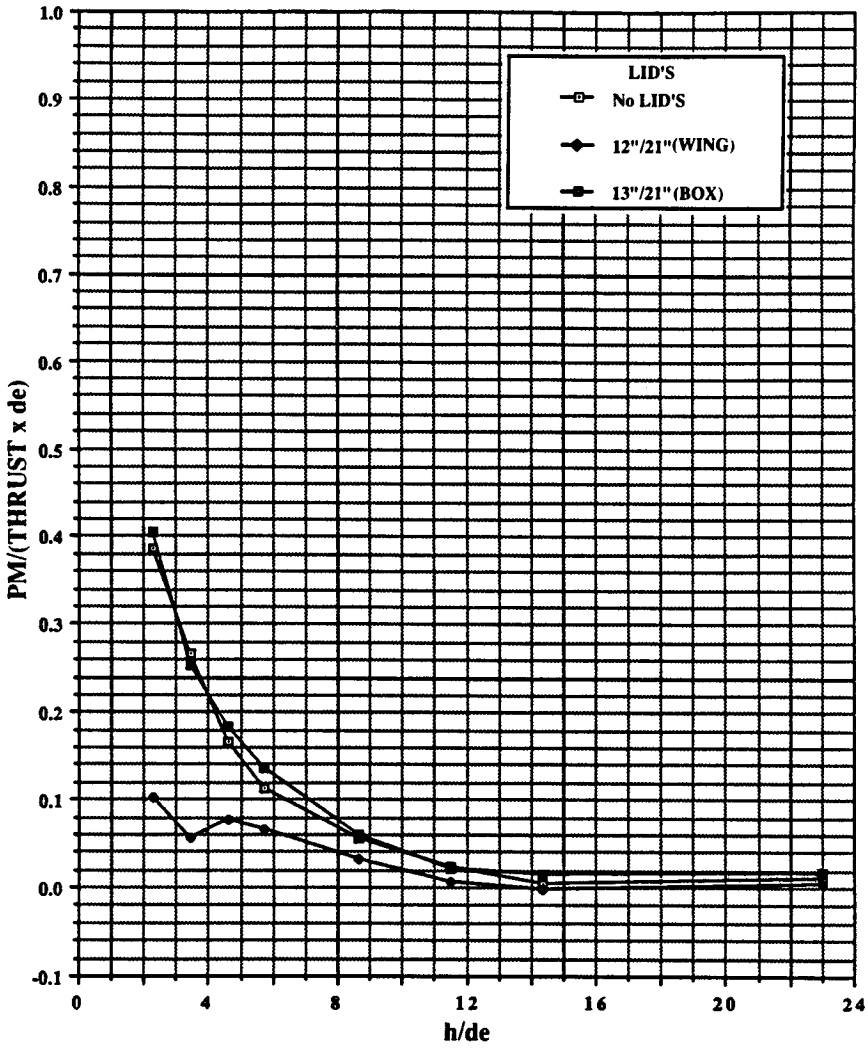

Figure 61. Effect of LIDs on jet-induced pitching moment on wing/body configuration in ground effect, both jets, NPR = 2.0.

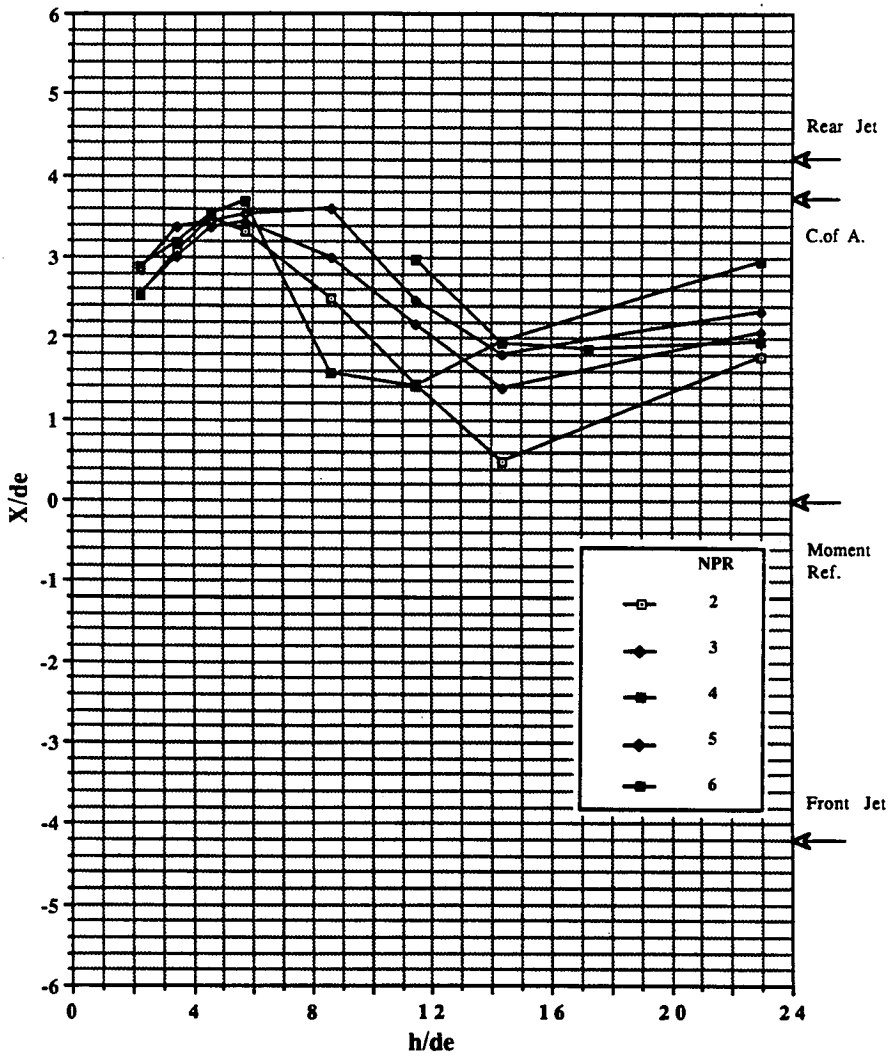

Figure 62. Effect of pressure ratio on jet-induced center of pressure (PM/lift) on delta-wing configuration in ground effect, both jets, no LIDs.

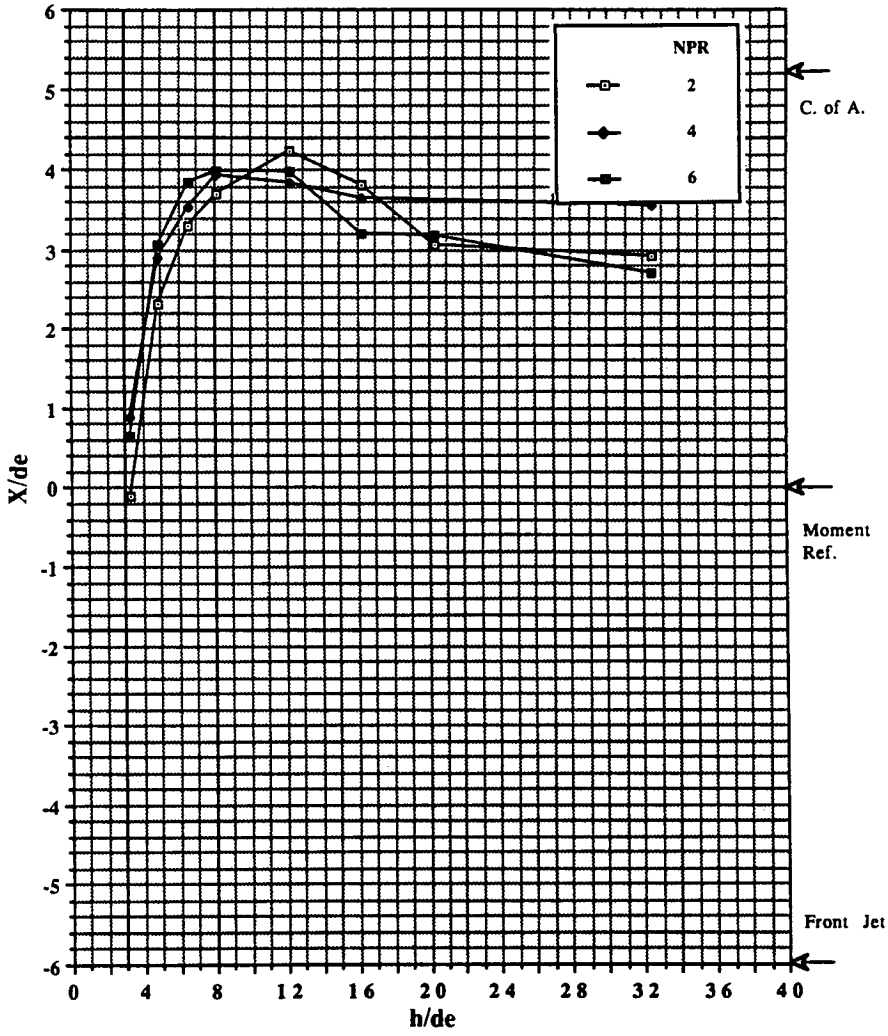

Figure 63. Effect of pressure ratio on jet-induced center of pressure (PM/lift) on delta-wing configuration in ground effect, front jet only, no LIDs.

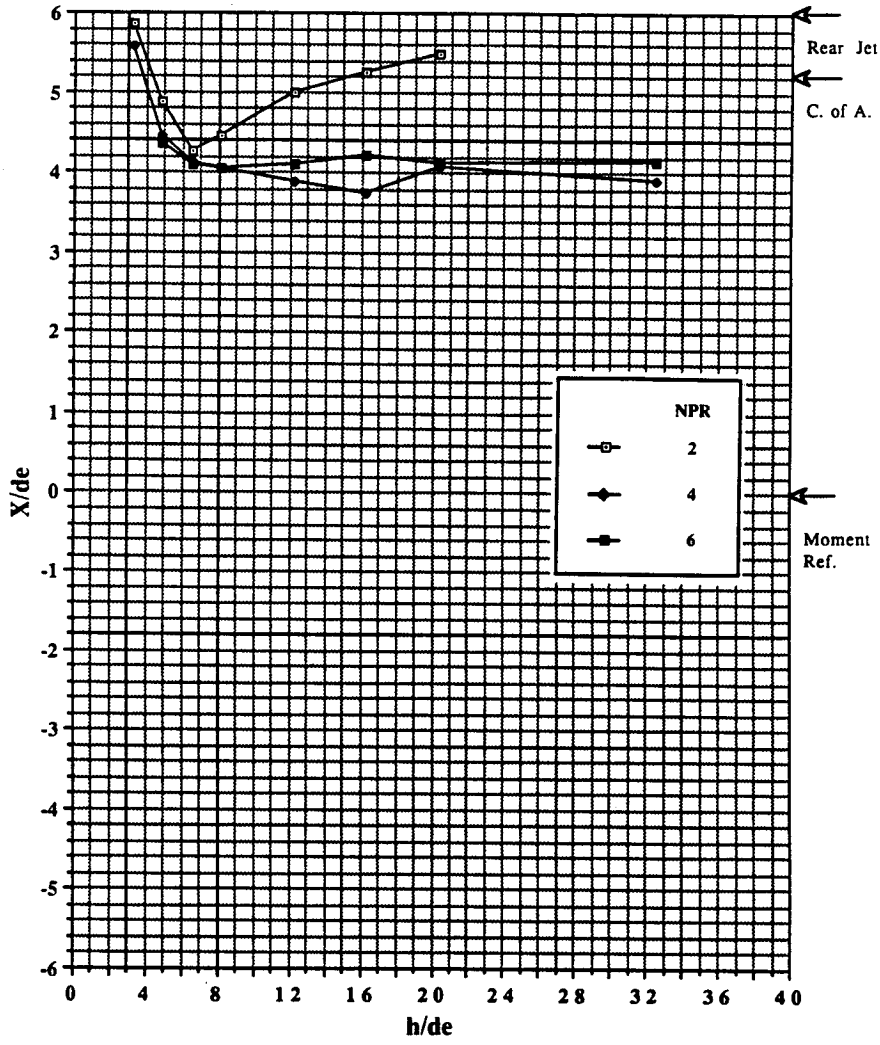

Figure 64. Effect of pressure ratio on jet-induced center of pressure (PM/lift) on delta-wing configuration in ground effect, rear jet only, no LIDs.

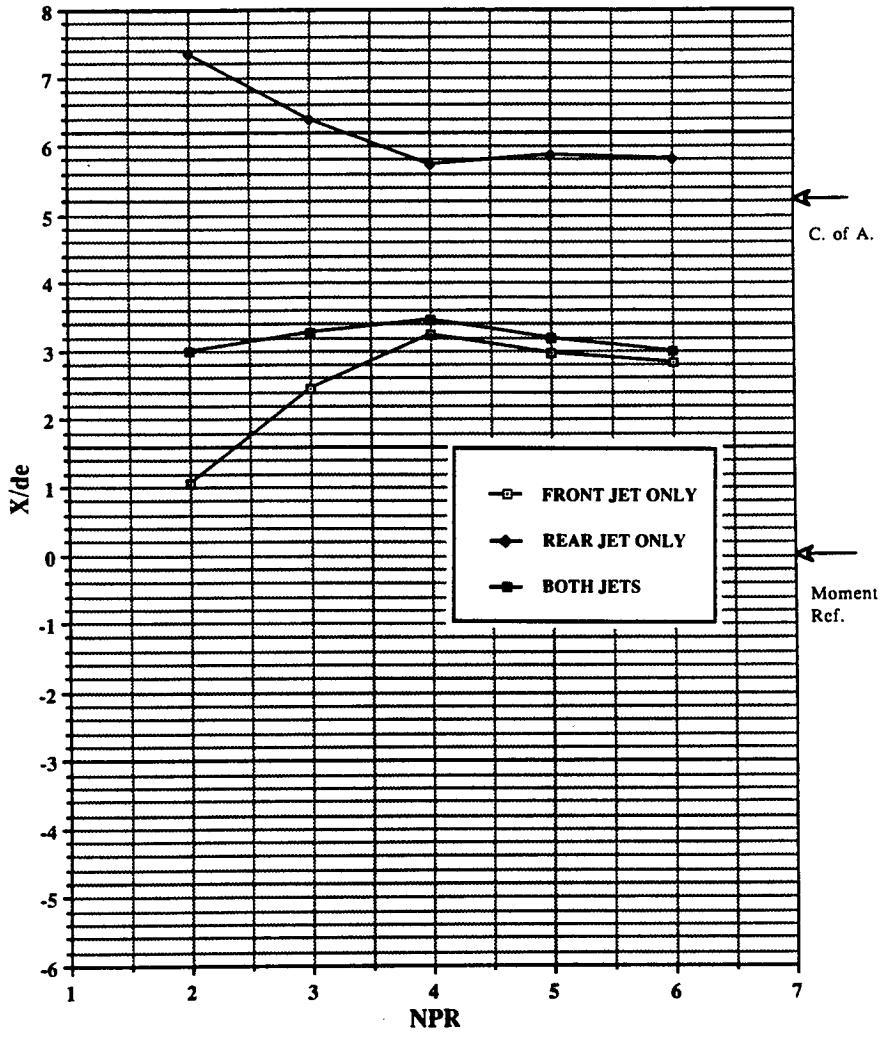

Figure 65. Jet-induced center of pressure (PM/lift) on delta-wing configuration out of ground effect, no LIDs.

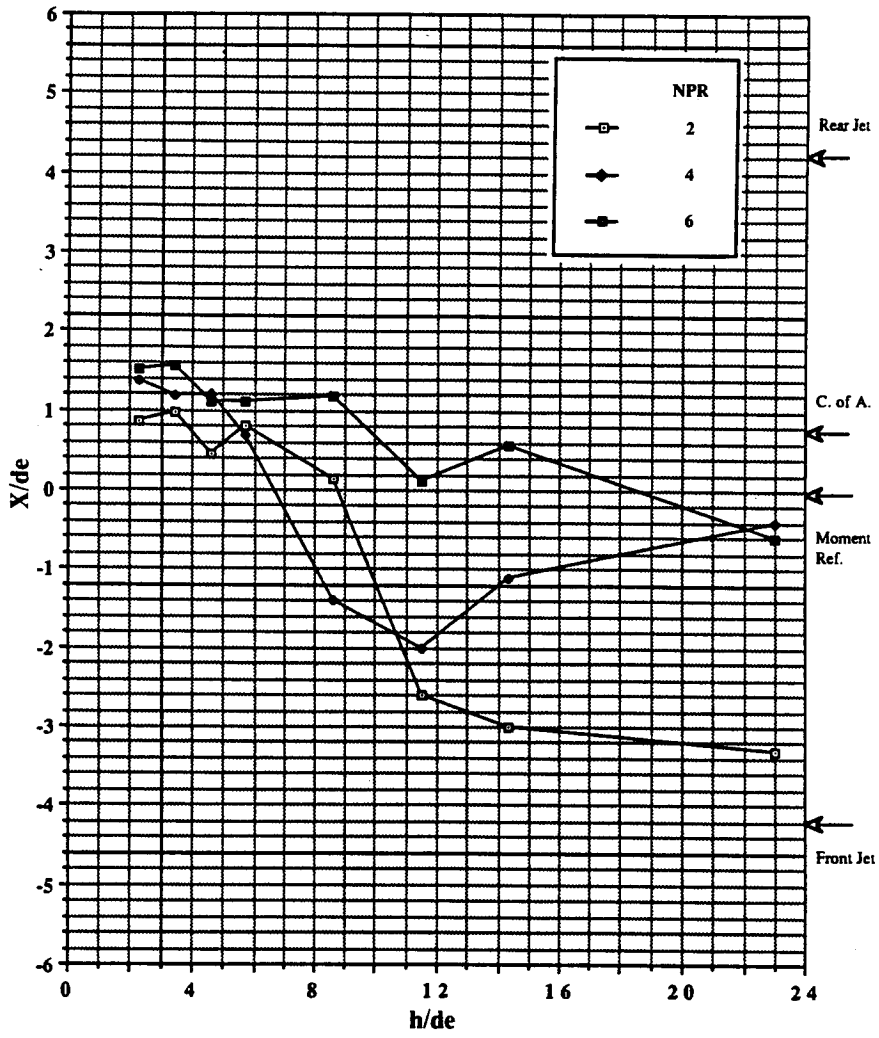

Figure 66. Effect of pressure ratio on jet-induced center of pressure (PM/lift) on body-alone configuration in ground effect, both jets, no LIDs.

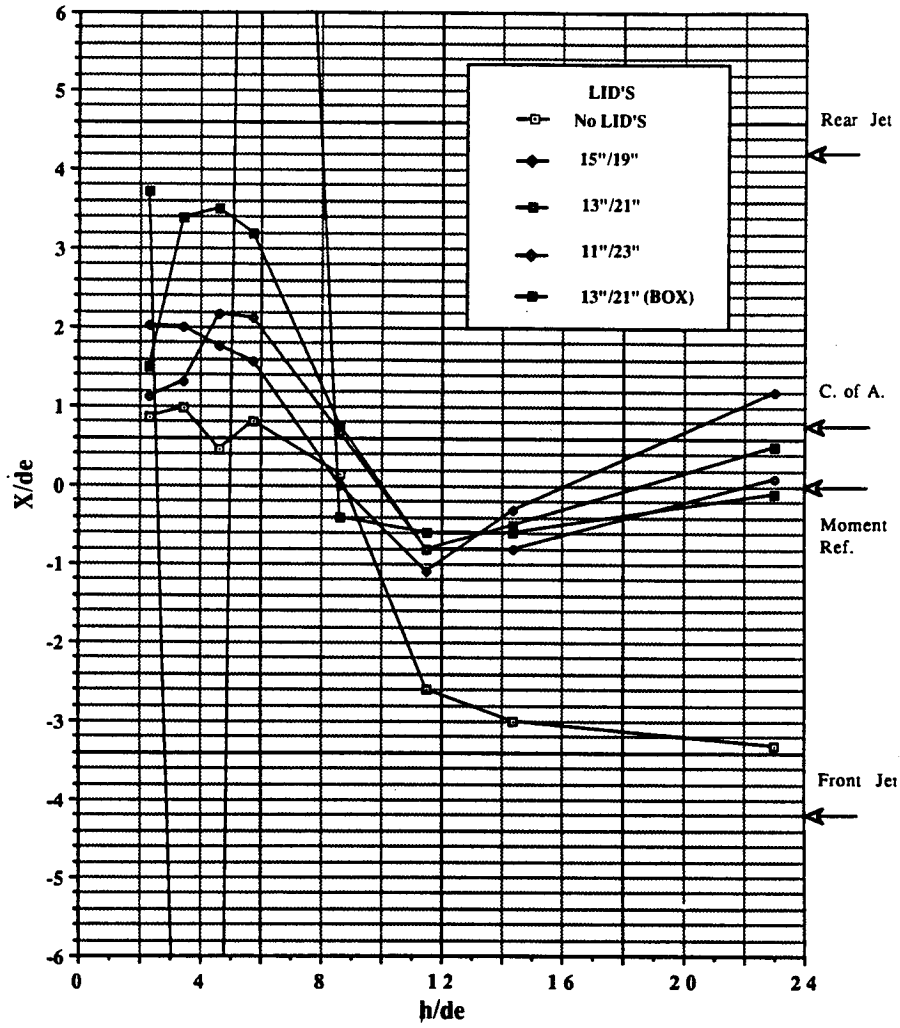

Figure 67. Effect of LIDs on jet-induced center of pressure (PM/lift) on body-alone configuration in ground effect, NPR = 2.0, both jets.

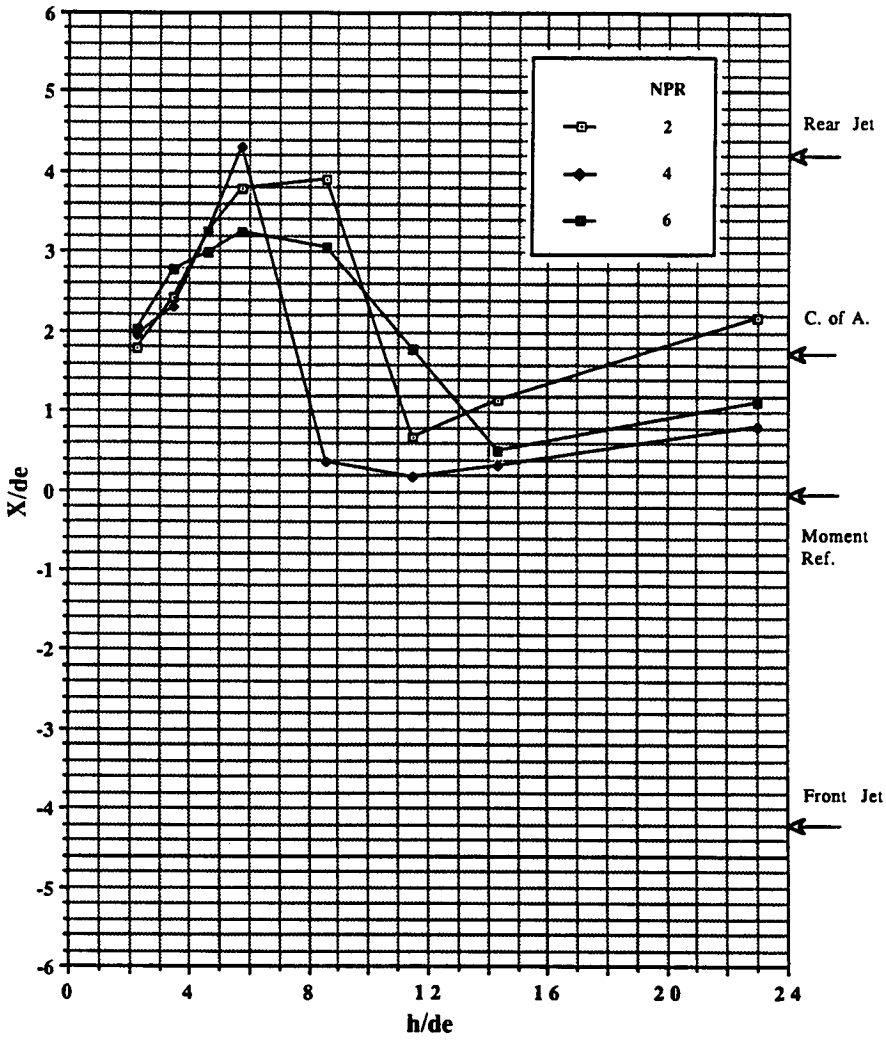

Figure 68. Effect of pressure ratio on jet-induced center of pressure (PM/lift) on wing/body configuration in ground effect, both jets, no LIDs.

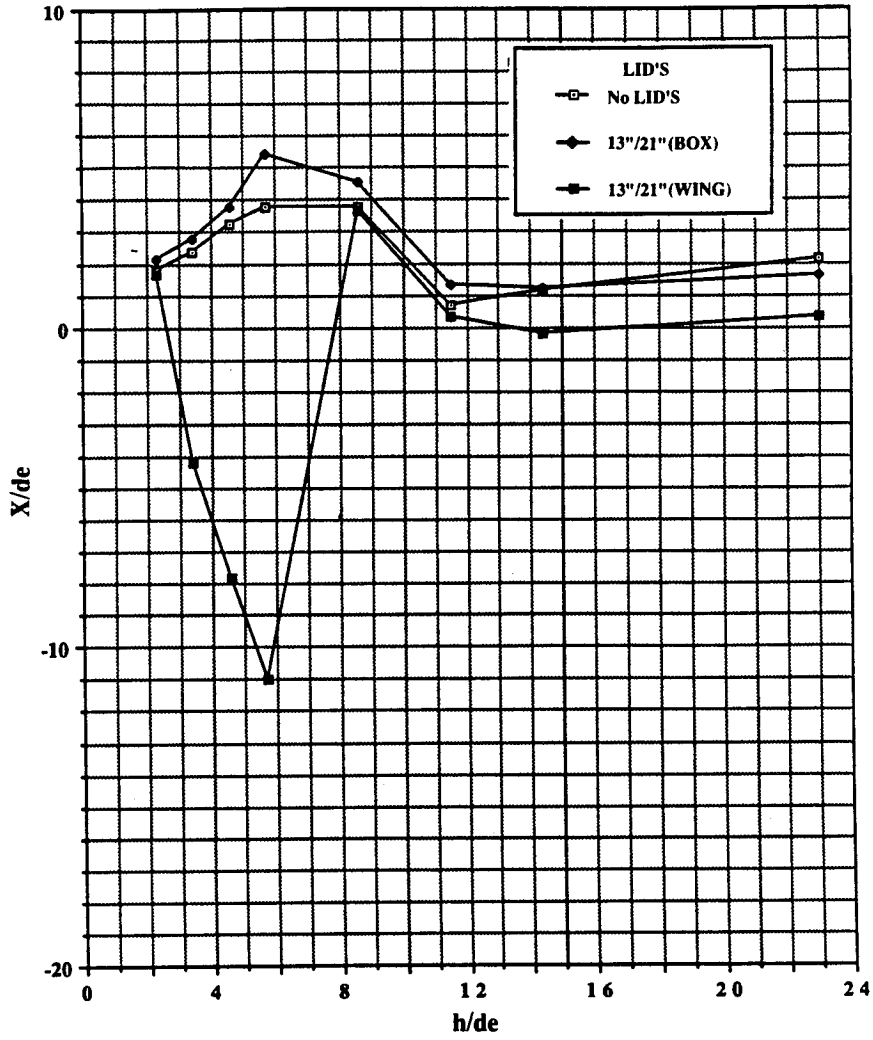

Figure 69. Effect of LIDs on jet-induced center of pressure (PM/lift) on wing/body configuration in ground effect, both jets, NPR = 2.0.

NASA
National Aeronautics and Space Administration

Report Documentation Page

1. Report No.	2. Government Accession No.	3. Recipient's Catalog No.
NASA TM-102817		

4. Title and Subtitle
Suckdown, Fountain Lift, and Pressures Induced on Several Tandem Jet V/STOL Configurations

5. Report Date
March 1991

6. Performing Organization Code

7. Author(s)
David C. Bellavia, Douglas A. Wardwell, Victor R. Corsiglia, and Richard E. Kuhn*
*STO-VL Technology, San Diego, California

8. Performing Organization Report No.
A-90144

10. Work Unit No.
505-61-71

9. Performing Organization Name and Address
Ames Research Center
Moffett Field, CA 94035-1000

11. Contract or Grant No.

13. Type of Report and Period Covered
Technical Memorandum

12. Sponsoring Agency Name and Address
National Aeronautics and Space Administration
Washington, DC 20546-0001

14. Sponsoring Agency Code

15. Supplementary Notes
Point of Contact: Douglas A. Wardwell, Ames Research Center, MS 247-2, Moffett Field, CA 94035-1000
(415) 604-6566 or FTS 464-6566

16. Abstract
As part of a program to improve the methods for predicting the suckdown and hot gas ingestion for jet V/STOL aircraft in ground effect, a data base is being created that provides a systematic variation of parameters so that a new empirical prediction procedure can be developed. The first series of tests in this program has been completed. This report describes suckdown, fountain lift, and pressures induced on several two-jet V/STOL configurations. It is one of three reports that present the data obtained from tests conducted at Lockheed Aeronautical Systems–Rye Canyon Facility and in the High Bay area of the 40- by 80-Foot Wind Tunnel complex at NASA Ames Research Center.

17. Key Words (Suggested by Author(s))	18. Distribution Statement
STOVL ground effects Powered lift ground effects V/STOL ground effects	Unclassified-Unlimited Subject Category - 02

19. Security Classif. (of this report)	20. Security Classif. (of this page)	21. No. of Pages	22. Price
Unclassified	Unclassified	154	A08

For sale by the National Technical Information Service, Springfield, Virginia 22161